Earth Mechanics

Fugro - Earth Mechanics
A JOINT VENTURE

SUBCONTRACTOR REPORTS
PRELIMINARY GEOTECHNICAL SITE CHARACTERIZATION

SAN FRANCISCO-OAKLAND BAY BRIDGE EAST SPAN SEISMIC SAFETY PROJECT

VOLUME 3 OF 4
(Fugro South, Inc., and University of Texas at Austin)

Prepared for
CALIFORNIA DEPARTMENT OF TRANSPORTATION

June 1998

Earth Mechanics

Fugro - Earth Mechanics
A JOINT VENTURE

7700 Edgewater Drive, Suite 848
Oakland, California 94621
Tel: (510) 633-5100
Fax: (510) 633-5101

June 24, 1998
Project No. 98-42-0035

California Department of Transportation
Engineering Service Center
Office of Structural Foundations
5900 Folsom Boulevard
Sacramento, California 95819-0128

Attention: Mr. Mark Willian
Contract Manager

Subcontractor Reports
Preliminary Geotechnical Site Characterization
SFOBB East Span Seismic Safety Project

Dear Mr. Willian:

The geologic and geotechnical studies for the San Francisco-Oakland Bay Bridge (SFOBB) East Span Seismic Safety Project are being conducted by Fugro-Earth Mechanics (a joint venture of Fugro West, Inc., and Earth Mechanics, Inc.) under California Department of Transportation (Caltrans) Contract 59A0053. The third task order for that contract included efforts for "Preliminary Site Exploration and Testing". Caltrans' notice to proceed for Task Order No. 3 (to Caltrans Contract 59A0053) was issued on January 26, 1998.

The Task Order No. 3 work scope included: 1) 14 marine borings, 2) 3 land borings on Yerba Buena Island, and 3) 3 seismic cone penetration test (CPT) soundings on the Oakland Mole. The borings include extensive in situ testing, soil sampling, rock coring, and downhole geophysical logging. Extensive laboratory testing programs were conducted on the soil samples and rock cores recovered from the borings.

As part of the execution of the preliminary geotechnical site investigations, services were obtained from several subcontractors who have submitted reports to Fugro-Earth Mechanics documenting the data they collected. Those reports are reproduced in a set of four volumes that include the following subcontractor reports:

Volume	Subcontractor	Report Subject
1	• Geovision • Welenco, Inc.	• Borehole Geophysics • Borehole Televiewer Logs
2	• NORCAL Geophysical Consultants, Inc. • COLOG, Inc. • Hughes Insitu Engineering, Inc.	• Seismic Surveys - Yerba Buena Island • BIPS Data - Yerba Buena Island • Pressuremeter Testing

Volume	Subcontractor	Report Subject
3	• Fugro South, Inc. • University of Texas at Austin	• Resonant Column and Cyclic Direct Simple Shear Tests • Dynamic Properties of Intact Soil Specimens
4	• GeoTest Unlimited	• Laboratory Rock Testing Program

On behalf of the project team, we appreciate the opportunity to contribute to the Caltrans' design of the new bridge to replace the existing SFOBB East Span. Please call if we can answer any questions relative to the information presented in the enclosed report.

Sincerely,

FUGRO WEST, INC.
(on behalf of Fugro-Earth Mechanics, a Joint Venture)

Thomas W. McNeilan, C.E., G.E.
Vice President

TWM:bki

Attachment

Copies Submitted: Mr. Mark Willian, Caltrans (1 + 1 unbound reproducible)
Mr. Reid Buell, Caltrans (2)
Dr. Abbas Abghari, Caltrans (1)
Dr. Brian Maroney, Caltrans (1)
Mr. Ade Akinsanya, Caltrans (1)
Mr. Steve Hulsebus, Caltrans (1)
Mr. Al Ely, T.Y. Lin/M&N (1)
Mr. Po Lam, Earth Mechanics (1)

SAN FRANCISCO-OAKLAND BAY BRIDGE
EAST SPAN SEISMIC SAFETY PROJECT

CALTRANS CONTRACT 59A0053

SUBCONTRACTOR REPORTS
PRELIMINARY GEOTECHNICAL
SITE CHARACTERIZATION

VOLUME 3 OF 4
(Fugro South, Inc., and University of Texas at Austin)

JUNE 1998

Prepared For:

CALIFORNIA DEPARTMENT OF TRANSPORTATION
Engineering Service Center
Office of Structural Foundations
5900 Folsom Boulevard
Sacramento, California 95819-0128

Prepared By:

FUGRO-EARTH MECHANICS
A Joint Venture
7700 Edgewater Drive, Suite 848
Oakland, California 94621

FUGRO SOUTH, INC.

FUGRO SOUTH, INC.
RESONANT COLUMN AND CYCLIC DIRECT SIMPLE SHEAR TESTS

FUGRO SOUTH, INC.

6100 Hillcroft (77081)
P.O. Box 740010
Houston, Texas 77274
Tel : (713) 778-5533
Fax: (713) 778-5544

June 24, 1998
Project No. 98-42-0035

Fugro-Earth Mechanics
7700 Edgewater Drive, Suite 848
Oakland, California 94621

Attention: Mr. Thomas W. McNeilan

Subject: Dynamic Testing

Dear Mr. McNeilan:

Dynamic geotechnical testing for the San Francisco-Oakland Bay Bridge (SFOBB) East Span Replacement was conducted by Fugro South. This data summary report summarizes the results of resonant column tests and cyclic direct simple shear tests that were performed in our Houston laboratories in June 1998.

The attached Data Summary Report includes a) a summary of the testing procedures used; b) tables and plots of results from five resonant column tests, and seven cyclic direct simple shear tests; and c) a brief discussion of the test results.

Please call if you have any questions.

Sincerely,

FUGRO SOUTH, INC.

Gregg Fiegel, Ph.D.
Project Engineer

Willard DeGroff
Laboratory Manager

GF/WD:bki

Attachment: Data Summary Report

C:\WINDOWS\TEMP\FUGSOUTH.DOC

FUGRO SOUTH, INC.

DATA SUMMARY REPORT
RESULTS OF RESONANT COLUMN AND STRAIN-CONTROLLED CYCLIC DIRECT SIMPLE SHEAR TESTS
SAN FRANCISCO-OAKLAND BAY BRIDGE
EAST SPAN SEISMIC SAFETY PROJECT

Prepared for:
FUGRO-EARTH MECHANICS
A JOINT VENTURE

June 1998

CONTENTS

		Page
1.0	INTRODUCTION	1
	1.1 Overview of Dynamic Testing	1
	1.2 Laboratory Classification Tests	1
2.0	RESONANT COLUMN TESTS	2
	2.1 Testing Procedure	2
	2.2 Test Results	3
	2.3 Discussion of Results	3
3.0	STRAIN-CONTROLLED CYCLIC DIRECT SIMPLE SHEAR TESTS	4
	3.1 Testing Procedure	4
	3.2 Test Results	5
	3.3 Discussion of Test Results	5

TABLES

	Table
Summary of Dynamic Testing Program	1
Summary of Resonant Column Test Results	
Metric	2a
English	2b
Effective Consolidation Stresses for the CSS Tests	
Metric	3a
English	3b
Summary of Cyclic Simple Shear Test Results	
Metric	4a
English	4b

APPENDICES

APPENDIX A RESULTS OF RESONANT COLUMN TESTS

APPENDIX B RESULTS OF CYCLIC SIMPLE SHEAR TESTS

1.0 INTRODUCTION

1.1 Overview of Dynamic Testing

The dynamic properties of six fine-grained soil samples were evaluated at the geotechnical testing laboratories of Fugro South, Inc., Houston, Texas. The six soil samples, tested (summarized in Table 1), were retrieved from five borings drilled by Fugro-Earth Mechanics for the San Francisco-Oakland Bay Bridge (SFOBB) Seismic Safety Project.

The samples were retrieved in thin-walled Shelby tubes [76-mm-OD, 72-mm-ID (3.0-inch-OD, 2.83-inch-ID) using push sampling techniques. The sample tubes were sealed with end caps and wax in the field prior to being transported to the laboratory.

Dynamic tests on the six samples were carried-out using resonant column (RC) and strain-controlled cyclic direct simple shear (CSS) test equipment. The following data summary report describes the dynamic laboratory testing procedures that were followed during the investigation and outlines the presentation of the test results. Summaries of test parameters and results are included within the report, together with the individual test data plots.

The purpose of the dynamic lab testing program was to: (a) determine the small-strain (low-amplitude) shear modulus, G_{max}, and material damping ratio, D_{min}, of each soil sample, (b) study the relationship between normalized shear modulus, G/G_{max}, and shear strain, γ, and (c) study the relationship between material damping ratio, D, and shear strain, γ. The RC tests were performed to characterize G and D for relatively small shear strains (<0.1percent). The CSS tests were performed to characterize G and D for large shear strains (0.1percent to 3percent).

Soil samples from several different San Francisco Bay area geologic units were examined. A summary of the samples tested is presented on Table 1. As shown in Table 1, dynamic tests were performed on samples from the Young Bay Mud (with comparatively low OCRs), from the upper, shallow portion of the Old Bay Mud (with comparatively high OCRs), and from the deeper section of the Old Bay Mud (with comparatively low OCRs). Five RC tests and seven CSS tests were performed. In four instances it was possible to perform RC and CSS tests on soil specimen taken from the same sample tube.

1.2 Laboratory Classification Tests

Classification tests and consolidation tests were performed on the six test specimens selected for dynamic laboratory testing. Summarized in Table 1 are water content, total unit weight, liquid limit, plasticity index, overconsolidation ratio (OCR), and void ratio results for each specimen. The table also provides, for each sample, a USCS classification, a geologic unit designation, penetration depth, an estimate of the in situ vertical effective stress, the coefficient

of lateral earth pressure at rest (K_o), the calculated mean effective confining stress (σ_o'), and a listing of the dynamic tests performed.

The mean effective confining stresses were computed using the in situ vertical effective stresses listed in Table 1 and the following relation:

$$\sigma_o' = [(1 + 2K_o)/3] * \sigma_{vo}'$$

The values of K_o required for the above relation were estimated using the empirical correlation developed by Mayne and Kulhawy (1982), which relates K_o to overconsolidation ratio. Estimated K_o values for the six samples are presented in Table 1.

2.0 RESONANT COLUMN TESTS

2.1 Testing Procedure

The five resonant column tests were performed on solid, cylindrical-shaped, soil specimens. These tests were numbered 09-7-49, 98-8-37, 98-9-53, 98-9-75, and 98-12-37. The diameters of the five specimens were approximately 38 mm, 53 mm, 38 mm, 38 mm, and 72 mm, respectively. Corresponding lengths for the five specimens were approximately 76 mm, 108 mm, 76 mm, 76 mm, and 142 mm. As evident, an approximate length to diameter ratio of 2:1 was achieved for all five specimens.

Each test specimen was back-pressure saturated to 138-276 kPa (20-40 psi) and then isotropically consolidated to three or four successive effective confining pressures (i.e., the tests were performed in stages). Effective confining pressures (σ_o') primarily equal to or greater than the mean effective in situ overburden pressure were used. During consolidation at each effective confining pressure, the variation of low amplitude or small-strain ($<10^{-4}$ percent) shear modulus (G) and material damping ratio (D) were measured as a function of time. Measurements began immediately after the confining pressure was applied and were taken at 0.5, 1, 2, 4, 8, 15, 30, 60 minutes, etc. Once primary consolidation was achieved, the G and D measurements were continued for approximately two log cycles of time. The measurements taken after primary consolidation were used to estimate the maximum shear modulus, G_{max}. A sinusoidal waveform was used to apply torque to the top of the specimen. It is noted that these low-amplitude shear moduli were calculated from data obtained after the frequency of the soil-oscillator system had been adjusted to vibrate at the undamped first mode frequency. The values of material damping were determined using the steady-state, magnification factor method.

During the resonant column tests, shear moduli (G) and material damping ratios (D) corresponding to moderate- to high-amplitude shear strains ($>10^{-4}$ percent) were also measured as a function of effective confining pressure. These values were measured during each test stage once the low-amplitude (small-strain) testing had been completed. The drainage lines were

closed during this portion of the test. For each test stage, the strain level was increased in small steps until the measured G value decreased to approximately 80 percent of G_{max} At this point, the moderate- to high-amplitude portion of the test was stopped and the soil specimen was allowed to drain and re-consolidate. Low-amplitude (small-strain) shear moduli were then measured. Measurements were taken until the G values approached the G value measured just before the moderate- to high-amplitude testing began. Failure in regaining this modulus may have been indicative of specimen degradation.

During the final test stage (i.e., the test stage with the highest effective confining pressure), moderate- to high-amplitude shear strain measurements of G and D were taken at incrementally higher strain levels until either the limits of the device were reached or oscillator instability occurred. G values measured during this final test stage were as small as 50 to 60 percent of G_{max}.

2.2 Test Results

The test conditions and results of the resonant column tests are summarized in Table 2a (Metric) and Table 2b (English), with the individual test data plots presented on Plates A.1 through A.5. The following plots are presented for each resonant column test:

- Low-Amplitude Shear Modulus vs. Time after Initiating Consolidation .. (semi-log)
- Low-Amplitude Material Damping Ratio vs. Time After Initiating Consolidation ..... (semi-log)
- Maximum Low-Amplitude Shear Modulus vs. Confining Pressure ..... (log-log)
- Shear Modulus vs. Time after Initiating High-Amplitude Sequence ..... (linear)
- Shear Modulus vs. Average Shear Strain ..... (semi-log)
- Normalized Shear Modulus vs. Average Shear Strain ..... (semi-log)
- Material Damping Ratio vs. Average Shear Strain ..... (semi-log)

The first three plots were obtained for each RC test during the low-amplitude test sequences. The remaining plots were obtained from the high-amplitude sequences.

2.3 Discussion of Results

As expected, the RC test results show that small-strain (low-amplitude) shear modulus (G_{max}) increases with increasing effective confining pressure. The G_{max} values also depend on the geologic unit from which the sample was taken. Larger values of G_{max} were measured for the Old Bay Mud samples as compared to the Young Bay Mud samples. In general the Old Bay Mud samples had comparatively higher in situ effective stresses and higher OCRs. Equations relating G_{max} and σ_o' are noted in the plots showing G_{max} as a function of effective confining pressure (see Appendix A).

In contrast, small-strain (low-amplitude) material damping ratios (D_{min}) did not appear to depend greatly on the effective confining pressure. Similar values of D_{min} were found for both the Young and Old Bay Mud samples for all of the confining pressures examined. The D_{min} values for all five samples, which are summarized in Tables 2a and 2b, generally ranged between 2 and 3 percent.

Plots of normalized shear modulus (G/G_{max}) and material damping ratio (D) as a function of shear strain (γ) are consistent with results found for other marine clays. The results show relatively little scatter and indicate that effective confining pressure has a small effect on the G/G_{max} and D relationships. When compared with the Young Bay Mud test results, the Old Bay Mud samples were found to have higher G/G_{max} values and lower D values for higher shear strain levels (>0.01percent).

3.0 STRAIN-CONTROLLED CYCLIC DIRECT SIMPLE SHEAR TESTS

3.1 Testing Procedure

The seven strain-controlled cyclic direct simple shear (CSS) tests were performed on small, puck-shaped soil specimens. Each specimen, after being trimmed from a larger sample, had an approximate height of about 18 mm and an approximate diameter of 65 to 66 mm. The seven tests were numbered 98-7-49-A, 98-7-49-B, 98-8-37-A, 98-8-37-B, 98-9-53, 98-11-73, and 98-11-37.

Ideally, the soil specimens were tested with OCRs and effective vertical consolidation stresses similar to those found in situ. Tables 3a (Metric) and 3b (English) summarize in situ and laboratory stress information for the seven CSS tests. Noted in the table for each sample are the test effective vertical consolidation stress and OCR. Stress conditions for samples 98-7-49-B, 98-8-37-B, 98-9-53, 98-11-73, and 98-12-37 were essentially the same as the in situ conditions. Note that samples 98-8-37-B and 98-12-37 were tested at slightly higher consolidation stresses but with similar OCRs. As indicated, samples 98-7-49-A and 98-8-37-A were tested under stress conditions different from those in situ. These samples were both tested in a normally consolidated condition with lab consolidation stresses higher than the approximated in situ vertical effective stress.

Soil samples were loaded incrementally during consolidation. During each CSS test, at least four load increments (stages) were used to achieve the final consolidation stress. At the test consolidation stress, specimen were allowed to consolidate for about one log cycle of time or 24 hours, whichever was less, past the end of primary consolidation (T_{100}).

After consolidation, the samples were subjected to sinusoidal cyclic horizontal loads at a frequency of 1.0 Hz. Constant volume conditions were maintained during the cyclic loading

portion of the test by locking the vertical loading piston in place. Changes in vertical stress during cyclic loading were used to evaluate pore-water pressure changes.

Each specimen was subjected to four levels of increasing nominal average cyclic shear strain, with re-consolidation (i.e., excess pore-water pressure dissipation) accommodated between each level of straining. Proposed for each CSS test were the nominal average shear strain levels and number of cycles summarized below. It is noted that the shear strains achieved during the tests do not always correspond exactly with the proposed strain levels. These differences stem from equipment control and measurement resolution limitations.

Strain Level	Average Shear Strain Level, ±γ (percent)	Number of Cycles, N
1	0.1 to 0.2	30
2	0.5	30
3	1.0	30
4	2.0 to 3.0	30

3.2 Test Results

The test conditions and results of the strain-controlled cyclic simple shear (CSS) tests are summarized in Tables 4a (Metric) and 4b (English), with the individual test data plots presented on Plates B.1 through B.7. The following plots are presented for each CSS test:

- Shear Modulus vs. Average Shear Strain ..... (semi-log)
- Material Damping Ratio vs. Average Shear Strain ..... (semi-log)
- Shear Modulus vs. Number of Cycles ..... (semi-log)
- Material Damping Ratio vs. Number of Cycles ..... (semi-log)
- Decrease in Vertical Stress Ratio vs. Number of Cycles ..... (semi-log)

3.3 Discussion of Test Results

As expected, the CSS test results show that shear moduli (G) and material damping ratios (D) depend on shear strain (γ). G values tend to decrease with increasing γ while D values tend to increase. G-γ and D-γ relationships show some dependence on effective stress conditions and OCR. Note that the G and D values included in these relationships are reported for the first loading cycle (N=1). Also, it is noted that G and D values associated with average shear strains less than about 0.2percent should be interpreted with some judgment. Measurement difficulties arise when attempting to run CSS tests at such small shear strains.

Normalized shear modulus values (G/G_{max}) were computed for the CSS test results, as was done for the RC tests. The required small-strain shear moduli (G_{max}) were estimated from

the G_{max} vs σ_o' relationships presented in Appendix A. The differences in the state of stress in the CSS test and RC test were accounted for by using the equation for mean effective confining stress discussed in Section 1.2. Mean effective confining stresses were calculated using the effective vertical consolidation stresses reported for each CSS test and the K_o values presented in Table 1. Note that this procedure assumes that the coefficient of horizontal stress in the CS test was equal to the in situ K_o.

G/G_{max} values found for the tests where the in situ stresses were accurately modeled (i.e., 98-7-49-B, 98-8-37-B, 98-9-53, 98-11-73, and 98-12-37) are consistent with the RC test results. A reasonably good transition exists between the two sets of results. Not surprisingly, the results for tests 98-7-49-A and 98-8-37-A are not as consistent. The differences are likely due to that fact that the stress conditions applied in the lab were different from those experienced in situ. The additional CSS test results help to illustrate the influence of stress history on the G/G_{max} relationships. At higher shear strains, the normally consolidated "A" samples have G/G_{max} values lower than those found for the overconsolidated "B" samples, which is consistent with comparisons between the Young and Old Bay Mud test results.

For all seven tests, reasonable transitions exist between the CSS and RC test results for material damping ratio (D). As was the case when examining the G/G_{max} relations, poorer transitions were found for tests 98-7-49-A and 98-8-37-A. The poorer transitions are most likely due to the fact that, during these tests, the stress conditions applied in the lab were different from those experienced in situ. For these two tests, the measured material damping ratios were higher than expected.

Finally, plots of shear modulus (G) versus the number of loading cycles (N) show that some degradation in shear modulus occurred during the CSS tests. Modulus degradation was larger for the Young Bay Mud samples than for the Old Bay Mud samples. Overall, the results appear to be consistent with results reported for other marine clays.

June 1998
Project No. 98-42-0035
SFOBB Task Order No. 3

Boring Number	98-7	98-8	98-8	98-9	98-9	98-11	98-12	98-19	98-20	98-20
Sample Number	49	37	71	53	75	73	37	34	27	91
Soil Classification (USCS)	CH	CH	CH	CH	CL	CH	CH	CH	CH	CL
Geologic Unit	OBM	YBM	OBM	OBM	OBM	OBM	YBM	YBM	YBM	OBM
Penetration Depth										
meters	16.0	12.2	24.1	37.9	65.4	62.9	15.1	11.1	8.4	70.4
feet	52.5	40.0	79.0	124.5	214.5	206.5	49.5	36.5	27.5	231.0
Water Content (%)	68	64	57	40	28	50	80	58	50	30
Total Unit Weight										
kN/m^3	15.7	16.0	16.8	17.8	18.5	17.0	15.1	16.2	16.8	18.9
pcf	100	102	107	113	118	108	96	103	107	120
Liquid Limit (%)	77	65	89	76	43	70	72	75	63	46
Plastic Limit (%)	31	25	36	27	21	29	30	22	27	27
In-situ Effective Vertical Stress, σ'_{vo}										
kPa	81	67	144	268	570	450	105	53	53	532
ksf	1.7	1.4	3.0	5.6	11.9	9.4	2.2	1.1	1.1	11.1
Overconsolidation Ratio (OCR)	7.6	2.4	5.2	3.1	1.4	2.2	0.9	2.9	1.6	2.0
Lateral Earth Pressure Coefficient, K_o	1.4	0.8	1.1	0.9	0.6	0.7	0.5	0.9	0.6	0.7
Test Mean Effective Stress, σ'_o										
kPa	101	57	158	249	412	374	67	48	38	431
ksf	2.1	1.2	3.3	5.2	8.6	7.8	1.4	1.0	0.8	9.0
Void Ratio, e	1.9	1.7	1.5	1.1	0.9	1.4	2.2	1.6	1.4	0.8
Tests Performed	RC	RC	RC	RC	RC		RC	RC	RC	RC
	CSS	CSS	TS	CSS		CSS	CSS	TS	TS	TS
Laboratory	Fugro	Fugro	UT	Fugro	Fugro	Fugro	Fugro	UT	UT	UT

Notes:
1. YBM = Young Bay Mud; OBM = Old Bay Mud
2. Lateral earth pressure coefficient at rest, $K_o \approx 0.5\ (OCR)^{0.5}$, after Mayne and Kulhawy (1982)
3. Calculated mean effective in-situ overburden stress, $\sigma'_o = [(1+2K_o)/3]\sigma'_{vo}$
4. RC = Resonant Column; TS = Torsional Shear; CSS = Cyclic Simple Shear

SUMMARY OF DYNAMIC TESTING PROGRAM
1998 Marine Borings
SFOBB East Span Seismic Safety Project

Sample No.	Depth (m)	Stage	σ_o' (kPa)	Initial w (%)	Final w (%)	e_{100}	γ_{max} (%)	G_{max} (MPa)	D_{min} (%)
98-7-49	16.0	1	191.4	61.5		1.60	5.26e-02	44.0	1.87
(OBM)		2	382.8			1.56	5.56e-02	55.0	1.86
		3	765.6			1.39	7.20e-02	96.1	1.83
		4	1531.2		38.1	1.00	1.35e-01	198.5	1.68
98-8-37	12.2	1	47.8	61.2		1.64	2.25e-02	15.7	2.35
(YBM)		2	95.6			1.59	2.84e-02	21.9	2.46
		3	191.2			1.34	3.80e-02	47.4	2.23
		4	430.6		42.9	0.87	9.68e-02	90.2	2.06
98-9-53	37.9	1	239.2	40.1		1.09	2.63e-02	61.6	2.31
(OBM)		2	478.4			1.05	3.85e-02	79.5	2.60
		3	956.8			0.96	4.85e-02	121.9	2.49
		4	1435.2		32.2	0.76	1.37e-01	153.1	2.78
98-9-75	65.4	1	205.7	30.2		0.78	2.69e-02	70.8	2.25
(OBM)		2	416.3			0.77	2.34e-02	100.7	2.27
		3	933.0			0.72	3.23e-02	147.8	2.44
		4	1866.0		22.1	0.63	3.82e-02	269.9	2.52
98-12-37	15.1	1	38.3	76.0		2.08	2.06e-02	10.6	2.18
(YBM)		2	76.6			2.00	3.79e-02	16.6	1.69
		3	153.1		64.0	1.77	2.04e-01	30.4	2.72
		4	---			---	---	---	---

Notes:
1. σ_o' = Effective confining pressure
2. w = Water content
3. e_{100} = Void ratio at T_{100}
4. T_{100} = Time at the end of primary consolidation
5. γ_{max} = Maximum average shear strain
6. G_{max} = Maximum shear modulus at low-amplitude shear strain
7. D_{min} = Material damping ratio at low-amplitude shear strain

SUMMARY OF RESONANT COLUMN TEST RESULTS (METRIC)

1998 Marine Borings

SFOBB East Span Seismic Safety Project

June 1998
Project No. 98-42-0035
SFOBB Task Order No. 3

Sample No.	Depth (ft)	Stage	σ_o' (ksf)	Initial w (%)	Final w (%)	e_{100}	γ_{max} (%)	G_{max} (ksf)	D_{min} (%)
98-7-49	52.5	1	4.0	61.5		1.60	5.26e-02	920	1.87
(OBM)		2	8.0			1.56	5.56e-02	1149	1.86
		3	16.0			1.39	7.20e-02	2008	1.83
		4	32.0		38.1	1.00	1.35e-01	4148	1.68
98-8-37	40.0	1	1.0	61.2		1.64	2.25e-02	329	2.35
(YBM)		2	2.0			1.59	2.84e-02	458	2.46
		3	4.0			1.34	3.80e-02	991	2.23
		4	9.0		42.9	0.87	9.68e-02	1885	2.06
98-9-53	124.5	1	5.0	40.1		1.09	2.63e-02	1287	2.31
(OBM)		2	10.0			1.05	3.85e-02	1661	2.60
		3	20.0			0.96	4.85e-02	2547	2.49
		4	30.0		32.2	0.76	1.37e-01	3200	2.78
98-9-75	214.5	1	4.3	30.2		0.78	2.69e-02	1479	2.25
(OBM)		2	8.7			0.77	2.34e-02	2104	2.27
		3	19.5			0.72	3.23e-02	3089	2.44
		4	39.0		22.1	0.63	3.82e-02	5640	2.52
98-12-37	49.5	1	0.8	76.0		2.08	2.06e-02	221	2.18
(YBM)		2	1.6			2.00	3.79e-02	346	1.69
		3	3.2		64.0	1.77	2.04e-01	636	2.72
		4	----			----	----	----	----

Notes:
1. σ_o' = Effective confining pressure
2. w = Water content
3. e_{100} = Void ratio at T_{100}
4. T_{100} = Time at the end of primary consolidation
5. γ_{max} = Maximum average shear strain
6. G_{max} = Maximum shear modulus at low-amplitude shear strain
7. D_{min} = Material damping ratio at low-amplitude shear strain

SUMMARY OF RESONANT COLUMN TEST RESULTS (ENGLISH)

1998 Marine Borings
SFOBB East Span Seismic Safety Project

Sample No.	Depth (m)	Approx. σ_{vo}' (kPa)	Max. σ_{vc}' (kPa)	Test σ_{vc}' (kPa)	OCR In situ	OCR Lab
98-7-49-A (OBM)	16.0	81.3	765.6	765.6	7.6	1.0
98-7-49-B (OBM)	16.0	81.3	717.7	95.7	7.6	7.5
98-8-37-A (YBM)	12.2	67.0	215.3	215.3	2.4	1.0
98-8-37-B (YBM)	12.2	67.0	239.2	95.7	2.4	2.5
98-9-53 (OBM)	37.9	267.9	861.3	263.2	3.1	3.3
98-11-73 (OBM)	62.9	449.8	909.1	445.0	2.2	2.0
98-12-37 (YBM)	15.1	105.3	191.4	191.4	0.9	1.0

Notes:
1. σ_{vo}' = Approximate in situ vertical effective stress
2. Max σ_{vc}' = Maximum effective vertical consolidation stress prior to cyclic loading
3. Test σ_{vc}' = Effective vertical consolidation stress during cyclic loading
4. OCR, In situ = Overconsolidation ratio found from consolidation test results
5. OCR, Lab = (Max σ_{vc}') / (Test σ_{vc}')

EFFECTIVE CONSOLIDATION STRESSES FOR THE CSS TESTS (METRIC)
1998 Marine Borings
SFOBB East Span Seismic Safety Project

Sample No.	Depth (ft)	Approx. σ_{vo}' (ksf)	Max. σ_{vc}' (ksf)	Test σ_{vc}' (ksf)	OCR In situ	OCR Lab
98-7-49-A (OBM)	52.5	1.7	16.0	16.0	7.6	1.0
98-7-49-B (OBM)	52.5	1.7	15.0	2.0	7.6	7.5
98-8-37-A (YBM)	40.0	1.4	4.5	4.5	2.4	1.0
98-8-37-B (YBM)	40.0	1.4	5.0	2.0	2.4	2.5
98-9-53 (OBM)	124.5	5.6	18.0	5.5	3.1	3.3
98-11-73 (OBM)	206.5	9.4	19.0	9.3	2.2	2.0
98-12-37 (YBM)	49.5	2.2	4.0	4.0	0.9	1.0

Notes:
1. σ_{vo}' = Approximate in situ vertical effective stress
2. Max σ_{vc}' = Maximum effective vertical consolidation stress prior to cyclic loading
3. Test σ_{vc}' = Effective vertical consolidation stress during cyclic loading
4. OCR, In situ = Overconsolidation ratio found from consolidation test results
5. OCR, Lab = (Max σ_{vc}') / (Test σ_{vc}')

EFFECTIVE CONSOLIDATION STRESSES FOR THE CSS TESTS (ENGLISH)
1998 Marine Borings
SFOBB East Span Seismic Safety Project

Sample No.	Depth (m)	σ_{vc}' (kPa)	Initial w (%)	Final w (%)	No. of Cycles, N	Avg. $\pm\gamma$ (%)	$G_{N=1}$ (MPa)	$G_{N=30}$ (MPa)	$D_{N=1}$ (%)
98-7-49-A	16.0	764.1	60.4		30	0.202	31.5	29.5	9.3
(OBM)		763.2			30	0.475	23.7	21.2	11.6
		763.4			30	1.094	15.8	13.6	16.3
		762.6		49.1	30	2.541	9.3	7.0	22.4
98-7-49-B	16.0	94.2	58.9		30	0.204	15.7	14.2	9.0
(OBM)		95.9			30	0.594	9.9	8.5	12.2
		94.5			30	1.268	6.3	5.4	14.6
		94.5		53.1	30	2.592	4.1	3.3	16.2
98-8-37-A	12.2	213.8	59.3		30	0.245	11.7	10.6	15.4
(YBM)		214.6			30	0.673	7.2	5.6	18.6
		214.0			30	1.431	4.2	3.1	21.6
		212.3		50.1	30	3.029	2.5	1.5	25.1
98-8-37-B	12.2	96.7	61.5		30	0.263	9.1	8.1	11.6
(YBM)		96.3			30	0.696	5.5	4.6	15.0
		96.1			30	1.369	3.5	2.8	16.4
		94.3		49.8	30	2.881	2.0	1.3	20.0
98-9-53	37.9	261.2	37.1		30	0.133	33.6	30.8	7.2
(OBM)		263.1			30	0.427	22.5	19.7	9.4
		262.9			30	0.962	15.0	13.3	12.2
		262.5		39.2	30	2.136	9.7	5.9	15.3
98-11-73	62.9	443.7	48.7		30	0.137	34.2	31.7	7.6
(OBM)		444.5			30	0.464	21.8	18.9	10.1
		445.5			30	1.059	14.2	12.0	13.1
		444.4		45.5	30	2.244	8.9	7.3	16.9
98-12-37	15.1	189.1	61.5		30	0.222	11.3	10.2	16.9
(YBM)		190.4			30	0.676	6.2	5.0	19.4
		188.7			30	1.409	3.7	2.6	23.9
		190.4		53.9	30	2.975	2.2	1.2	26.5

Notes:
1. σ_{vc}' = Effective vertical consolidation stress during cyclic loading
2. w = Water content
3. N = Number of loading cycles
4. Avg. $\pm\gamma$ = Average shear strain, single amplitude
5. $G_{N=1}$ = Shear modulus at N=1
6. $G_{N=30}$ = Shear modulus at N=30
7. $D_{N=1}$ = Material damping ratio at N=1

SUMMARY OF CYCLIC SIMPLE SHEAR TEST RESULTS (METRIC)

1998 Marine Borings

SFOBB East Span Seismic Safety Project

Sample No.	Depth (ft)	σ_{vc}' (ksf)	Initial w (%)	Final w (%)	No. of Cycles, N	Avg. $\pm\gamma$ (%)	$G_{N=1}$ (ksf)	$G_{N=30}$ (ksf)	$D_{N=1}$ (%)
98-7-49-A	52.5	15.969	60.4		30	0.202	658.2	617.3	9.3
(OBM)		15.951			30	0.475	494.3	442.9	11.6
		15.955			30	1.094	331.0	284.8	16.3
		15.939		49.1	30	2.541	195.0	147.2	22.4
98-7-49-B	52.5	1.969	58.9		30	0.204	327.4	297.6	9.0
(OBM)		2.004			30	0.594	206.4	176.8	12.2
		1.975			30	1.268	132.5	113.0	14.6
		1.975		53.1	30	2.592	85.8	68.7	16.2
98-8-37-A	40.0	4.469	59.3		30	0.245	245.1	222.5	15.4
(YBM)		4.486			30	0.673	149.9	117.9	18.6
		4.472			30	1.431	87.8	64.8	21.6
		4.436		50.1	30	3.029	52.3	30.9	25.1
98-8-37-B	40.0	2.020	61.5		30	0.263	191.2	169.5	11.6
(YBM)		2.013			30	0.696	114.6	96.3	15.0
		2.008			30	1.369	73.8	57.6	16.4
		1.970		49.8	30	2.881	41.9	27.7	20.0
98-9-53	124.5	5.460	37.1		30	0.133	702.8	644.4	7.2
(OBM)		5.499			30	0.427	470.0	412.2	9.4
		5.495			30	0.962	313.7	277.6	12.2
		5.487		39.2	30	2.136	202.6	123.2	15.3
98-11-73	206.5	9.274	48.7		30	0.137	715.5	663.4	7.6
(OBM)		9.291			30	0.464	456.3	394.5	10.1
		9.311			30	1.059	296.3	251.3	13.1
		9.288		45.5	30	2.244	185.9	152.9	16.9
98-12-37	49.5	3.953	61.5		30	0.222	235.6	212.4	16.9
(YBM)		3.979			30	0.676	128.9	105.5	19.4
		3.944			30	1.409	77.5	53.9	23.9
		3.979		53.9	30	2.975	45.8	25.7	26.5

Notes:
1. σ_{vc}' = Effective vertical consolidation stress during cyclic loading
2. w = Water content
3. N = Number of loading cycles
4. Avg. $\pm\gamma$ = Average shear strain, single amplitude
5. $G_{N=1}$ = Shear modulus at N=1
6. $G_{N=30}$ = Shear modulus at N=30
7. $D_{N=1}$ = Material damping ratio at N=1

SUMMARY OF CYCLIC SIMPLE SHEAR TEST RESULTS (ENGLISH)

1998 Marine Borings
SFOBB East Span Seismic Safety Project

APPENDIX A
RESULTS OF RESONANT COLUMN TESTS

June 1998
Project No. 98-42-0035
SFOBB Task Order No. 3

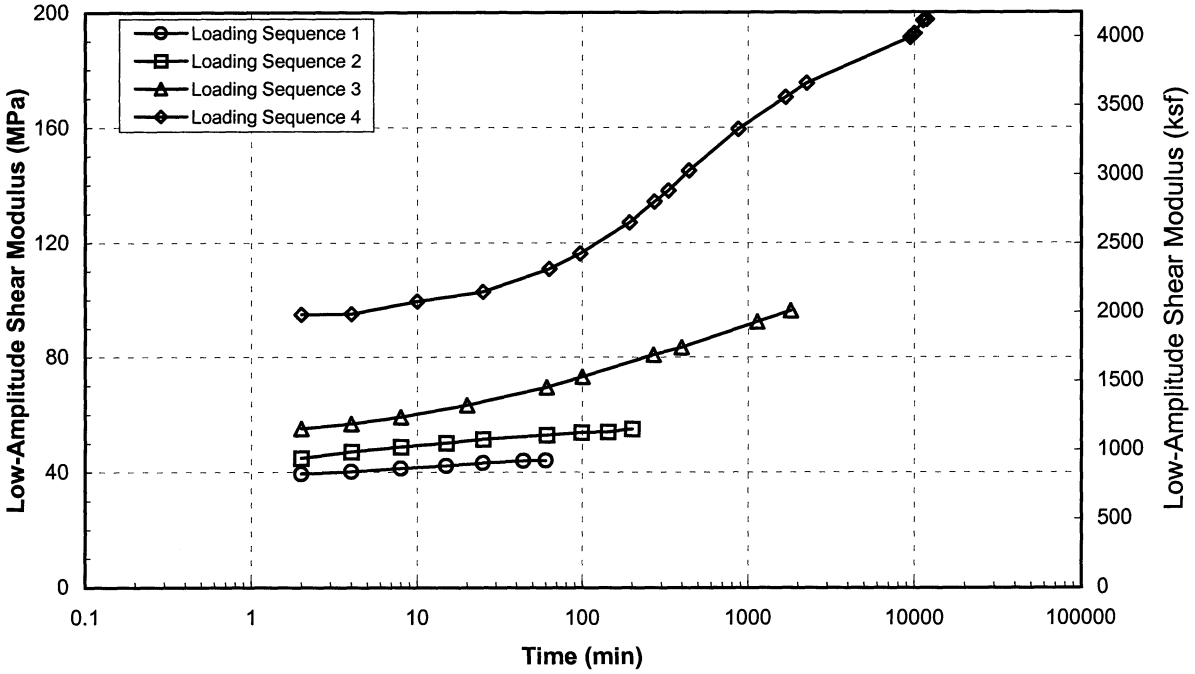

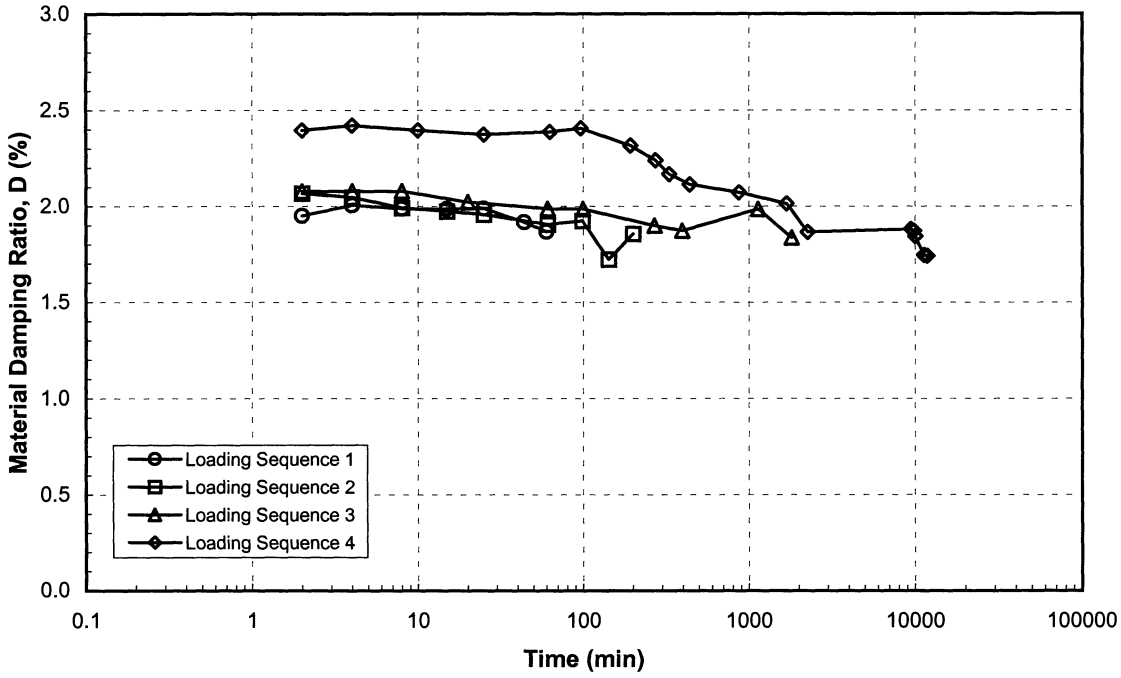

RESONANT COLUMN TEST RESULTS
Sample No. 49 - Penetration: 16.0 m
Boring 98-7
SFOBB East Span Seismic Safety Project

F:\wp_in\caltrans\gregg\9807_49m.xls\Gm,D vs Time

PLATE A.1a

June 1998
Project No. 98-42-0035
SFOBB Task Order No. 3

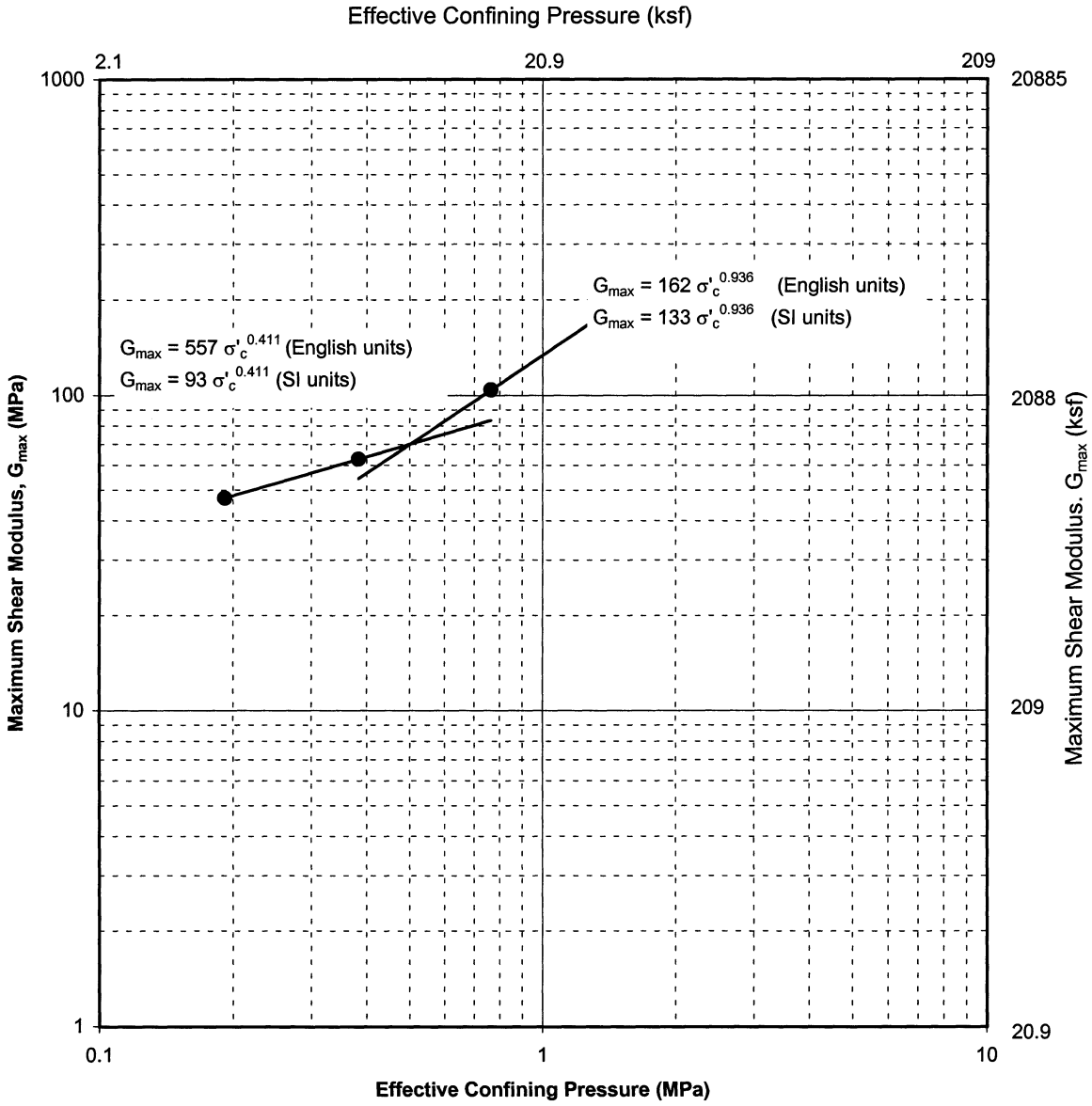

RESONANT COLUMN TEST RESULTS
Sample No. 49 - Penetration: 16.0 m
Boring 98-7
SFOBB East Span Seismic Safety Project

F:\wp_in\caltrans\gregg\9807_49m.xls\Gmax vs Confine

PLATE A.1b

June 1998
Project No. 98-42-0035
SFOBB Task Order No. 3

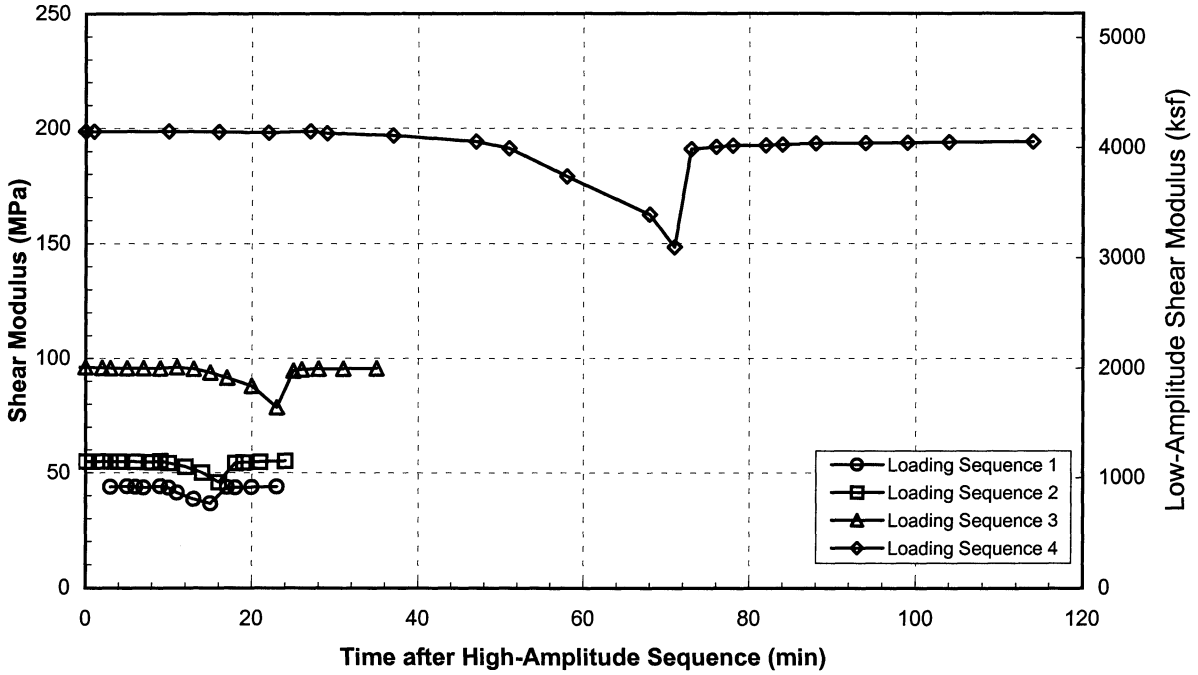

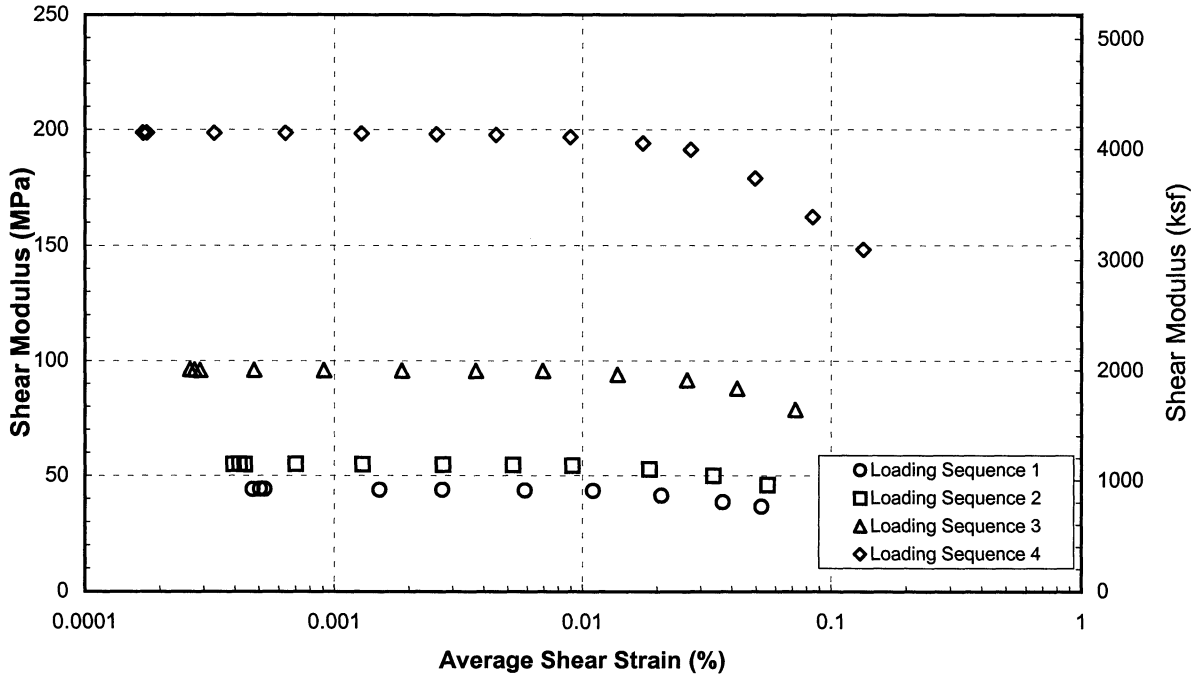

RESONANT COLUMN TEST RESULTS
Sample No. 49 - Penetration: 16.0 m
Boring 98-7
SFOBB East Span Seismic Safety Project

F:\wp_in\caltrans\gregg\9807_49m.xls\G vs T,S

PLATE A.1c

June 1998
Project No. 98-42-0035
SFOBB Task Order No. 3

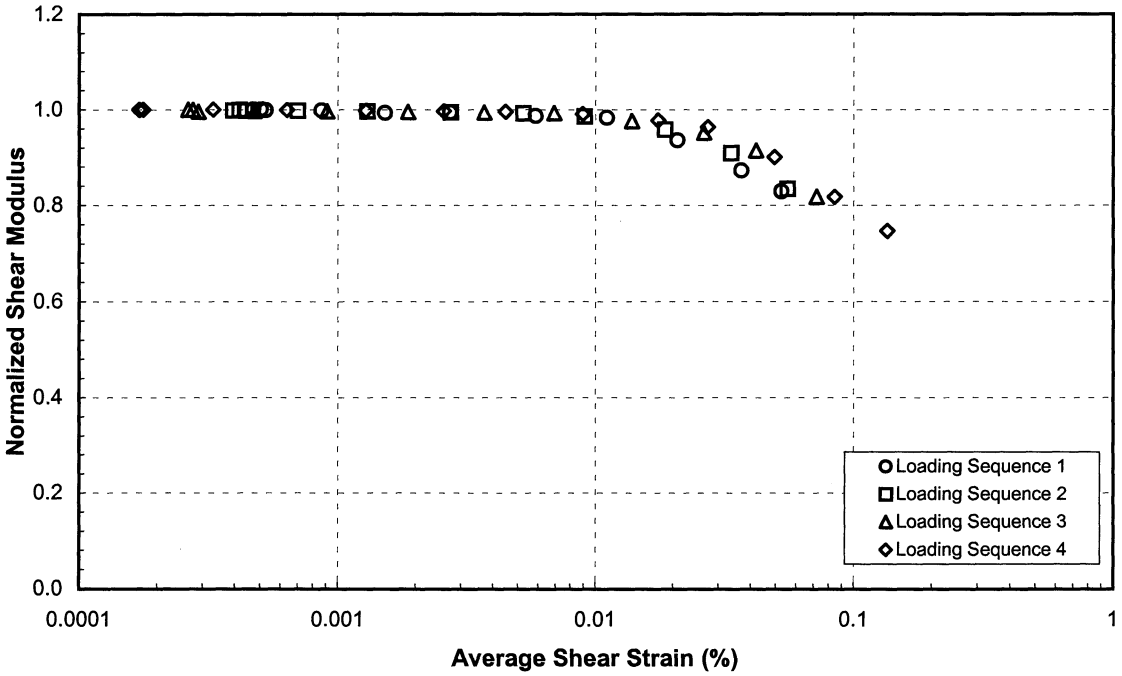

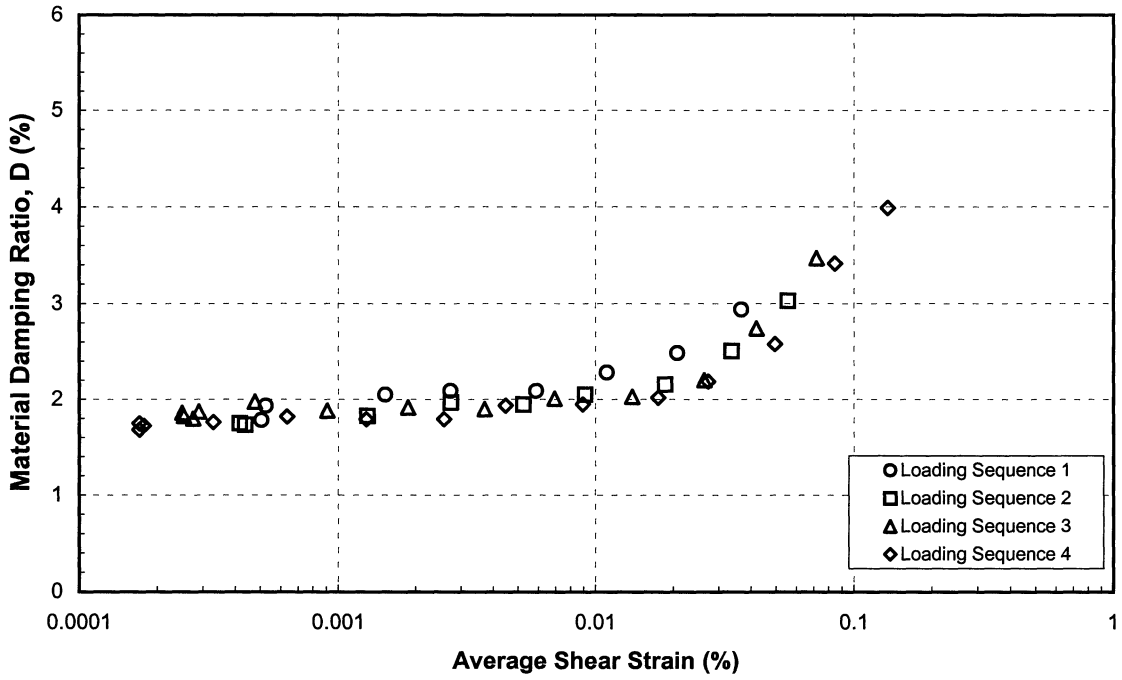

RESONANT COLUMN TEST RESULTS
Sample No. 49 - Penetration: 16.0 m
Boring 98-7
SFOBB East Span Seismic Safety Project

F:\wp_in\caltrans\gregg\9807_49m.xls\G,D vs S

PLATE A.1d

June 1998
Project No. 98-42-0035
SFOBB Task Order No. 3

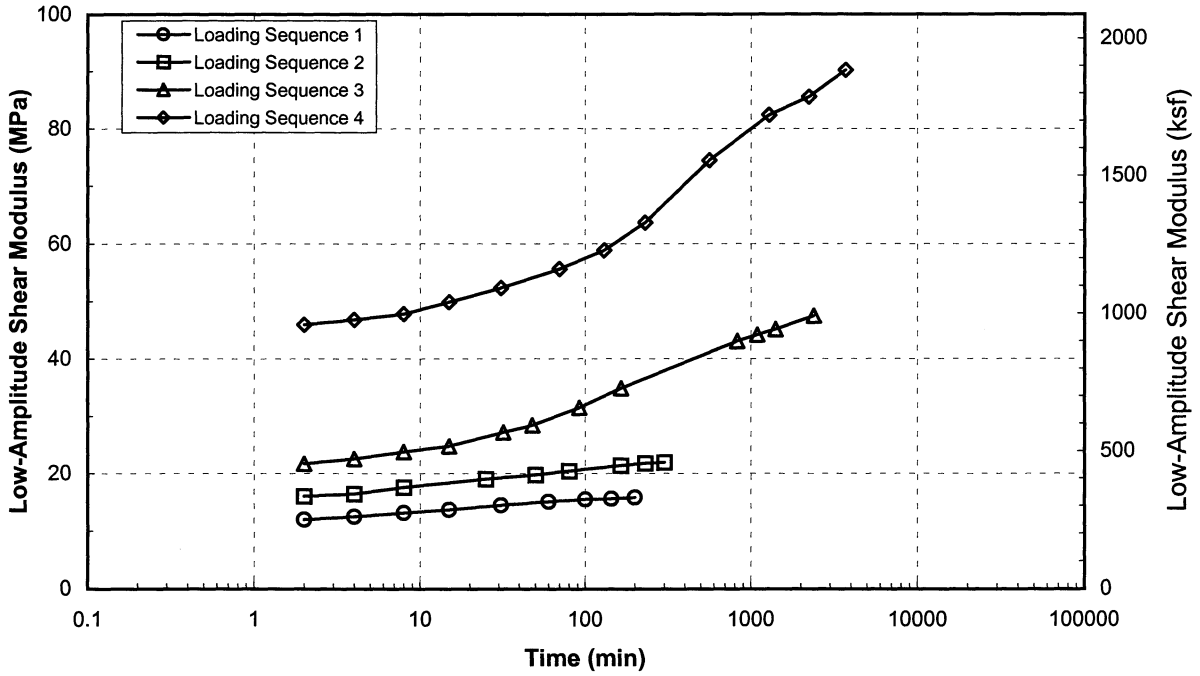

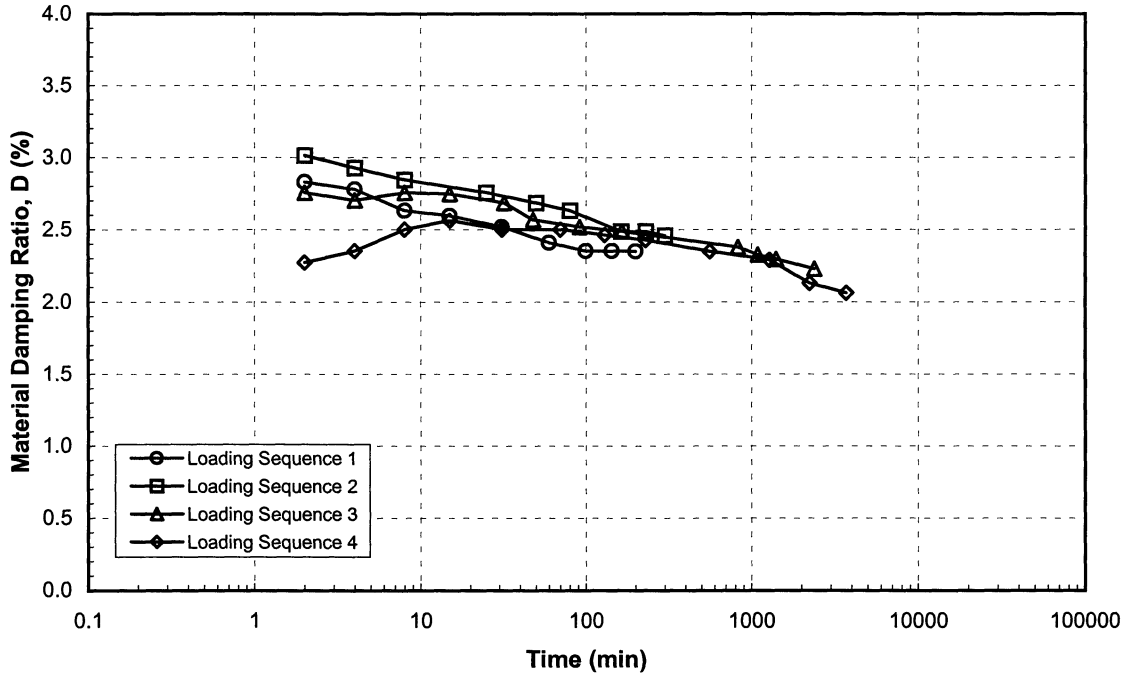

RESONANT COLUMN TEST RESULTS
Sample No. 37 - Penetration: 12.2 m
Boring 98-8
SFOBB East Span Seismic Safety Project

F:\wp_in\caltrans\gregg\9808_37.xls\Gm,D vs Time

PLATE A.2a

June 1998
Project No. 98-42-0035
SFOBB Task Order No. 3

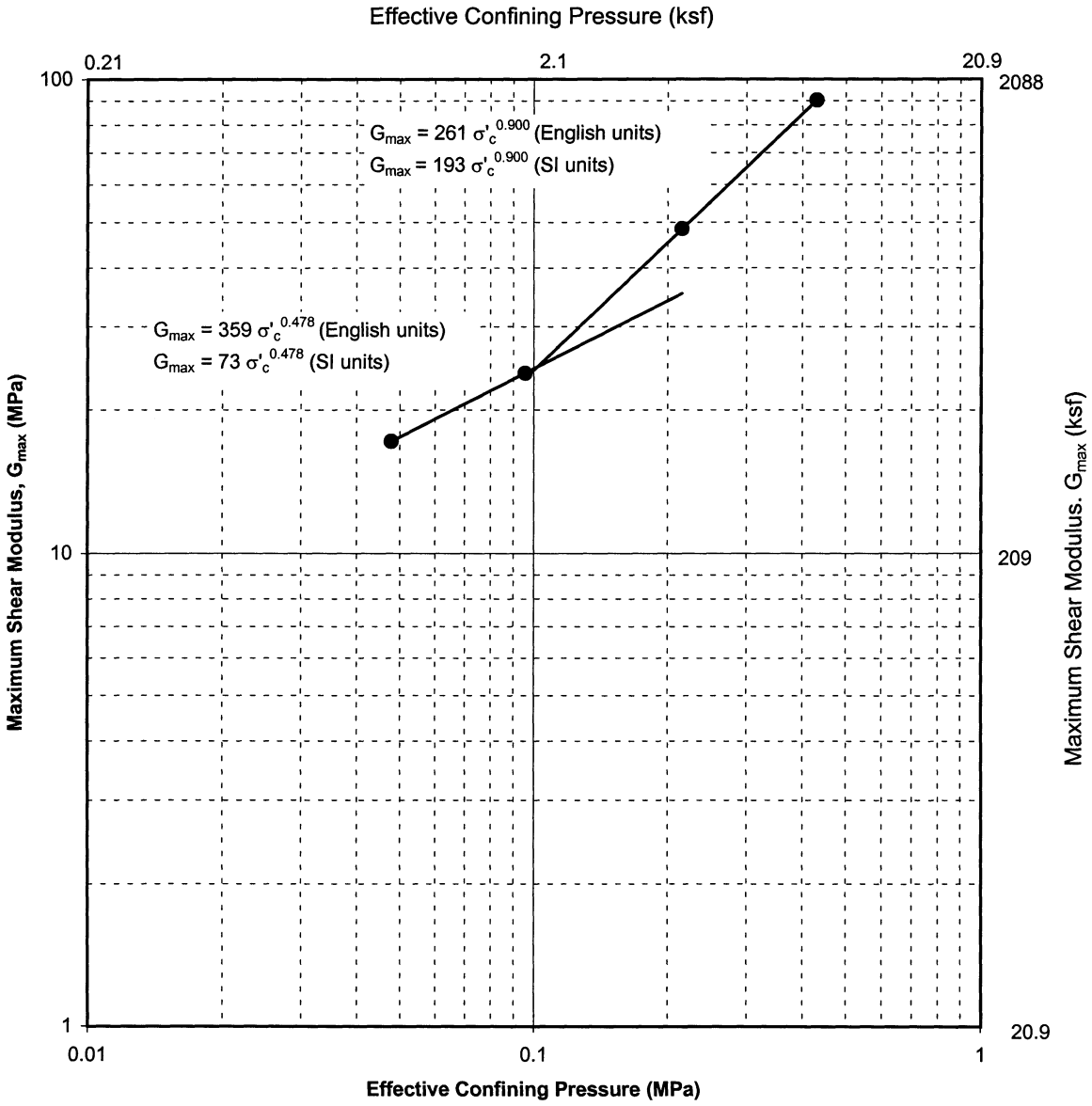

RESONANT COLUMN TEST RESULTS
Sample No. 37 - Penetration: 12.2 m
Boring 98-8
SFOBB East Span Seismic Safety Project

F:\wp_in\caltrans\gregg\9808_37.xls\Gmax vs Confine

PLATE A.2b

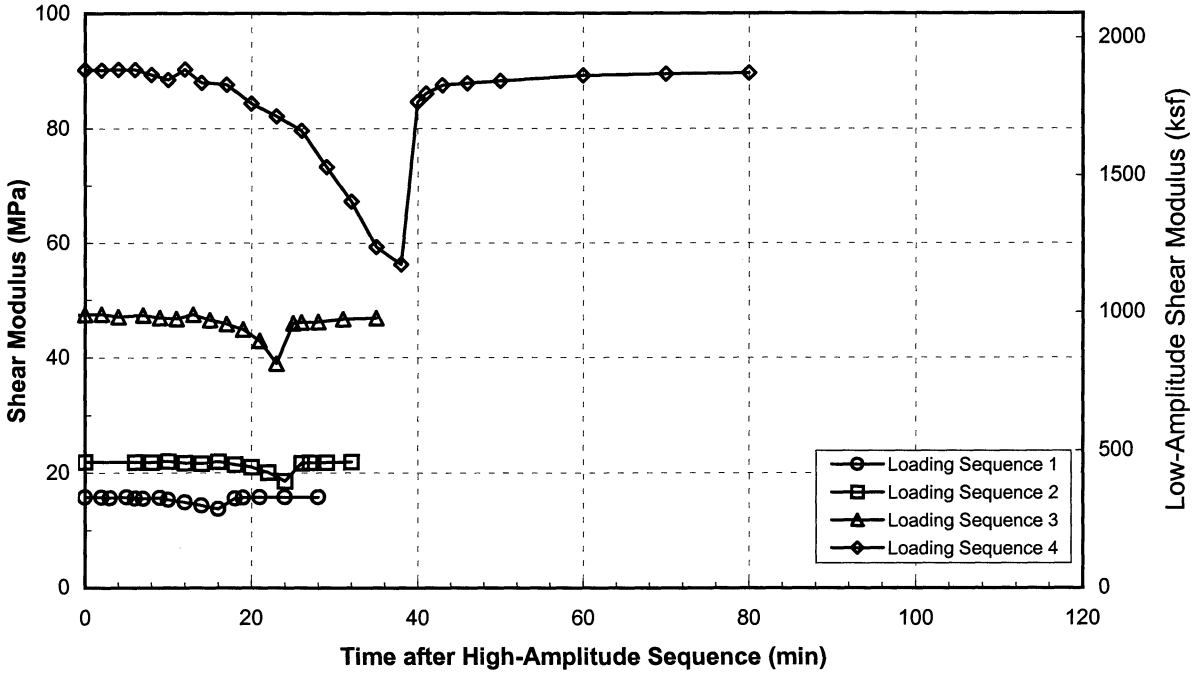

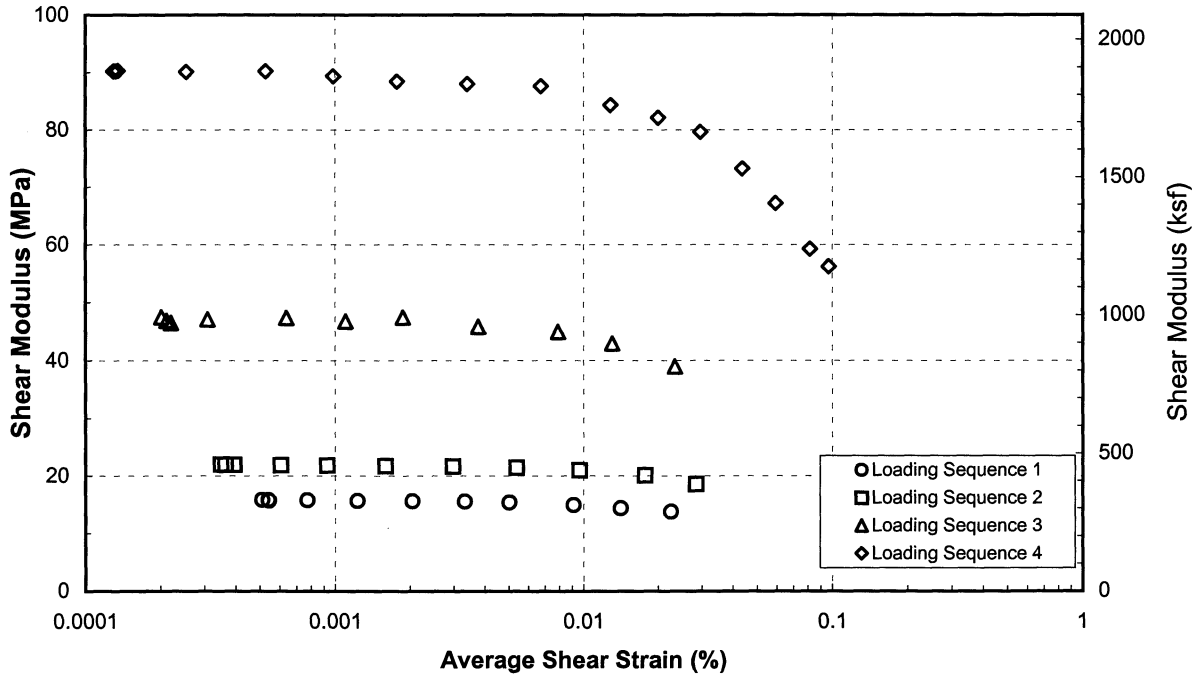

RESONANT COLUMN TEST RESULTS
Sample No. 37 - Penetration: 12.2 m
Boring 98-8
SFOBB East Span Seismic Safety Project

F:\wp_in\caltrans\gregg\9808_37.xls\G vs T,S

PLATE A.2c

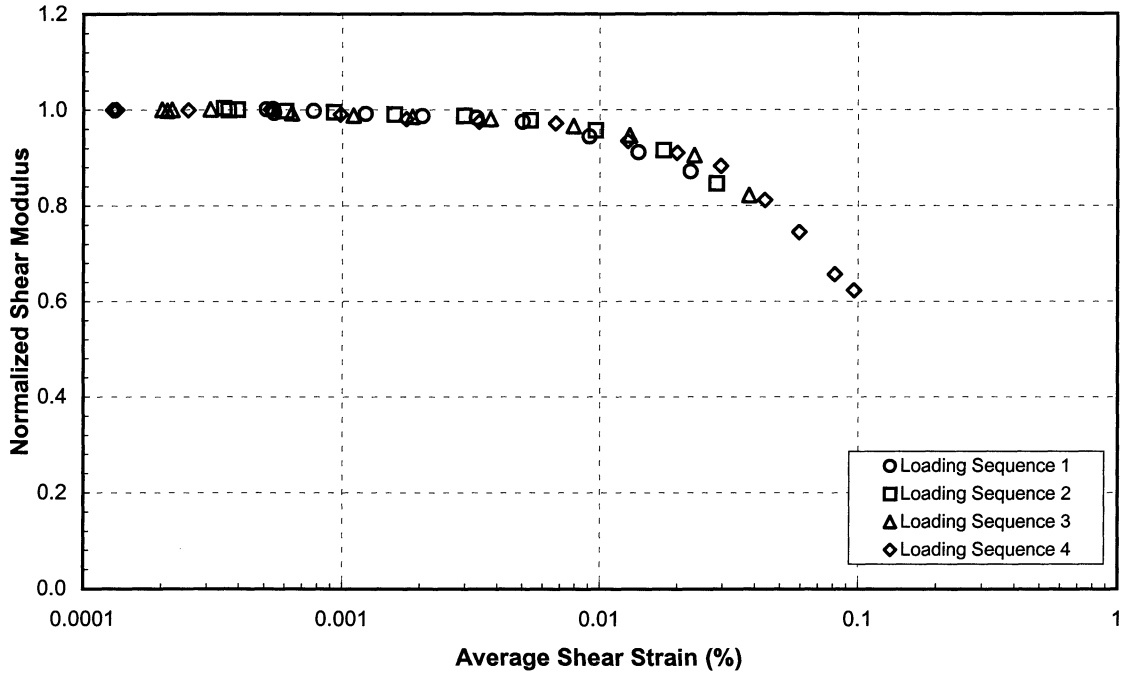

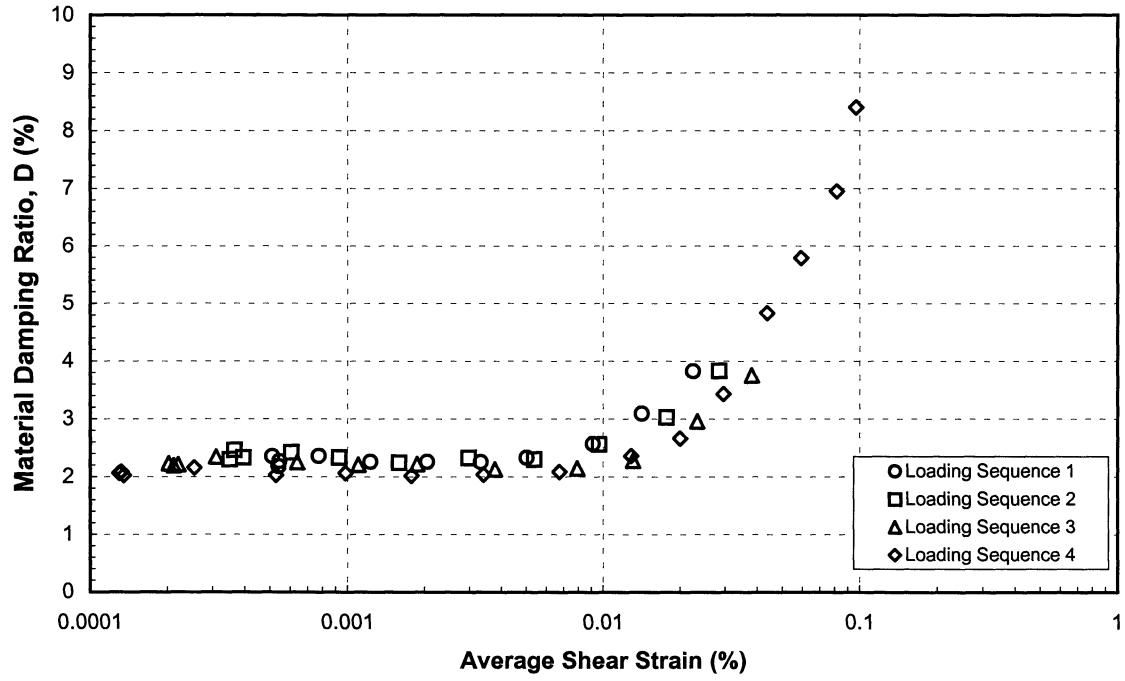

RESONANT COLUMN TEST RESULTS
Sample No. 37 - Penetration: 12.2 m
Boring 98-8
SFOBB East Span Seismic Safety Project

F:\wp_in\caltrans\gregg\9808_37.xls\G,D vs S

PLATE A.2d

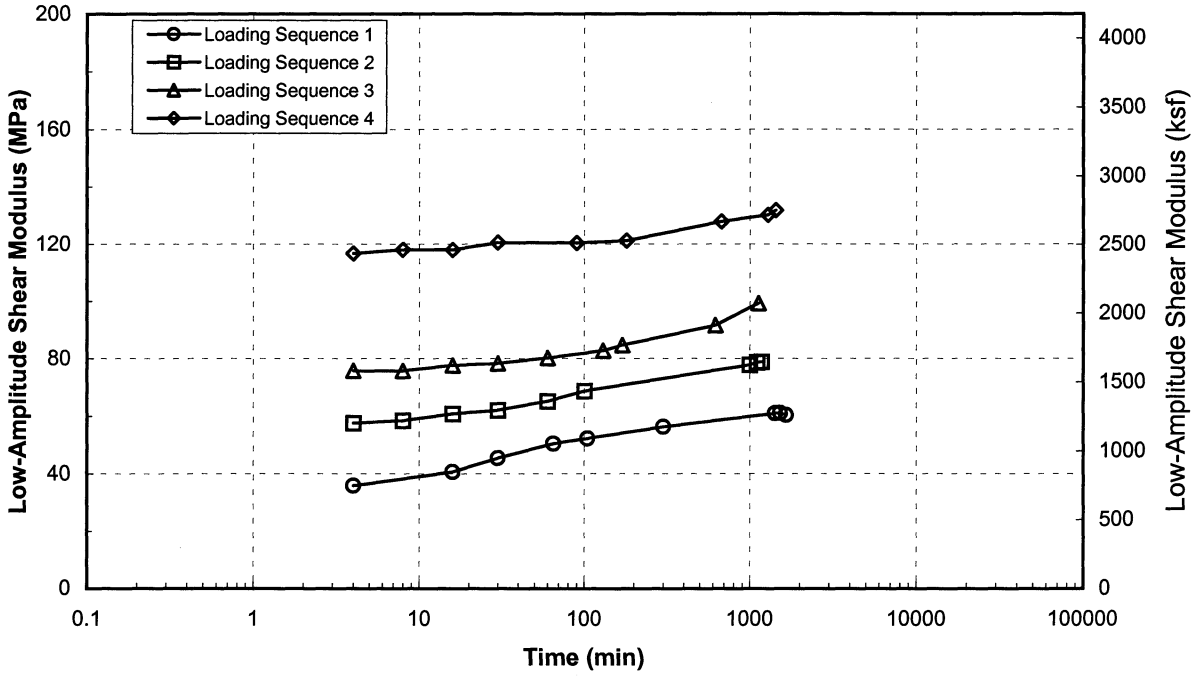

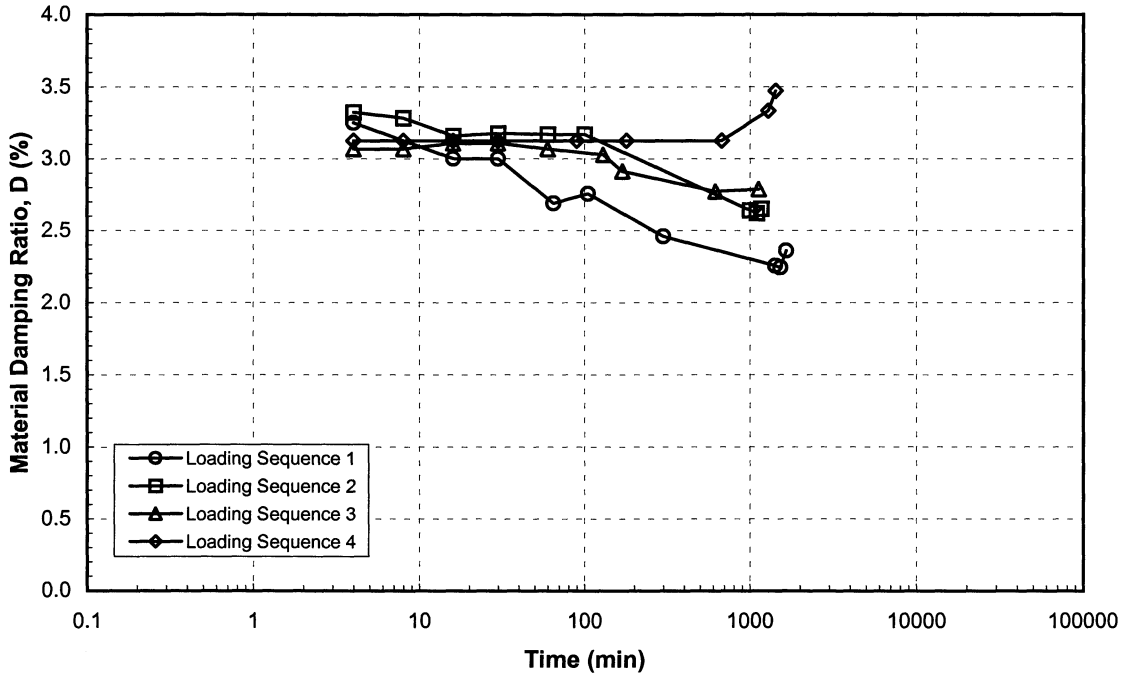

RESONANT COLUMN TEST RESULTS
Sample No. 53 - Penetration: 37.9 m
Boring 98-9
SFOBB East Span Seismic Safety Project

F:\wp_in\caltrans\gregg\9809_53.xls\Gm,D vs Time

PLATE A.3a

June 1998
Project No. 98-42-0035
SFOBB Task Order No. 3

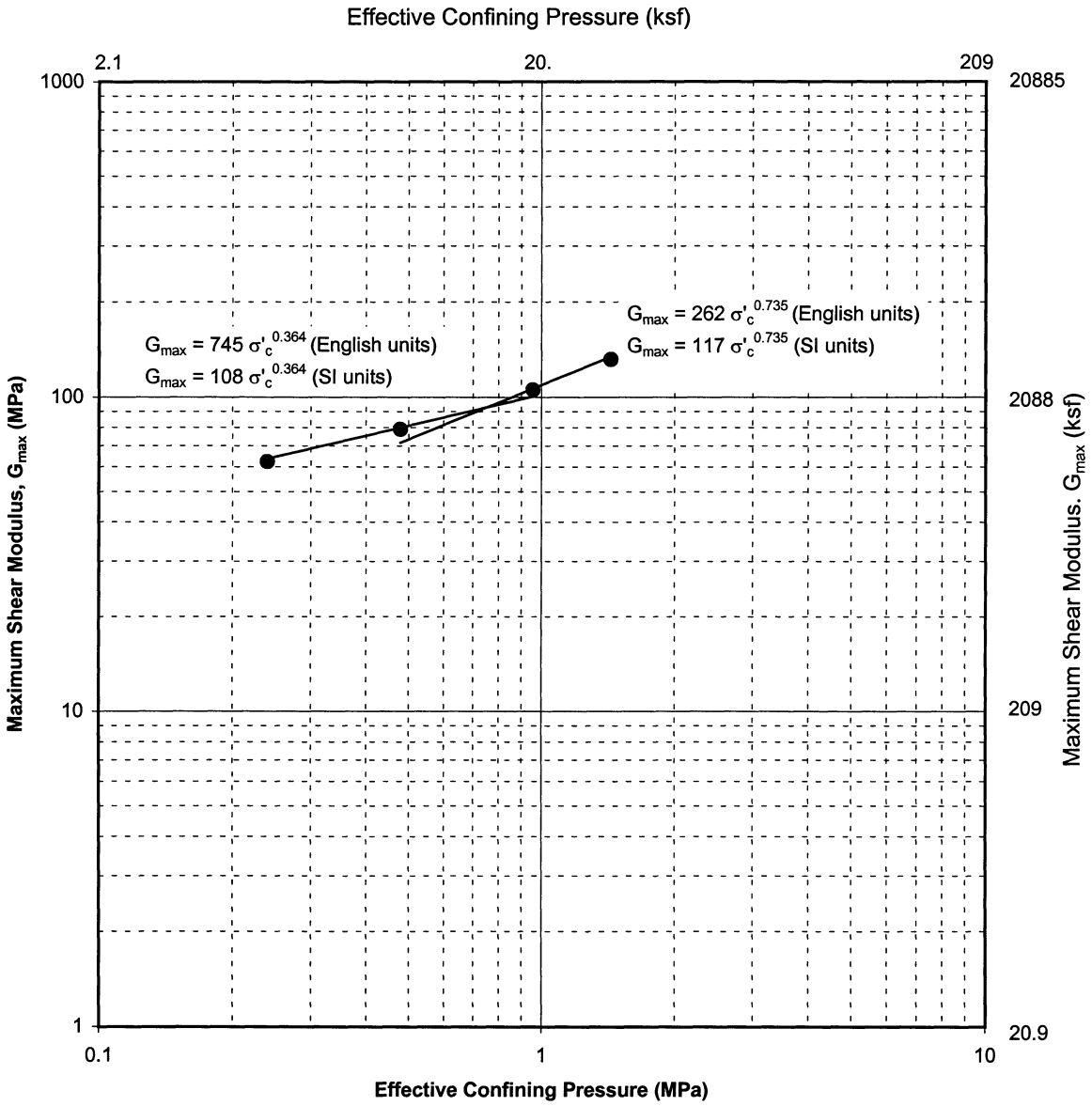

RESONANT COLUMN TEST RESULTS
Sample No. 53 - Penetration: 37.9 m
Boring 98-9
SFOBB East Span Seismic Safety Project

F:\wp_in\caltrans\gregg\9809_53.xls\Gmax vs Confine

PLATE A.3b

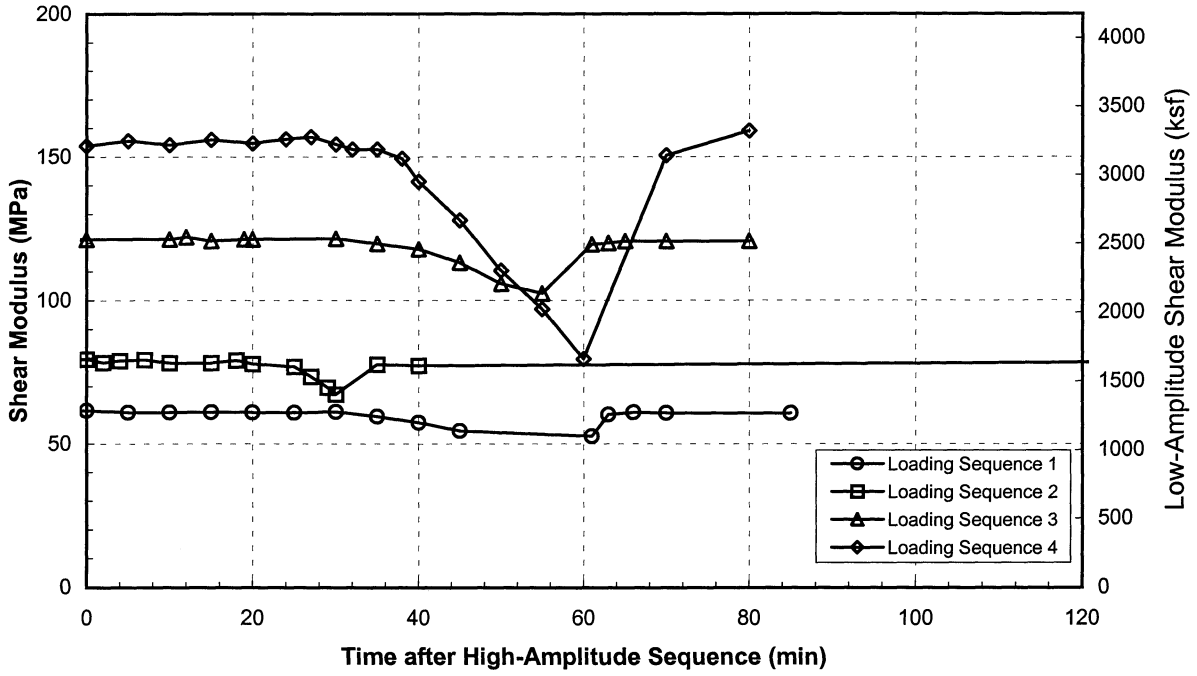

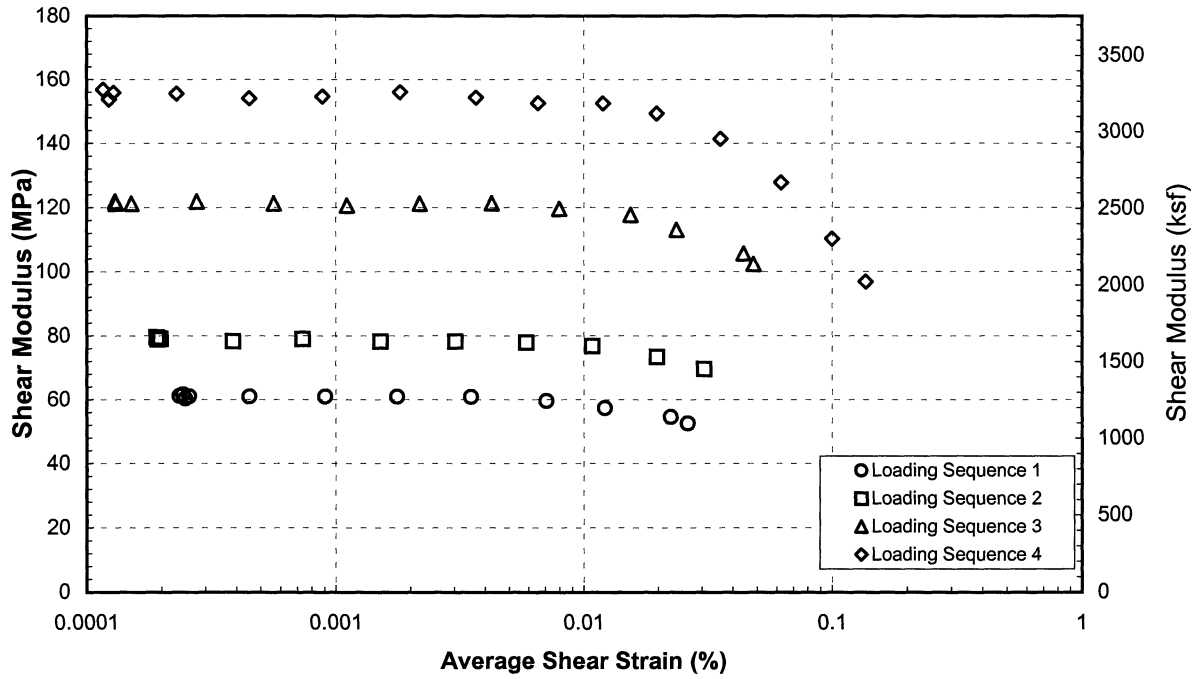

RESONANT COLUMN TEST RESULTS
Sample No. 53 - Penetration: 37.9 m
Boring 98-9
SFOBB East Span Seismic Safety Project

F:\wp_in\caltrans\gregg\9809_53.xls\G vs T,S

PLATE A.3c

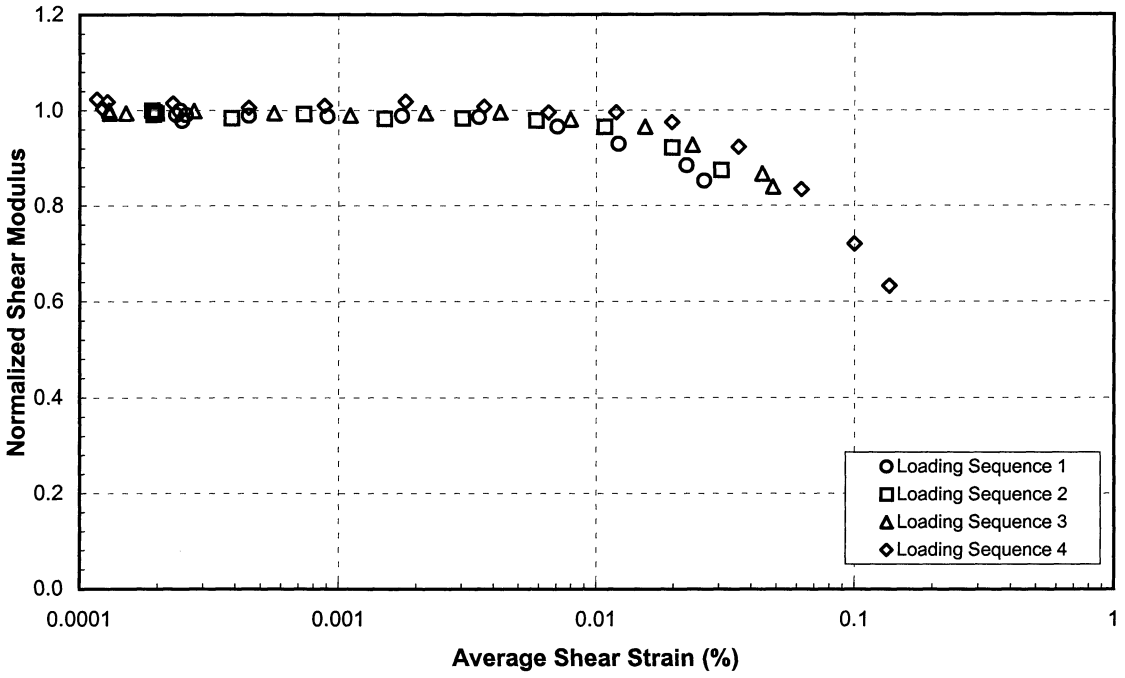

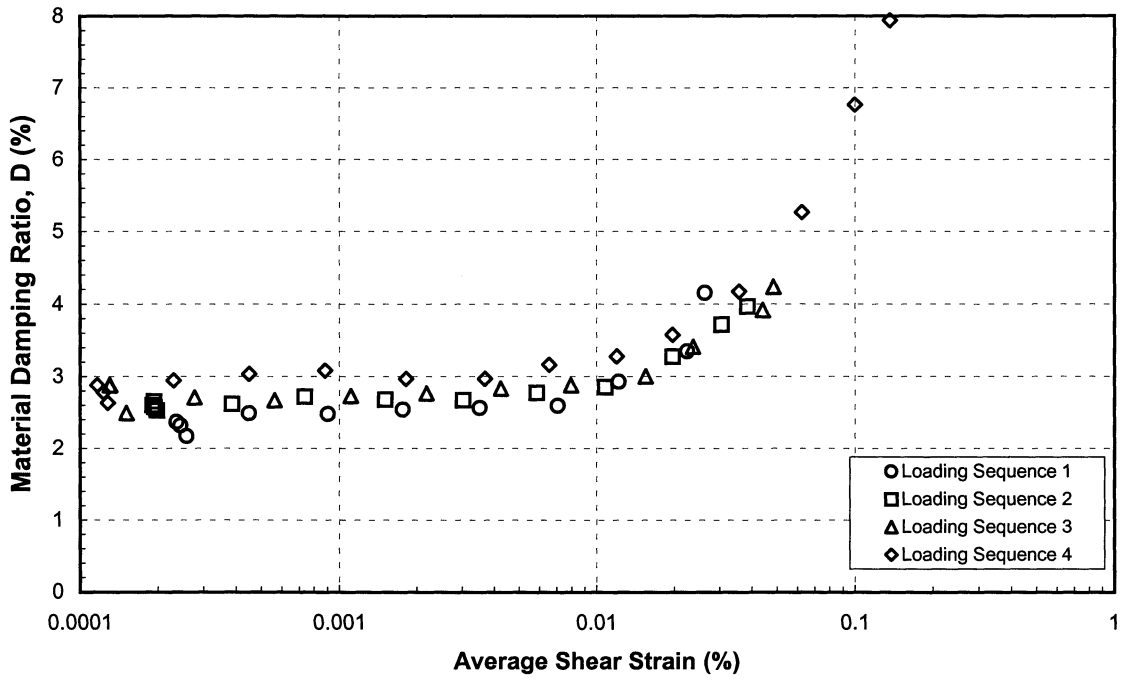

RESONANT COLUMN TEST RESULTS
Sample No. 53 - Penetration: 37.9 m
Boring 98-9
SFOBB East Span Seismic Safety Project

F:\wp_in\caltrans\gregg\9809_53.xls\G,D vs S

PLATE A.3d

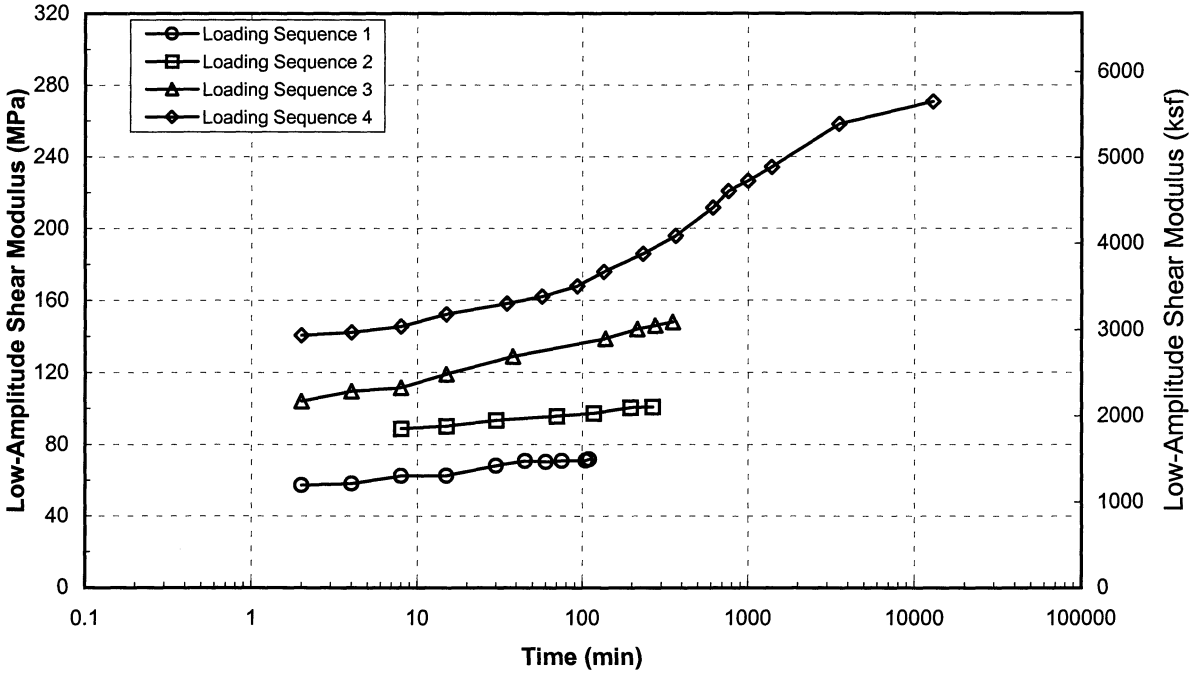

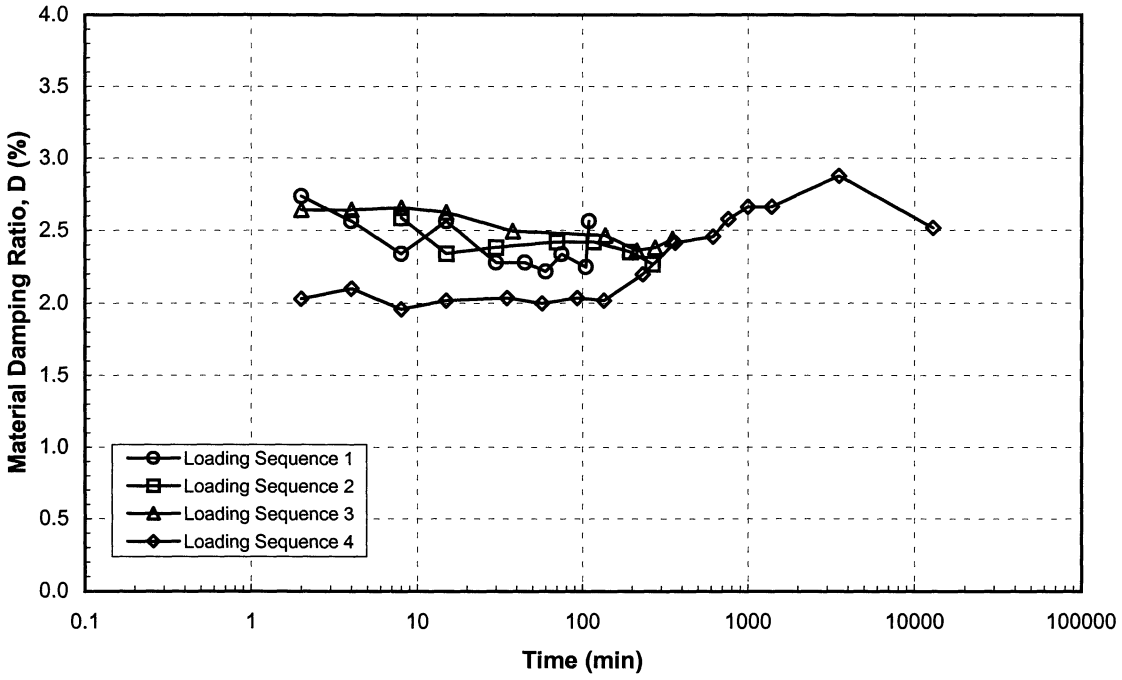

RESONANT COLUMN TEST RESULTS
Sample No. 75 - Penetration: 65.4 m
Boring 98-9
SFOBB East Span Seismic Safety Project

F:\wp_in\caltrans\gregg\9809_75m.xls\Gm,D vs Time

PLATE A.4a

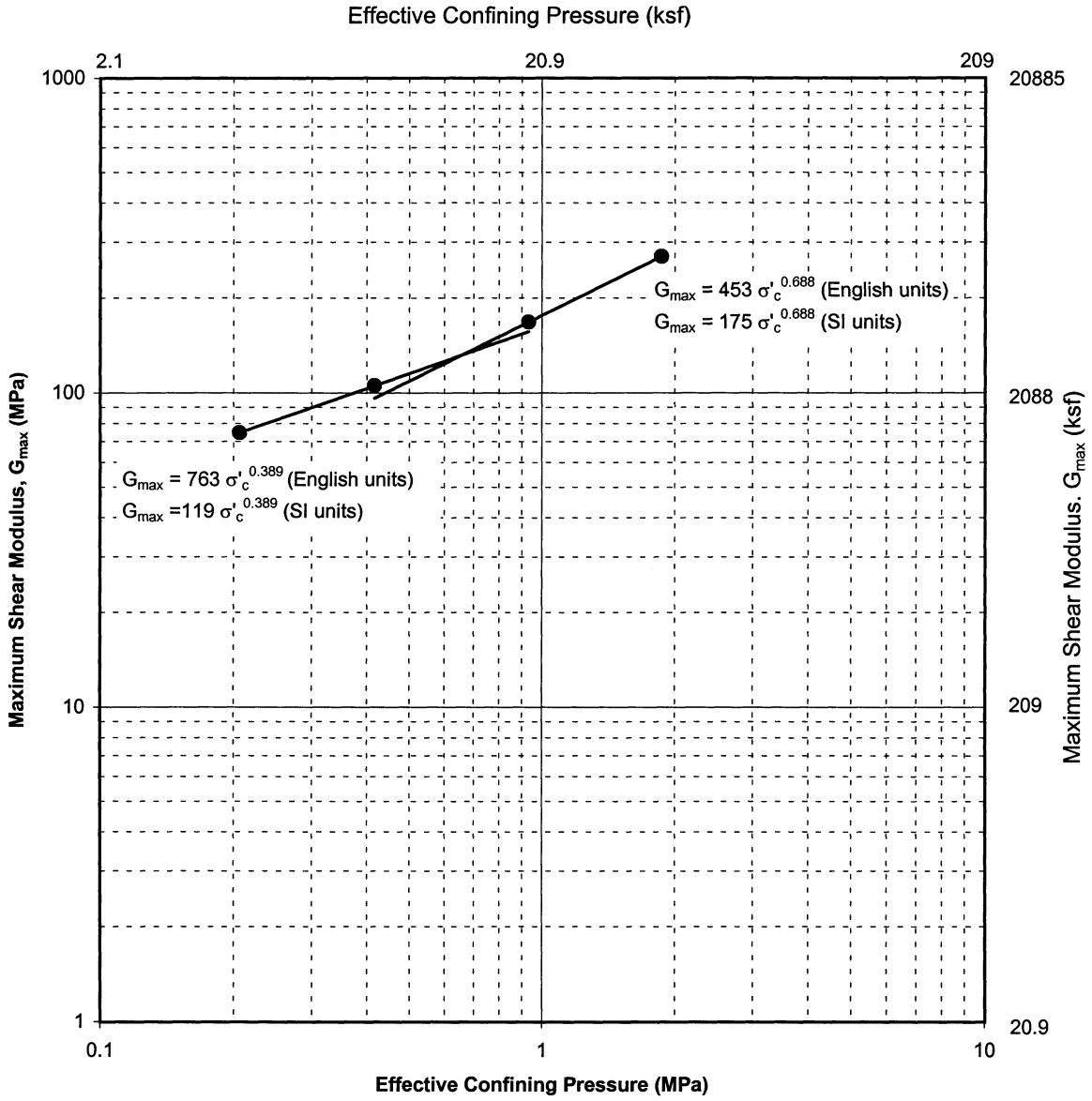

RESONANT COLUMN TEST RESULTS
Sample No. 75 - Penetration: 65.4 m
Boring 98-9
SFOBB East Span Seismic Safety Project

F:\wp_in\caltrans\gregg\9809_75m.xls\Gmax vs Confine

PLATE A.4b

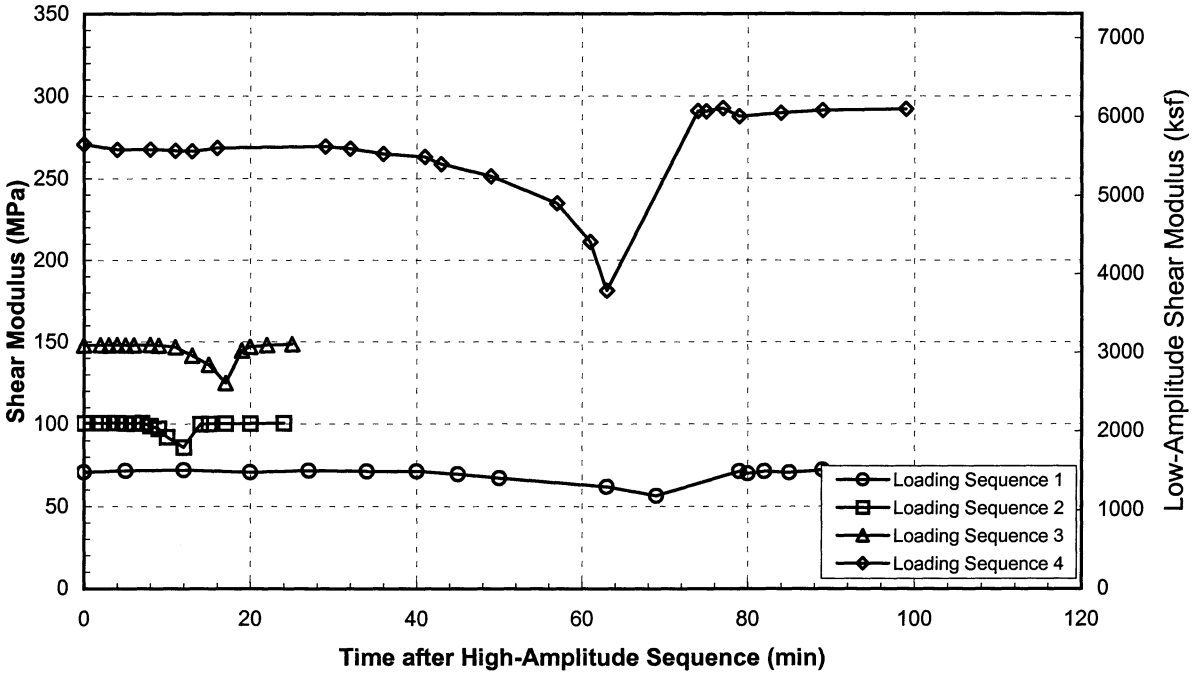

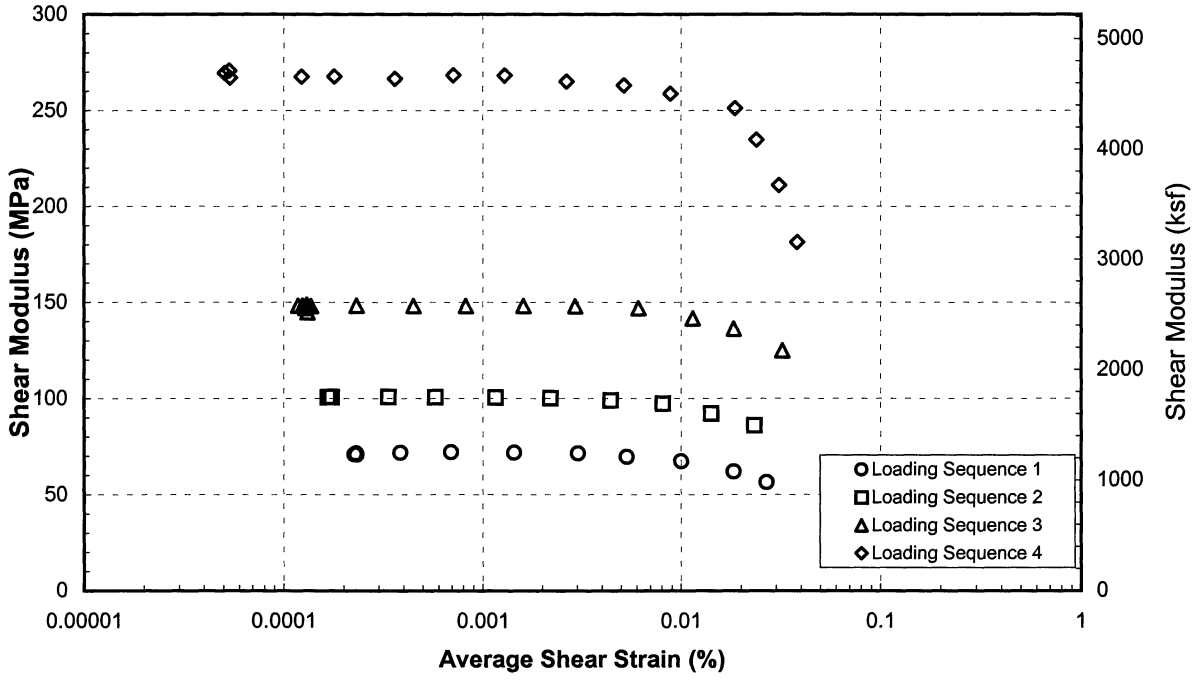

RESONANT COLUMN TEST RESULTS
Sample No. 75 - Penetration: 65.4 m
Boring 98-9
SFOBB East Span Seismic Safety Project

F:\wp_in\caltrans\gregg\9809_75m.xls\G vs T,S

PLATE A.4c

June 1998
Project No. 98-42-0035
SFOBB Task Order No. 3

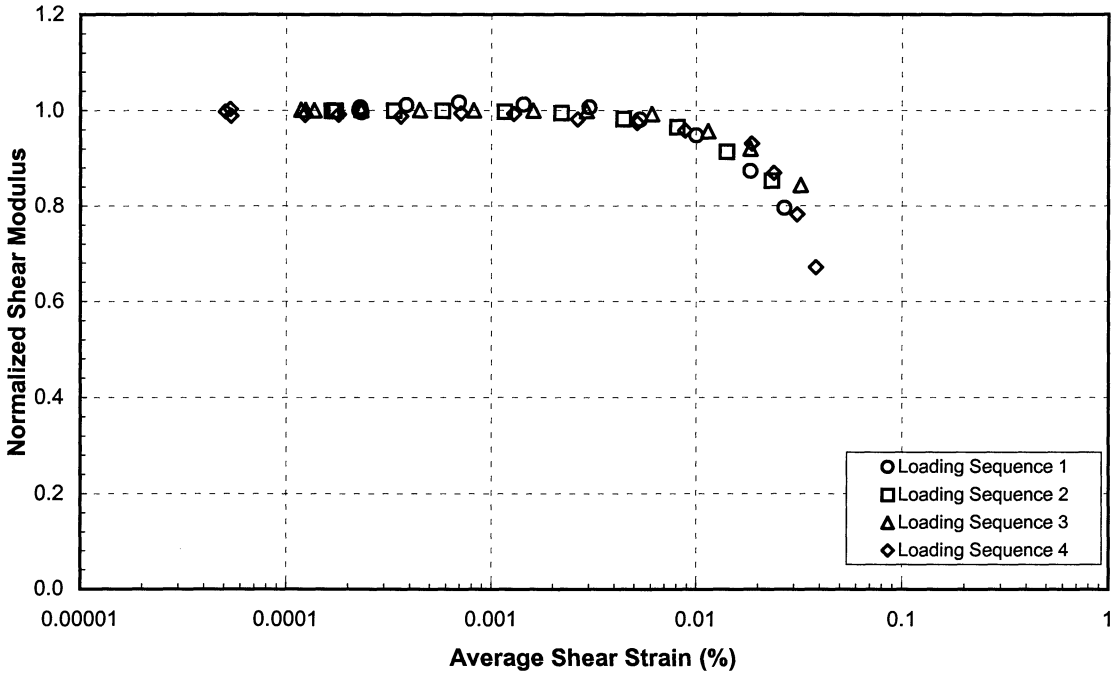

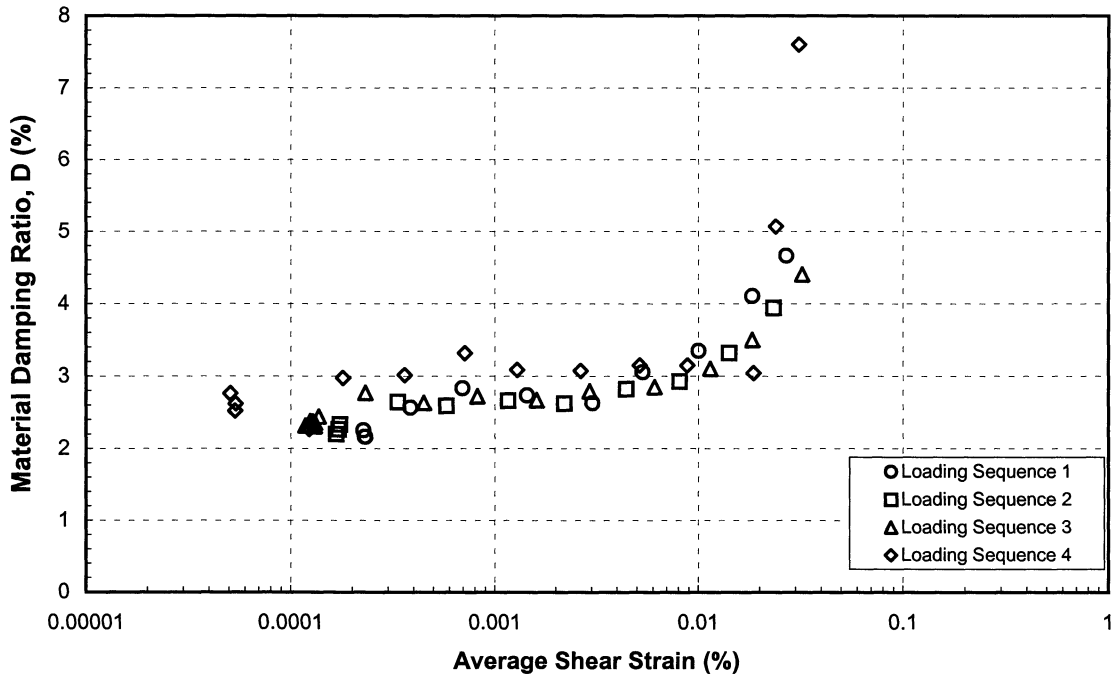

RESONANT COLUMN TEST RESULTS
Sample No. 75 - Penetration: 65.4 m
Boring 98-9
SFOBB East Span Seismic Safety Project

F:\wp_in\caltrans\gregg\9809_75m.xls\G,D vs S

PLATE A.4d

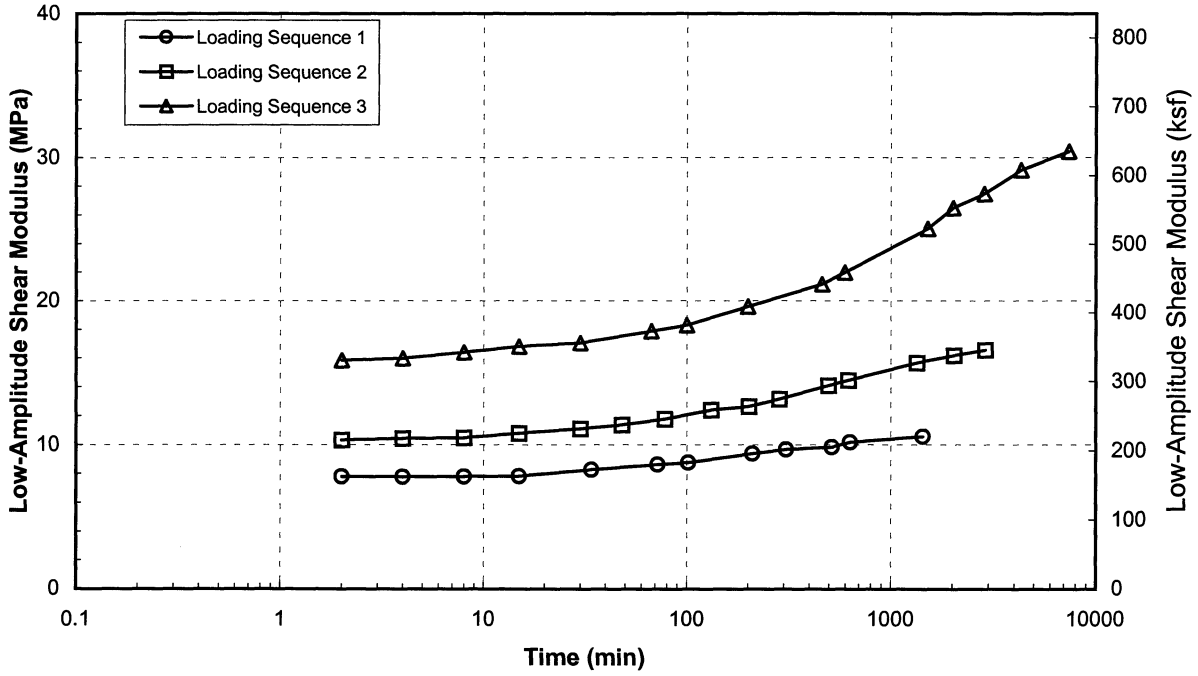

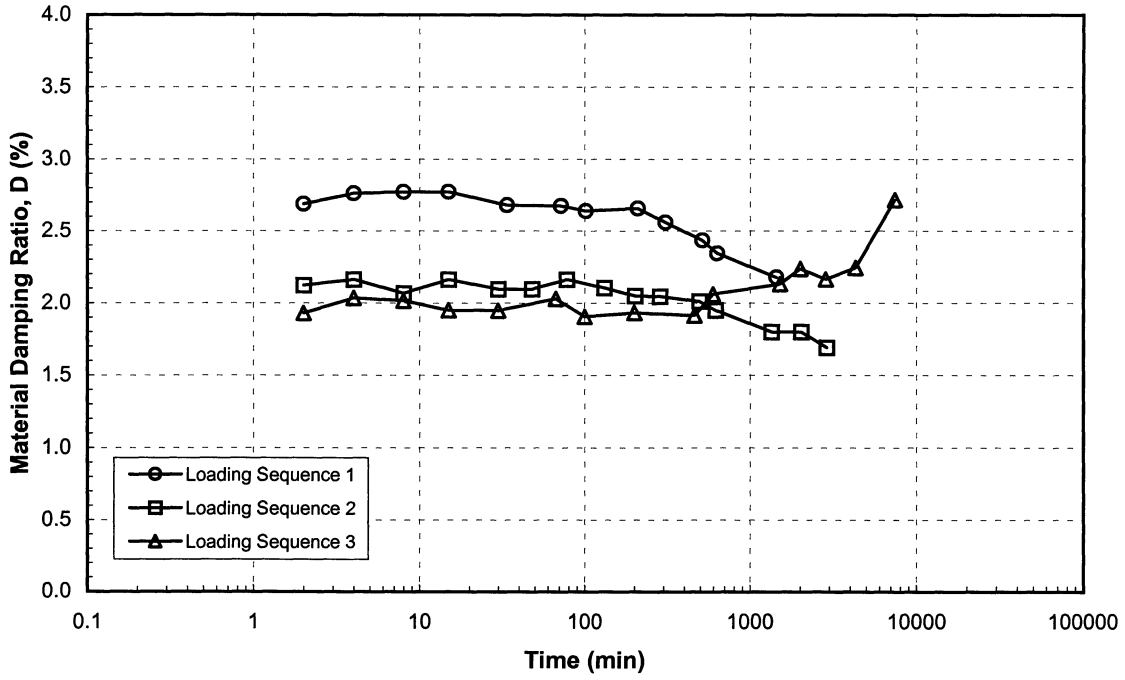

RESONANT COLUMN TEST RESULTS
Sample No. 37 - Penetration: 15.1 m
Boring 98-12
SFOBB East Span Seismic Safety Project

F:\wp_in\caltrans\gregg\9812_37.xls\Gm,D vs Time

PLATE A.5a

June 1998
Project No. 98-42-0035
SFOBB Task Order No. 3

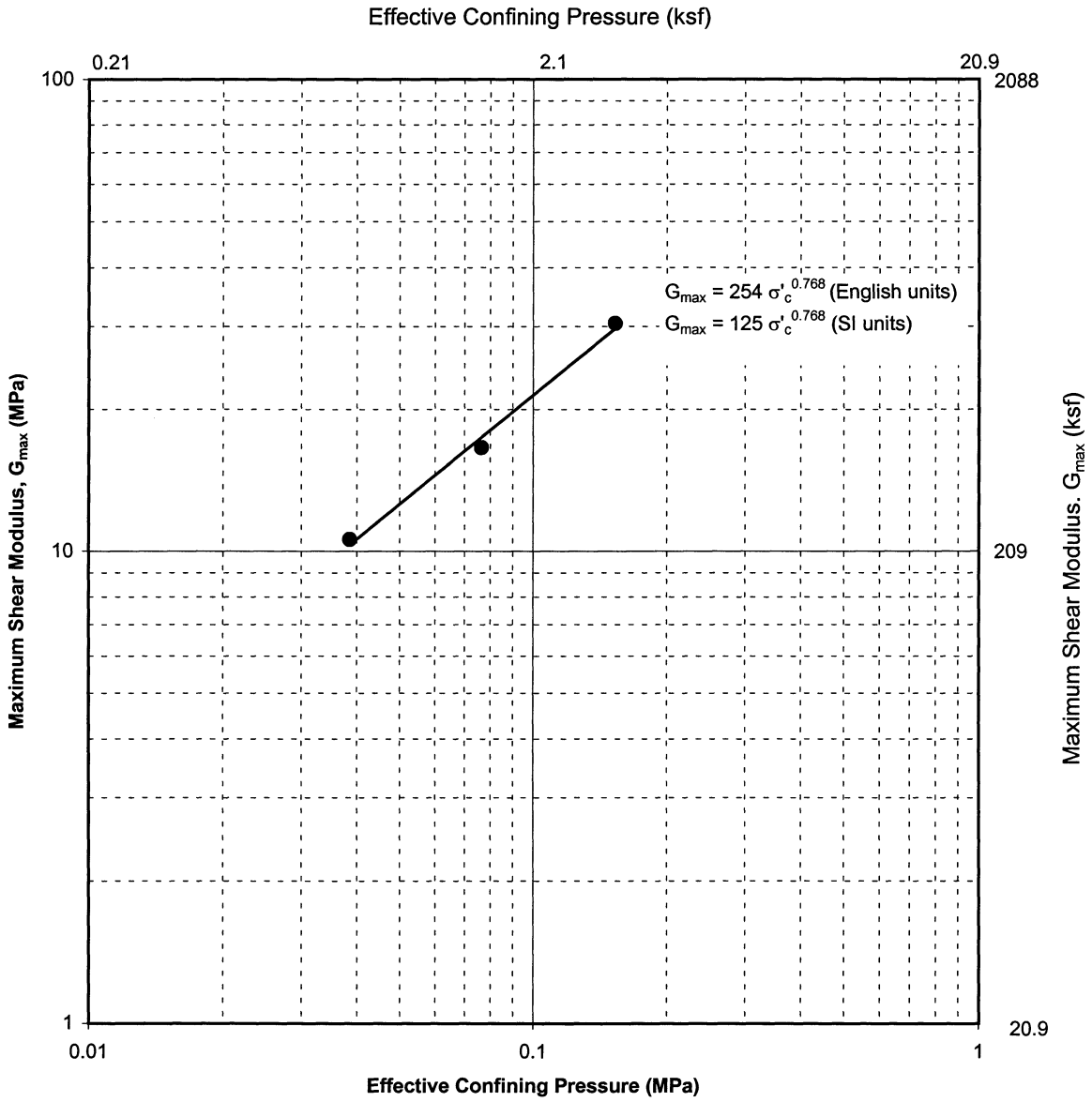

RESONANT COLUMN TEST RESULTS
Sample No. 37 - Penetration: 15.1 m
Boring 98-12
SFOBB East Span Seismic Safety Project

F:\wp_in\caltrans\gregg\9812_37.xls\Gmax vs Confine

PLATE A.5b

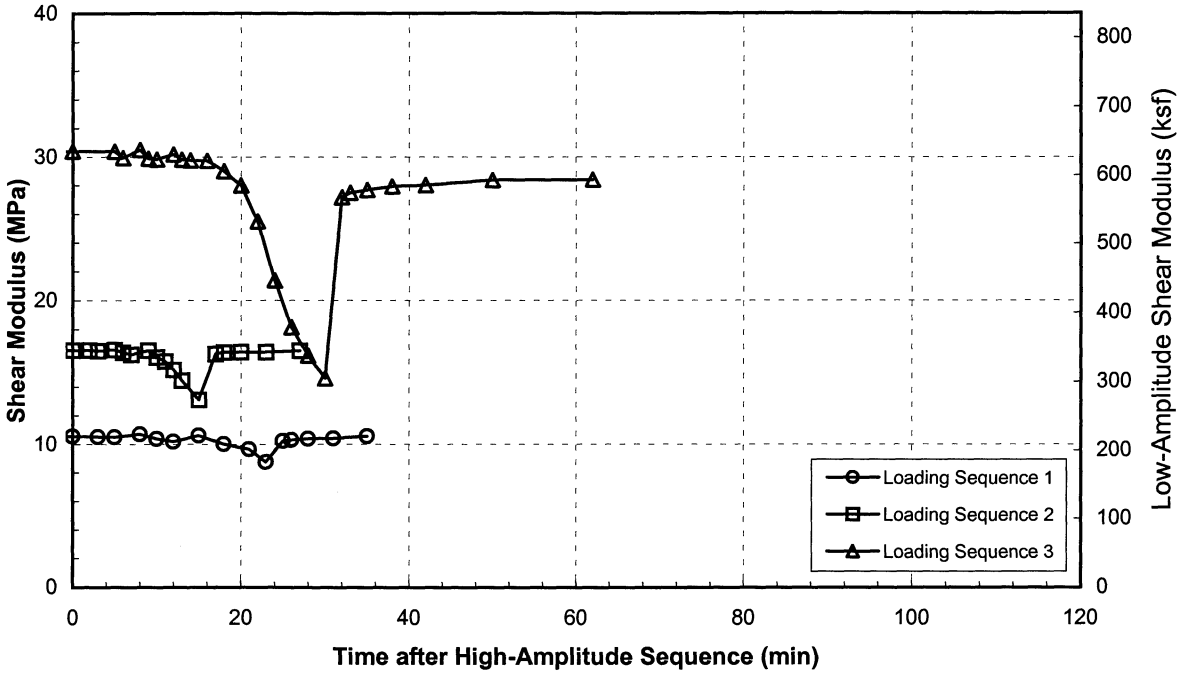

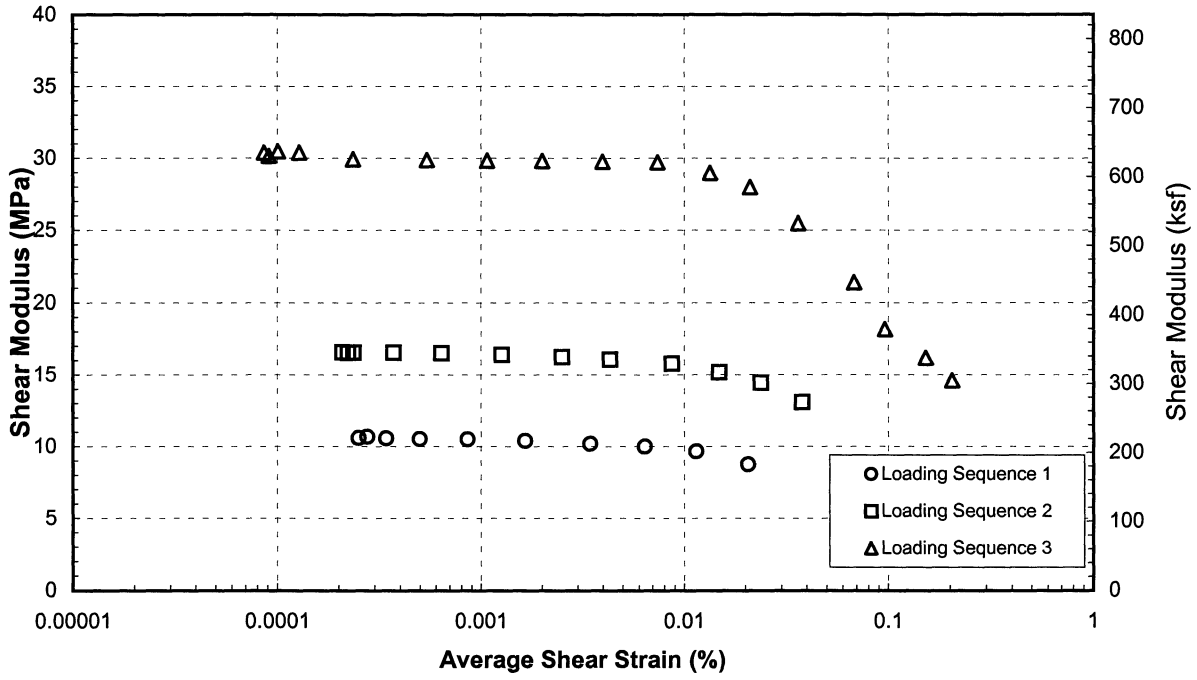

RESONANT COLUMN TEST RESULTS
Sample No. 37 - Penetration: 15.1 m
Boring 98-12
SFOBB East Span Seismic Safety Project

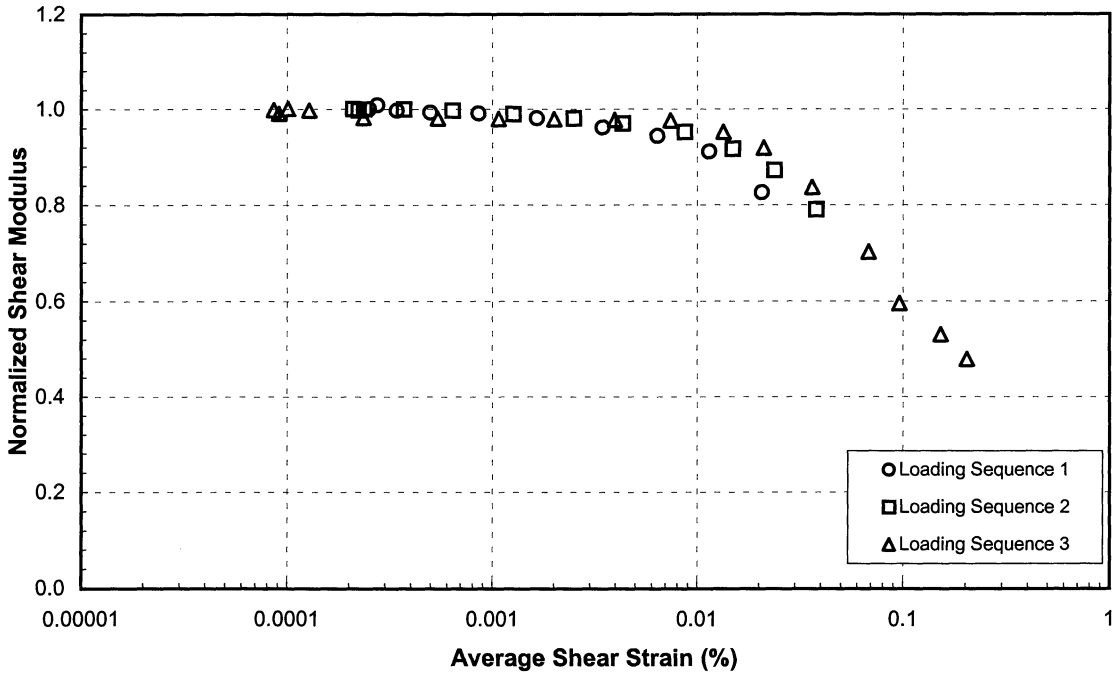

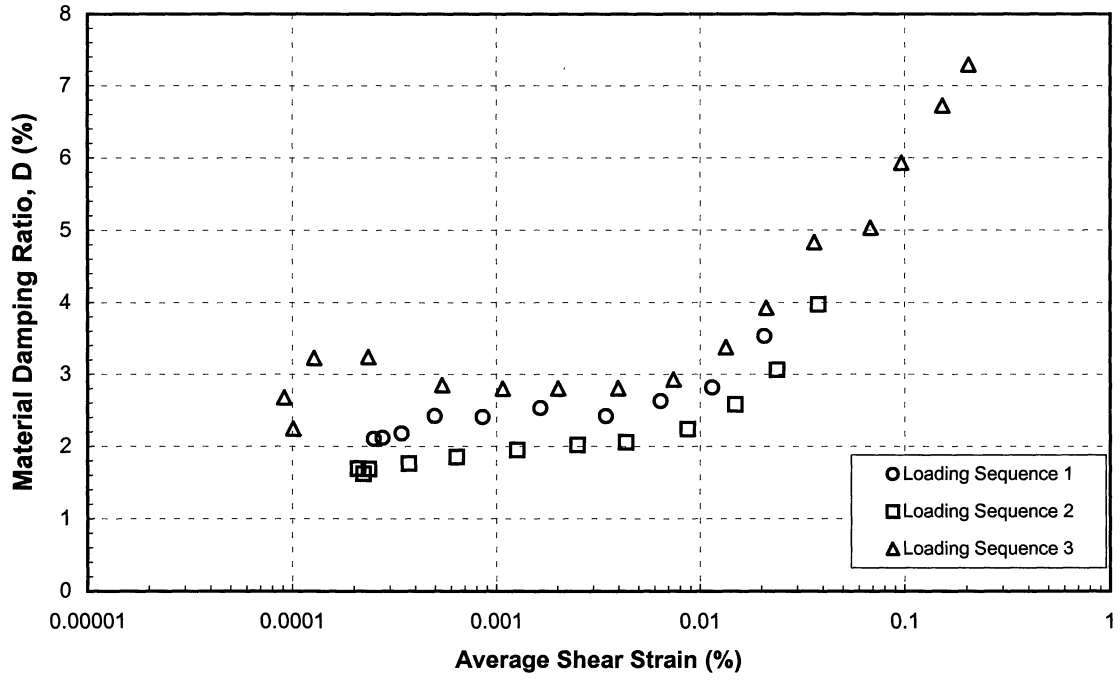

RESONANT COLUMN TEST RESULTS
Sample No. 37 - Penetration: 15.1 m
Boring 98-12
SFOBB East Span Seismic Safety Project

F:\wp_in\caltrans\gregg\9812_37.xls\G,D vs S

PLATE A.5d

APPENDIX B
RESULTS OF CYCLIC SIMPLE SHEAR TESTS

June 1998
Project No. 98-42-0035
SFOBB Task Order No. 3

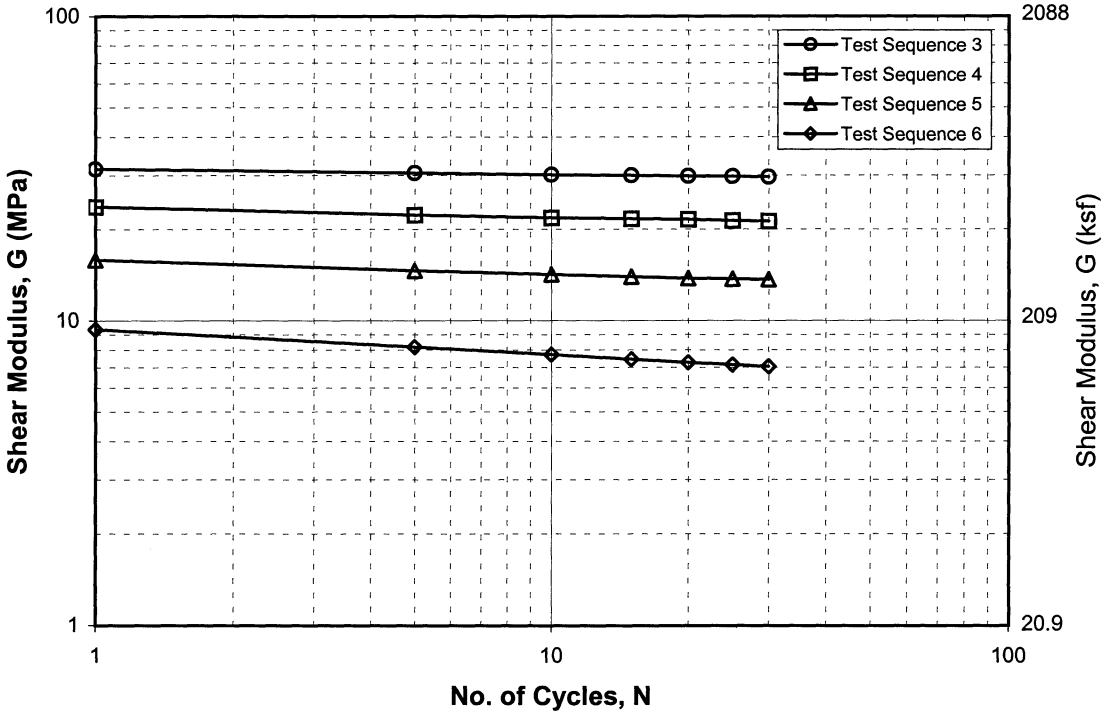

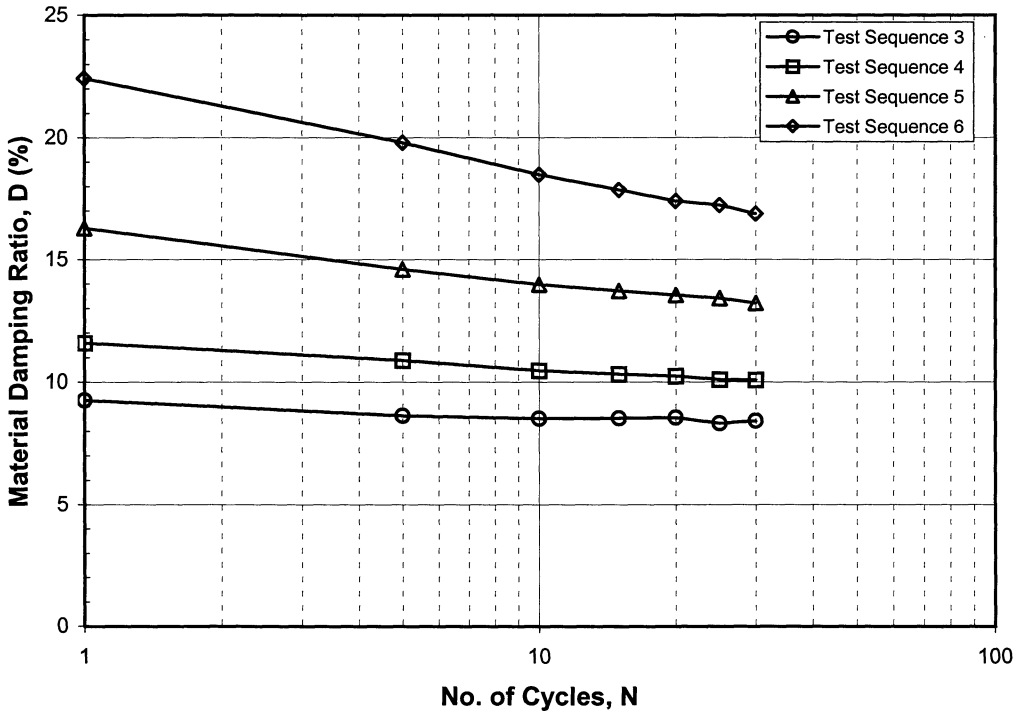

CYCLIC SIMPLE SHEAR TEST RESULTS
Sample No. 49 - Penetration: 15.9 m
Boring 98-7
SFOBB East Span Seismic Safety Project

F:\wp_in\caltrans\gregg\css\98-7-49.xls\G,D vs N

PLATE B-1a

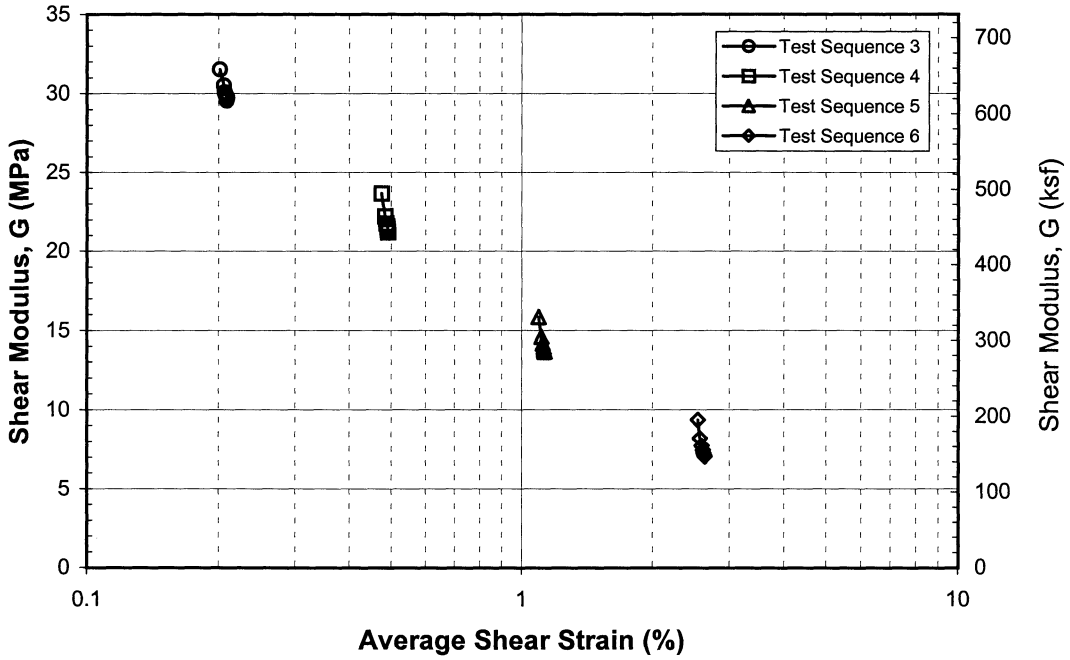

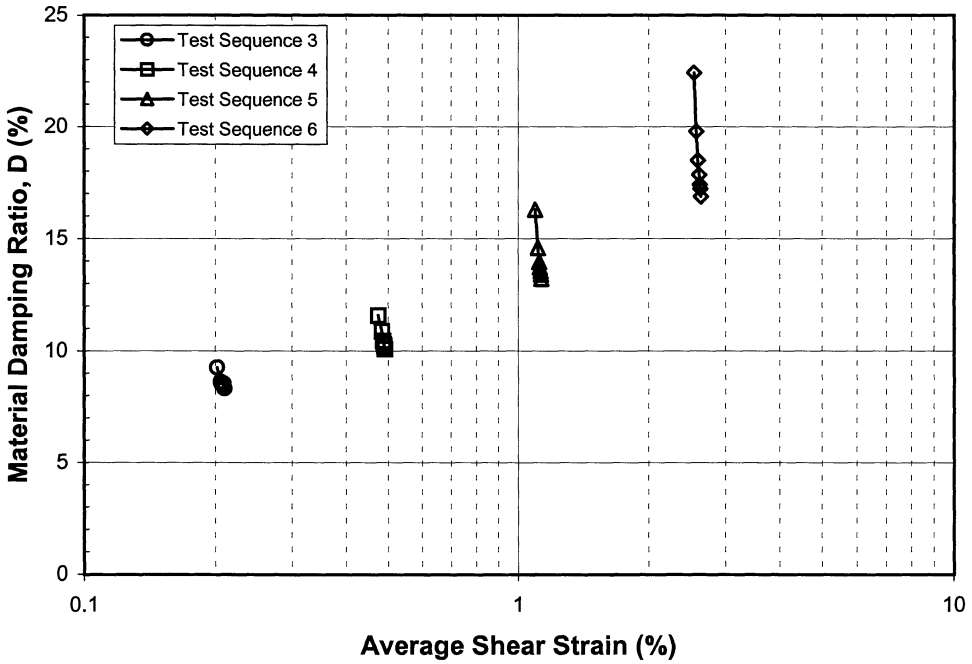

CYCLIC SIMPLE SHEAR TEST RESULTS
Sample No. 49 - Penetration: 15.9 m
Boring 98-7
SFOBB East Span Seismic Safety Project

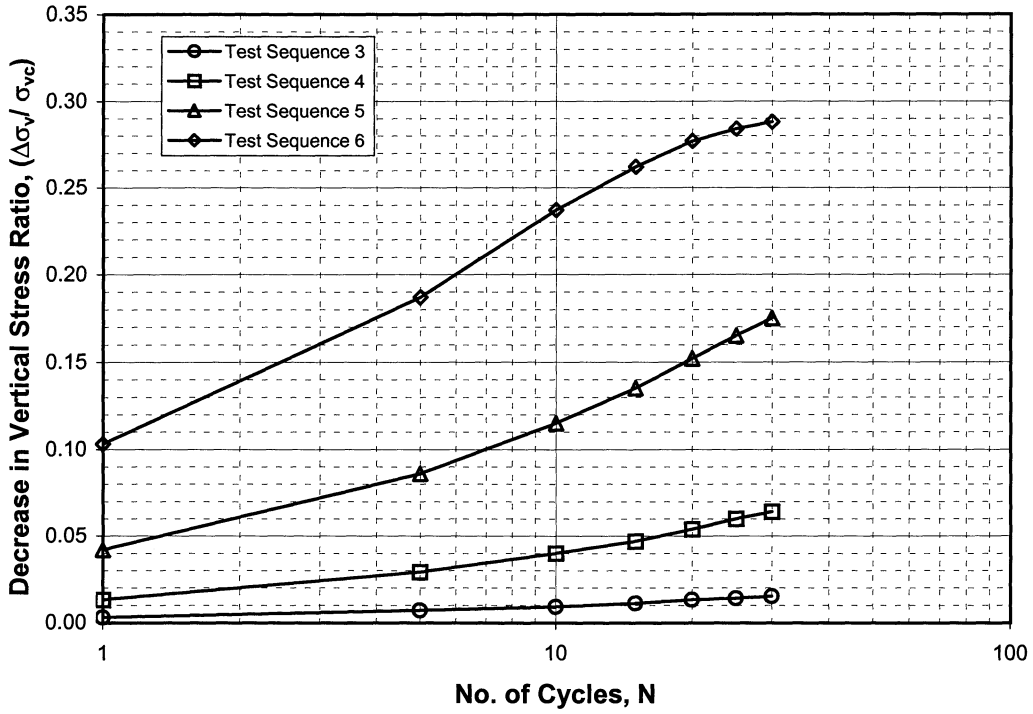

CYCLIC SIMPLE SHEAR TEST RESULTS
Sample No. 49 - Penetration: 15.9 m
Boring 98-7
SFOBB East Span Seismic Safety Project

June 1998
Project No. 98-42-0035
SFOBB Task Order No. 3

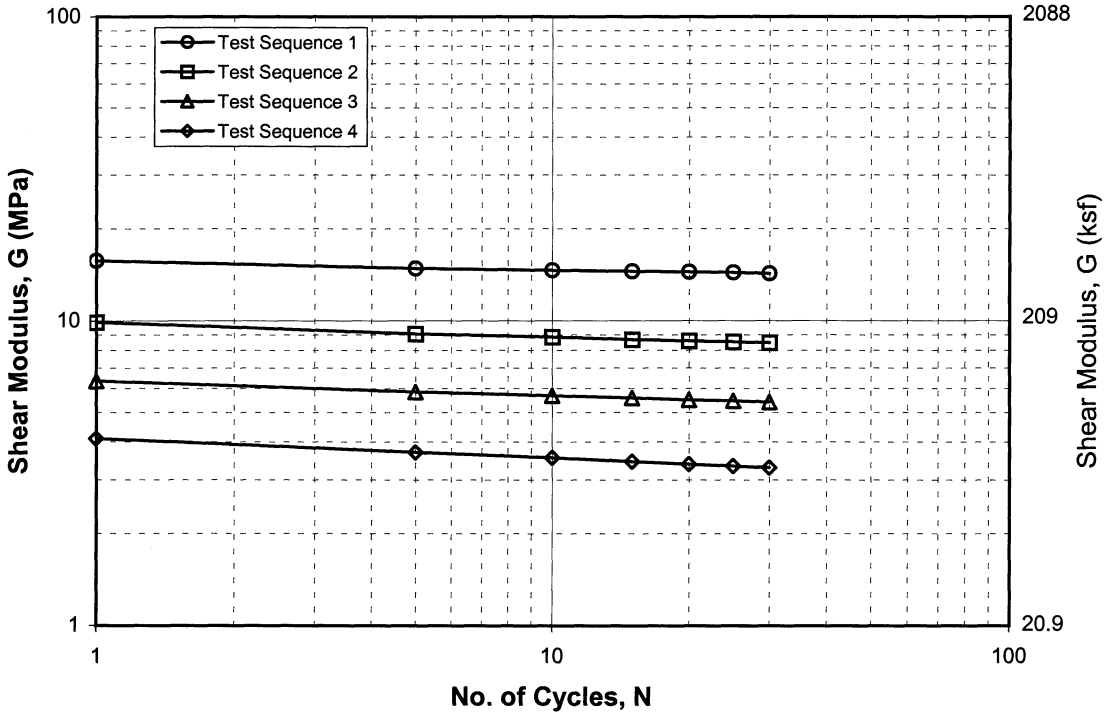

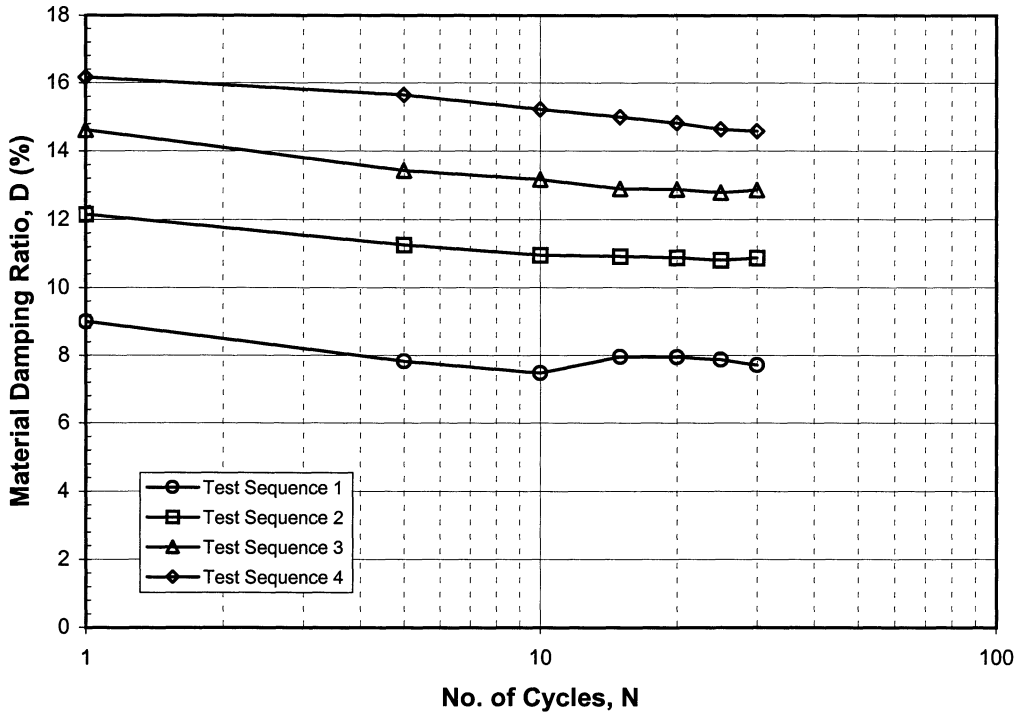

CYCLIC SIMPLE SHEAR TEST RESULTS
Sample No. 49B - Penetration: 15.8 m
Boring 98-7
SFOBB East Span Seismic Safety Project

F:\wp_in\caltrans\gregg\css\98-7-49b.xls\G,D vs N

PLATE B-2a

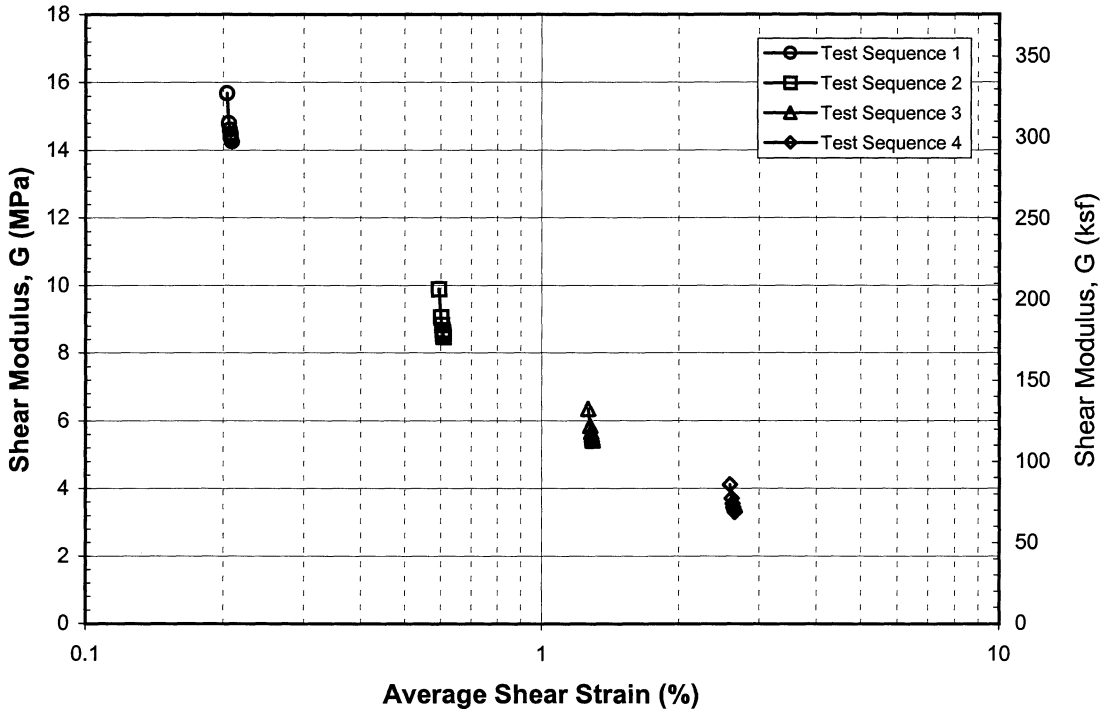

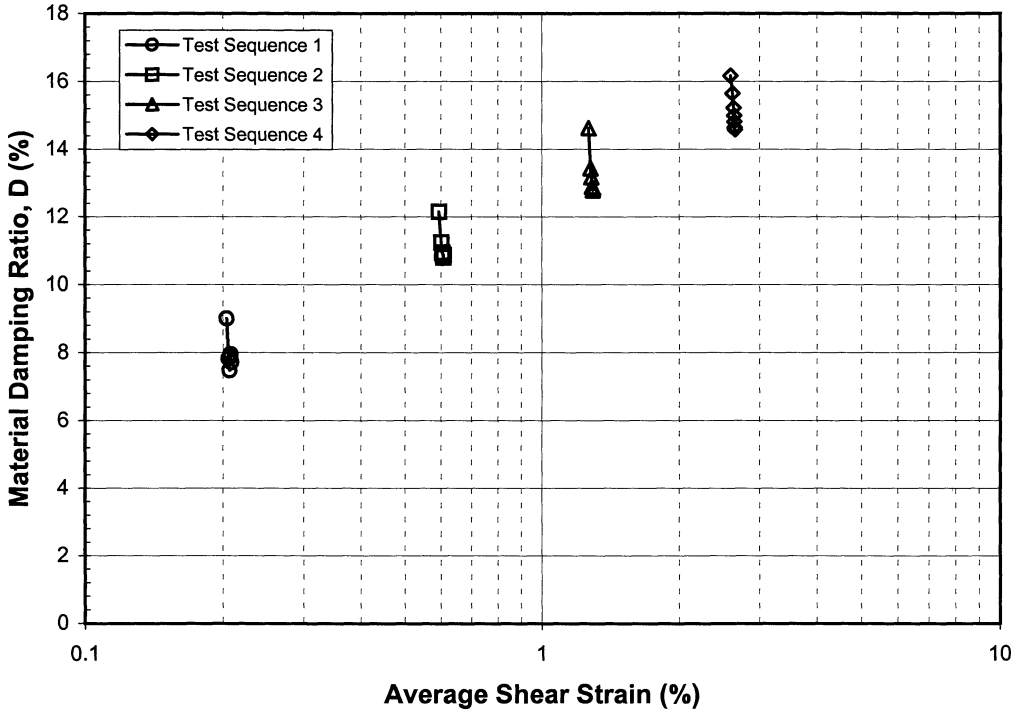

CYCLIC SIMPLE SHEAR TEST RESULTS
Sample No. 49B - Penetration: 15.8 m
Boring 98-7
SFOBB East Span Seismic Safety Project

F:\wp_in\caltrans\gregg\css\98-7-49b.xls\G,D vs S

PLATE B-2b

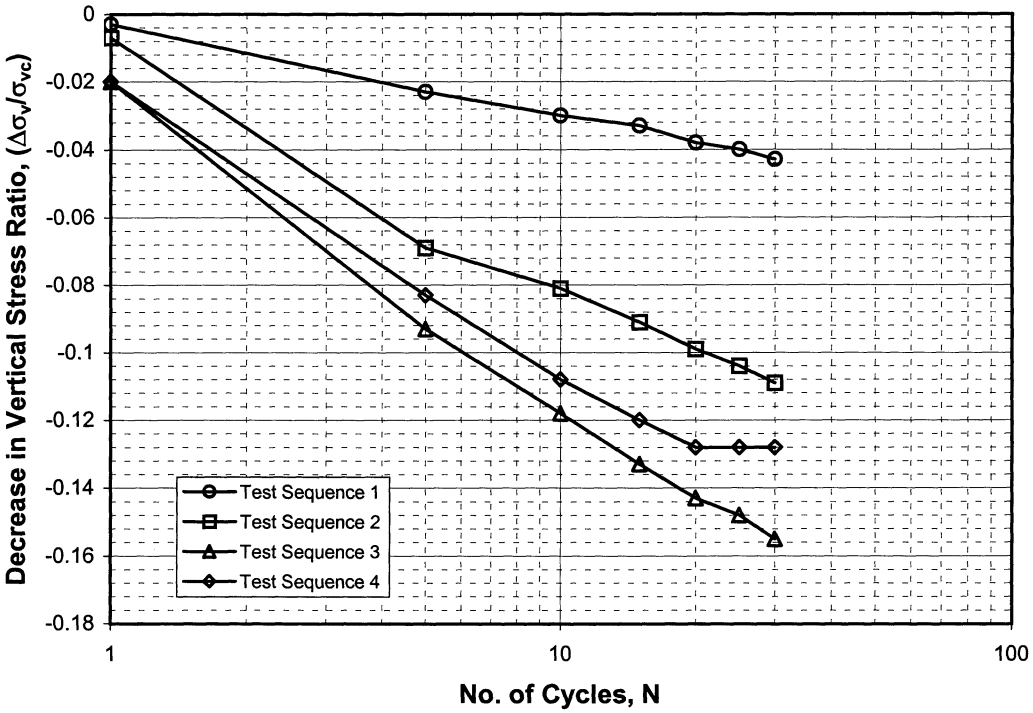

CYCLIC SIMPLE SHEAR TEST RESULTS
Sample No. 49B - Penetration: 15.8 m
Boring 98-7
SFOBB East Span Seismic Safety Project

F:\wp_in\caltrans\gregg\css\98-7-49b.xls\DVSR vs N

PLATE B-2c

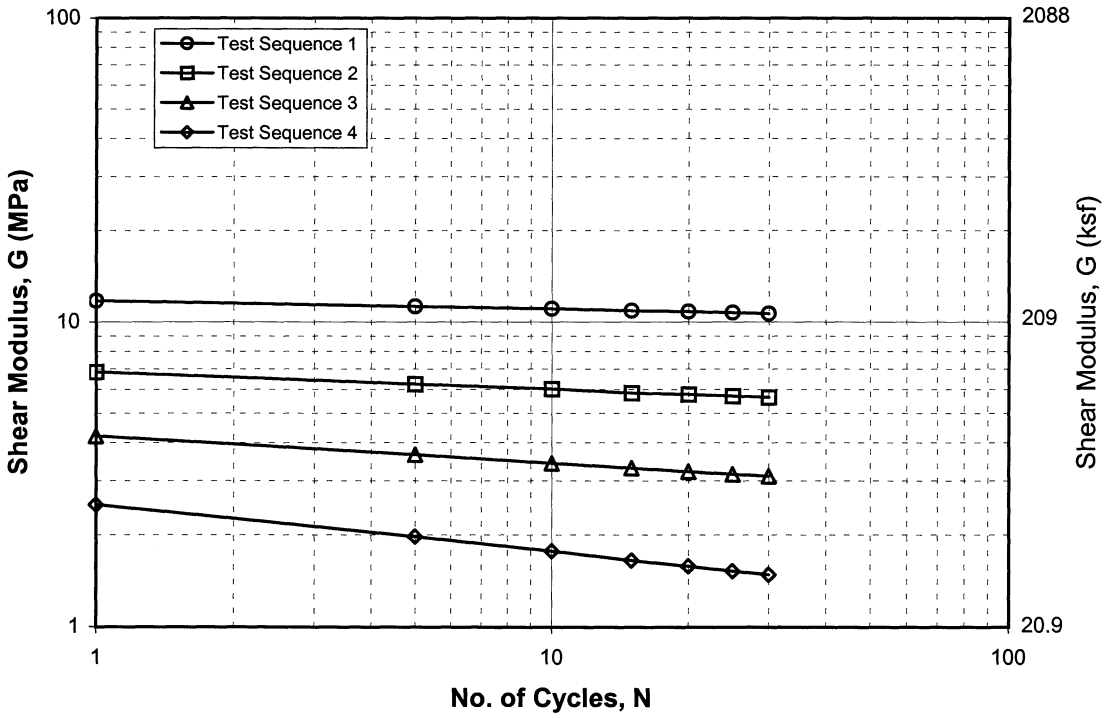

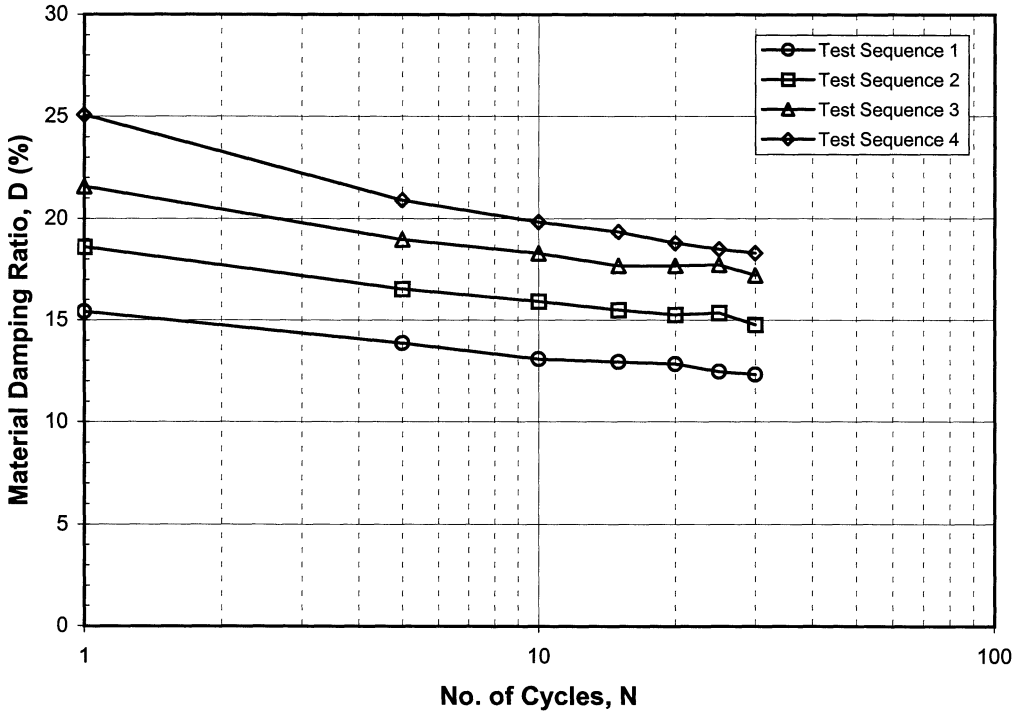

CYCLIC SIMPLE SHEAR TEST RESULTS
Sample No. 37 - Penetration: 11.9 m
Boring 98-8
SFOBB East Span Seismic Safety Project

F:\wp_in\caltrans\gregg\css\98-8-37.xls\G,D vs N

PLATE B-3a

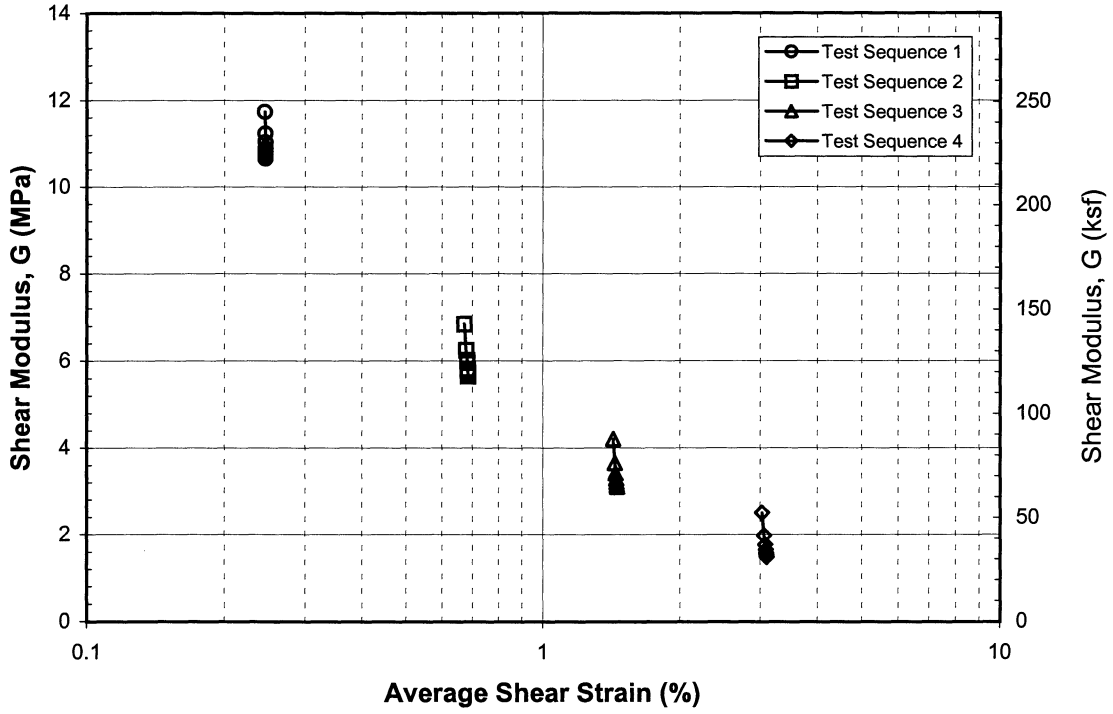

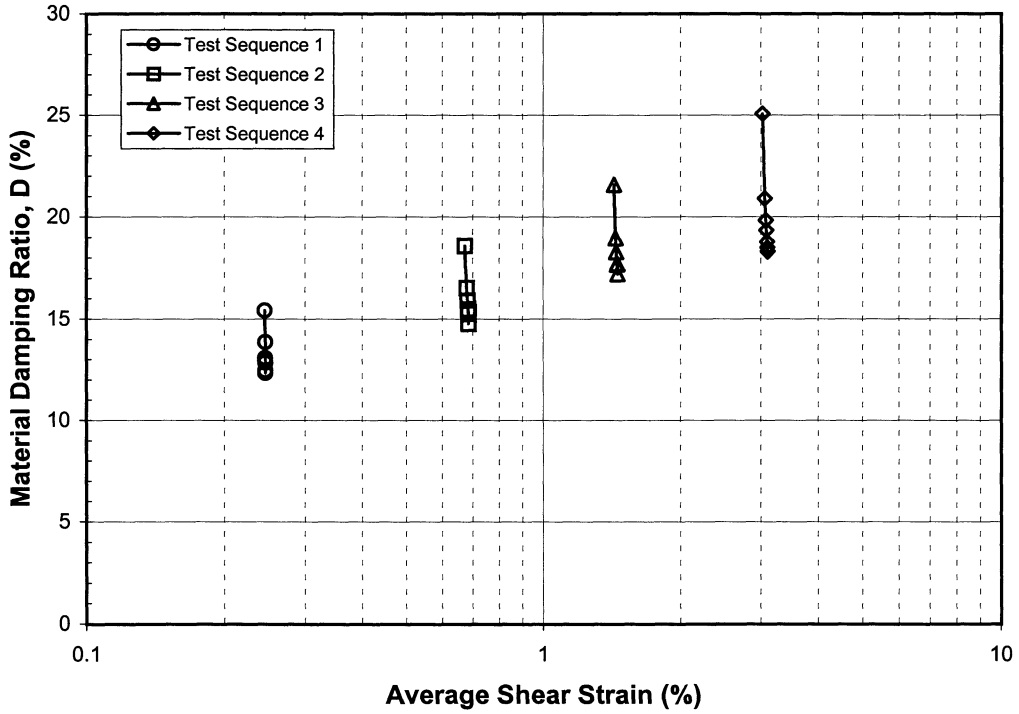

CYCLIC SIMPLE SHEAR TEST RESULTS
Sample No. 37 - Penetration: 11.9 m
Boring 98-8
SFOBB East Span Seismic Safety Project

F:\wp_in\caltrans\gregg\css\98-8-37.xls\G,D vs S

PLATE B-3b

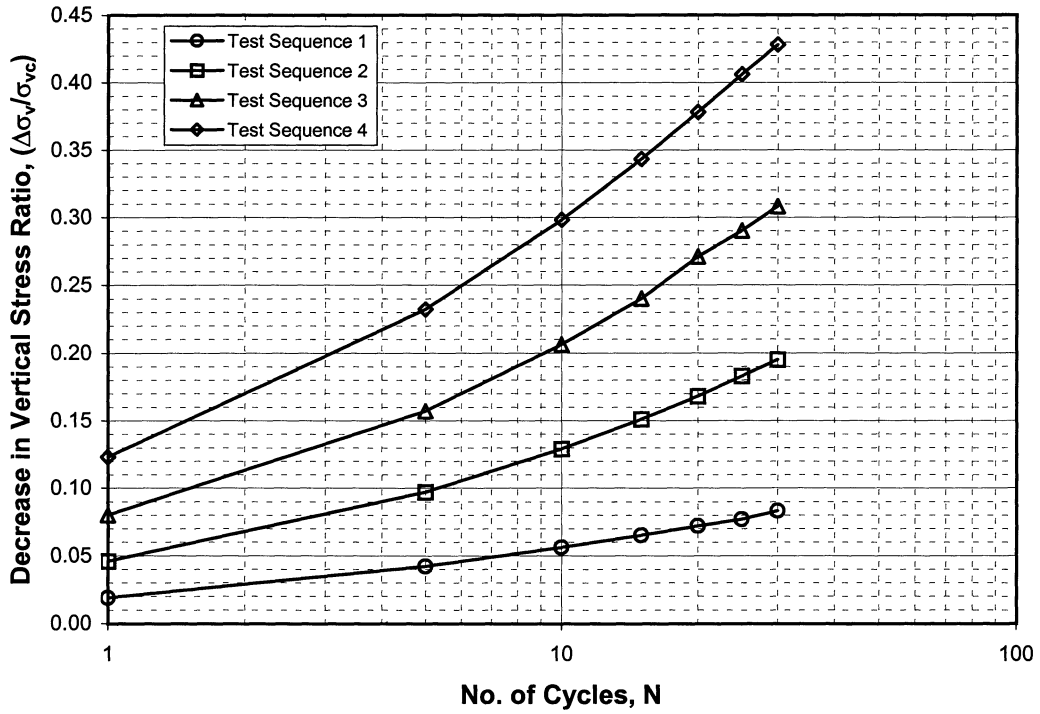

CYCLIC SIMPLE SHEAR TEST RESULTS
Sample No. 37 - Penetration: 11.9 m
Boring 98-8
SFOBB East Span Seismic Safety Project

F:\wp_in\caltrans\gregg\css\98-8-37.xls\DvSR vs N

PLATE B-3c

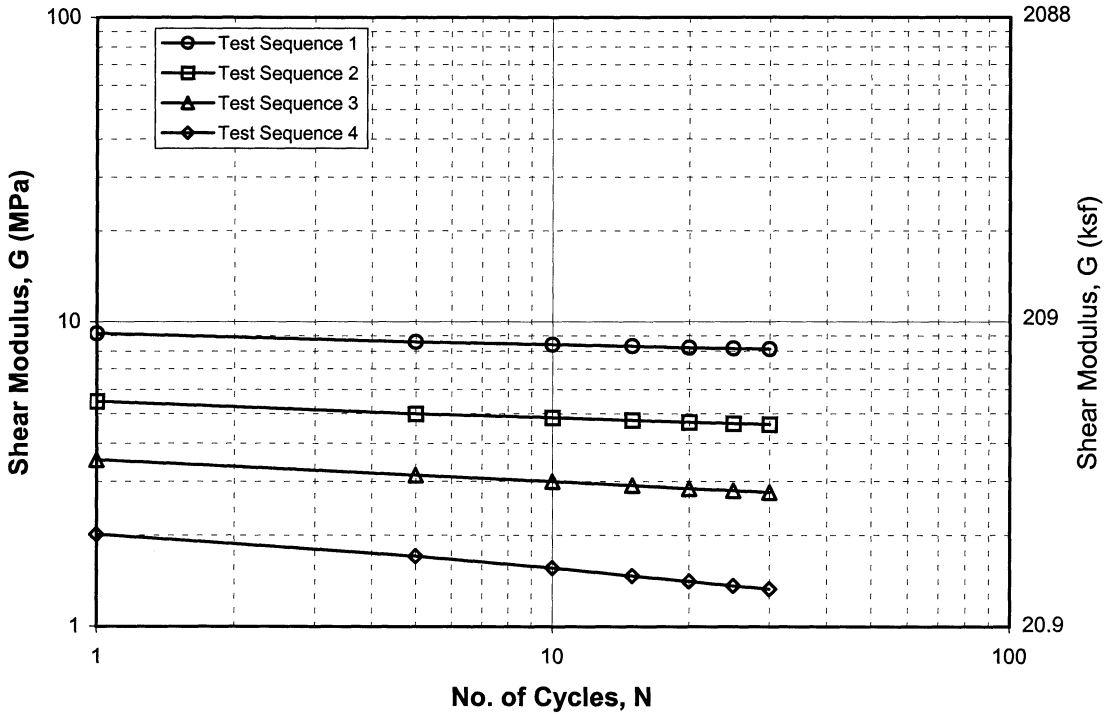

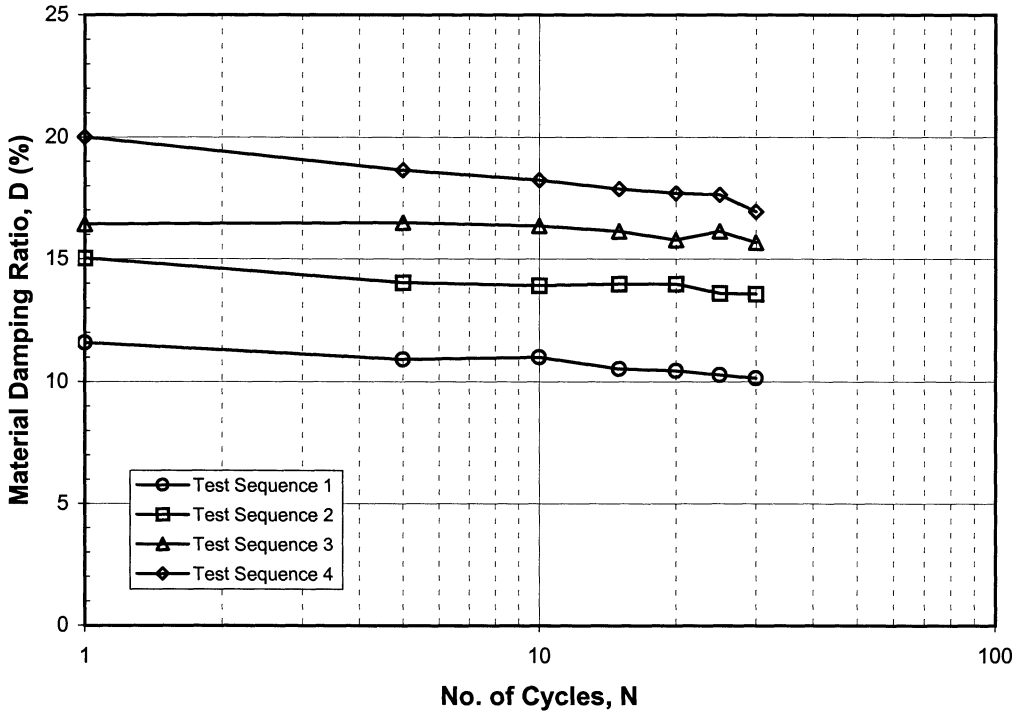

CYCLIC SIMPLE SHEAR TEST RESULTS
Sample No. 37D - Penetration: 11.9 m
Boring 98-8
SFOBB East Span Seismic Safety Project

F:\wp_in\caltrans\gregg\css\98-8-37d.xls\G,D vs N

PLATE B-4a

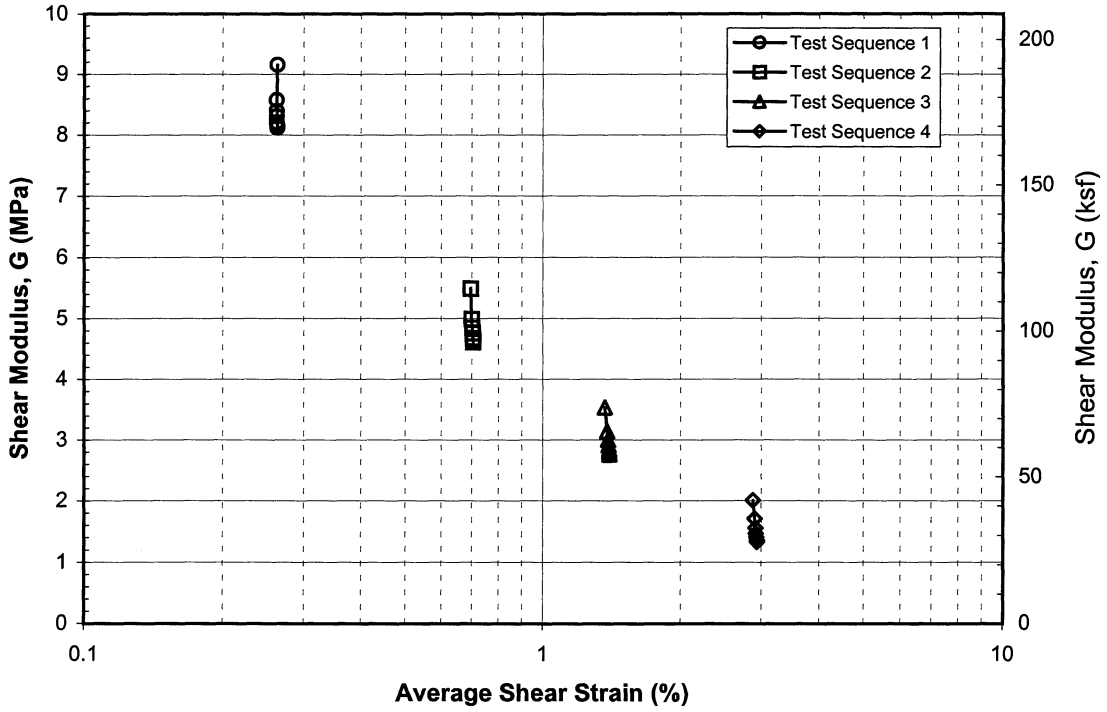

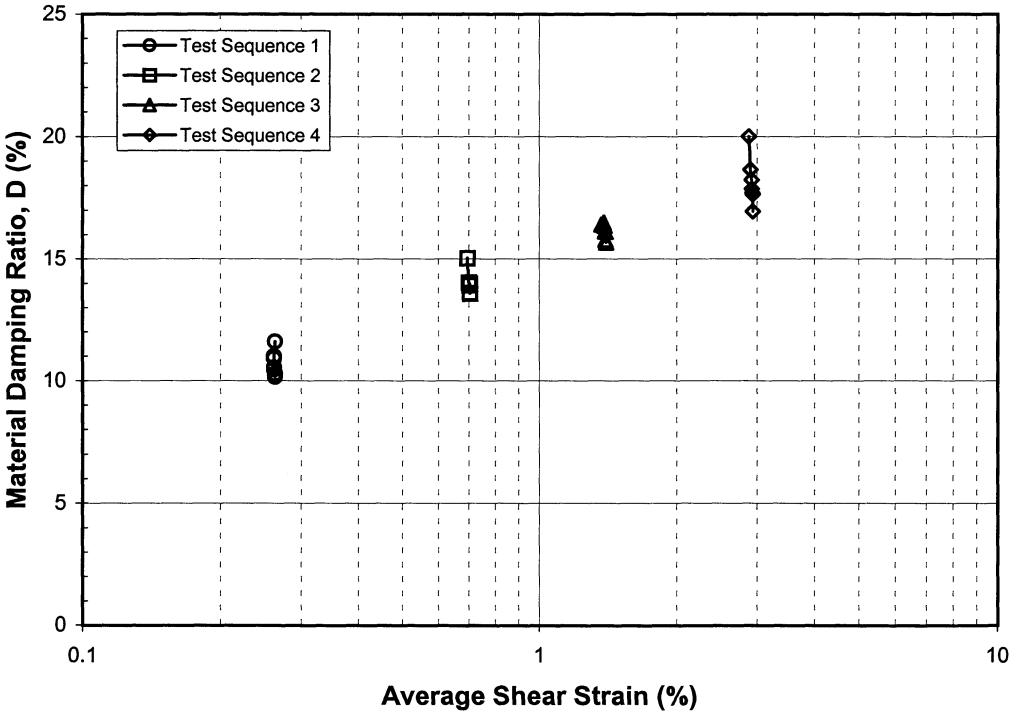

CYCLIC SIMPLE SHEAR TEST RESULTS
Sample No. 37D - Penetration: 11.9 m
Boring 98-8
SFOBB East Span Seismic Safety Project

F:\wp_in\caltrans\gregg\css\98-8-37d.xls\G,D vs S

PLATE B-4b

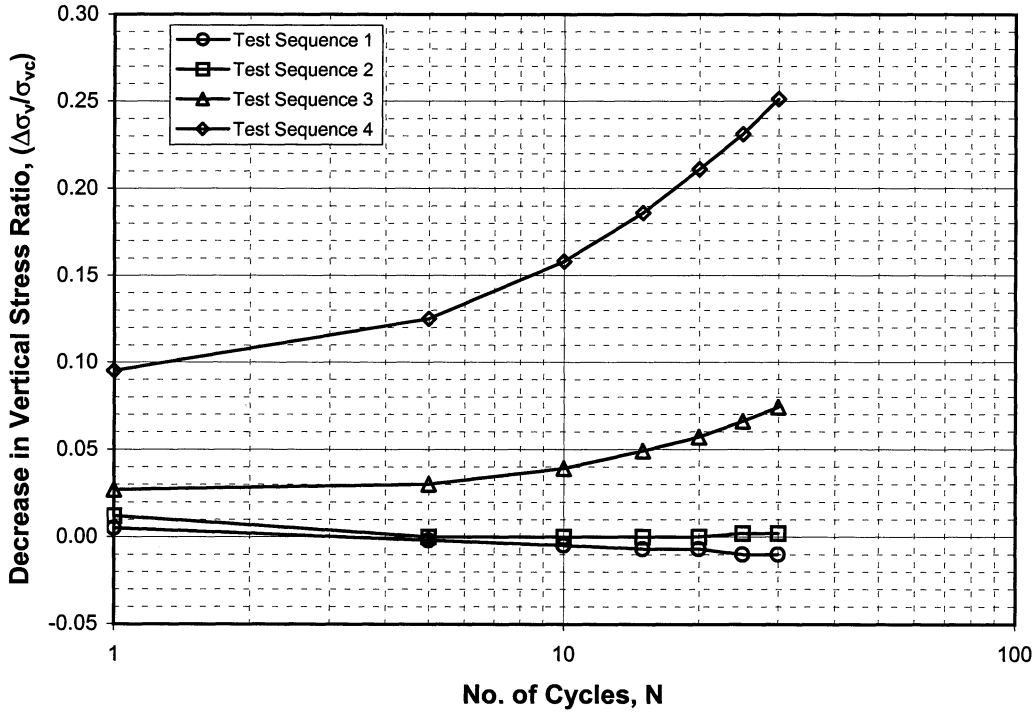

CYCLIC SIMPLE SHEAR TEST RESULTS
Sample No. 37D - Penetration: 11.9 m
Boring 98-8
SFOBB East Span Seismic Safety Project

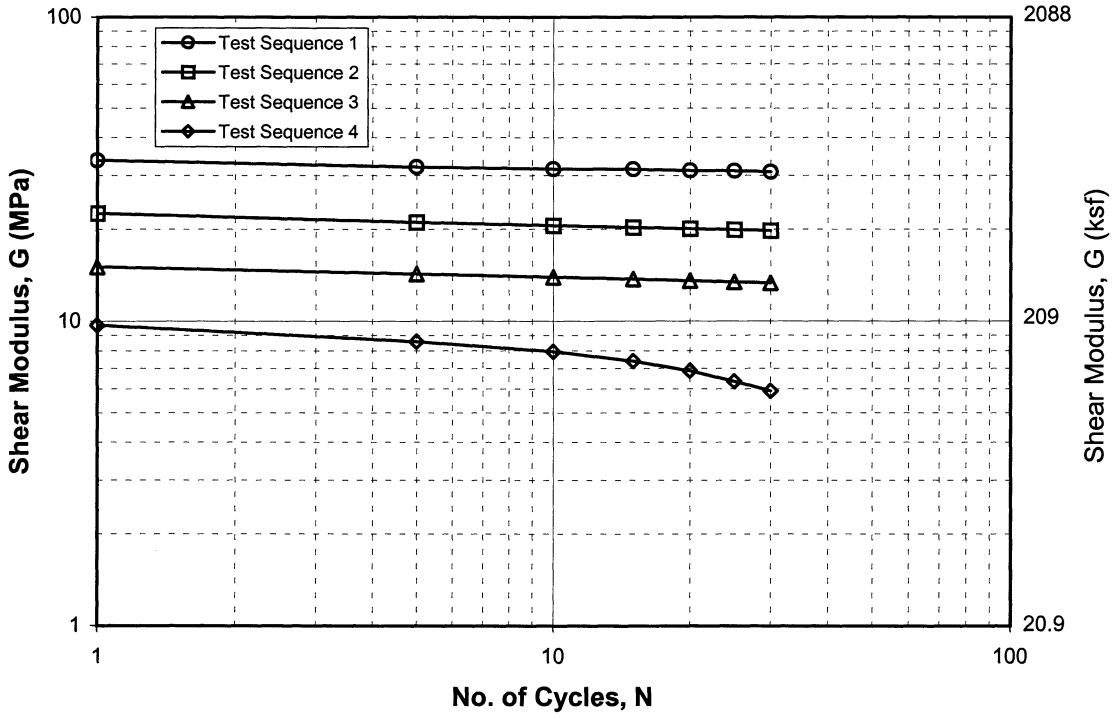

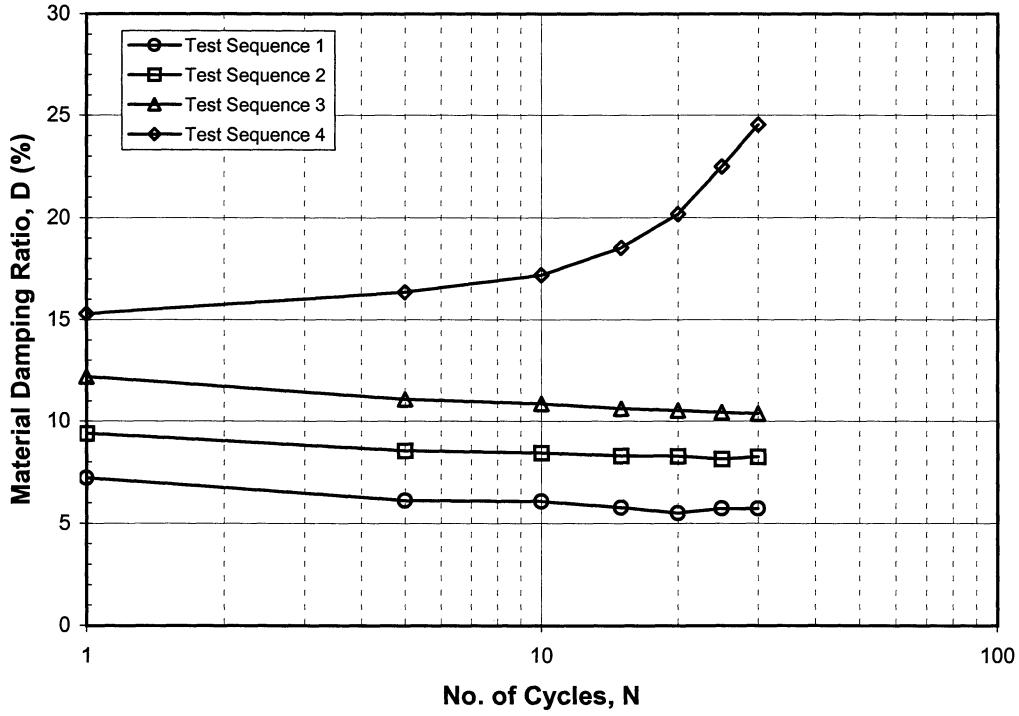

CYCLIC SIMPLE SHEAR TEST RESULTS
Sample No. 53 - Penetration: 37.9 m
Boring 98-9
SFOBB East Span Seismic Safety Project

F:\wp_in\caltrans\gregg\css\98-9-53.xls\G,D vs N

PLATE B-5a

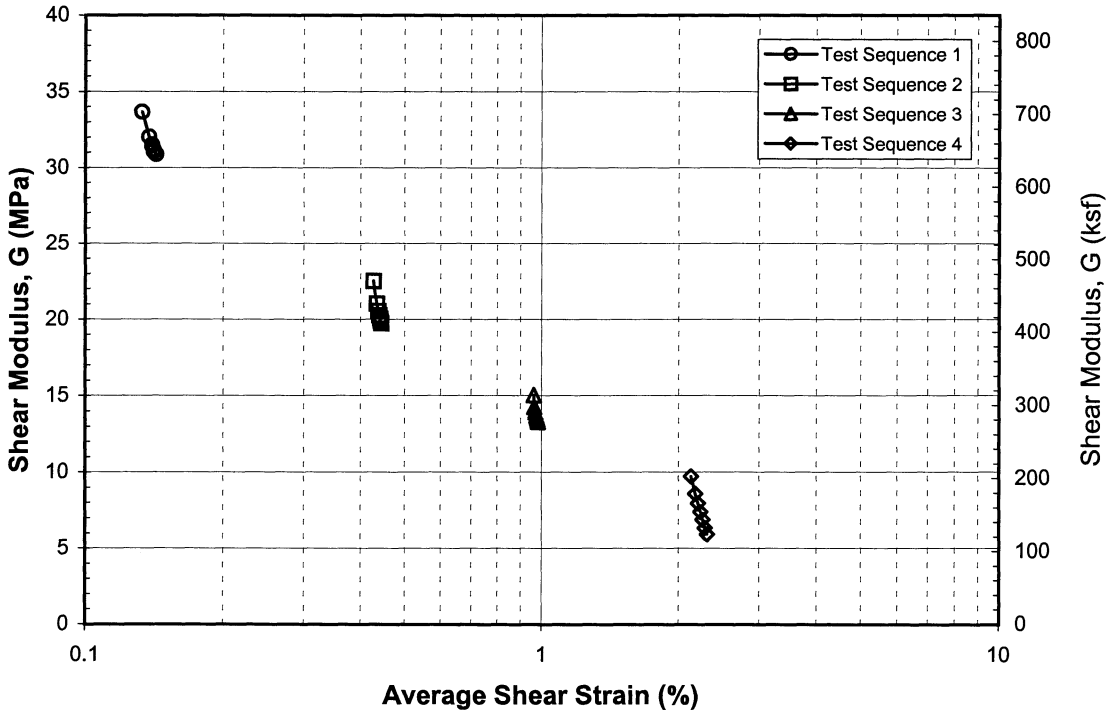

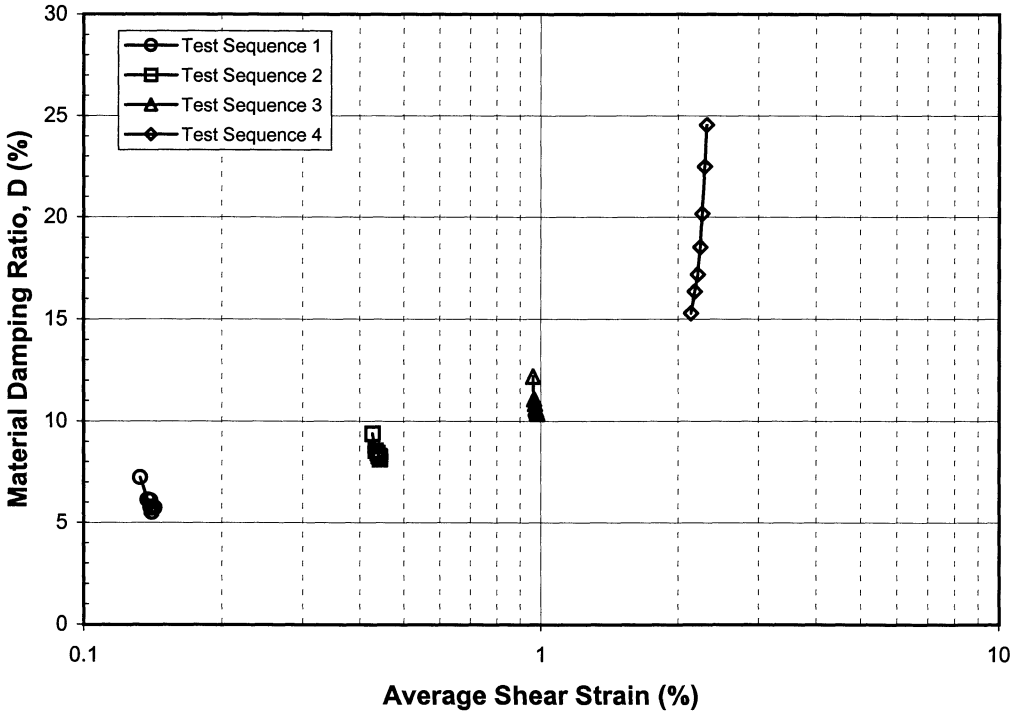

CYCLIC SIMPLE SHEAR TEST RESULTS
Sample No. 53 - Penetration: 37.9 m
Boring 98-9
SFOBB East Span Seismic Safety Project

F:\wp_in\caltrans\gregg\css\98-9-53.xls\G,D vs S

PLATE B-5b

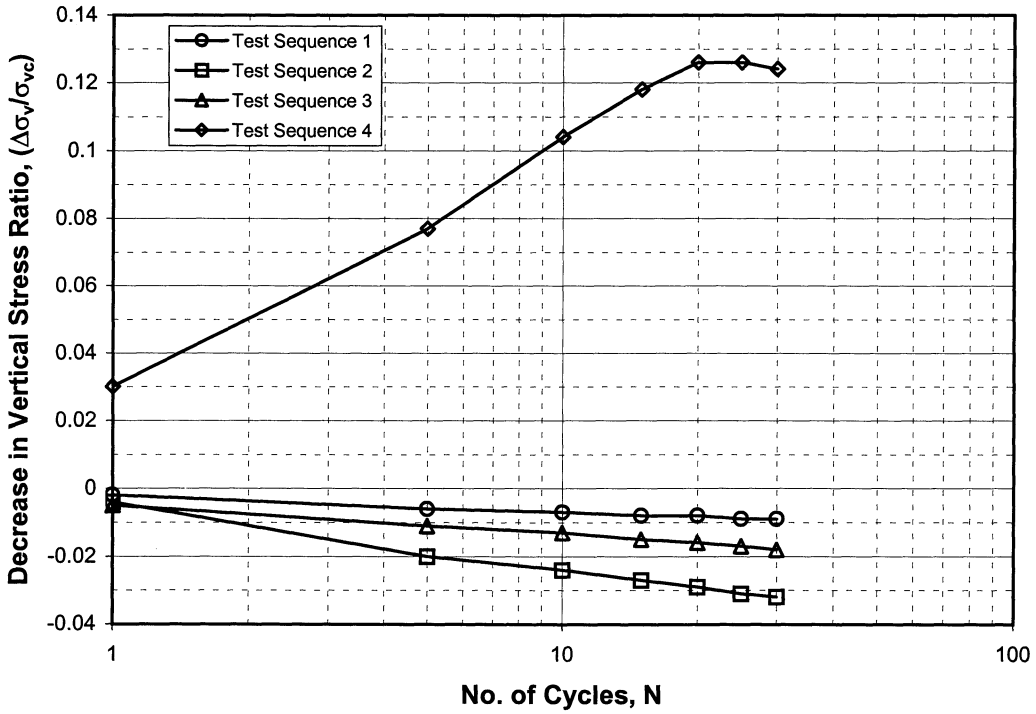

CYCLIC SIMPLE SHEAR TEST RESULTS
Sample No. 53 - Penetration: 37.9 m
Boring 98-9
SFOBB East Span Seismic Safety Project

June 1998
Project No. 98-42-0035
SFOBB Task Order No. 3

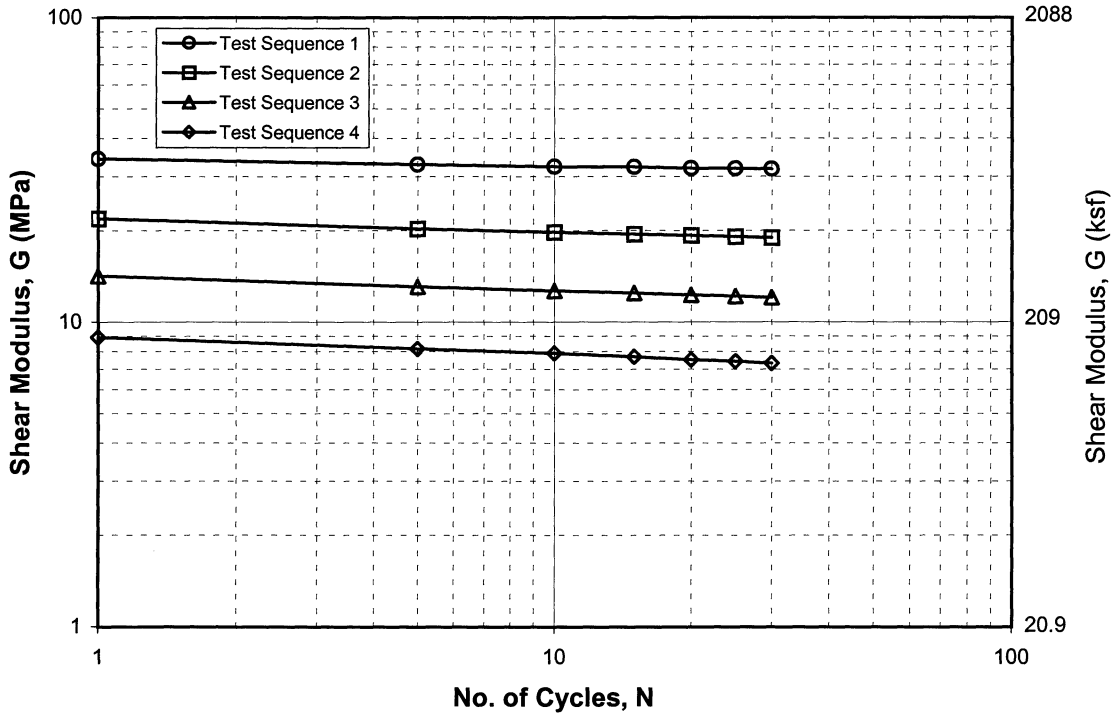

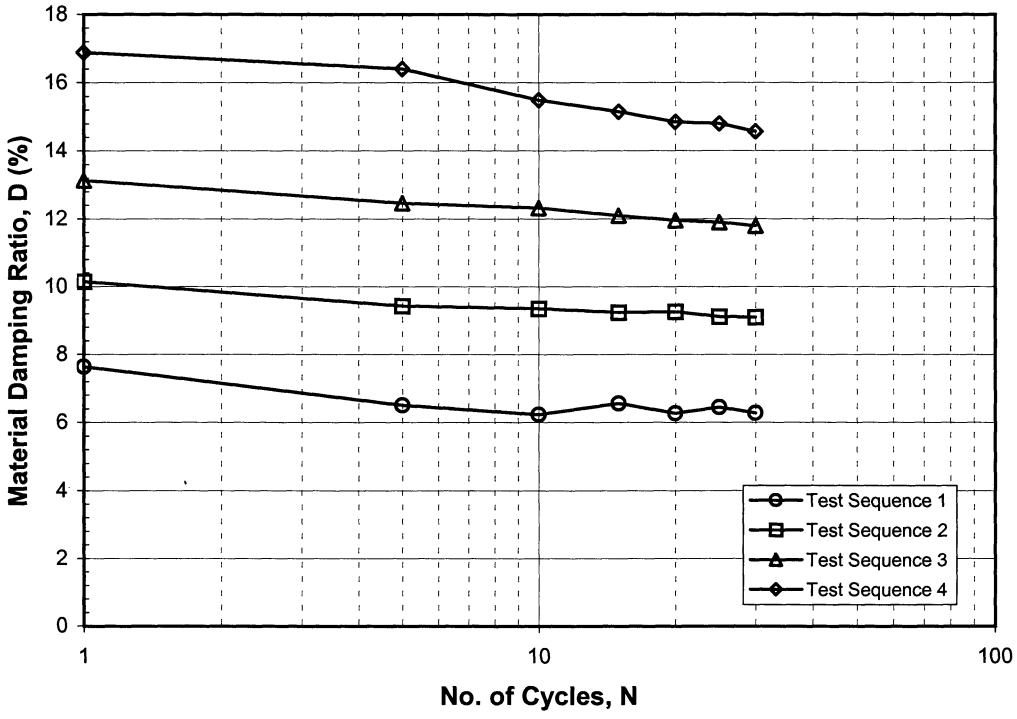

CYCLIC SIMPLE SHEAR TEST RESULTS
Sample No. 73 - Penetration: 62.7 m
Boring 98-11
SFOBB East Span Seismic Safety Project

F:\wp_in\caltrans\gregg\css\9811-73.xls\G,D vs N

PLATE B-6a

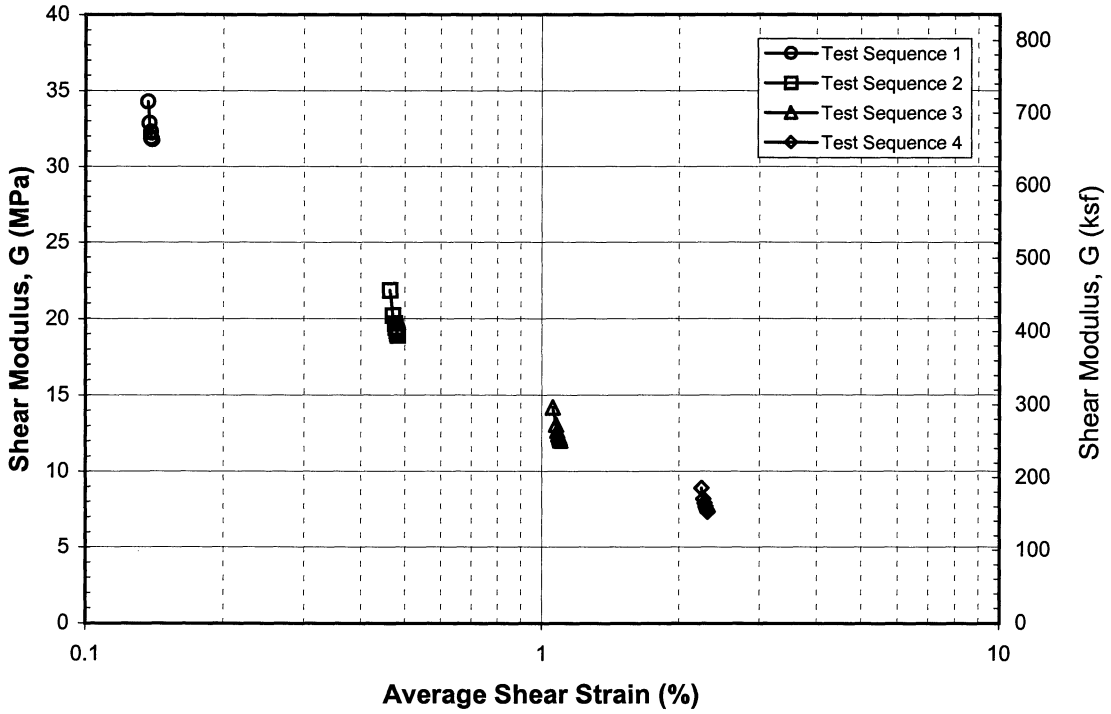

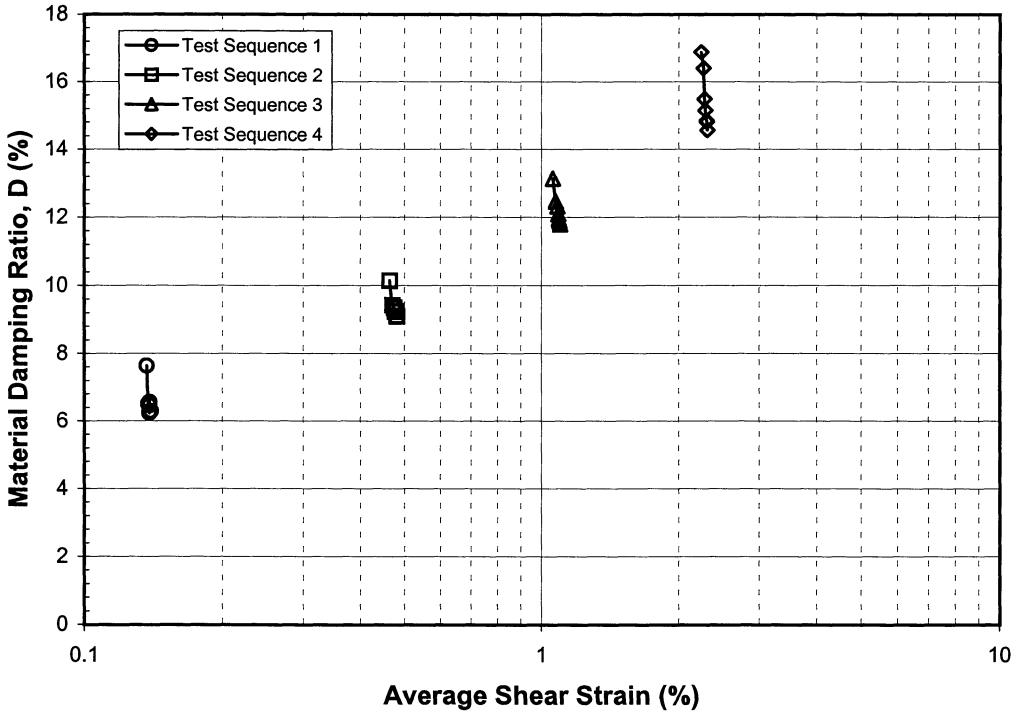

CYCLIC SIMPLE SHEAR TEST RESULTS
Sample No. 73 - Penetration: 62.7 m
Boring 98-11
SFOBB East Span Seismic Safety Project

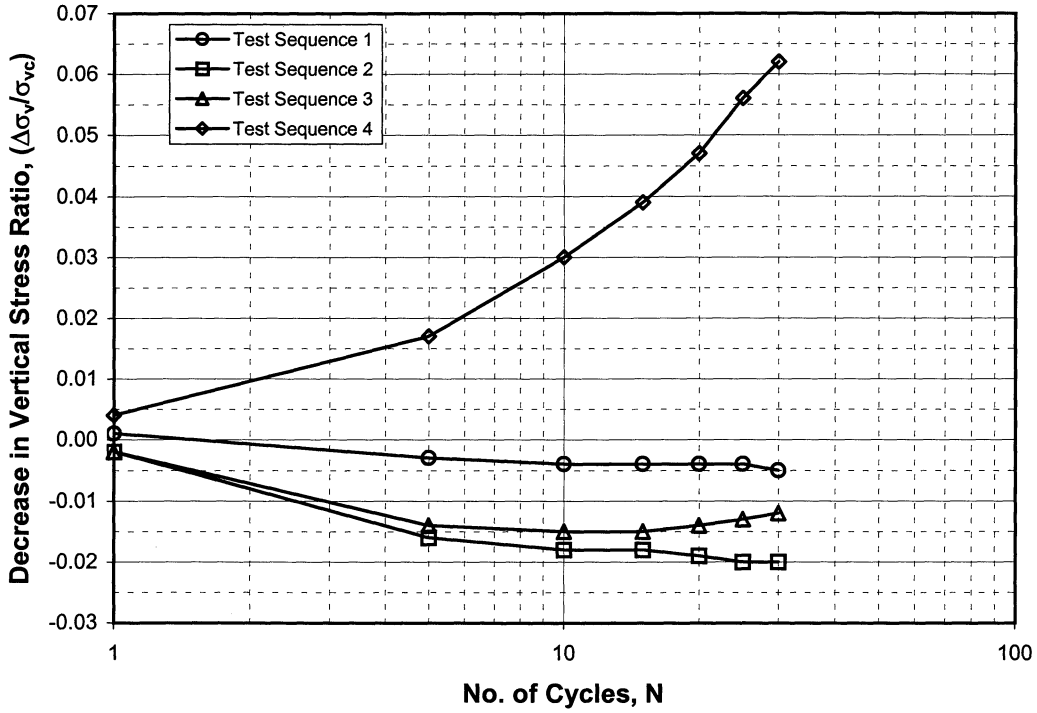

CYCLIC SIMPLE SHEAR TEST RESULTS
Sample No. 73 - Penetration: 62.7 m
Boring 98-11
SFOBB East Span Seismic Safety Project

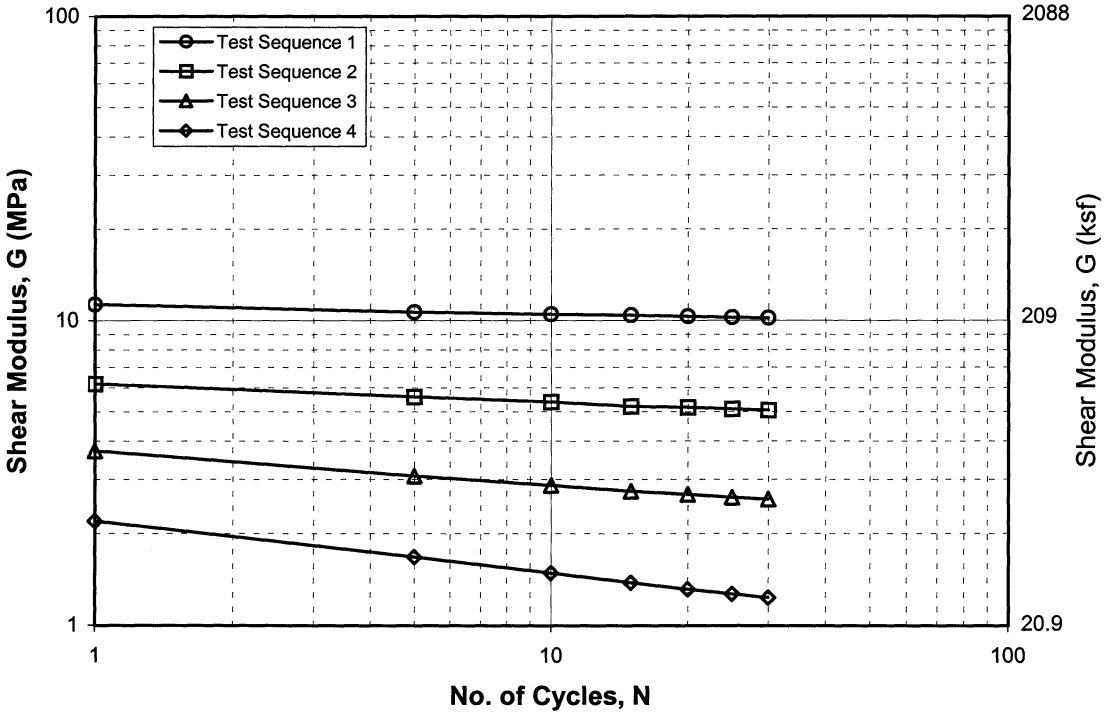

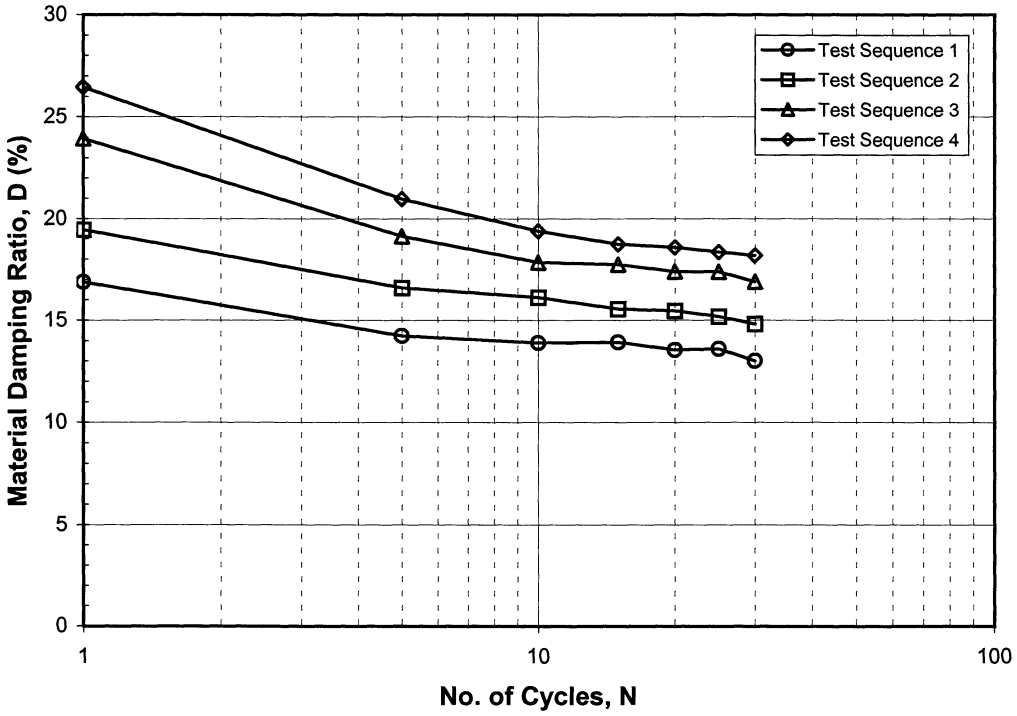

CYCLIC SIMPLE SHEAR TEST RESULTS
Sample No. 37B - Penetration: 12.1 m
Boring 98-12
SFOBB East Span Seismic Safety Project

F:\wp_in\caltrans\gregg\css\9812-37b.xls\G,D vs N

PLATE B-7a

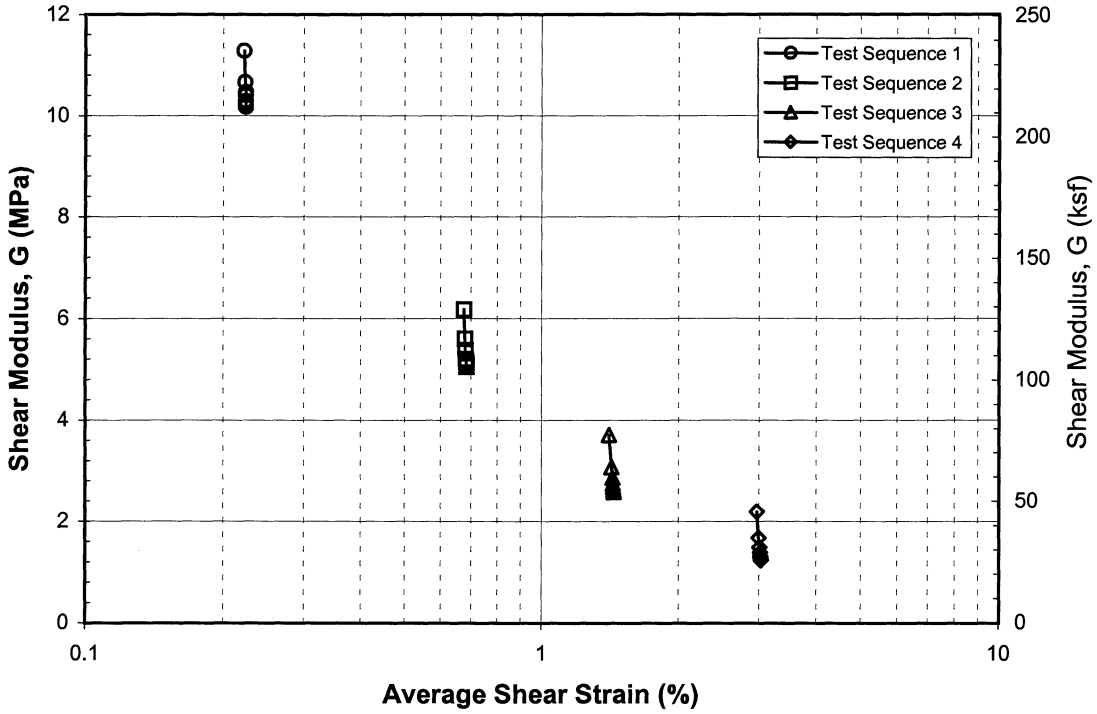

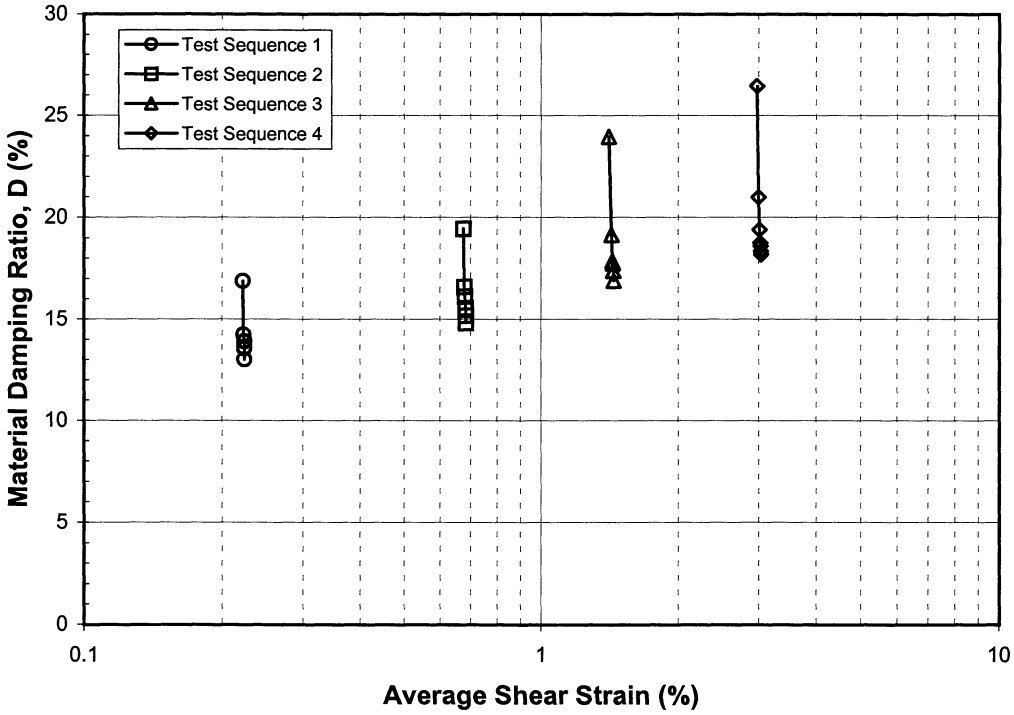

CYCLIC SIMPLE SHEAR TEST RESULTS
Sample No. 37B - Penetration: 12.1 m
Boring 98-12
SFOBB East Span Seismic Safety Project

F:\wp_in\caltrans\gregg\css\9812-37b.xls\G,D vs S

PLATE B-7b

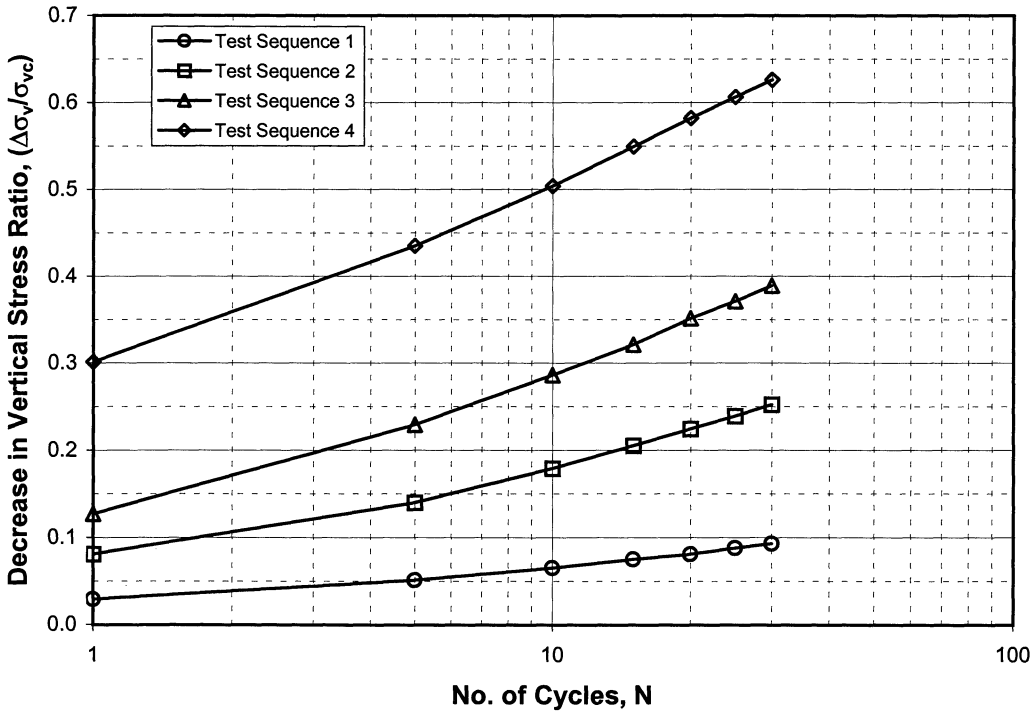

CYCLIC SIMPLE SHEAR TEST RESULTS
Sample No. 37B - Penetration: 12.1 m
Boring 98-12
SFOBB East Span Seismic Safety Project

UNIVERSITY OF TEXAS AT AUSTIN

UNIVERSITY OF TEXAS AT AUSTIN
DYNAMIC PROPERTIES OF INTACT SOIL SPECIMENS

COLLEGE OF ENGINEERING

THE UNIVERSITY OF TEXAS AT AUSTIN

Department of Civil Engineering • Austin, Texas 78712-1076
Geotechnical Engineering • (512) 471-4929 • FAX (512) 471-6548

July 3, 1998

Mr. Tom McNeilan
Fugro West, Inc.
5855 Olivas Park Dr.
Ventura, CA 93003-7672

Dear Tom:

Attached are a bound and an unbound copy of our final report documenting the dynamic laboratory testing of the four intact specimens that you sent us. We have enjoyed the work and hope to interact with you again in future projects.

Best regards,

Kenneth H. Stokoe, II
Cockrell Family Regents Chair No.9

LABORATORY EVALUATION OF THE DYNAMIC PROPERTIES OF INTACT SOIL SPECIMENS: SAN FRANCISCO-OAKLAND BAY BRIDGE, EAST-SPAN SEISMIC SAFETY PROJECT, PHASE I - SITE CHARACTERIZATION

for

A Joint Venture of:
Fugro, Inc. and Earth Mechanics, Inc.

Fugro West, Inc.
5855 Olivas Park Drive
Ventura, California 93003 - 7672

by

Kenneth H. Stokoe, II
Mehmet B. Darendeli
Farn-Yuh Menq

July 1, 1998

Geotechnical Engineering Report GR98-8
Geotechnical Engineering Center
Civil Engineering Department
The University of Texas at Austin

TABLE OF CONTENTS

LIST OF TABLES iii

LIST OF FIGURES iv

1. INTRODUCTION 1

2. DYNAMIC LABORATORY TESTS 4

   2.1. Test Program 5
   2.2. Test Results 10

3. DISCUSSION OF RESULTS 12

   3.1. Small-Strain Shear Modulus and Material Damping Ratio 12
   3.2. Nonlinear Shear Modulus and Material Damping Ratio 27

4. REFERENCES 43

APPENDIX A: TEST EQUIPMENT, MEASUREMENT TECHNIQUES AND DISCUSSION OF EQUIPMENT CONSTANTS A.1

APPENDIX B: UTA-10-A BOREHOLE ID : 98 - 20
SAMPLE NO. = 27 DEPTH = 27.5 ft (8.4 m) B.1

APPENDIX C: UTA-10-B BOREHOLE ID : 98 - 19
SAMPLE NO. = 34 DEPTH = 36.5 ft (11.1 m) C.1

APPENDIX D: UTA-10-C BOREHOLE ID : 98 - 8
SAMPLE NO. = 71 DEPTH = 79.0 ft (24.1 m) D.1

APPENDIX E: UTA-10-D BOREHOLE ID : 98 - 20
SAMPLE NO. = 91 DEPTH = 231 ft (70.4 m) E.1

LIST OF TABLES

Table 1 Initial Properties of Specimens Tested from the Easy Bay Bridge Site..... 2

Table 2 Summary of Resonant Column and Torsional Shear Tests Performed on the Specimens from the Easy Bay Bridge Site..... 6

Table 3 A and n Dimensionless Constants from the Least-Squares Fits to the Hardin (1978) Equation..... 19

Table 4 Reference Strain ($\gamma_{r,G}$) Values for the G/G_{max} - log γ Curves Based on the Hardin and Drnevich (1972) Equation 32

Table 5 Damping Curve Coefficients ($\gamma_{r,D}$ and D_{min}) for the D - log γ Curves..... 39

LIST OF FIGURES

Figure 1 Grain Size Distribution Curves of Samples from the East Bay Bridge Site..... 3

Figure 2 Testing Procedure Used in the Torsional Shear (TS) Test to Investigate the Effects of Strain Amplitude, Number of Loading Cycles, and Excitation Frequency on G and D of Intact Soil Specimens from the East Bay Bridge Site..... 8

Figure 3 Testing Procedure Used in the Resonant Column (RC) Test to Investigate the Effect of Strain Amplitude on G and D Intact Soil Specimens from the East Bay Bridge Site..... 9

Figure 4 Variation in Low-Amplitude Shear Modulus with Effective Isotropic Confining Pressure from Resonant Column (RC) Tests of Soil Specimens from the East Bay Bridge Site..... 13

Figure 5 Variation in Low-Amplitude, Void-Ratio-Adjusted Shear Modulus with Effective Isotropic Confining Pressure from Resonant Column (RC) Tests of Soil Specimens from the East Bay Bridge Site..... 14

Figure 6 Best-Fit Curve to log G_{max} x F(e) - log σ_o' Relationship from Resonant Column (RC) Tests of Specimen UTA-10-A from the East Bay Bridge Site..... 15

Figure 7 Best-Fit Curve to log G_{max} x F(e) - log σ_o' Relationship from Resonant Column (RC) Tests of Specimen UTA-10-B from the East Bay Bridge Site..... 16

Figure 8 Best-Fit Curve to log G_{max} x F(e) - log σ_o' Relationship from Resonant Column (RC) Tests of Specimen UTA-10-C from the East Bay Bridge Site..... 17

Figure 9 Best-Fit Curve to log G_{max} x F(e) - log σ_o' Relationship from Resonant Column (RC) Tests of Specimen UTA-10-D from the East Bay Bridge Site..... 18

Figure 10 Variation in Low-Amplitude Material Damping Ratio with Effective Isotropic Confining Pressure from Resonant Column (RC) Tests of Soil Specimens from the East Bay Bridge Site..... 20

Figure 11 Variation in Void Ratio with Effective Isotropic Confining Pressure from Resonant Column (RC) Tests of Soil Specimens from the East Bay Bridge Site..... 22

Figure 12 Variation in Low-Amplitude Shear Modulus with Loading Frequency at the Estimated Mean Effective Confining Pressure from Resonant Column (RC) and Torsional Shear (TS) Tests of Soil Specimens from the East Bay Bridge Site..... 23

Figure 13 Variation in Normalized Low-Amplitude Shear Modulus with Loading Frequency at the Estimated Mean Effective Confining Pressure from Resonant Column (RC) and Torsional Shear (TS) Tests of Soil Specimens from the East Bay Bridge Site..... 24

Figure 14 Variation in Low-Amplitude Material Damping Ratio with Loading Frequency at the Estimated Mean Effective Confining Pressure from Resonant Column (RC) and Torsional Shear (TS) Tests of Soil Specimens from the East Bay Bridge Site..... 25

Figure 15 Variation in Normalized Low-Amplitude Material Damping Ratio with Loading Frequency at the Estimated Mean Effective Confining Pressure from Resonant Column (RC) and Torsional Shear (TS) Tests of Soil Specimens from the East Bay Bridge Site..... 26

Figure 16 Variation in Shear Modulus with Shearing Strain at the Estimated Mean Effective Confining Pressure from Resonant Column (RC) and Torsional Shear (TS) Tests of Soil Specimens from the East Bay Bridge Site..... 28

Figure 17 Variation in Normalized Shear Modulus with Shearing Strain at the Estimated Mean Effective Confining Pressure from Resonant Column (RC) Tests of Soil Specimens from the East Bay Bridge Site..... 29

Figure 18 Variation in Normalized Shear Modulus with Shearing Strain at the Estimated Mean Effective Confining Pressure from Torsional Shear (TS) Tests of Soil Specimens from the East Bay Bridge Site..... 30

Figure 19 Variation in Normalized Shear Modulus with Shearing Strain at the Estimated Mean Effective Confining Pressure from Resonant Column (RC) and Torsional Shear (TS) Tests of Soil Specimens from the East Bay Bridge Site..... 31

Figure 20 Best Fits of the Hyperbolic Equation to the Variation in Normalized Shear Modulus with Shearing Strain at the Estimated Mean Effective Confining Pressure from Resonant Column (RC) Tests of Soil Specimens from the East Bay Bridge Site..... 33

Figure 21 Best Fits of the Hyperbolic Equation to the Variation in Normalized Shear Modulus with Shearing Strain at the Estimated Mean Effective Confining Pressure from Torsional Shear (TS) Tests of Soil Specimens from the East Bay Bridge Site..... 34

Figure 22 Variation in Material Damping Ratio with Shearing Strain at the Estimated Mean Effective Confining Pressure from Resonant Column (RC) Tests of Soil Specimens from the East Bay Bridge Site..... 36

Figure 23 Variation in Material Damping Ratio with Shearing Strain at the Estimated Mean Effective Confining Pressure from Torsional Shear (TS) Tests of Soil Specimens from the East Bay Bridge Site..... 37

Figure 24 Variation in Material Damping Ratio with Shearing Strain at the Estimated Mean Effective Confining Pressure from Resonant Column (RC) and Torsional Shear (TS) Tests of Soil Specimens from the East Bay Bridge Site..... 38

Figure 25 Best Fits to the Variation in Material Damping Ratio with Shearing Strain at the Estimated Mean Effective Confining Pressure from Resonant Column (RC) Tests of Soil Specimens from the East Bay Bridge Site. 40

Figure 26 Best Fits to the Variation in Material Damping Ratio with Shearing Strain at the Estimated Mean Effective Confining Pressure from Torsional Shear (TS) Tests of Soil Specimens from the East Bay Bridge Site..... 41

1. INTRODUCTION

The dynamic properties of four intact soil samples from the site of the new San Francisco - Oakland Bay Bridge (termed the new East Bay Bridge herein) were evaluated in the Soil Dynamics Laboratory at the University of Texas at Austin (UTA). The samples were taken from three borings in San Francisco Bay by Fugro West, Inc. using a push-tube sampler with a latch-out assembly. Four sealed Shelby tube sections of intact material were delivered to the Geotechnical Engineering Center at UTA in early June, 1998. Each Shelby tube section was a thin-walled steel tube with an outside diameter of 3 in. (7.6 cm), a wall thickness of 1/16 in. (0.16 cm), and a length of about 6 in. (15.2 cm). The samples were recovered from Boring 98-20 (Sample Nos. 27 and 91), Boring 98-19 (Sample No. 34) and Boring 98-8 (Sample No. 71).

Before dynamic testing, each sample was extruded from the Shelby tube section. The samples were trimmed into circular, cylindrical specimens with a nominal height of 4 in. (10.2 cm) and a nominal diameter of 2 in. (5.1 cm). Trimming was quite easy and straightforward. However, Specimen UTA-10-A from Sample No. 27 was found to contain several thin metal strips which were each about 3 in. (7.6 cm) long by about 1 in. (2.5 cm) wide. These metal strips were removed from the periphery of the soil sample during trimming, resulting in an intact specimen.

All four intact specimens were dynamically tested using combined resonant column and torsional shear (RCTS) equipment as described in Section 2. Initial properties of these specimens are given in Table 1. Three of the specimens classify as CH materials and the fourth specimen classify as a CL material in the Unified Soil Classification System. Grain size distribution curves of these samples are presented in Figure 1.

This work was performed for a joint venture between Fugro, Inc. and Earth Mechanics, Inc. The project is termed the East-Span Seismic Safety Project: Phase I - Site Characterization. The project number is 98 - 420035, and Mr. Tom McNeilan is the contact person at Fugro West, Inc.

Table 1 Initial Properties of Specimens Tested from the East Bay Bridge Site

Sample No. (UT ID)	Specimen Depth ft (m)	Soil Type (Unified Soil Classification)	Water Content %	Dry Unit Weight pcf (gr/cm^3)	Liquid Limit %	Plasticity Index %	R_{200}[1] %	Void Ratio[2] e	Specimen Diameter in. (cm)	Specimen Height in. (cm)	Specific Gravity[3] G_s	Degree of Saturation %
27 (UTA-10-A)	27.5 (8.4)	Fat Clay (CH)	50	71 (1.14)	63	36	7	1.38	2.02 (5.12)	3.83 (9.73)	2.70	98
34 (UTA-10-B)	36.5 (11.1)	Fat Clay (CH)	58	65 (1.03)	75	43	3	1.61	2.04 (5.17)	3.96 (10.05)	2.70	97
71 (UTA-10-C)	79.0 (24.1)	Fat Clay (CH)	57	68 (1.08)	89	53	4	1.50	2.01 (5.11)	3.94 (10.02)	2.70	~100
91 (UTA-10-D)	231 (70.5)	Lean Clay (CL)	30	92 (1.48)	46	19	9	0.83	2.02 (5.14)	3.53 (8.97)	2.70	98

Notes:

1. R_{200} = Percent of soil sample by weight remaining on #200 sieve.
2. Void ratios were calculated based on the assumed value of G_s.
3. G_s was assumed equal to 2.70.

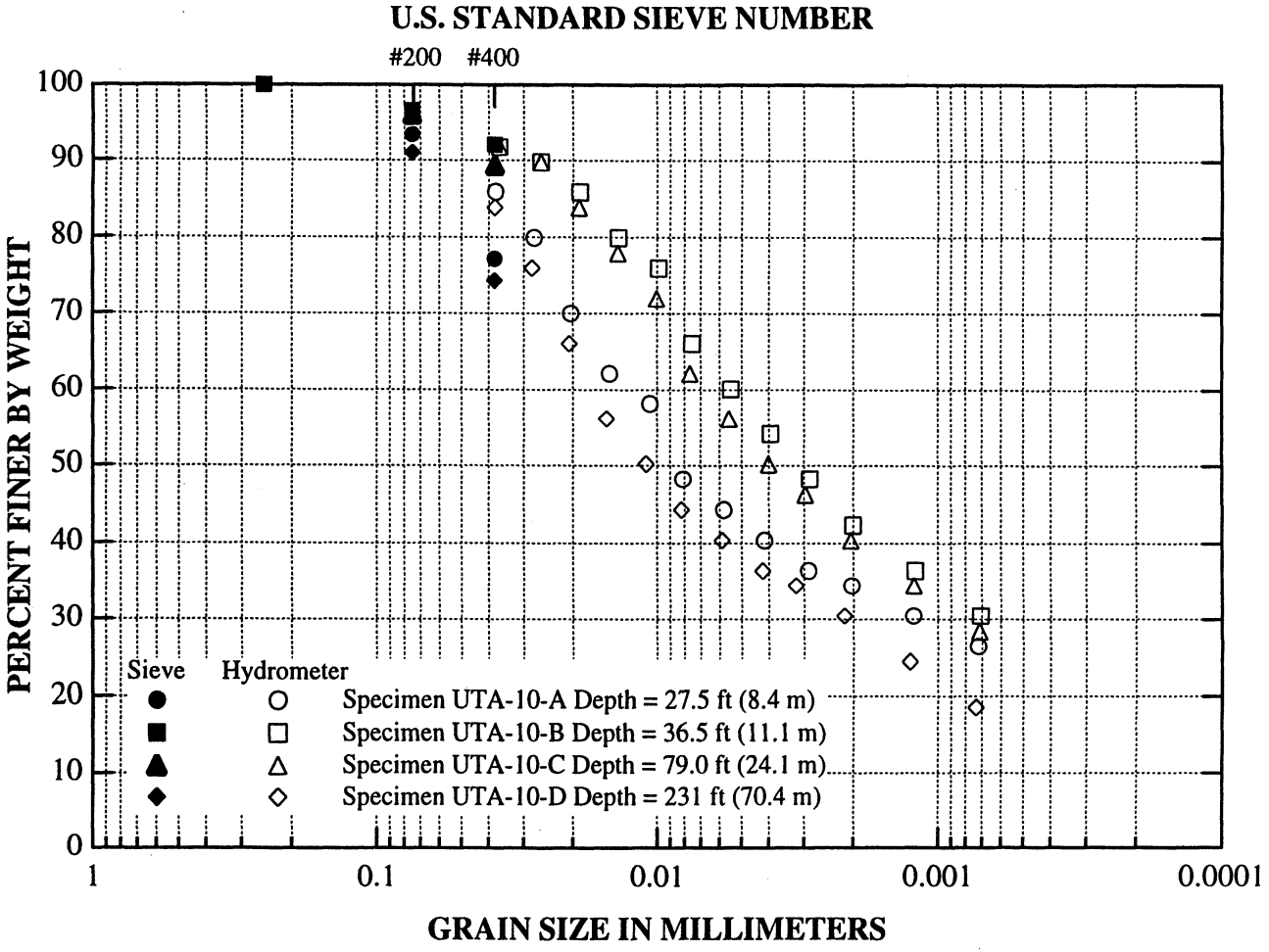

Figure 1 Grain Size Distribution Curves of Samples from the East Bay Bridge Site.

2. DYNAMIC LABORATORY TESTS

Combined resonant column and torsional shear (RCTS) equipment was used to investigate the dynamic characteristics of the four intact specimens. This equipment is described in detail in Appendix A. Verification of the equipment constants is described in Section A.5 of Appendix A. The dynamic characteristics of concern are the shear modulus, G, and the material damping ratio in shear, D. These parameters were evaluated to determine the influence of the following variables on them.

1. Magnitude of the isotropic state of stress, σ_o'.

   Five isotropic pressures were used for each specimen which ranged from below to above the estimated in situ mean effective stress at the sample depth.

2. Time of confinement at each isotropic state of stress, t.

   Confinement times at each pressure were at least 1000 minutes for all specimens.

3. Shearing strain amplitude, γ.

   Strains ranged from the small-strain range, less than about 0.001% for these fine grained soils, to rather large strain amplitudes, above 0.1%.

4. Number of cycles of loading, N.

   Ten cycles of loading were used in the torsional shear (TS) test followed by about 1000 cycles in the resonant column (RC) test.

5. Excitation frequency, f.

   Frequencies ranging from 0.1 Hz to about 5 Hz were used in the TS test while the frequency associated with resonance in the RC test varied with soil stiffness and ranged from between 19 Hz and 107 Hz.

6. Stress History.

   Nonlinear values of G and D were evaluated at consolidation states in the normally consolidated and overconsolidated ranges.

2.1. Test Program

Dynamic testing of each soil specimen involved the evaluation of G and D over a range of isotropic confining pressures. Typically, five isotropic confining pressures were used in a loading sequence, with the isotropic confining pressure, σ_o', doubled upon completion of the required tests at the previous pressure. Low-amplitude resonant column testing was performed at each level of σ_o' to determine the effects of magnitude of confinement and time of confinement on the small-strain shear modulus, G_{max}, and small-strain material damping ratio, D_{min}. Low-amplitude dynamic tests are defined as those tests in which the resonant amplitude did not exceed 0.003% and was well below that level except for the softest specimens at the lowest confining pressures.

For each laboratory specimen, the range in confining pressures was based on the estimated in situ mean effective stress, σ_m'. The estimated in situ mean effective stress, σ_m', was determined by assuming the following: 1) the water table exists above the top of the soil deposit, 2) the total unit weight of the soil was determined by measuring the volume and weight of the trimmed specimen before testing or by measuring an intact section of the sample after extrusion from the Shelby tube, and 3) the effective coefficient of earth pressure at rest, K_o', was assumed to be in the range of 0.5 to 0.75. The resulting values of σ_m' for each sample are given in Table 2. Once the value of σ_m' was estimated, the range in confining pressures over which G and D would be evaluated was determined. Isotropic confining pressures which ranged from below to above σ_m' were selected.

A summary of all confining pressures at which low-amplitude resonant column tests were performed is given in Table 2. In addition to small-strain testing, high-amplitude tests were also performed on each specimen at two or more confining pressures, with one pressure typically at the estimated in situ mean effective stress and another at four times the estimated in situ mean effective stress. Also, for two of the four specimens, high-amplitude testing was performed at an unloading pressure which was 0.25 times the maximum pressure in the loading sequence. High-amplitude testing is defined as any test in which the peak shearing strain exceeds 0.003%. High-amplitude

Table 2 Summary of Resonant Column and Torsional Shear Tests Performed on the Specimens from the East Bay Bridge Site

Sample No. (UT ID)	Specimen Depth ft (m)	Estimated In-Situ Mean Effective Stress[1], σ'_m psf (kPa)	Isotropic Test Pressure		
			Low-Amplitude RC and TS Tests[2] psf (kPa)	High-Amplitude RC Tests[3] psf (kPa)	High-Amplitude TS Tests[3] psf (kPa)
27 (UTA-10-A)	27.5 (8.4)	1007 (48)	288,576,1152,2304,4608,1152 (14,28,55,110,221,55)	1152,4608,1152 (55,221,55)	1152,4608,1152 (55,221,55)
34 (UTA-10-B)	36.5 (11.1)	1205 (58)	288,576,1152,2304,4608 (14,28,55,110,221)	1152,4608 (55,221)	1152,4608 (55,221)
71 (UTA-10-C)	79.0 (24.1)	2296 (110)	576,1152,2304,4608,9216,2304 (28,55,110,221,442,110)	2304,9216,2304 (110,442,110)	2304,9216,2304 (110,442,110)
91 (UTA-10-D)	231 (70.5)	8824 (423)	2160,4320,8640,17280,34560 (104,207,414,828,1657)	8640,34560 (414,1657)	8640,34560 (414,1657)

Notes:

1. Estimated in-situ mean effective stress based on an effective coefficient of earth pressure at rest between 0.5 and 0.75.
2. Low-amplitude tests were performed at shearing strains below 0.003 %.
3. High-amplitude tests were performed at shearing strains above 0.003 %.

testing was composed of two series of tests. The first involved cyclic torsional shear (TS) testing as illustrated in Figure 2. A complete set of torsional shear tests requires about two hours to perform at an individual confining pressure. Torsional shear tests were conducted with the drainage line open, and involved shearing strains, γ, from less than 0.001% to above 0.1%. The majority of the measurements were performed at 0.5 Hz and are labeled as TS1 in Figure 2. However, two sets of TS tests at $\gamma \approx 0.001\%$ and $\gamma \approx 0.01\%$ were conducted to evaluate the effect of excitation frequency on G and D at these strains. In these tests (denoted as TS2 in Figure 2), ten cycles of loading were applied at about four different frequencies ranging from 0.1 Hz to about 5 Hz.

After the TS tests were completed, confinement of the sample was continued at the given confining pressure, and a series of high-amplitude resonant column (RC) tests was performed. However, before high-amplitude RC testing commenced, small-strain RC tests were performed to determine if any changes in the soil skeleton had occurred from the TS tests. In all cases, essentially no changes in G_{max} or D_{min} from the TS tests were measured.

Once the small-strain datum was re-established after the TS tests, high-amplitude resonant column testing was conducted to evaluate the influence of strain amplitude on G and D. This series of tests is illustrated in Figure 3. A complete set of resonant column tests that took about two hours to perform, was performed with the drainage line open just as in the case of the TS tests, and typically involved shearing strains from less than 0.001% to about 0.1%, depending on the soil stiffness. In these tests, about 1000 cycles of loading were required at each strain measurement.

Upon completion of the high-amplitude RC tests, low-amplitude RC tests were again performed to determine if any changes in the soil skeleton had occurred from the high-amplitude tests. In some cases, changes occurred. At that point, confinement of the sample at σ_m' was continued until G_{max} and D_{min} returned to the values before the high-amplitude tests or the change in values was noted in the next stage of testing.

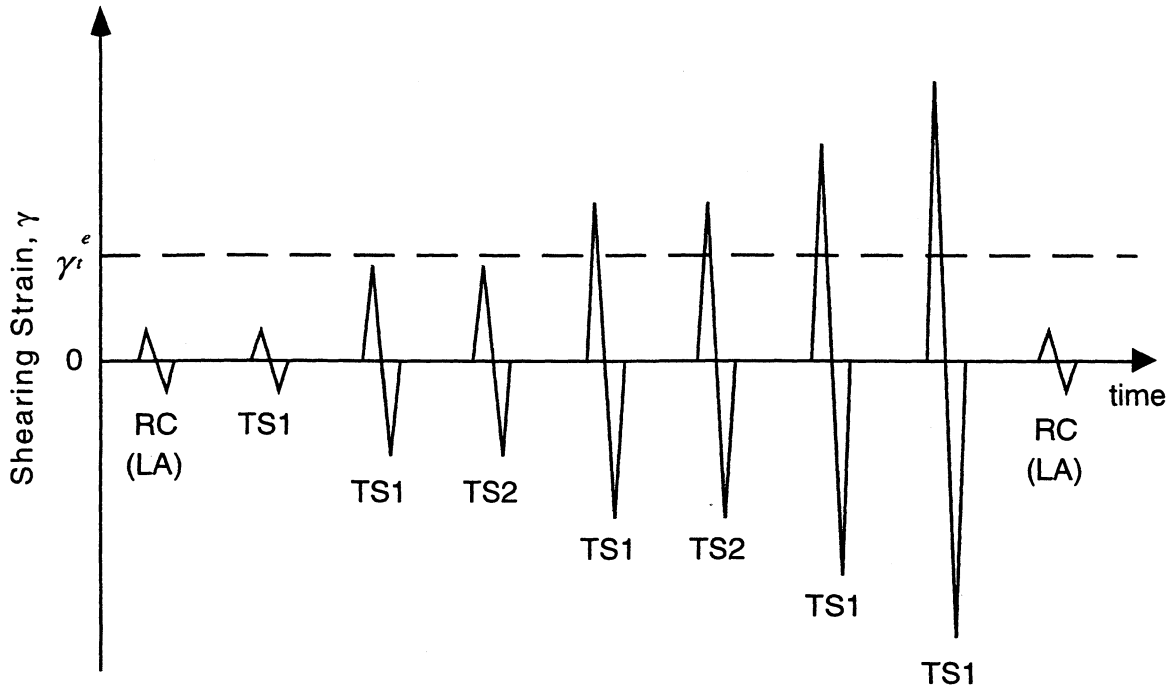

γ_t^e = elastic threshold strain; below γ_t^e, G is constant and equal to G_{max}

RC (LA) = resonant column test at low-amplitudes (strains < 0.003%)

TS1 = torsional shear test in which 10 cycles are applied at 0.5 Hz.

TS2 = torsional shear test in which 10 cycles are applied at each of approximately 4 frequencies between 0.1 to about 5 Hz.

Figure 2 Testing Procedure Used in the Torsional Shear (TS) Test to Investigate the Effects of Strain Amplitude, Number of Loading Cycles, and Excitation Frequency on G and D of Intact Soil Specimens from the East Bay Bridge Site.

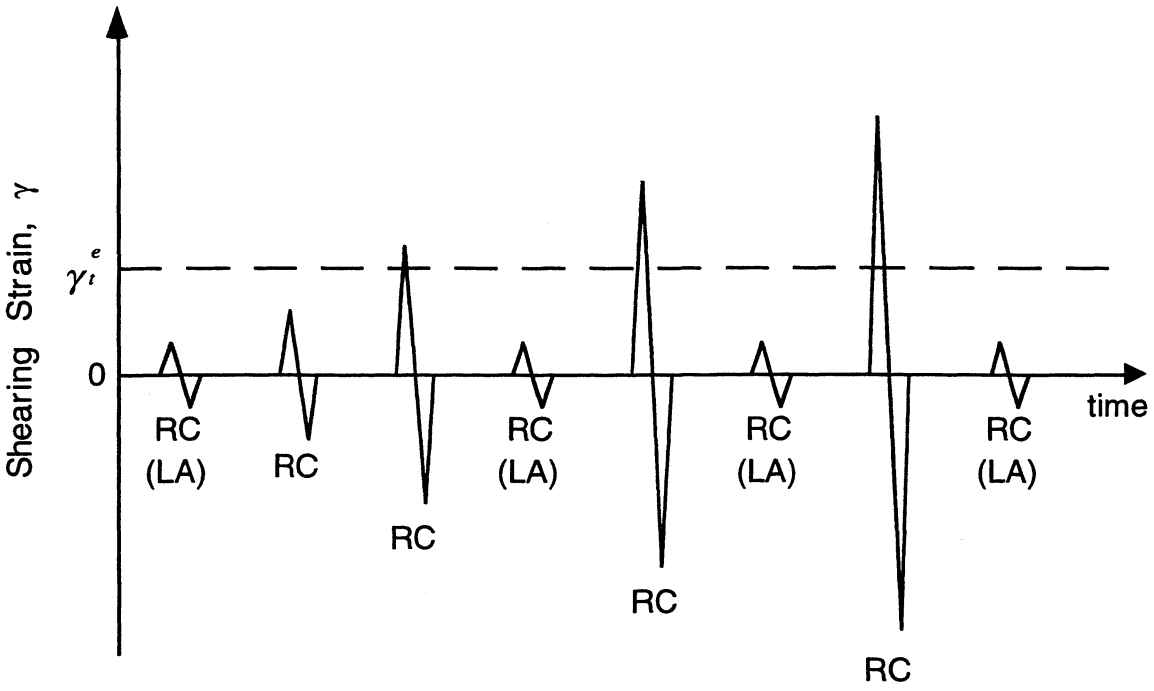

γ_t^e = elastic threshold strain; below γ_t^e, G is constant and equal to G_{max}

RC (LA) = resonant column test at low-amplitudes (strains < 0.003%)

RC = resonant column test in which about 1000 cycles of loading is applied during each measurement

Figure 3 Testing Procedure Used in the Resonant Column (RC) Test to Investigate the Effect of Strain Amplitude on G and D Intact Soil Specimens from the East Bay Bridge Site.

2.2. Test Results

The results of the RC and TS tests are shown in Appendices B through E for Specimens UTA-10-A through UTA-10-D (Sample Nos. 27, 34, 71 and 91), respectively. Each appendix presents all test results from one specimen. As an example, consider the general presentation of dynamic test results presented in Appendix B. The dynamic tests results are presented as follows:

1. Figure B.1 shows the variation in low-amplitude shear wave velocity with magnitude and duration of isotropic confining pressure from resonant column tests

2. Figure B.2 shows the variation in low-amplitude shear modulus with magnitude and duration of isotropic confining pressure from resonant column tests

3. Figure B.3 shows the variation in low-amplitude material damping ratio with magnitude and duration of isotropic confining pressure from resonant column tests

4. Figure B.4 shows the variation in void ratio with magnitude and duration of isotropic confining pressure from resonant column tests

5. Figure B.5 shows the variation in low-amplitude shear wave velocity with effective confining pressure from resonant column tests

6. Figure B.6 shows the variation in low-amplitude shear modulus with effective confining pressure from resonant column tests

7. Figure B.7 shows the variation in low-amplitude material damping ratio with effective confining pressure from resonant column tests

8. Figure B.8 shows the variation in void ratio with effective confining pressure from resonant column tests

9. Figure B.9 shows the comparison of the variation in shear modulus with shearing strain, stress history and isotropic effective confining pressure from RCTS tests

10. Figure B.10 shows the comparison of the variation in normalized shear modulus with shearing strain, stress history and isotropic effective confining pressure from RCTS tests

11. Figure B.11 shows the comparison of the variation in material damping ratio with shearing strain, stress history and isotropic effective confining pressure from RCTS tests

12. Figure B.12 shows the comparison of the variation in normalized material damping ratio with shearing strain, stress history and isotropic effective confining pressure from RCTS tests

13. Figure B.13 shows the comparison of the variation in shear modulus with loading frequency, shearing strain, stress history and isotropic effective confining pressure from RCTS tests

14. Figure B.14 shows the comparison of the variation in material damping ratio with loading frequency, shearing strain, stress history and isotropic effective confining pressure from RCTS tests

15. Table B.1 shows the variation in low-amplitude shear modulus, low-amplitude material damping ratio and void ratio with effective isotropic confining pressure from RC tests

16. Table B.2 shows the variation in shear modulus, normalized shear modulus and material damping ratio with shearing strain from RC tests at an effective confining pressure of 8 psi (1.15 ksf = 55.2 kPa)

17. Table B.3 shows the variation in shear modulus, normalized shear modulus and material damping ratio with shearing strain from TS tests at an effective confining pressure of 8 psi (1.15 ksf = 55.2 kPa)

18. Table B.4 shows the variation in shear modulus, normalized shear modulus and material damping ratio with shearing strain from RC tests at an effective confining pressure of 32 psi (4.61 ksf = 220.9 kPa)

19. Table B.5 shows the variation in shear modulus, normalized shear modulus and material damping ratio with shearing strain from TS tests at an effective confining pressure of 32 psi (4.61 ksf = 220.9 kPa)

20. Table B.6 shows the variation in shear modulus, normalized shear modulus and material damping ratio with shearing strain from RC tests at an effective confining pressure of 8 psi (unloading)

21. Table B.7 shows the variation in shear modulus, normalized shear modulus and material damping ratio with shearing strain from TS tests at an effective confining pressure of 8 psi (unloading)

3. DISCUSSION OF RESULTS

3.1. Small-Strain Shear Modulus and Material Damping Ratio

Small-Strain Shear Modulus

The variations of small-strain (low-amplitude) shear modulus, G_{max}, with effective isotropic confining pressure, σ_o', for the four specimens are presented in a summary form in Figure 4. Only the values of G_{max} measured in the loading series are shown in Figure 4. The small-strain shear moduli have also been adjusted for void ratio using the F(e) term presented by Hardin (1978). The Hardin (1978) equation is:

$$G_{max} * F(e) = A * P_a^{(1-n)} * \sigma_o'^{(n)} \quad (1)$$

where;

$F(e) = 0.3 + 0.7e^2$,

e = void ratio,

σ_o' = effective isotropic confining pressure in the same units as P_a,

P_a equals one atmosphere (2117 psf or 101 kPa), and

A and n are dimensionless constants.

The log G_{max} * F(e) - log σ_o' relationships are presented in Figure 5. Each void-ratio-adjusted relationship is fitted with the basic Hardin (1978) equation presented in Equation 1. The fitted relationships are shown by the solid line in Figures 6 through 9 for Specimens UTA-10-A through UTA-10-D (Samples Nos. 27, 34, 71 and 91), respectively.

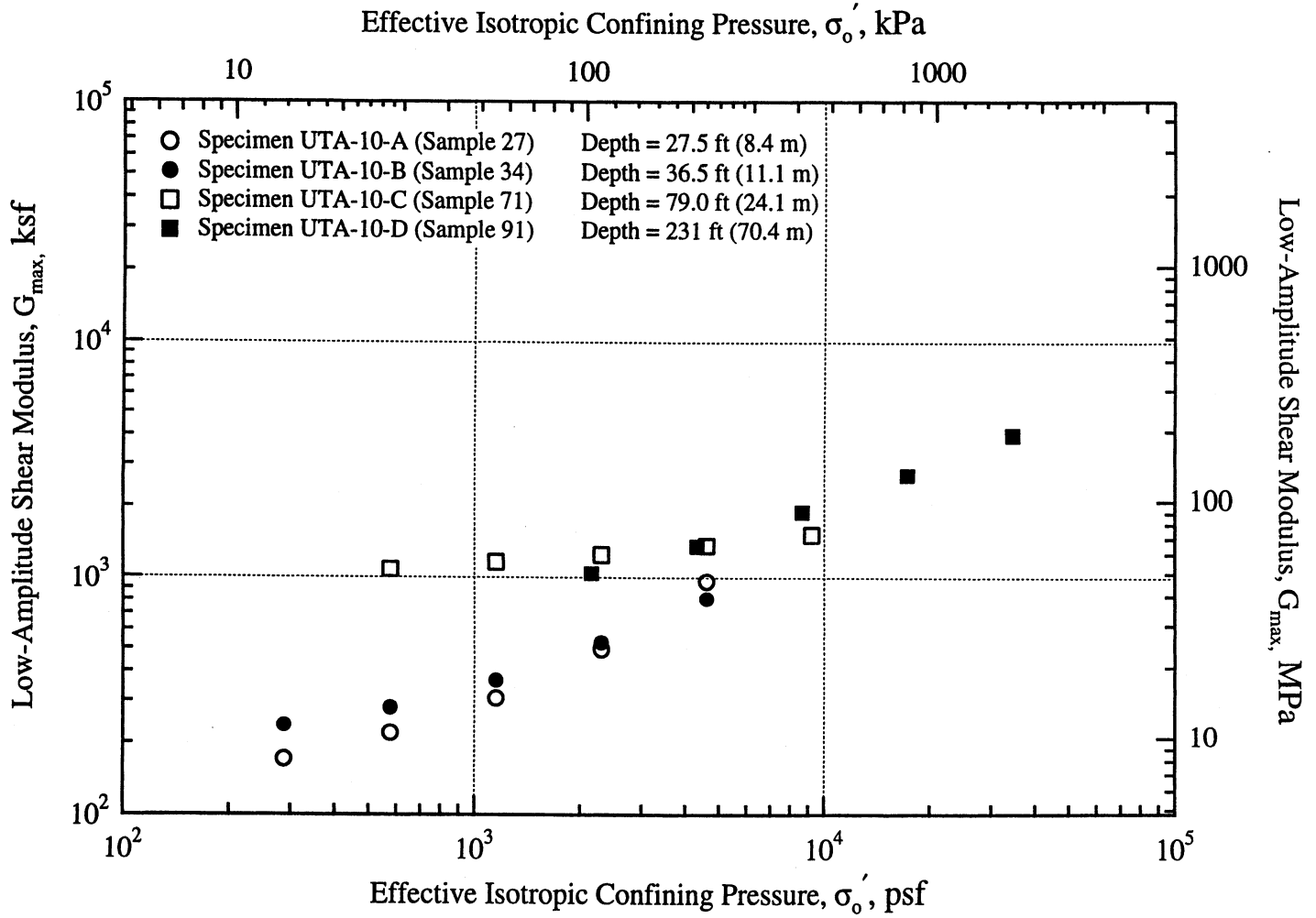

Figure 4 Variation in Low-Amplitude Shear Modulus with Effective Isotropic Confining Pressure from Resonant Column (RC) Tests of Soil Specimens from the East Bay Bridge Site.

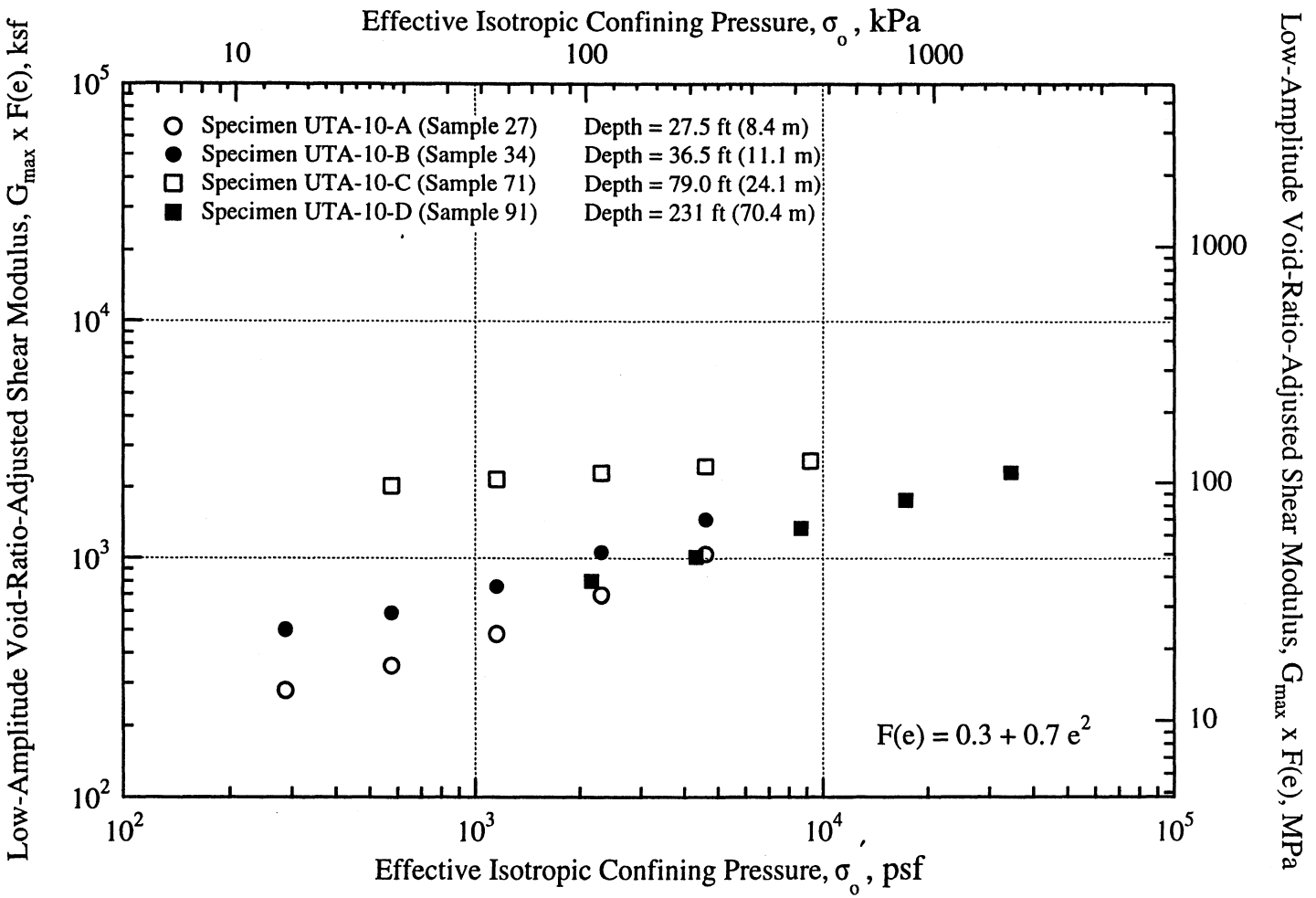

Figure 5 Variation in Low-Amplitude, Void-Ratio-Adjusted Shear Modulus with Effective Isotropic Confining Pressure from Resonant Column (RC) Tests of Soil Specimens from the East Bay Bridge Site.

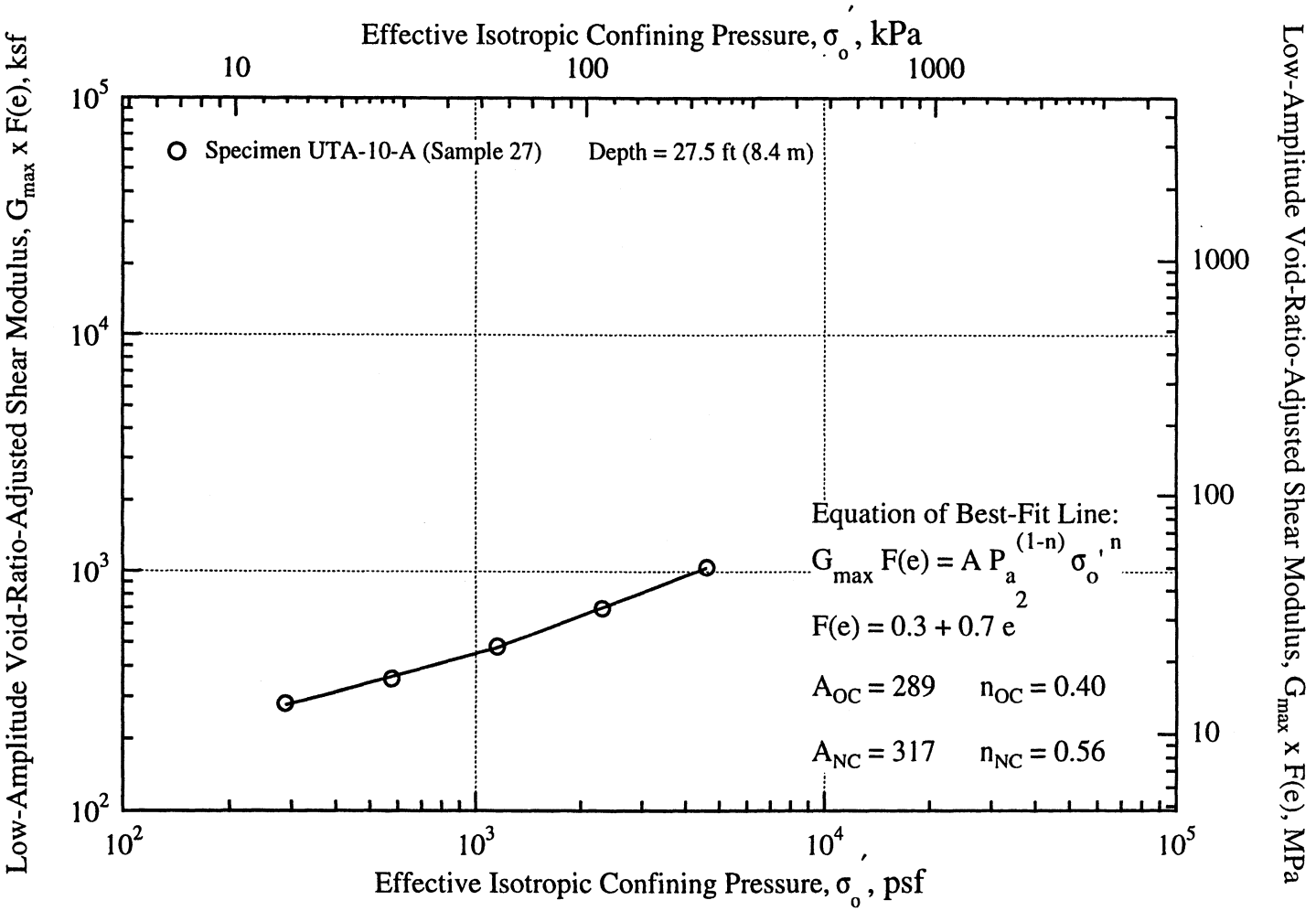

Figure 6 Best-Fit Curve to log G_{max} x F(e) - log σ_o' Relationship from Resonant Column (RC) Tests of Specimen UTA-10-A from the East Bay Bridge Site.

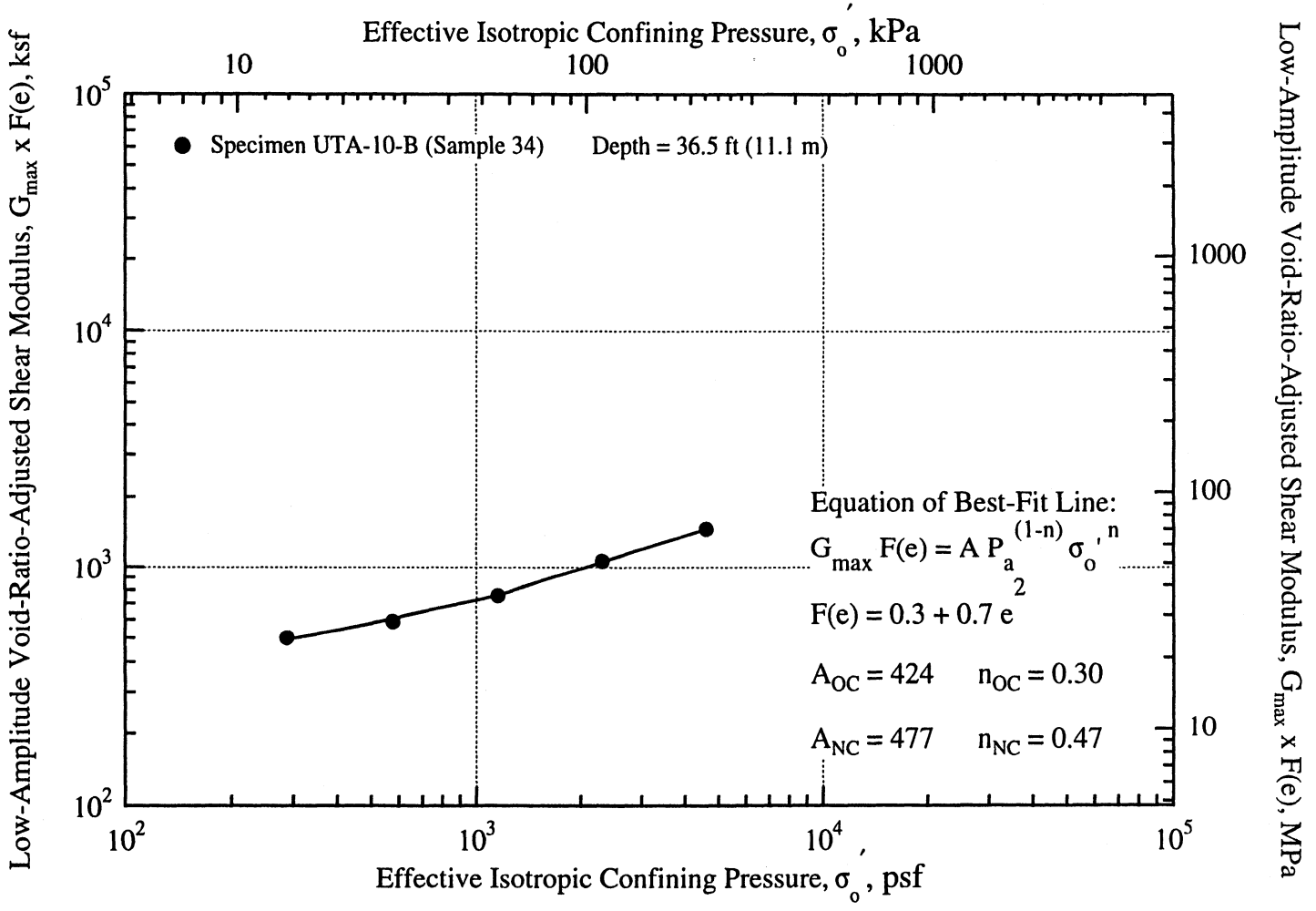

Figure 7 Best-Fit Curve to log G_{max} x F(e) - log σ_o' Relationship from Resonant Column (RC) Tests of Specimen UTA-10-B from the East Bay Bridge Site.

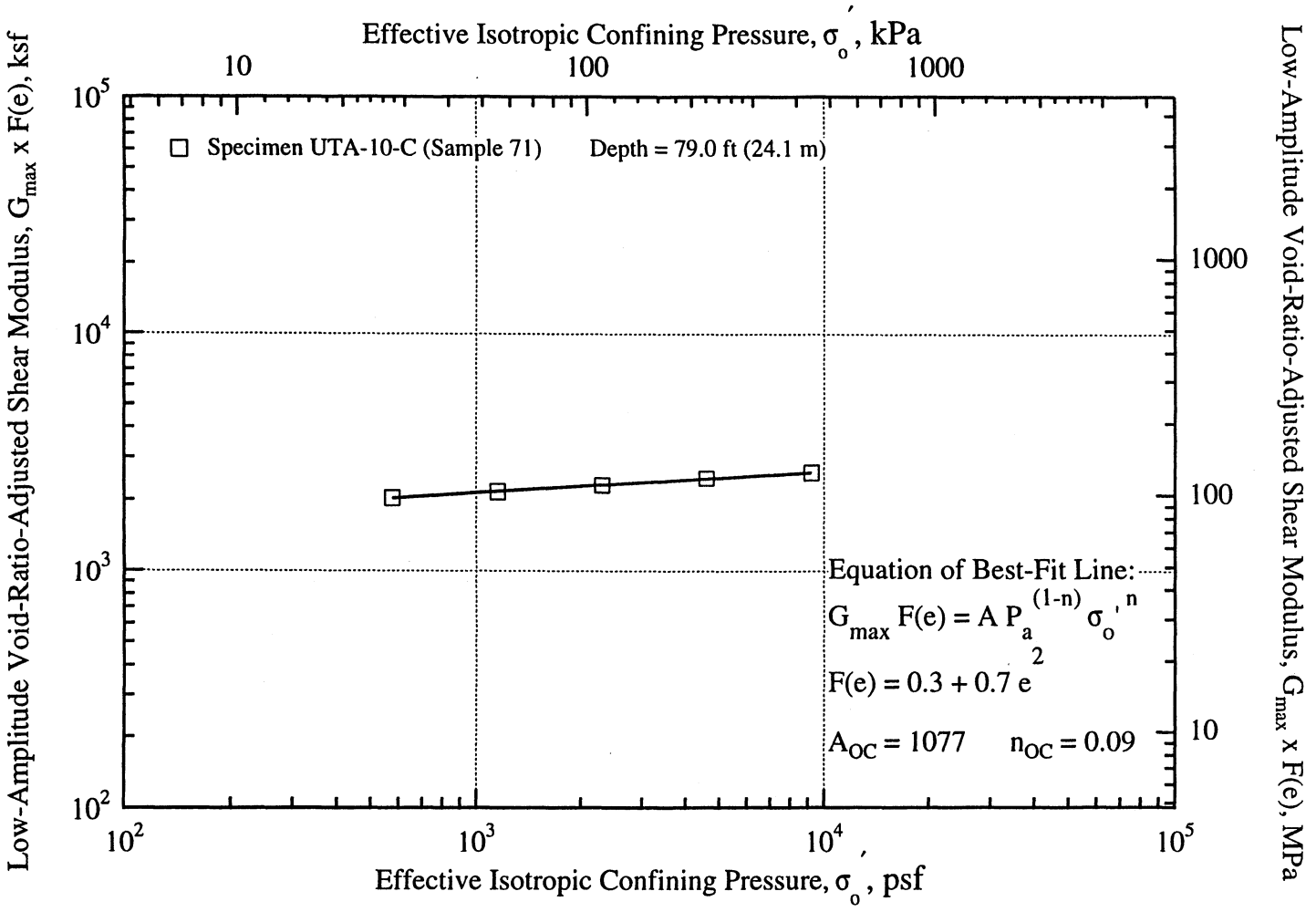

Figure 8 Best-Fit Curve to log G_{max} x F(e) - log σ_o' Relationship from Resonant Column (RC) Tests of Specimen UTA-10-C from the East Bay Bridge Site.

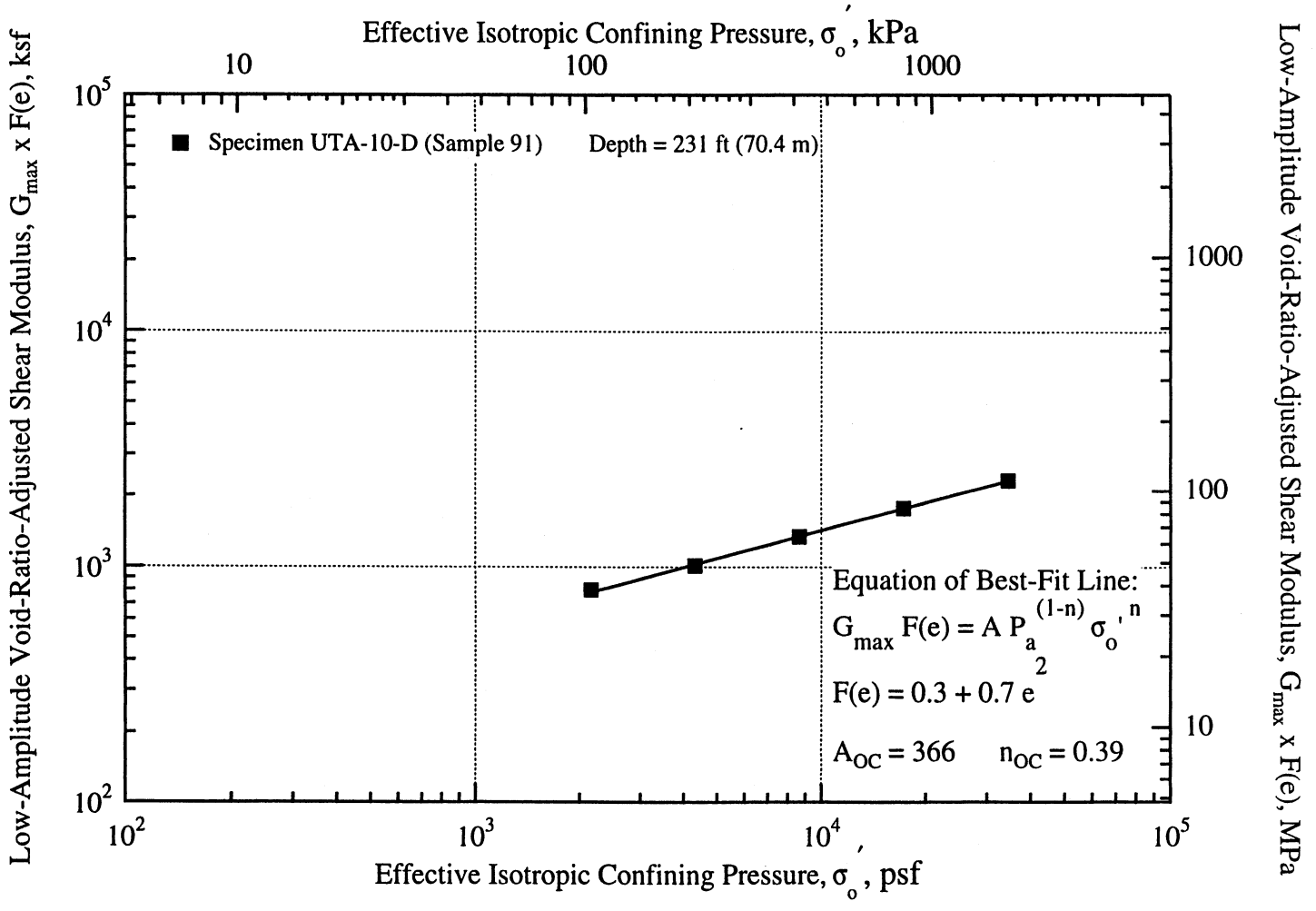

Figure 9 Best-Fit Curve to log G_{max} x F(e) - log σ_o' Relationship from Resonant Column (RC) Tests of Specimen UTA-10-D from the East Bay Bridge Site.

For all four specimens, comparisons of the measurements with Hardin's equation show that these soils exhibit some "memory" of stress history; that is, they show the effect of overconsolidation. The constants of the best-fit lines calculated by least-squares fitting are summarized in Table 3. The two shallower specimens UTA-10-A (Sample No. 27) and UTA-10-B (Sample No. 34) exhibit overconsolidated behavior followed by normally consolidated behavior over the loading pressure sequence used in these tests. The values of n in the normally consolidated stress range in these fits of 0.47 to 0.56 are within the range of expected values. On the other hand, the two deeper specimens exhibit only overconsolidated behavior over the loading pressures used in these tests, indicating that the overconsolidation ratios associated with these two specimens are greater than 4.

Table 3 A and n Dimensionless Constants from the Least-Squares Fits to the Hardin (1978) Equation.

	Overconsolidated		Normally Consolidated	
Sample Number (Specimen ID)	A	n	A	n
27 (UTA-10-A)	289	0.40	317	0.56
34 (UTA-10-B)	424	0.30	477	0.47
71 (UTA-10-C)	1077	0.09	–	–
91 (UTA-10-D)	366	0.39	–	–

Small-Strain Material Damping Ratio

The variations of the small-strain material damping ratio, D_{min}, with effective isotropic confining pressure, σ_o', for the four specimens are presented in Figure 10. As expected, there is a decrease in D_{min} with increasing σ_o' (Kim, 1991; Hwang, 1997; and Darendeli, 1997).

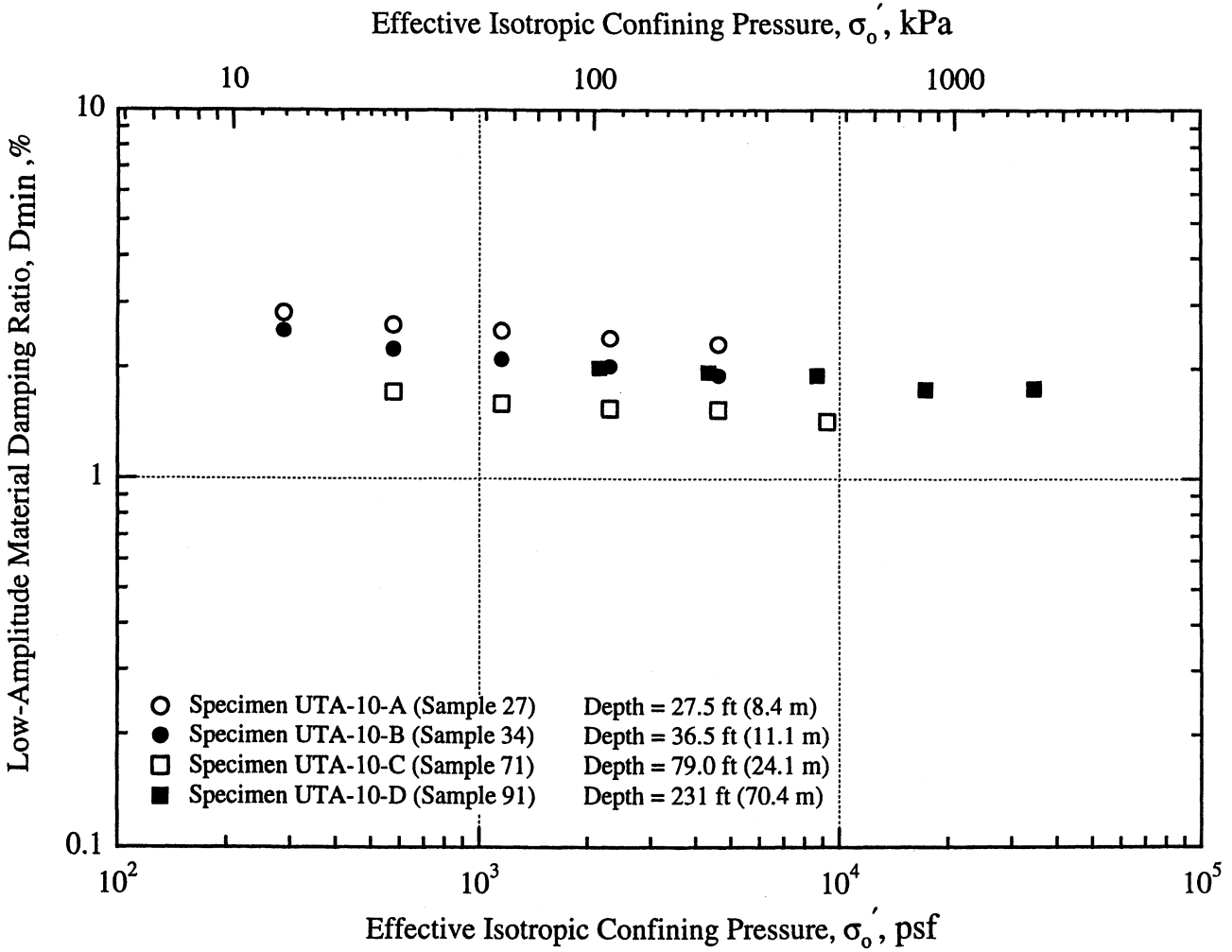

Figure 10 Variation in Low-Amplitude Material Damping Ratio with Effective Isotropic Confining Pressure from Resonant Column (RC) Tests of Soil Specimens from the East Bay Bridge Site.

Void Ratio

The variations in void ratio with σ_o' for all specimens are shown in Figure 11. All four specimens exhibited a similar trend with void ratio decreasing as σ_o' increased.

Excitation Frequency

Figure 12 shows the effect of loading frequency on shear modulus at low strains (γ = 0.001 %) for the laboratory specimens. Figure 13 shows the same data normalized by the respective values of G_{max} at a loading frequency of 1 Hz, $G_{max\,1Hz}$.

Figure 14 shows the effect of loading frequency on the material damping ratio at low strains (γ = 0.001 %) for the laboratory specimens. Figure 15 shows the same data normalized by the respective values of D_{min} at a loading frequency of 1 Hz, $D_{min\,1Hz}$.

As seen in Figures 12 through 15, there is a more pronounced effect of frequency on D_{min} than G_{max}. This result is typical of all soils (Kim, 1991; Hwang, 1997; and Darendeli, 1997). The main effect of frequency on G_{max} and D_{min} occurs at frequencies above 1 Hz. (In the range of 0.01 to 1 Hz, there is very little effect of frequency on G_{max} and D_{min}.) Since the RC tests involve measurements at the resonant frequency of the specimen (19 to 107 Hz in these particular tests) and the TS tests involve measurements at considerably lower frequencies (0.01 to 5 Hz), the frequency dependency of G_{max} and D_{min} can easily be evaluated with combined RC and TS testing.

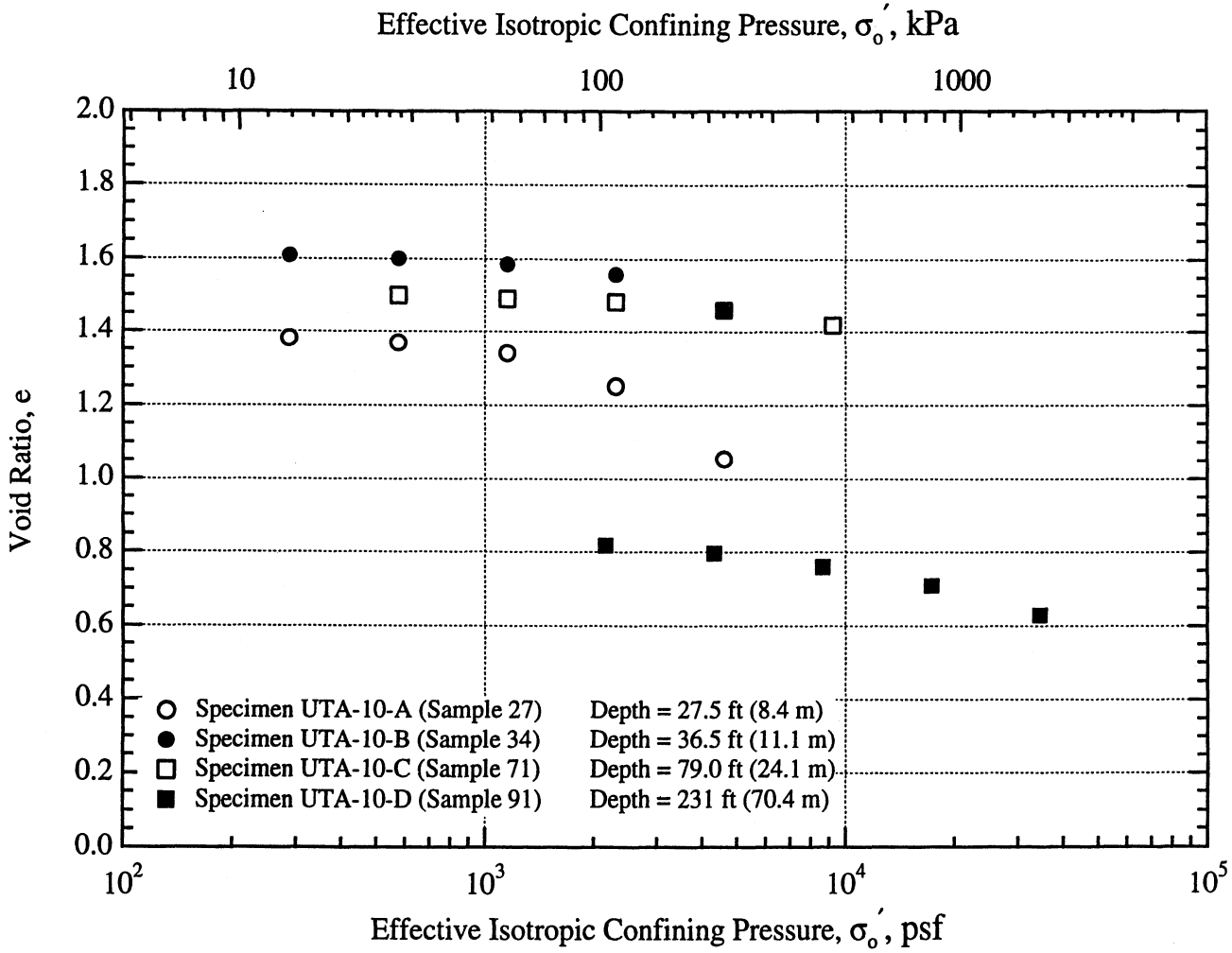

Figure 11 Variation in Void Ratio with Effective Isotropic Confining Pressure from Resonant Column (RC) Tests of Soil Specimens from the East Bay Bridge Site.

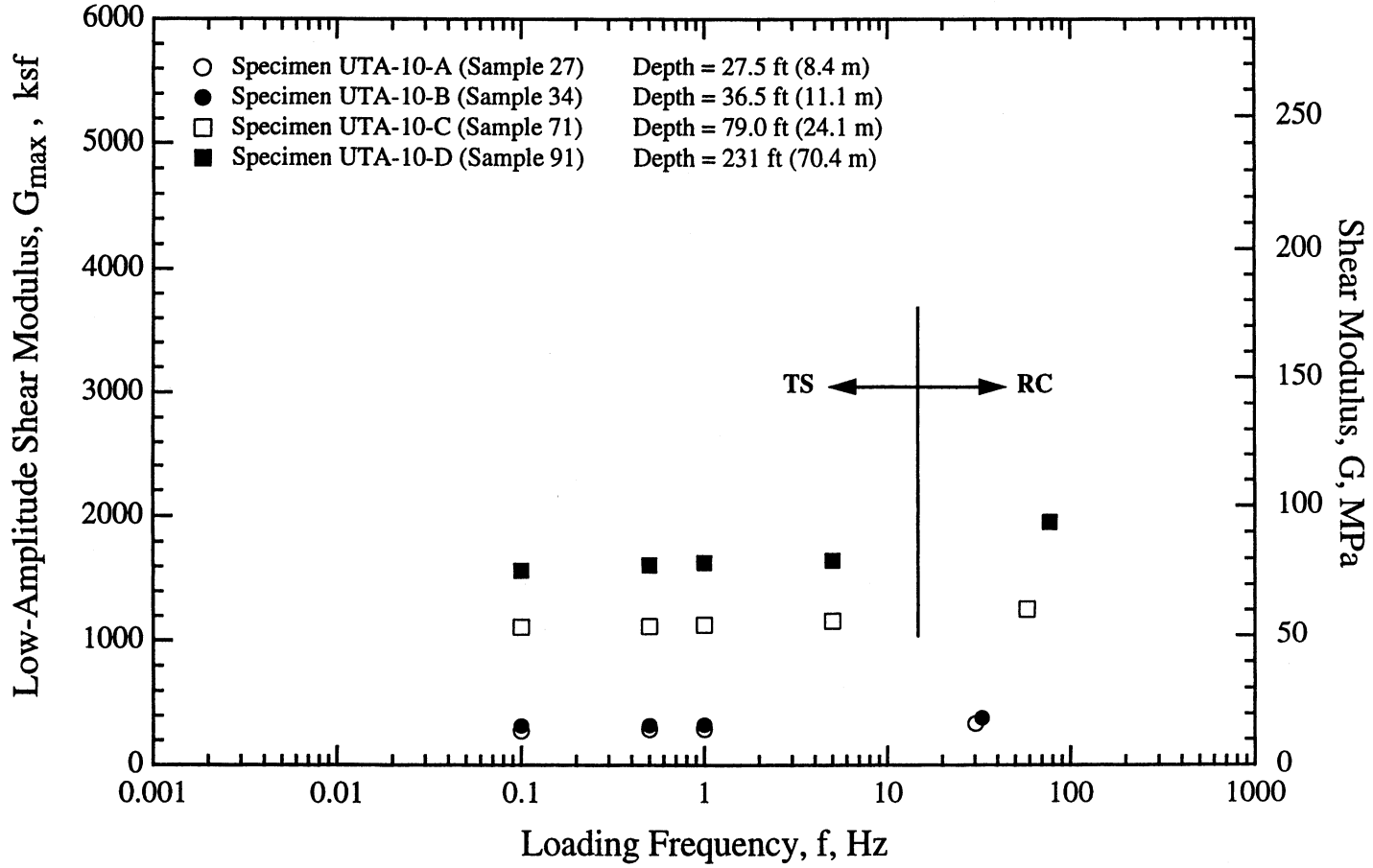

Figure 12 Variation in Low-Amplitude Shear Modulus with Loading Frequency at the Estimated Mean Effective Confining Pressure from Resonant Column (RC) and Torsional Shear (TS) Tests of Soil Specimens from the East Bay Bridge Site.

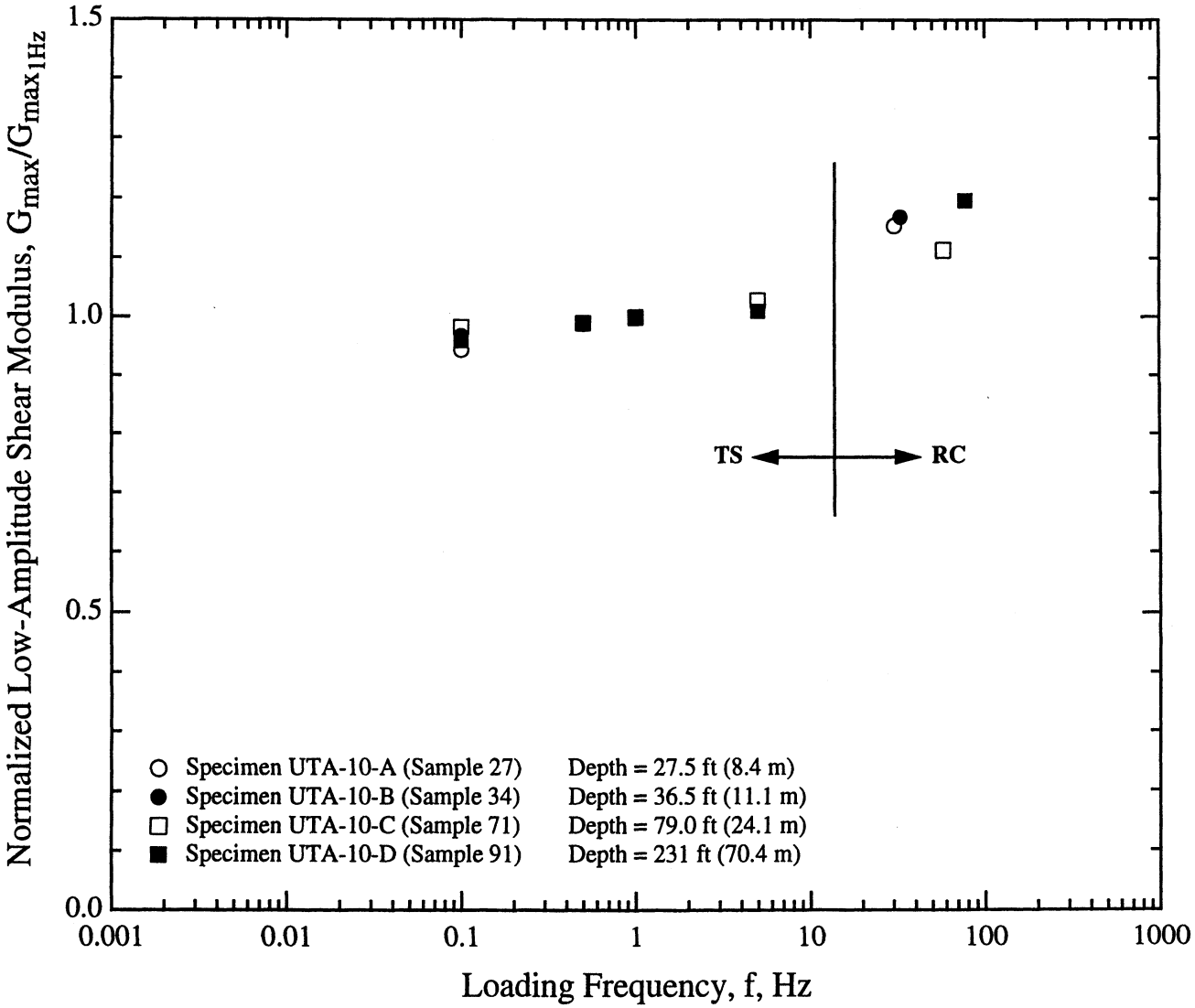

Figure 13 Variation in Normalized Low-Amplitude Shear Modulus with Loading Frequency at the Estimated Mean Effective Confining Pressure from Resonant Column (RC) and Torsional Shear (TS) Tests of Soil Specimens from the East Bay Bridge Site.

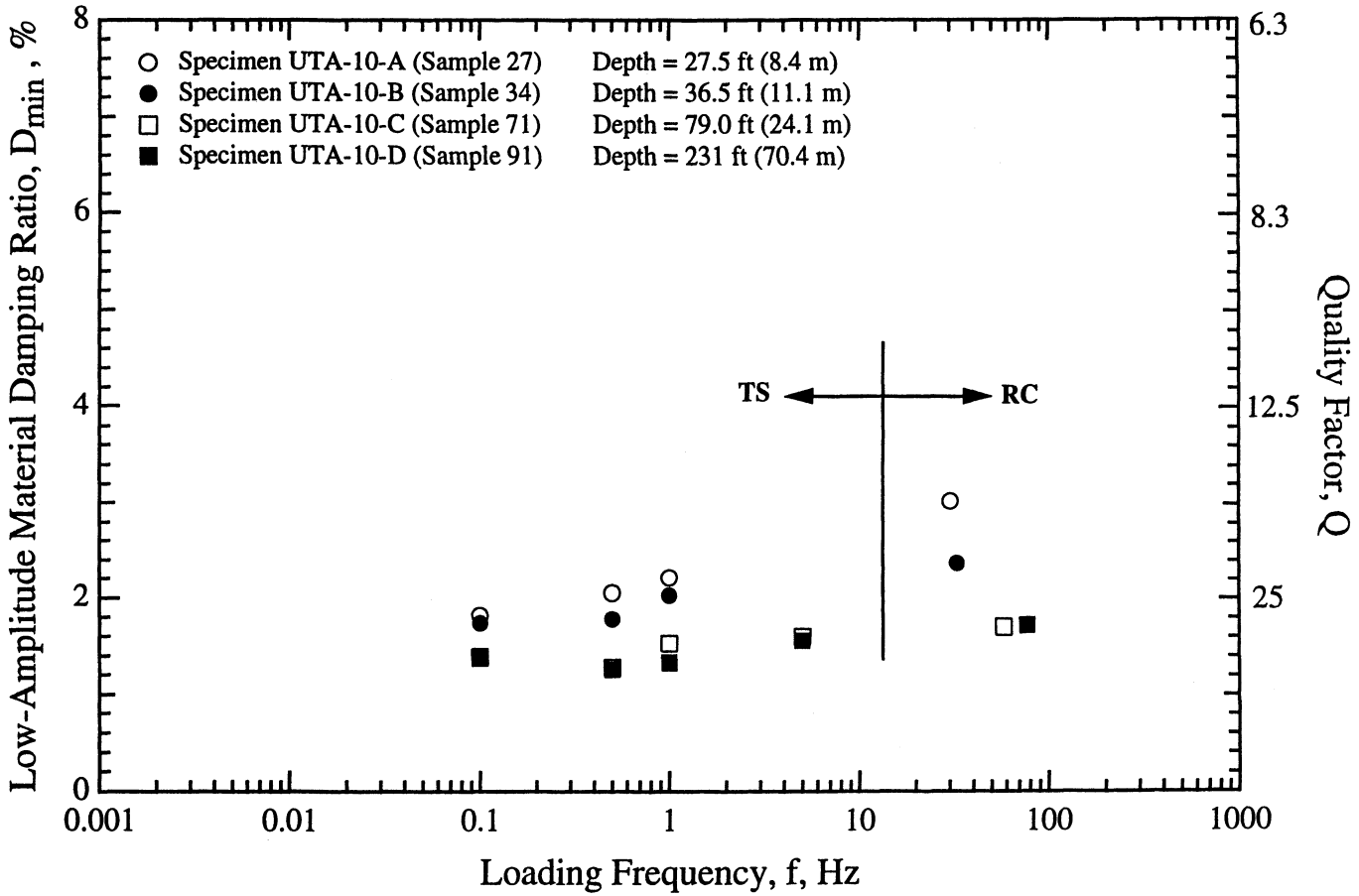

Figure 14 Variation in Low-Amplitude Material Damping Ratio with Loading Frequency at the Estimated Mean Effective Confining Pressure from Resonant Column (RC) and Torsional Shear (TS) Tests of Soil Specimens from the East Bay Bridge Site.

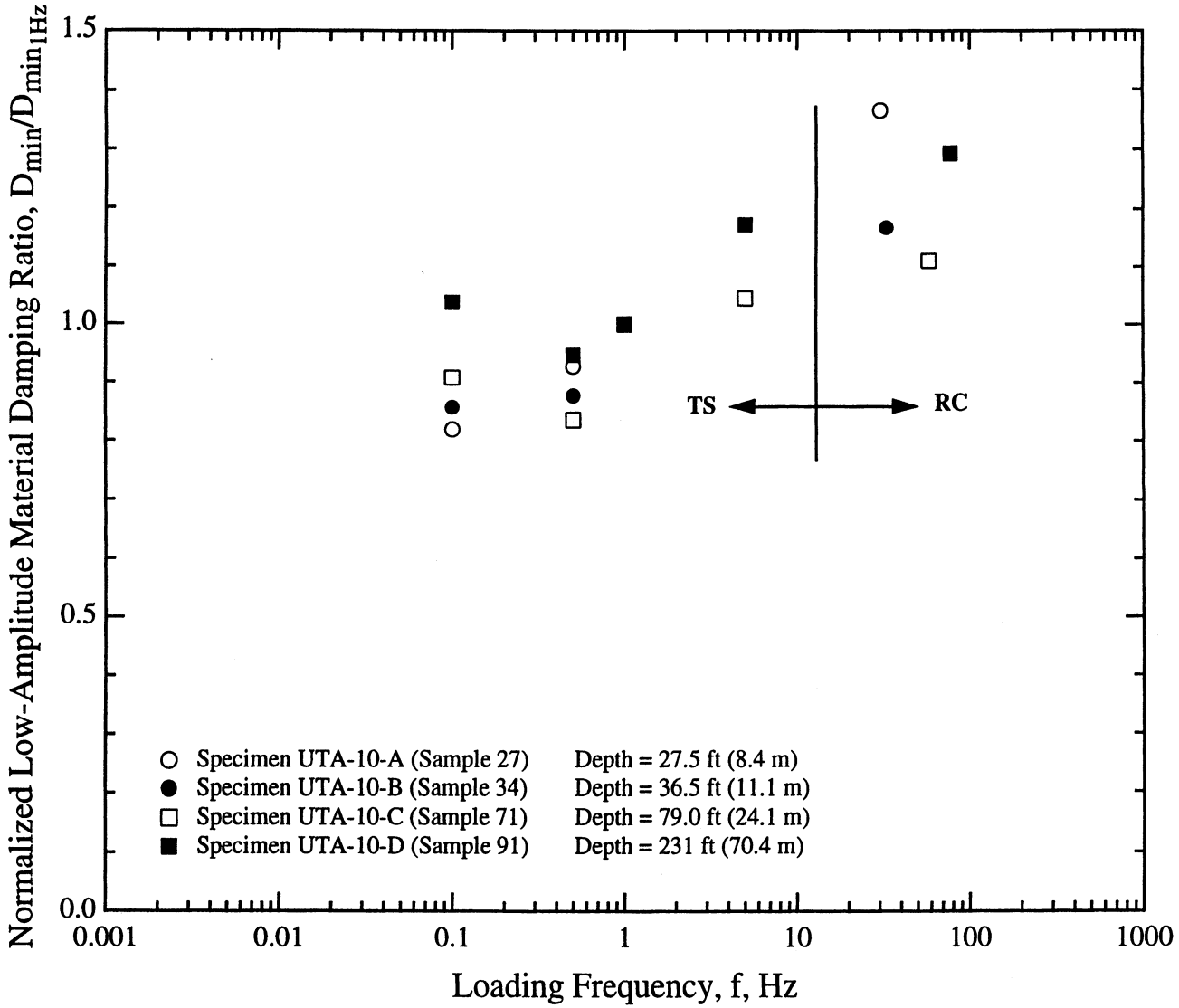

Figure 15 Variation in Normalized Low-Amplitude Material Damping Ratio with Loading Frequency at the Estimated Mean Effective Confining Pressure from Resonant Column (RC) and Torsional Shear (TS) Tests of Soil Specimens from the East Bay Bridge Site.

3.2. Nonlinear Shear Modulus and Material Damping Ratio

G - log γ Relationships

Results of all G - log γ relationships determined by the RC and TS tests are presented in Figure 16. It can be seen in this figure that the G - log γ relationships determined by the RC and TS tests are slightly different, mainly due to the effect of measurement frequency on G as discussed above for G_{max}. The normalized shear modulus (G/G_{max}) - log γ relationships are shown in Figures 17 through 19. The figures are arranged so that the first figure (Figure 17) shows the RC results. The next figure (Figure 18) shows the TS results. Figure 19 shows a comparison of the RC and TS results.

In Figures 17 through 19, the G/G_{max} - log γ relationship recommended by Seed et al. (1986) for sands is shown for comparison purposes. In addition, the separate relationships for sands and clays recommended by Idriss (1990) are also shown. As seen in Figure 19, the values for each cohesive specimen lie above the range proposed by Seed et al. (1986) as one would expect when comparing the behavior of sands and clays. The measured relationships cluster around the relationship suggested for clays by Idriss (1990). It is also clear that the loading frequency has a negligible effect on the normalized shear modulus curves. The modulus reduction curves are observed to shift to the right (specimens exhibiting more linear behavior) with increasing plasticity and increasing confining pressure.

Reference strains were determined for the normalized shear modulus curves using the hyperbolic equation recommended by Hardin and Drnevich (1972). The hyperbolic equation can be expressed as:

$$\frac{G}{G_{max}} = \frac{1}{1 + \frac{\gamma}{\gamma_{r,G}}} \qquad (2)$$

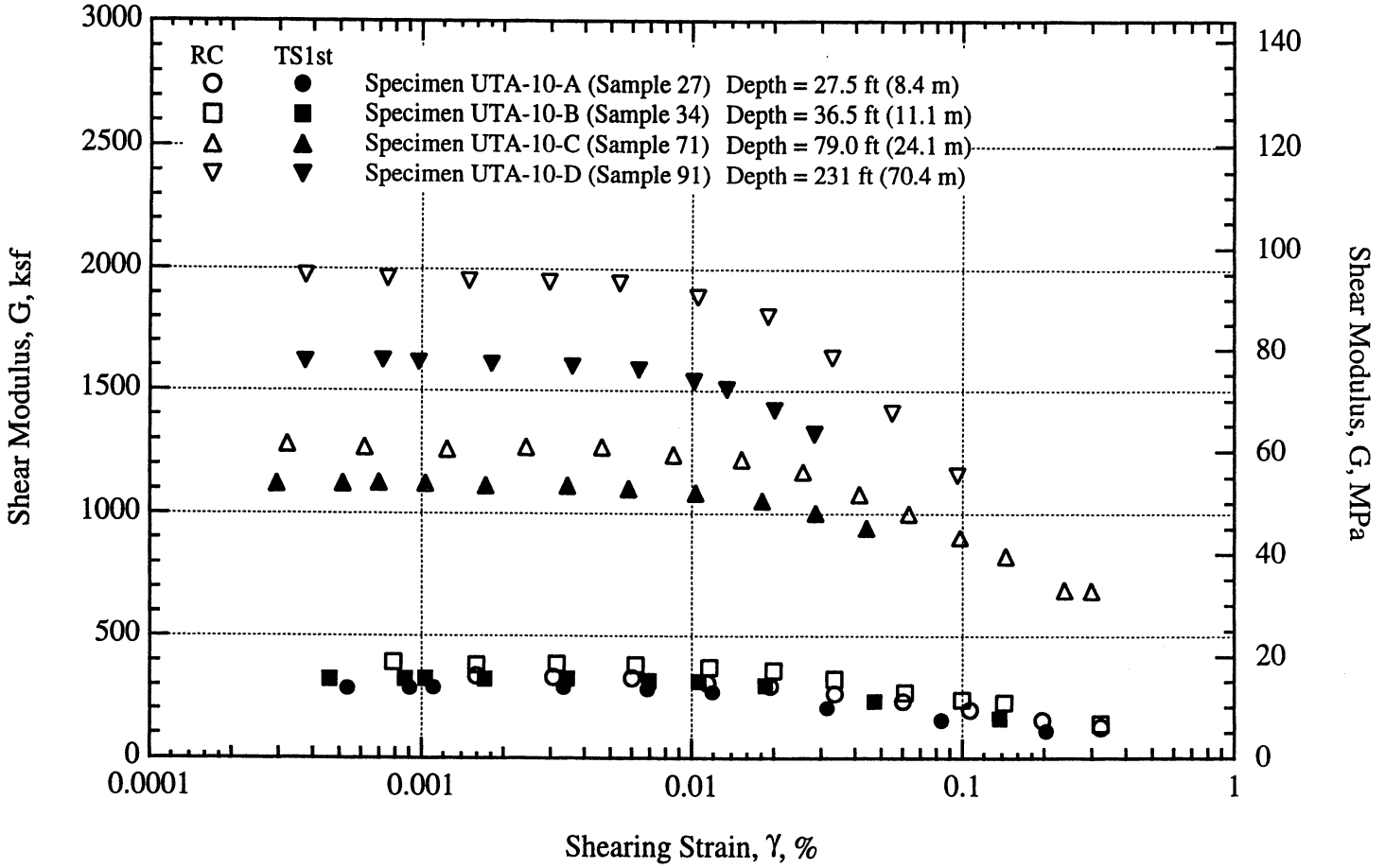

Figure 16 Variation in Shear Modulus with Shearing Strain at the Estimated Mean Effective Confining Pressure from Resonant Column (RC) and Torsional Shear (TS) Tests of Soil Specimens from the East Bay Bridge Site.

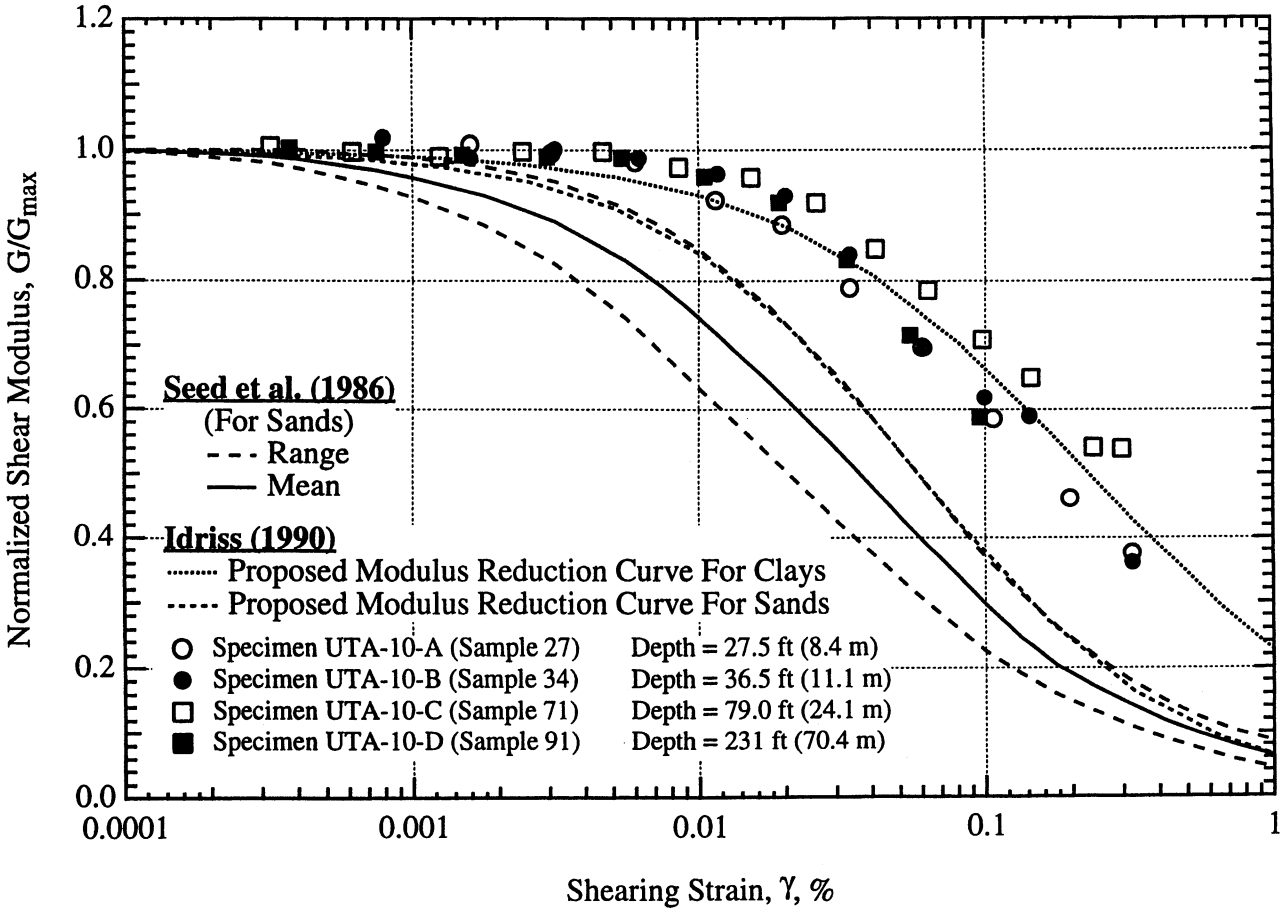

Figure 17 Variation in Normalized Shear Modulus with Shearing Strain at the Estimated Mean Effective Confining Pressure from Resonant Column (RC) Tests of Soil Specimens from the East Bay Bridge Site.

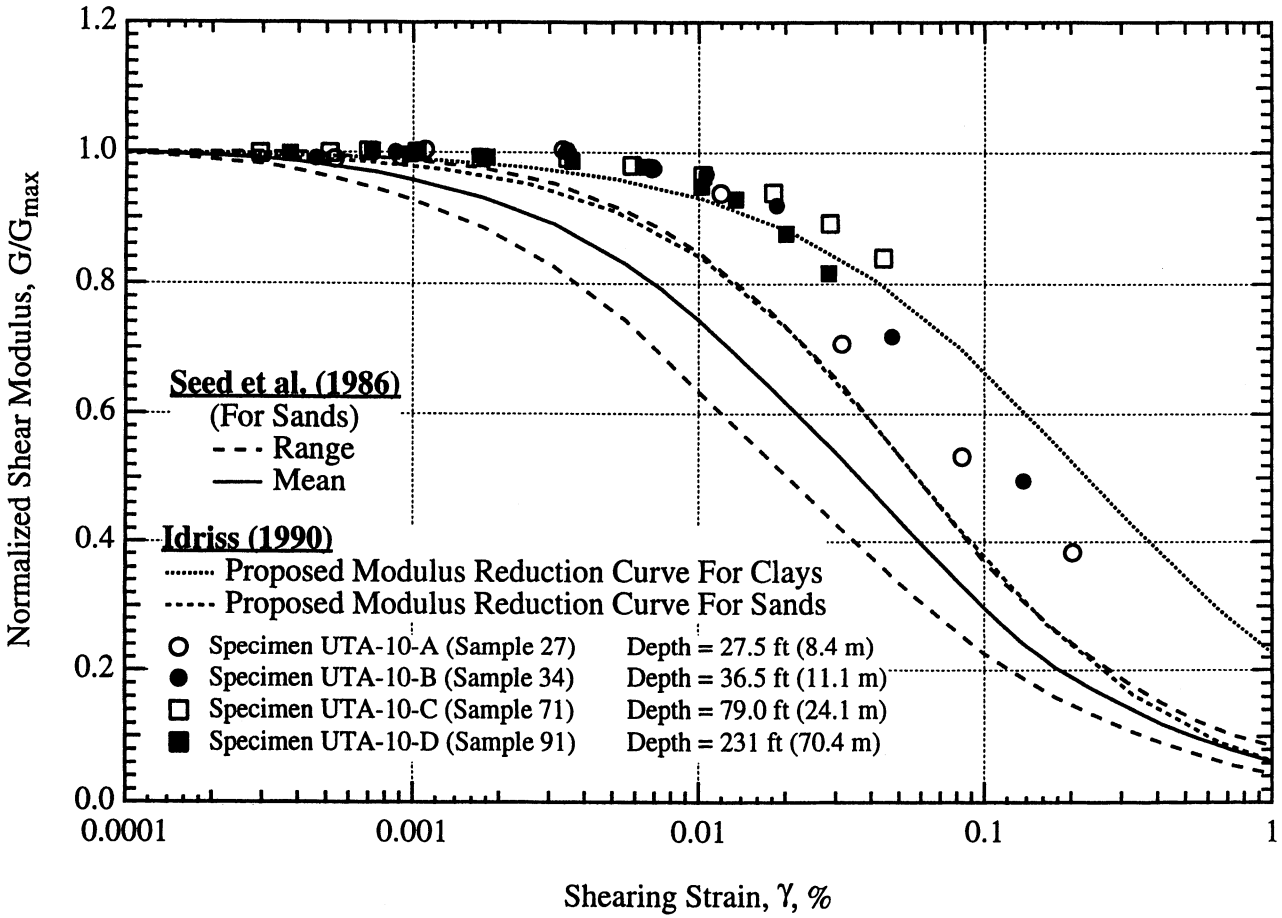

Figure 18 Variation in Normalized Shear Modulus with Shearing Strain at the Estimated Mean Effective Confining Pressure from Torsional Shear (TS) Tests of Soil Specimens from the East Bay Bridge Site.

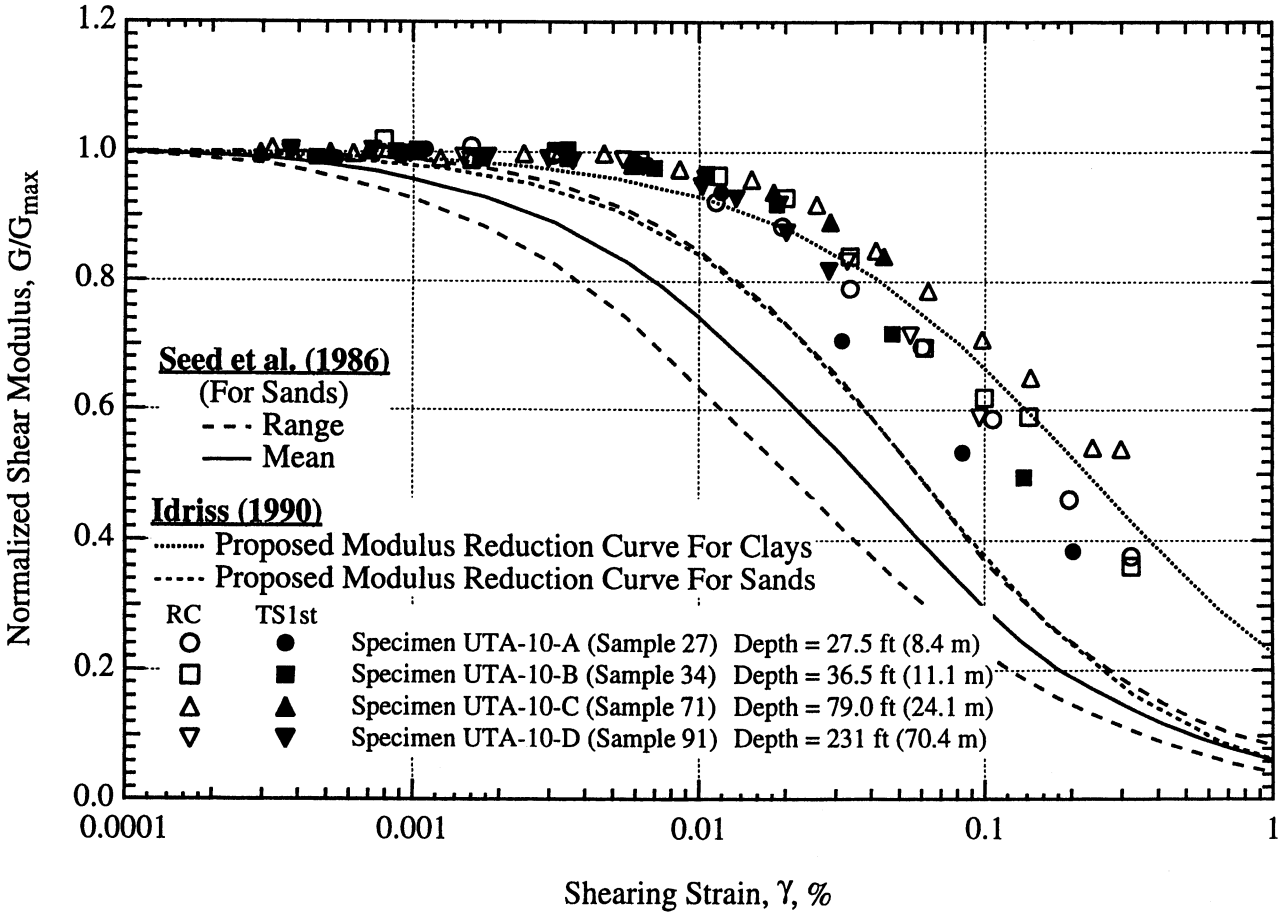

Figure 19 Variation in Normalized Shear Modulus with Shearing Strain at the Estimated Mean Effective Confining Pressure from Resonant Column (RC) and Torsional Shear (TS) Tests of Soil Specimens from the East Bay Bridge Site.

where

γ = any given strain, and

$\gamma_{r, G}$ = the reference strain with respect to the shear modulus.

The reference strain is used simply for curve fitting purposes. The value of $\gamma_{r, G}$ is equal to the shearing strain at which G/G_{max} equals 0.5.

Best fits of the hyperbolic equation to the G/G_{max} - log γ relationships for the RC and TS results are shown in Figures 20 and 21, respectively. Values of the reference strain with respect to the shear modulus for these fits for both the RC and TS tests are summarized in Table 4. In each case, the reference strains determined for the RC and TS results are quite close, with the values from the RC test being slightly higher.

Table 4 Reference Strain ($\gamma_{r, G}$) Values for the G/G_{max} - log γ Curves Based on the Hardin and Drnevich (1972) Equation.

Sample Number (Specimen ID)	Reference Strain Values, $\gamma_{r, G}$ (%)	
	RC Results	TS 1st Cycle Results
27 (UTA-10-A)	1.59E-1	1.05E-1
34 (UTA-10-B)	1.78E-1	1.40E-1
71 (UTA-10-C)	2.79E-1	2.40E-1
91 (UTA-10-D)	1.48E-1	1.45E-1

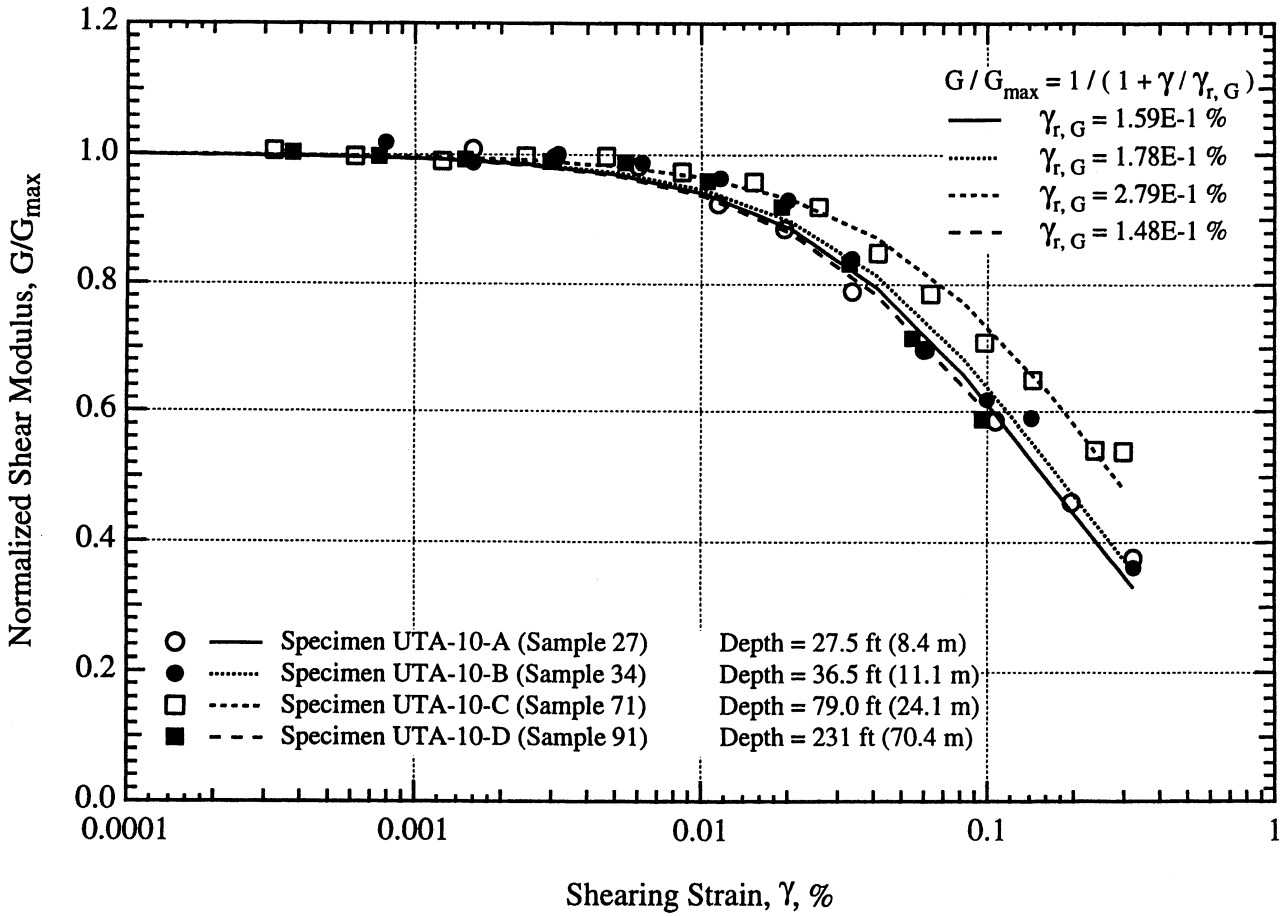

Figure 20 Best Fits of the Hyperbolic Equation to the Variation in Normalized Shear Modulus with Shearing Strain at the Estimated Mean Effective Confining Pressure from Resonant Column (RC) Tests of Soil Specimens from the East Bay Bridge Site.

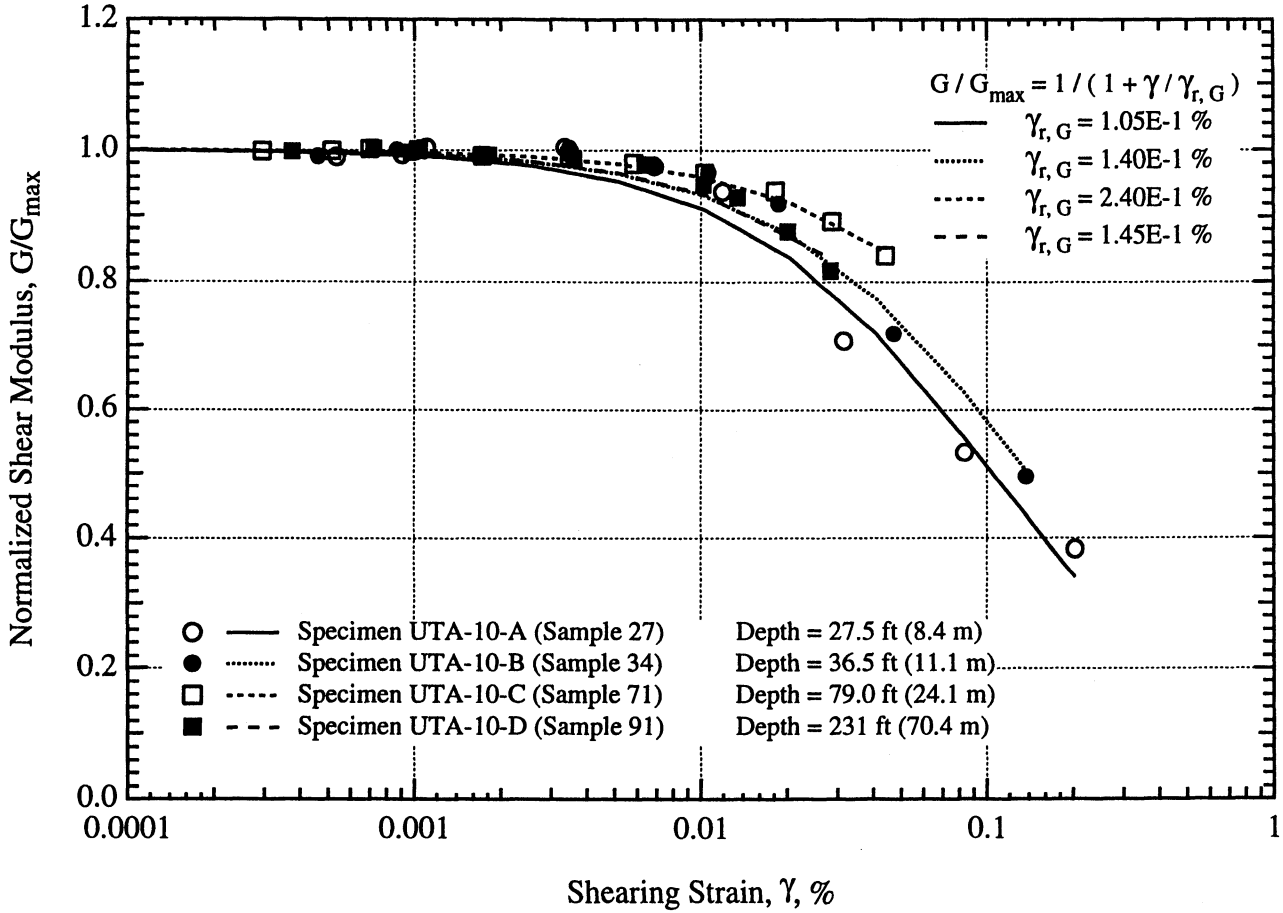

Figure 21 Best Fits of the Hyperbolic Equation to the Variation in Normalized Shear Modulus with Shearing Strain at the Estimated Mean Effective Confining Pressure from Torsional Shear (TS) Tests of Soil Specimens from the East Bay Bridge Site.

D - log γ Relationships

Figures 22 through 24 show the D-log γ relationships for the four specimens. The figures are arranged so that Figure 22 shows the RC results, Figure 23 shows the TS results, and Figure 24 shows a comparison of the RC and TS results. The values of D_{min} measured in the RC tests are higher than the D_{min} values measured in the TS tests, as shown in Figure 24. This difference is due to the frequency effect as discussed above and as shown for other soils (Kim, 1991; Hwang, 1997; and Darendeli, 1997). This general relationship between values of D measured in the RC and TS tests is observed to exist for all specimens at strains below about 0.005 %. At higher strains in the range of 0.01 to 0.1 %, the values of D from the TS tests increase slightly more rapidly with strain and become more similar to the values of D determined in the RC tests. This trend at higher strains seems to be related to the plasticity of the soil (Stokoe et al., 1994). Also, the highest value of D measured at the largest strain (about 0.15 %) for the two shallow specimens should be viewed cautiously. The strain amplitude varied significantly during these free-vibration decay measurements and the strain at which the values of D are shown could be underestimated.

In Figures 22 through 24, the D - log γ relationship recommended by Seed et al. (1986) for sands is shown for comparison purposes. The general curve proposed by Idriss (1990) for sands and clays is also shown. At very low strains, the measured values of D tend to be slightly above the proposed relationships. Also, at strains between 0.01 and 0.1 %, the measured values of D for all specimens range from below the recommended curve by Idriss (1990) to the values recommended by Idriss at a strain of about 0.1%.

Best-fit curves were determined for the material damping ratio measurements using the equation from Darendeli (1997) which was patterned after Hardin and Drnevich (1972) as:

$$\frac{D}{D_{min}} = 1 + \frac{\gamma}{\gamma_{r,D}} \qquad (3)$$

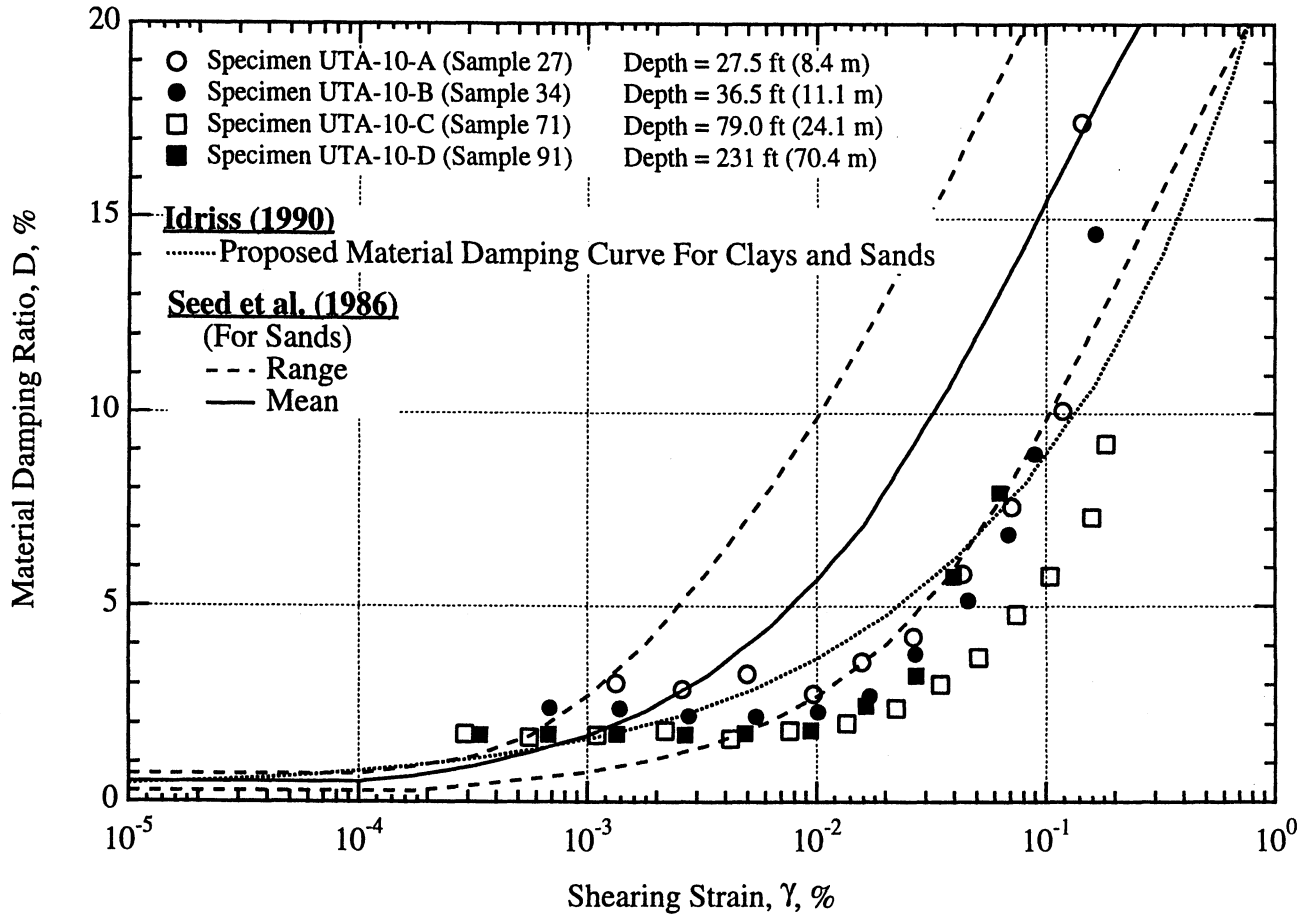

Figure 22 Variation in Material Damping Ratio with Shearing Strain at the Estimated Mean Effective Confining Pressure from Resonant Column (RC) Tests of Soil Specimens from the East Bay Bridge Site.

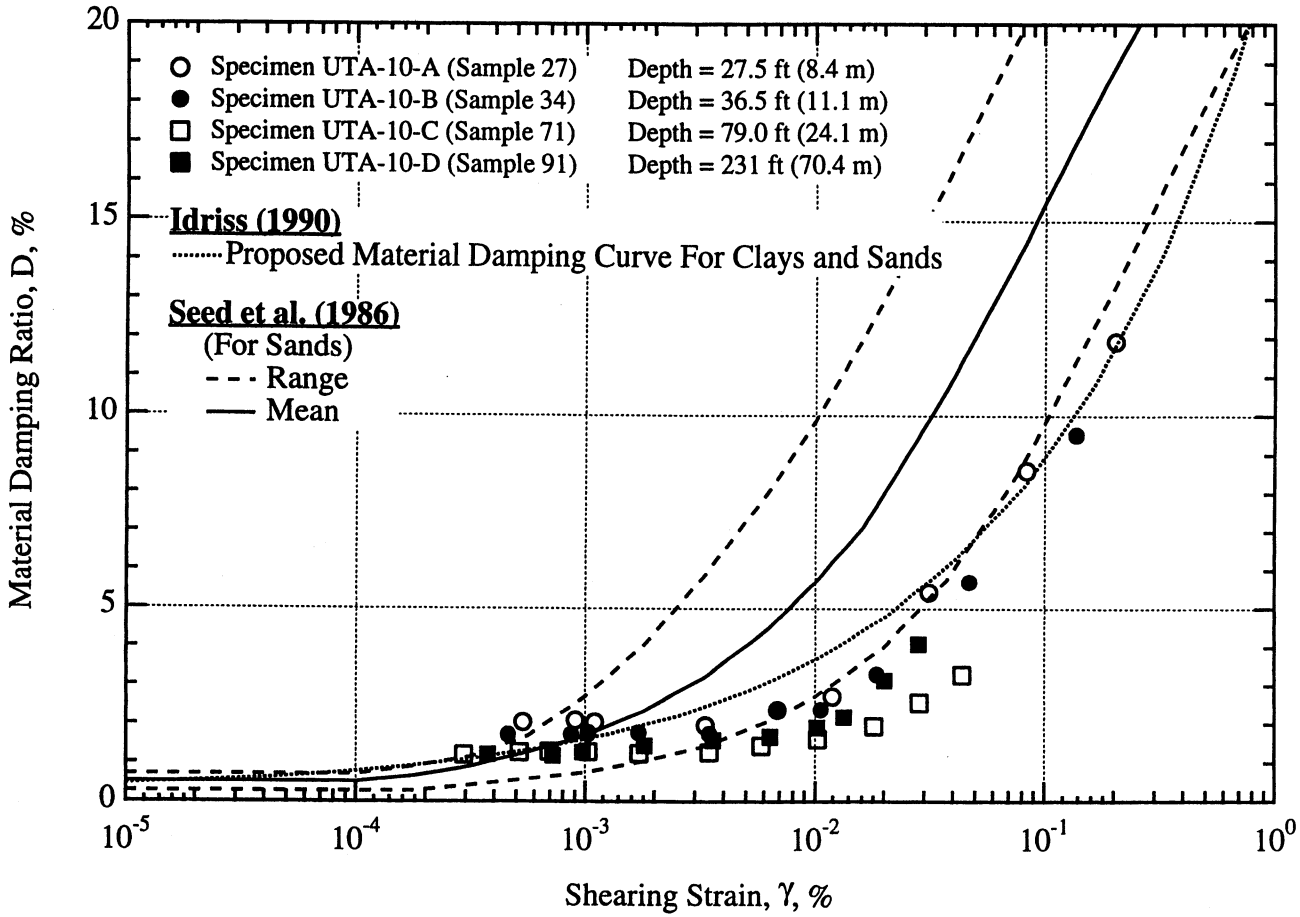

Figure 23 Variation in Material Damping Ratio with Shearing Strain at the Estimated Mean Effective Confining Pressure from Torsional Shear (TS) Tests of Soil Specimens from the East Bay Bridge Site.

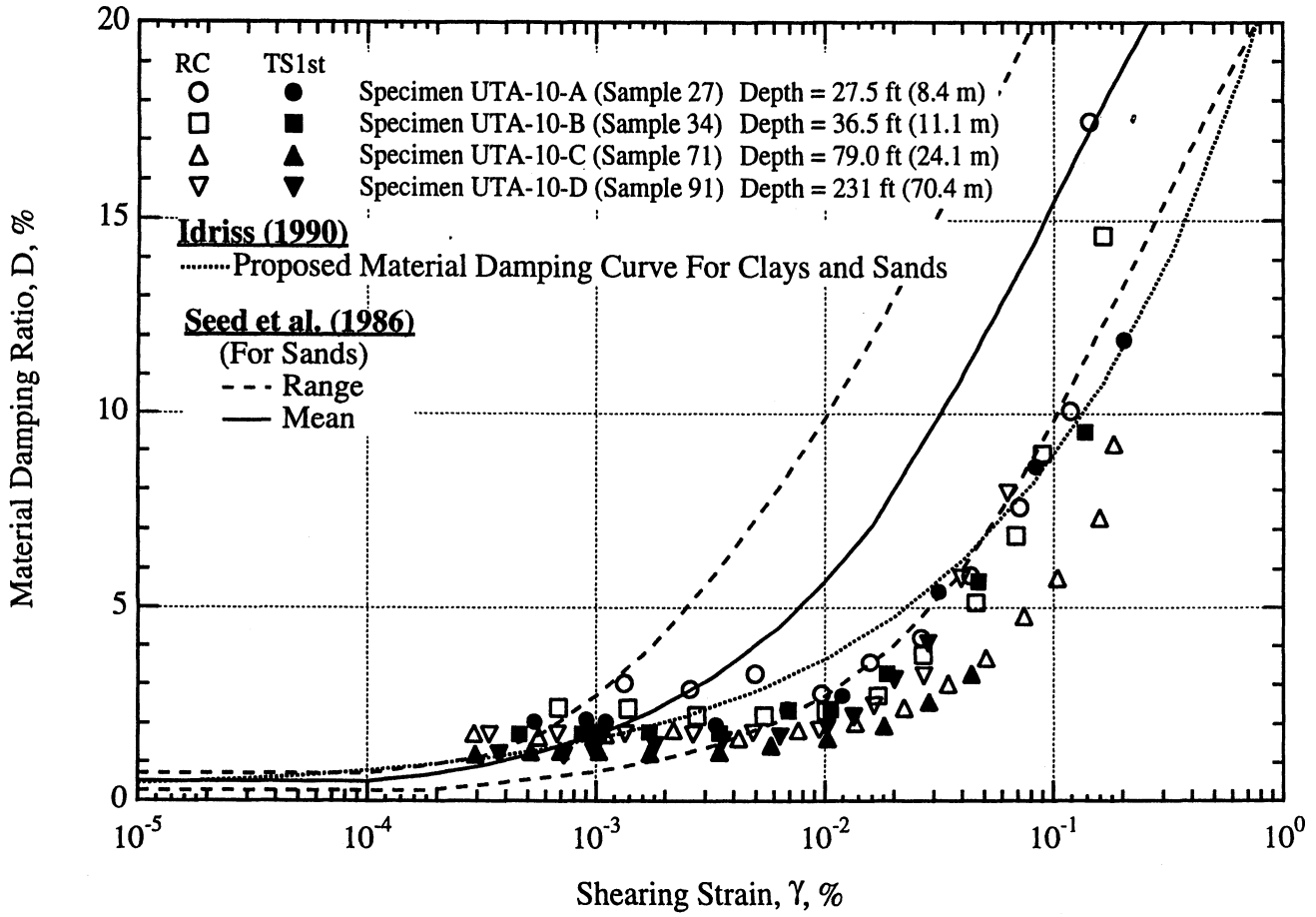

Figure 24 Variation in Material Damping Ratio with Shearing Strain at the Estimated Mean Effective Confining Pressure from Resonant Column (RC) and Torsional Shear (TS) Tests of Soil Specimens from the East Bay Bridge Site.

where

γ = any given strain, and

$\gamma_{r, D}$ = the reference strain with respect to material damping.

The equation presented above was used for only curve fitting purposes. It is worthwhile noting that the value of $\gamma_{r, D}$ is equal to the shearing strain at which D/D_{min} equals 2.

Best fits of the above equation to the D - log γ relationships for the RC and TS results are shown in Figures 25 and 26, respectively. Values of the reference strain with respect to material damping and values of D_{min} for these fits for both the RC and TS tests are summarized in Table 5.

Table 5 Damping Curve Coefficients ($\gamma_{r, D}$ and D_{min}) for the D - log γ Curves

Sample Number (Specimen ID)	Reference Strain Values, $\gamma_{r, D}$ (%)			
	RC Results		TS 1st Cycle Results	
	D_{min}	$\gamma_{r, D}$	D_{min}	$\gamma_{r, D}$
27 (UTA-10-A)	3.00	3.76E-2	2.04	3.78E-2
34 (UTA-10-B)	2.37	3.09E-2	1.69	2.86E-2
71 (UTA-10-C)	1.71	4.47E-2	1.28	2.83E-2
91 (UTA-10-D)	1.68	1.86E-2	1.50	1.28E-2

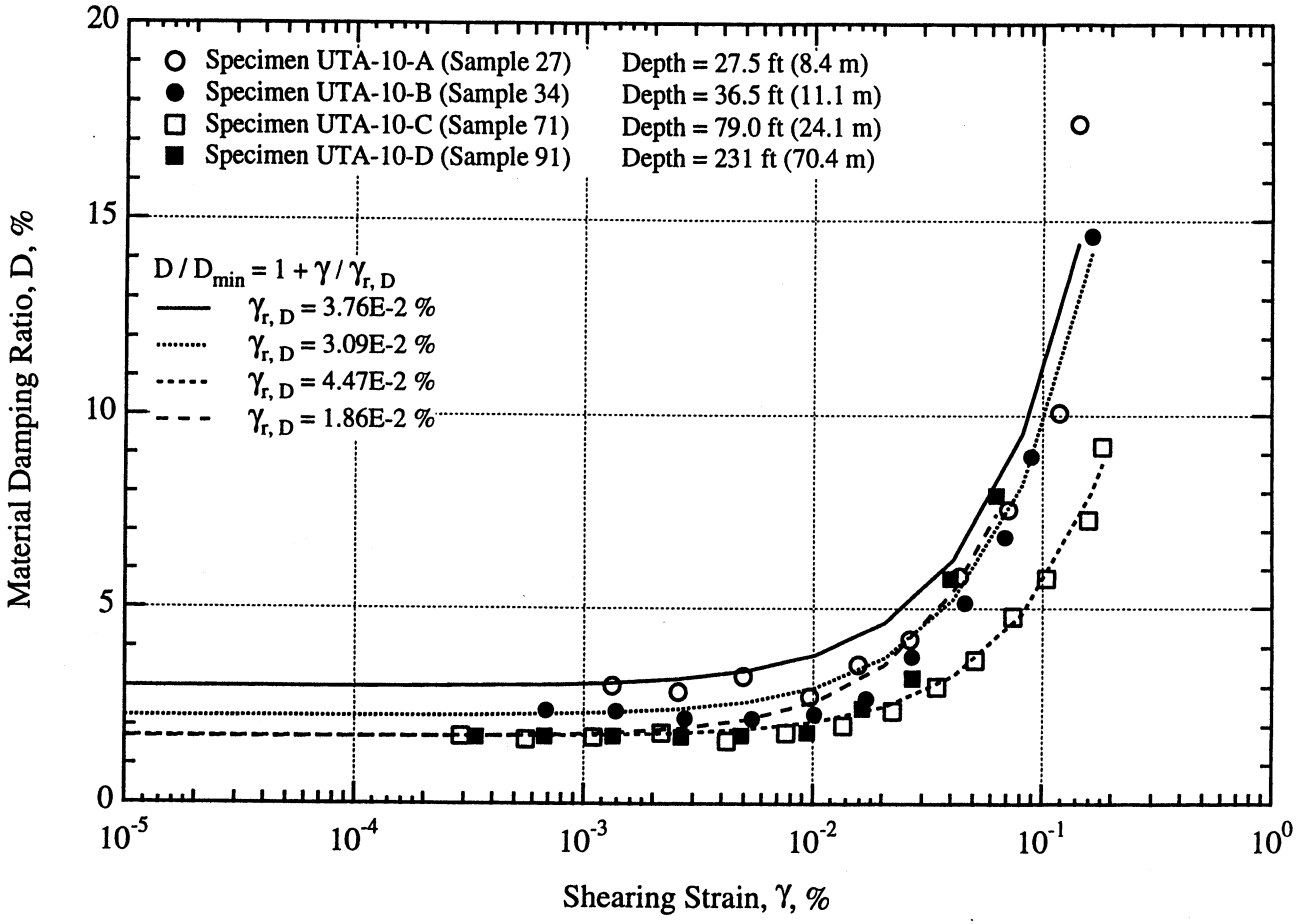

Figure 25 Best Fits to the Variation in Material Damping Ratio with Shearing Strain at the Estimated Mean Effective Confining Pressure from Resonant Column (RC) Tests of Soil Specimens from the East Bay Bridge Site.

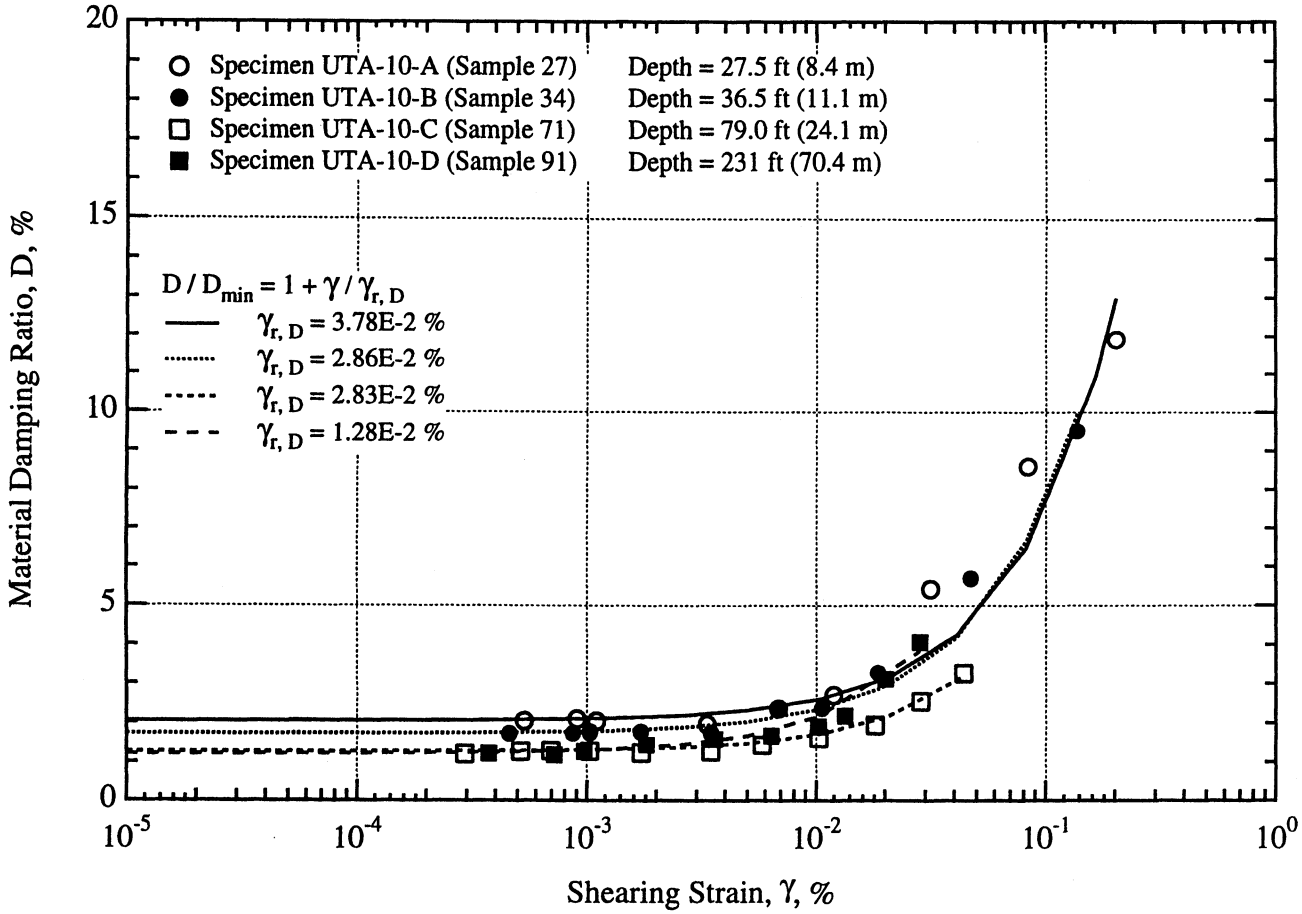

Figure 26 Best Fits to the Variation in Material Damping Ratio with Shearing Strain at the Estimated Mean Effective Confining Pressure from Torsional Shear (TS) Tests of Soil Specimens from the East Bay Bridge Site.

4. REFERENCES

Darendeli, M.B. (1997), "Dynamic Properties of Soils Subjected to 1994 Northridge Earthquake," shows M.S. Thesis, Geotechnical Engineering, Department of Civil Engineering, University of shows Texas at Austin, December.

Hardin, B.O. (1978), "The Nature of Stress-Strain Behavior for Soils," Proceedings, Geotechnical Engineering Division Specialty Conference on Earthquake Engineering and Soil Dynamics, Vol. I, ASCE, Pasadena, CA, June, pp. 3-90.

Hardin, B.O. and V.P. Drnevich (1972), "Shear Modulus and Damping in Soils: Design Equations and Curves," Journal of the Soil Mechanics and Foundations Division, ASCE, Vol. 98, No. SM6, Proc. Paper 9006, July.

Hwang, S.K. (1997), "Dynamic Properties of Natural Soils," Ph.D. Dissertation, Geotechnical Engineering, Department of Civil Engineering, University of Texas at Austin, May.

Idriss, I.M., (1990), "Response of Soft Sites During Earthquakes," H. Bolton Seed Memorial Symposium Proceedings, Vol. 2, Editor J. Michael Duncan, pp. 273-289.

Kim, D.S. (1991), "Deformational Characteristics of Soils at Small to Intermediate Strains from Cyclic Tests," Ph.D. Dissertation, Geotechnical Engineering, Department of Civil Engineering, University of Texas at Austin, August.

Seed, H.B., R.T. Wong, I.M. Idriss, and K. Tokimatsu (1986), "Moduli of Damping Factors For Dynamic Analyses of Cohesionless Soils," Journal of the Soil Mechanics and Foundations Division, Vol. 112, No. SM11, pp. 1016-1032.

Stokoe, K.H. II, H.K. Hwang, J.N.-K. Lee, and R.D. Andrus (1994), "Effects of Various Parameters on the Stiffness and Damping of Soils at Small to Medium Strains," Proceedings, International Symposium on Pre-Failure Deformation Characteristics of Geomaterials, Vol. I, Japanese Society of Soil Mechanics and Foundation Engineering, Sapporo, Japan, September, pp. 785-816.

APPENDIX A

TESTING EQUIPMENT, MEASUREMENT TECHNIQUES AND EQUIPMENT CALIBRATION

APPENDIX A

TESTING EQUIPMENT, MEASUREMENT TECHNIQUES AND EQUIPMENT CALIBRATION

A.1 INTRODUCTION

In this study, combined resonant column and torsional shear (RCTS) equipment was employed to evaluate the dynamic properties of undisturbed soil specimens. This equipment was originally developed by Prof. Stokoe following earlier developments by Professors Hardin and Drnevich. The equipment has undergone continued modifications and improvements over the past two decades by the graduate students under Prof. Stokoe's guidance (Isenhower, 1979; Lodde, 1982; Ni, 1987; Kim, 1991; and Hwang, 1997).

The RCTS equipment is a fixed-free system that applies torsional excitation at the top of a cylindrical soil specimen while the bottom of the specimen is fixed. The excitation is applied with a driving system composed of coils and magnets. Static and dynamic response data are collected with measurement systems composed of an accelerometer, an LVDT, and two proximitors. With this arrangement, testing is performed without constraining the top of the specimen, hence, the "free" portion of the fixed-free configuration is accomplished. The boundary conditions reduce the

problem into a simple theoretical solution of wave propagation through the specimen.

In this appendix, a detailed description of the testing equipment is presented along with information on the theory of testing and the equipment calibration. Figures and tables that are originally produced by Seon-Keun Hwang (1997) are used throughout this appendix to illustrate the equipment, testing methods and calibration procedures.

A.2 General Overview Of RCTS Equipment And Testing Methods

Testing of a soil specimen in the RCTS device is accomplished in two different ways. One way is employing the resonant column portion of the device which is based on measuring the resonance characteristics of a soil specimen subjected to certain boundary conditions. The other way is employing the torsional shear portion of the device which is based on slow cycling and evaluating the stress-strain hysteresis loop through measuring the torque applied to the top of the specimen and the resulting rotation of the specimen.

A.2.1 Resonant Column Test

In case of resonant column testing, the basic principle is measurement of the resonance characteristics of a specimen with known geometry subjected

to simple boundary conditions. For the case of the resonant column device at The University of Texas at Austin (UTA), the specimen shape is a right circular cylinder that is fixed at the bottom and free at the top. The specimen is subjected to a dynamic torsional loading as shown in Figure A.1.

As the specimen is excited in torsion, the dynamic material properties are measured at first-mode resonance. First-mode resonance is generated by applying harmonic loading through a rigid top cap on the specimen to which a drive plate is attached with four screws. The magnets on the drive plate are displaced by applying a current in the form of a harmonic forcing function through drive coils which surround the magnets in a noncontacting fashion. A simple sketch of the test setup is presented in Figure A.2a.

A frequency response curve is determined by sweeping the driving current through frequencies and measuring the resulting output from the accelerometer attached to the drive plate. The point where the response is a maximum is called the resonant peak and the frequency at this point is the resonant frequency as illustrated in Figure A.2b.

Using the geometry of the specimen, the boundary conditions, and the calibration constants, the shear wave velocity (V_s) is calculated from the resonant frequency. The shear modulus (G) is then determined using this value. The peak accelerometer output is used in estimating the peak shearing strain (γ). The material damping ratio (D) is evaluated using the frequency

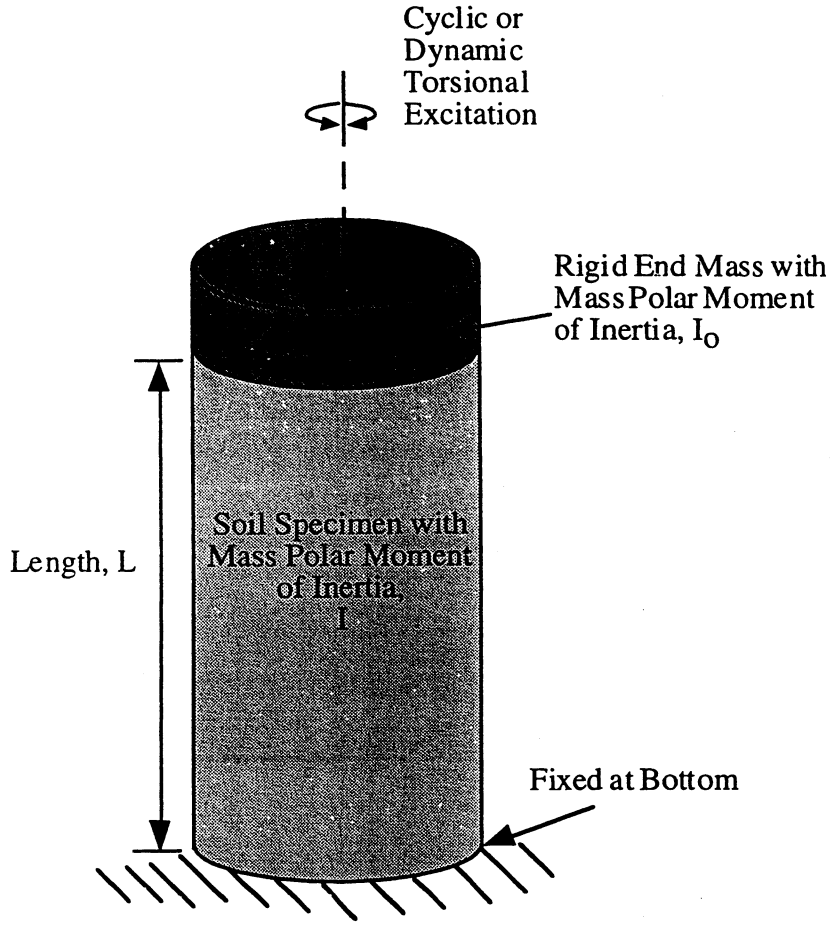

Figure A.1 Idealized Fixed-Free RCTS Test Configuration (from Hwang 1997)

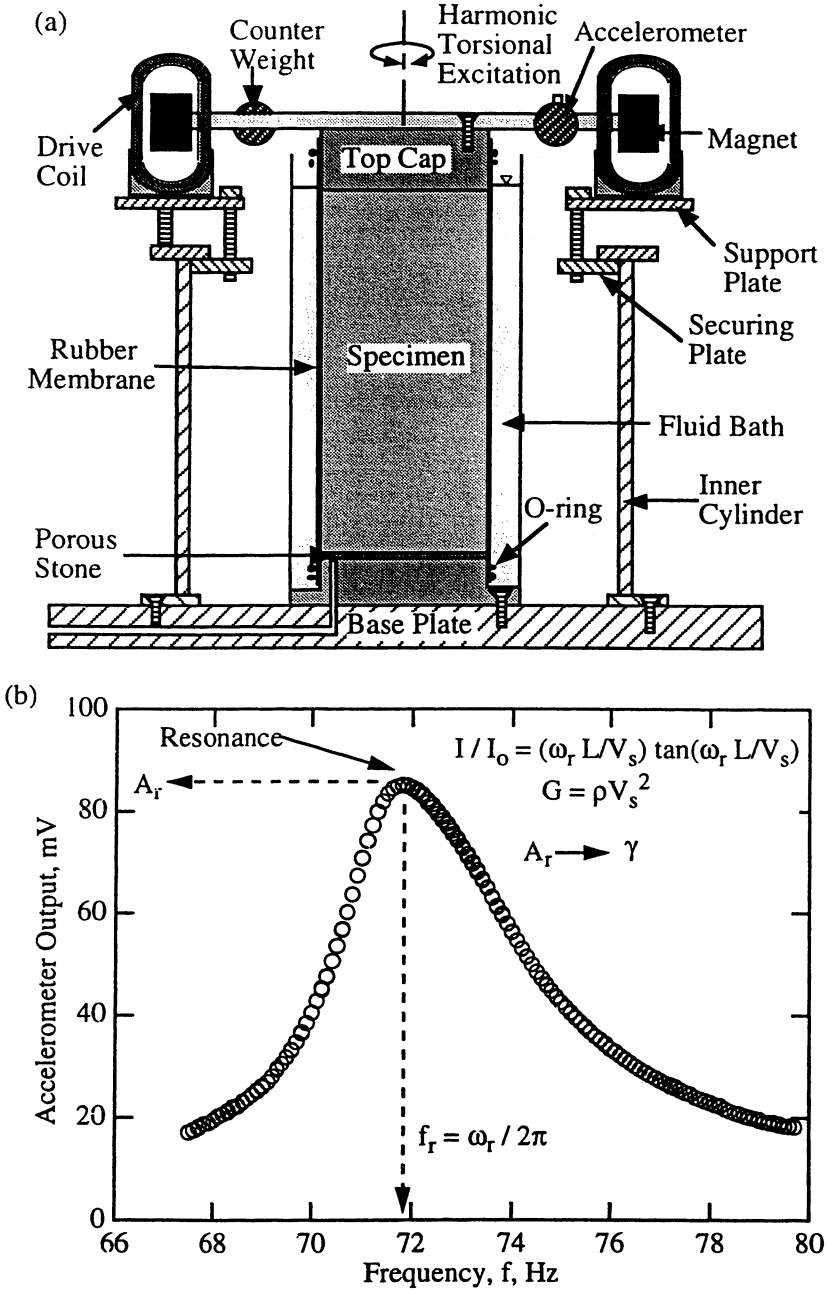

Figure A.2 Side View of a Fixed-Free Resonant Column Test Set-Up (a) and a Typical Frequency Response Curve Determined During Testing (b) (from Hwang 1997)

response curve (half-power bandwidth method) and the free-vibration decay curve.

The free-vibration decay curve is recorded by resonating the specimen in steady-state motion at the resonant frequency and then quickly shutting off the driving power. The displacement of the specimen starts to decay exponentially and the slope of the semi-log plot of displacement versus number of cycles of movement is used to evaluate the material damping ratio as illustrated in Figure A.3.

The half-power bandwidth method is based on evaluating the shape of the frequency response curve around the resonance peak as illustrated in Figure A.4.

A.2.2 Torsional Shear Test

In torsional shear test, the basic principle is the application of a known torque at the top of the specimen at a predetermined frequency and measurement of the resulting twist (displacement) of the top of the specimen. Thus, the soil specimen is subjected to a cyclic shearing stress at low frequencies. The stress applied to the specimen and the resulting strain are measured simultaneously. The hysteresis loop formed from this loading condition is measured for each loading cycle and is used in calculation of cyclic (also called "dynamic" herein) material properties.

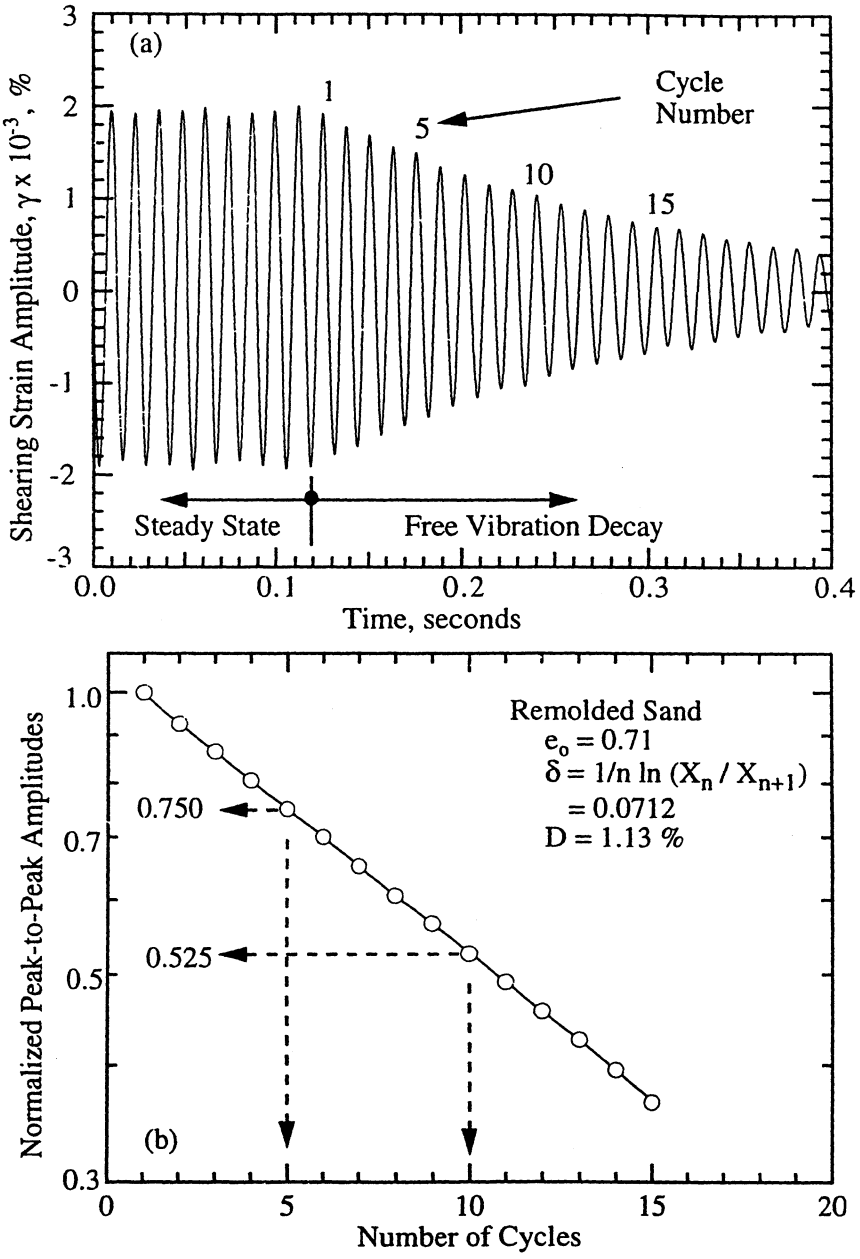

Figure A.3 Typical Free-Vibration Decay Curve (a) and Material Damping Measurement (b) in the Resonant Column Test for Remolded Sand (from Hwang 1997)

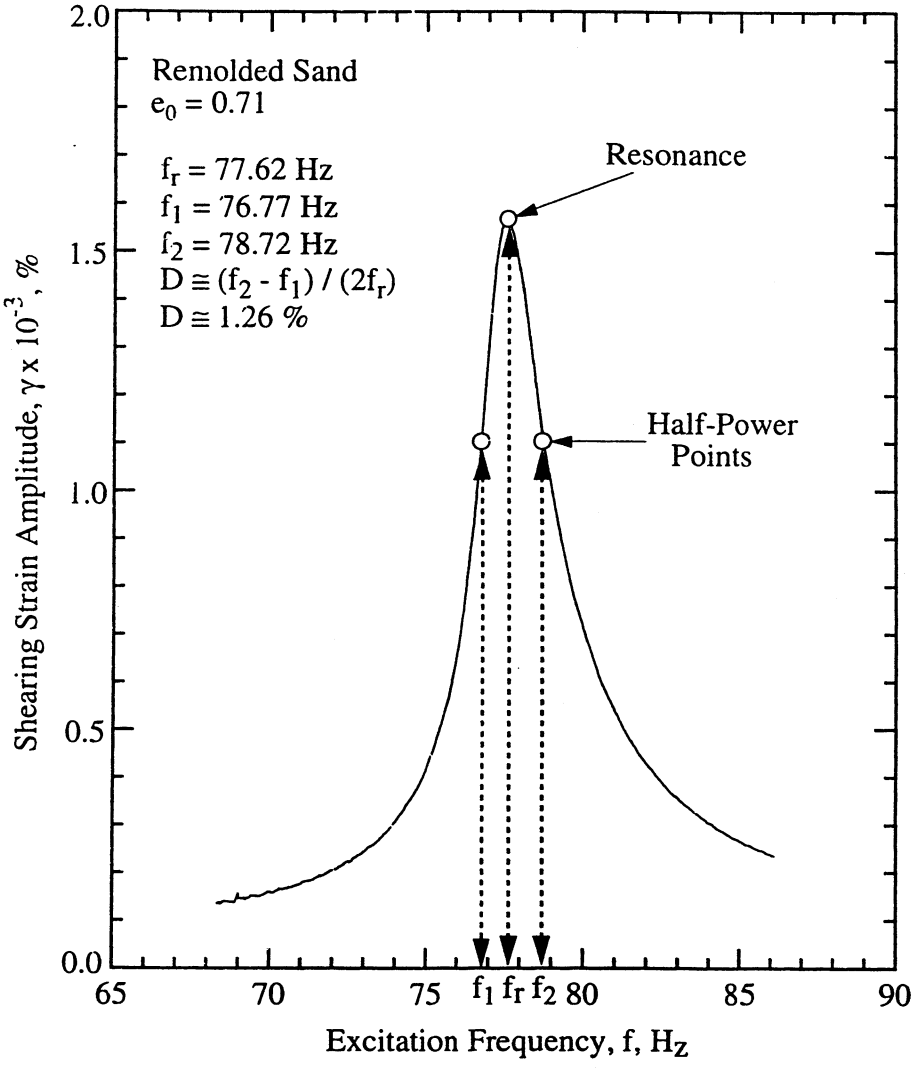

Figure A.4 Typical Material Damping Ratio Measurement from Frequency Response Curve in the Resonant Column Test Using the Half-Power Bandwidth Method (from Hwang 1997)

As illustrated in Figure A.5a, the displacement at the top of the specimen is measured with proximitors while the current applied at the drive coil is simultaneously recorded. The displacement is used in calculation of the shearing strain and the current in the coils is used to evaluate the shearing stress. The resulting hysteresis loop is then used in calculation of shear modulus (G) and material damping ratio (D) of the soil specimen as illustrated in Figure A.5b.

A.3 Resonant Column And Torsional Shear Testing Equipment And Methods

In Figure A.6, a detailed drawing of the RCTS equipment is presented. The system is composed of a confinement system (which is not shown in this figure), a drive system, a height-change measurement system, and a motion monitoring system. The equipment has been automated by Ni (1987).

A.3.1 RCTS Confinement System

A cross-sectional view of the confinement system is presented in Figure A.7. It is composed of an outer hollow cylinder, two square plates and four fixing rods. The outer hollow cylinder has a wall thickness of 0.25 in. (0.64 cm) and an outside diameter of 8.5 in. (21.6 cm). Each square plate has the dimensions of 9 in. x 9 in. x 1 in. (23 cm x 23 cm x 2.54 cm). The

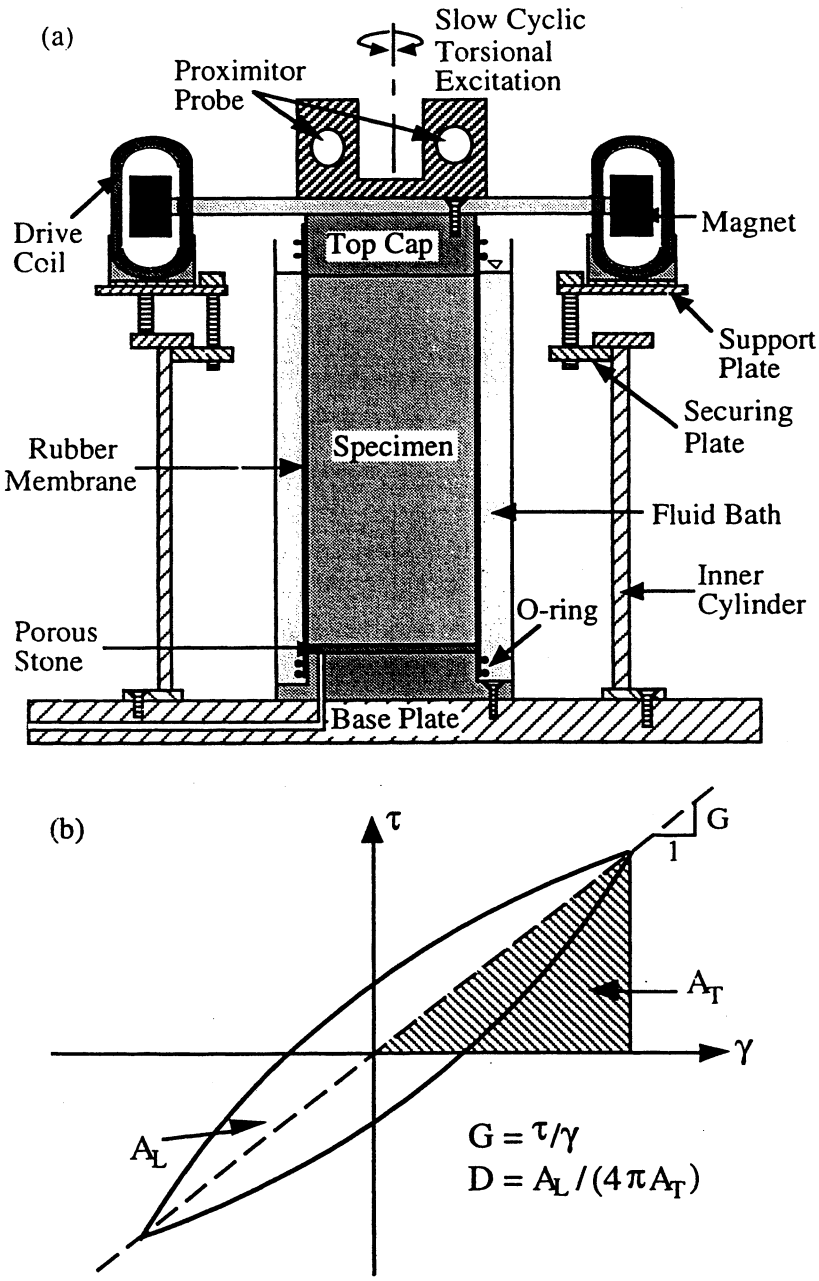

Figure A.5 Side View of a Fixed-Free Torsional Shear Test Set-Up (a) and a Typical Hysteretic Loop for Measurement of Shear Modulus and Material Damping Ratio (b) (from Hwang 1997)

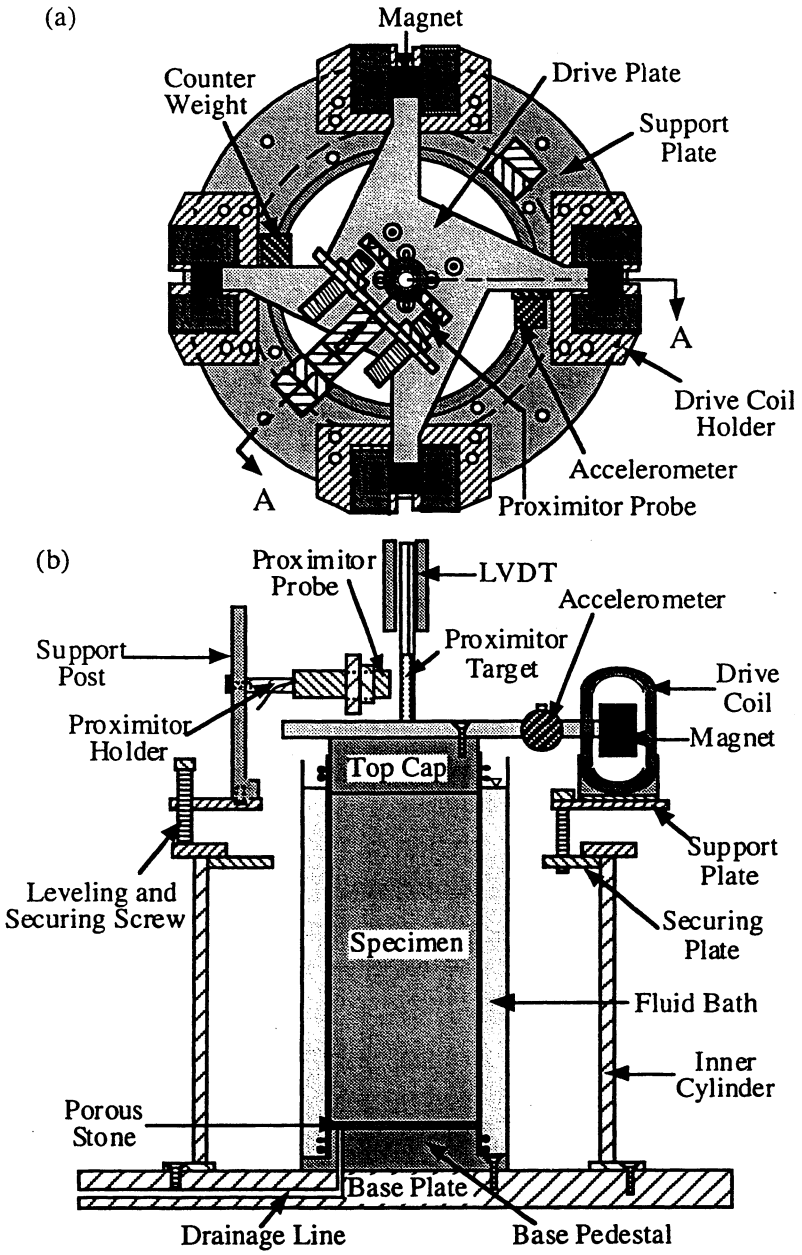

Figure A.6 General Configuration of RCTS Equipment; Top View (a) Section AA (b) (from Hwang 1997)

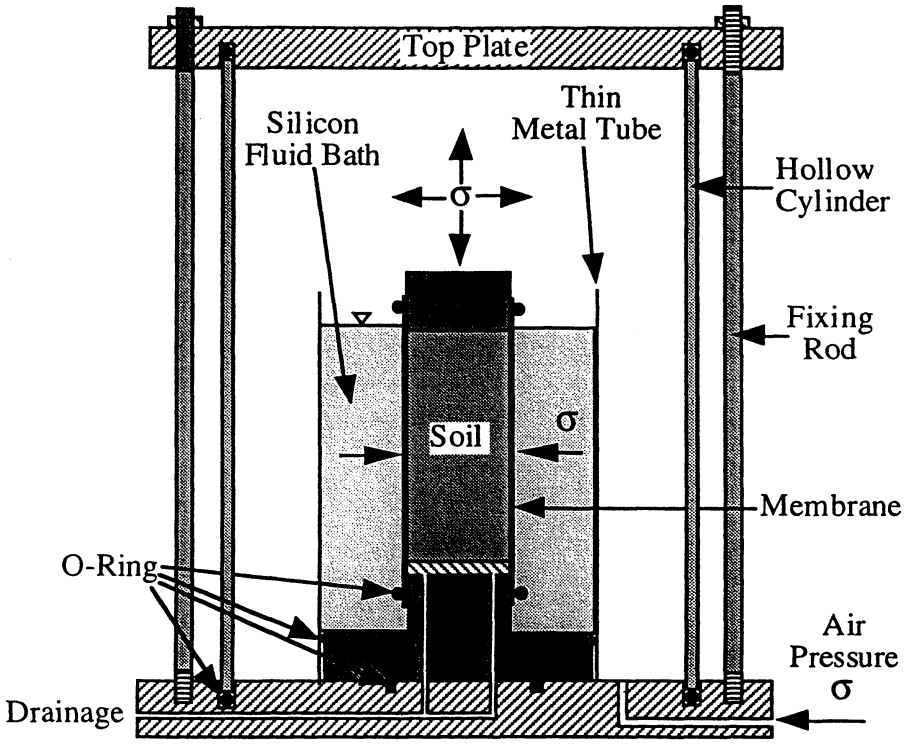

Figure A.7 Simplified Cross-Sectional View of Confinement System (from Hwang 1997)

fixing rods are 20 in. (51 cm) long and 0.5 in. (1.27 cm) in diameter. All these components are made of stainless steel to prevent any reaction with the electro-magnetic driving system. The bottom plate is rigidly fixed to the support table. Rubber o-rings are used between the end plates and the cylinder to ensure that the system is air tight. This system is designed to withstand a maximum internal air pressure of 600 psi (4137 kPa).

After the confining cell is assembled, air pressure is supplied through a pressure line in the bottom plate. This pressure is regulated by either a Fairchild model 30 (2 to 100 psi (14 to 689 kPa)) or a Tescom model 44-2200 (3 to 500 psi (21 to 3447 kPa)) regulator. The pressure source is either the building air supply (up to 60 psi (up to 414 kPa)) or an industrial nitrogen gas container (up to 2500 psi (17 MPa)).

During the testing stage, the specimen is seated on a base pedestal that is connected to a drainage line in the bottom plate. The specimen is sealed with a membrane and a silicon fluid bath is placed around the membrane to prevent air migration into the specimen. The air pressure is then applied to the chamber. Thus, an isotropic confining pressure is applied to the specimen through the fluid bath. The air pressure is monitored with either a Bordon type pressure gage or a Validyne DP15 pressure transducer. It is also possible to monitor the pore water pressure in the specimen with a pressure transducer connected to the drainage line.

A.3.2 Drive System

The drive system is composed of a drive plate (four Alnico No.8 magnets and an aluminum plate that connects them to the top cap), eight drive coils (located around the magnets by fixing to a support plate), a power amplifier (HP 6824A) and a function generator (HP 3314A). The details of the drive plate are presented in Figure A.6, and the schematic diagram of the drive system is presented in Figure A.8.

The function generator is used to create a sinusoidal output at a certain frequency and a desired voltage level. This current is transferred to the drive coils, and it is used to drive the magnet located inside the coil. The aluminum plate transfers the applied force to the top cap. Thus, the specimen is dynamically loaded in torsion. In case of high-amplitude tests, the output from the function generator is amplified before being transferred to the drive coils.

The maximum torque applied to the specimen is a function of the strength of the magnets, characteristics of the drive coils, the gap between the magnets and the drive coils, length of the arms of the aluminum plate and finally the input current. This system is described in Ray (1983) in further detail.

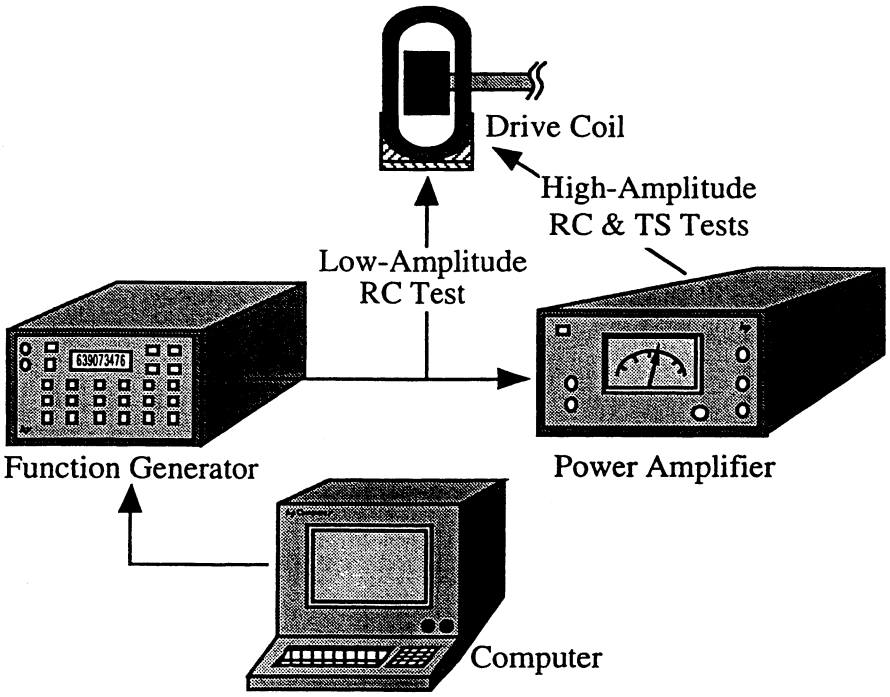

Figure A.8 Schematic Diagram of the Torsional Drive System (from Hwang 1997)

A.3.3 Height-Change Measurement System

The height-change measurement system is composed of an LVDT (CRL model SH-200-53R), a function generator (HP 3314A), and a digital voltmeter (HP 3458A). The LVDT is arranged in such a manner that the boundary condition at the top of the specimen is free. Thus, the core rod in the LVDT is attached at the center of the top cap. The LVDT coil housing is attached to a support post and monitoring is accomplished without any physical contact between the core and the housing. The function generator is used to create a 500-Hz, 4.77-V input current at the coil housing. Then, the voltage output from the LVDT is monitored with the voltmeter. Using the appropriate equipment constant, the actual height of a specimen is calculated at the time of each test. This value is used in estimating the mass density, length and mass polar moment of inertia of the specimen at all times during testing, and these values are used in calculation of the shear modulus of a soil sample. A schematic diagram of the height-change measurement system is presented in Figure A.9.

A.3.4 Motion Monitoring System

The frequencies involved in the resonant column (RC) and torsional shear (TS) tests are different. In case of RC tests, the testing frequency is a function of the boundary conditions and geometry of the specimen.

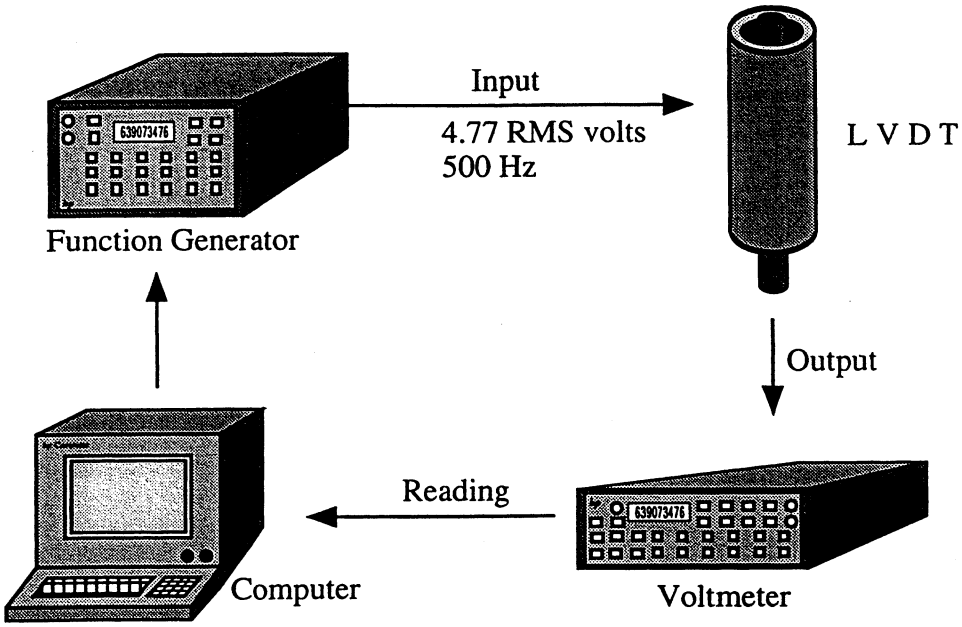

Figure A.9 Schematic Diagram of the Height-Change Measuring System (from Hwang 1997)

However, in TS tests, the testing frequency is a predetermined value and is at least an order of magnitude smaller than that used in the RC test. The frequencies involved in TS tests (0.05 to 10 Hz) are very low. At such low frequencies, measurement of displacement can only be achieved with a proximitor. In case of RC tests, the higher frequencies (more than 20 Hz) permit the use of accelerometers. The voltage readings from the accelerometers are then converted to displacement data.

A.3.4.1 Resonant Column Test

The devices involved in motion monitoring during an RC test are; an accelerometer (Columbia Research Lab. model 3021), a charge amplifier (Columbia Research Lab. model 4102M), a frequency counter (HP 5334A), a digital voltmeter (HP 3458A) and a digital oscilloscope (Nicolet 20929-01). Figure A.10 presents a schematic diagram of the motion monitoring system in the RC test.

As the specimen responds to the dynamic loading through the drive coils, the accelerometer senses the motion of the specimen. The signal is sent through a charge amplifier that conditions the output to be linear in the range of acceleration levels. Then the conditioned output is monitored simultaneously at the frequency counter, the voltmeter and the digital oscilloscope. The voltmeter measures the amplitude of the signal while the

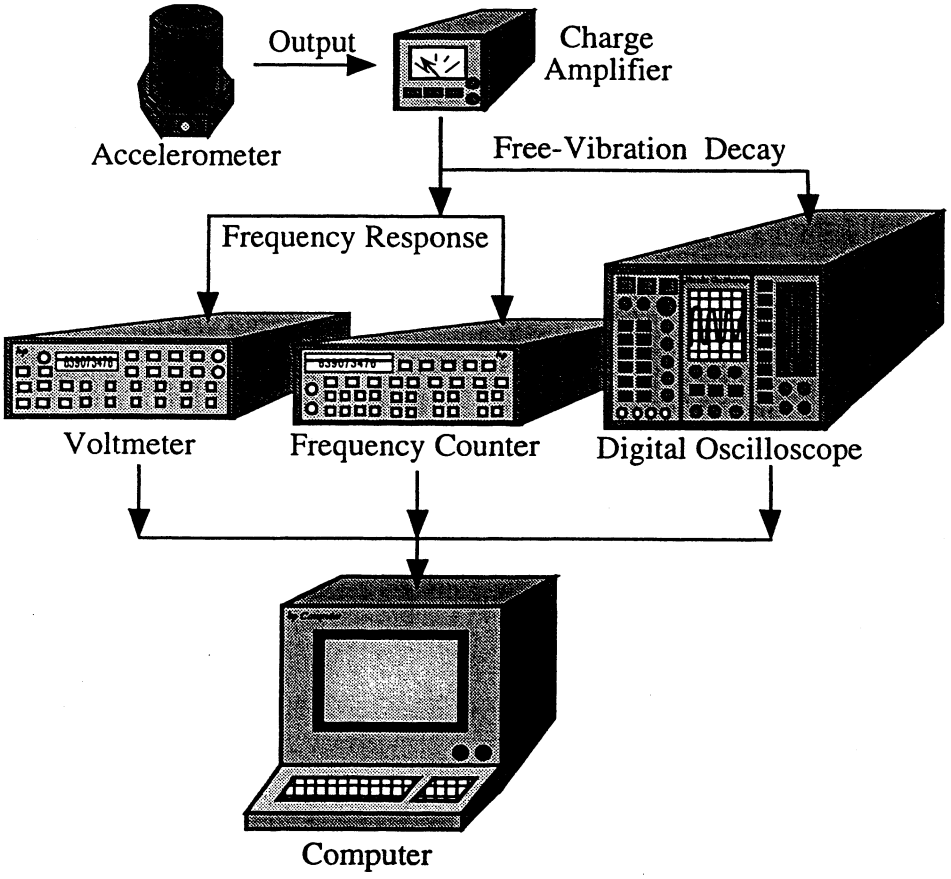

Figure A.10 Schematic Diagram of The Motion Monitoring System in The Resonant Column Test (from Hwang 1997)

frequency counter determines the frequency. The digital oscilloscope displays the signal in the time domain. The frequency response curve of the specimen is recorded in the memory of the computer by dumping the data from voltmeter and frequency counter continuously. Then customized computer software automatically determines the maximum accelerometer output. The frequency that corresponds to this data in the frequency domain is the resonant frequency. Using the complete response curve, the material damping ratio is estimated by the half-power bandwidth method. The resonant frequency is used in calculation of the shear wave velocity and shear modulus. Finally, the shearing strain is estimated by converting the maximum accelerometer output to actual displacement at the top of the specimen.

After estimation of the resonant frequency, the function generator drives the specimen at this frequency in steady-state motion. Then, the power to the coils is turned off and the response of the specimen is recorded in the time domain by using the digital oscilloscope. The data is later dumped to the computer. The computer software is employed in calculating a best-fit to the free vibration decay curve. The constant of exponential fit is used in calculation of material damping ratio from the free-vibration decay curve.

A.3.4.2 Torsional Shear Test

Due to the low frequencies involved in TS testing, the accelerometers can not be used in monitoring cyclic motion. As an alternative, proximitors are employed in TS testing. The system is based on measuring the width of an air-gap between a proximity probe and a proximity target. Thus, it directly measures displacements instead of measuring acceleration and converting it into displacement (as in the case of accelerometers). The system is composed of a proximity target, two proximity probes (Bently Nevada M 300-00), two proximitors (Bently Nevada M 20929-01), a DC power supply (Lambda M-11-902), a custom-made DC shifter, an operational amplifier (Tektronix TM 504 with AM501), a digital signal filter (Wavetek Brickwall Filter System 716), a function generator (HP 3314A), and a digital oscilloscope (Nicolet 20929-01). A schematic diagram of the motion monitoring system in the TS test is presented in Figure A.11.

As shown in Figure A.6, the U-shaped proximity target is attached at the center of the drive plate and the proximity probes are attached to a support post. The proximity probes are connected to proximitors which are powered with a DC power supply. The probes sense the width of the air-gap between the target and the probe tip, and the signal is conditioned at the proximitors.

Before starting the test, the signal from the proximitors is sent to a DC shifter, and the output is adjusted to a zero reading. Then the DC shifter is

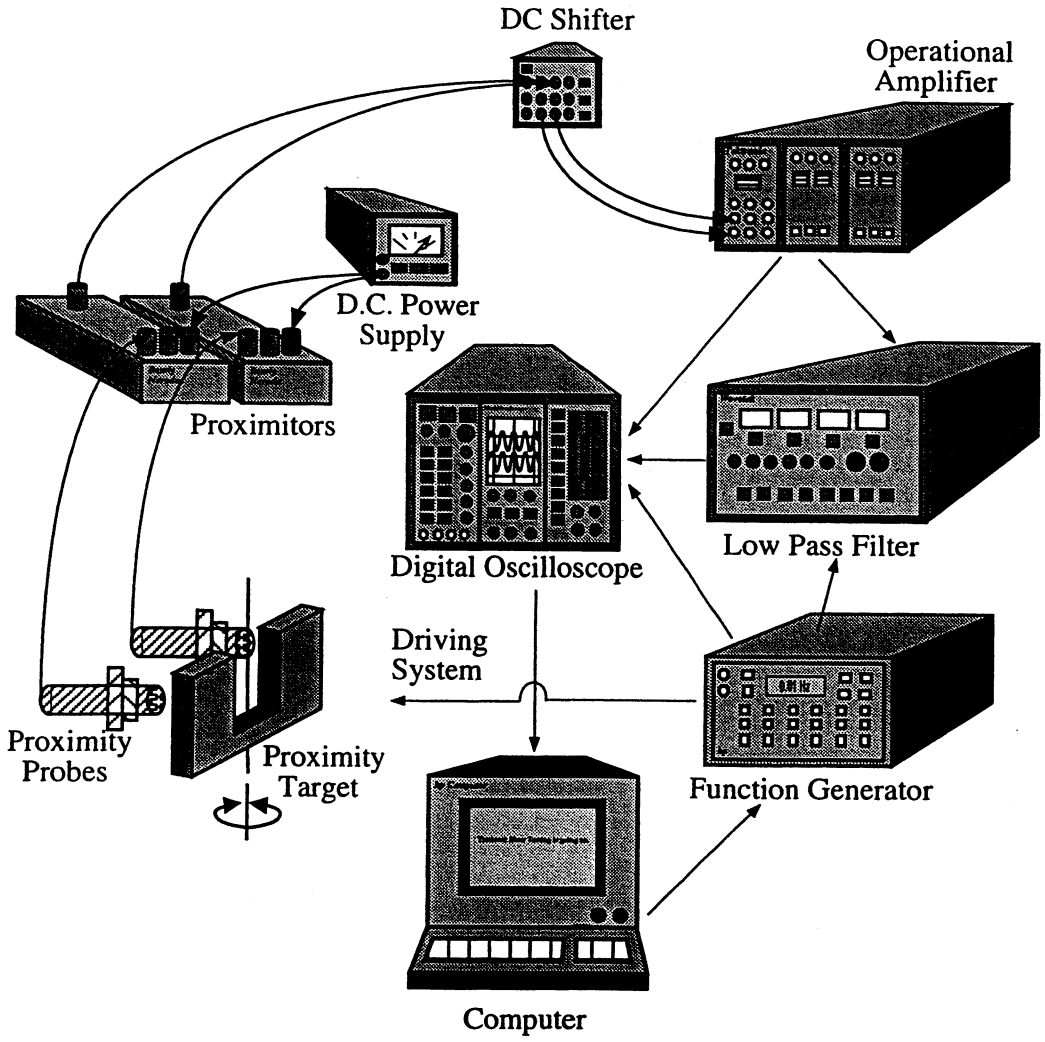

Figure A.11 Schematic Diagram of the Motion Monitoring System in the Torsional Shear Test (3000 Proximitor System) (from Hwang 1997)

connected to the operational amplifier that combines the two signals and outputs the difference of the two. The output is then filtered and displayed at the oscilloscope along with the signal that represents the driving force. The data are then converted into stress and strain by the software in the computer in order to plot the observed hysteresis loop. The area of the loop is used in the calculation of the material damping ratio, and the orientation of the loop (slope of the line connecting the end points of the loop) is used in the calculation of the shear modulus (as illustrated in Figure A.5b).

A.4 Theory Of Analysis of Resonant Column And Torsional Shear Tests

As mentioned above, there are two ways of determining dynamic soil properties with combined RCTS equipment. This section briefly explains the theory and calculations involved in measuring these properties.

A.4.1 Resonant Column Test

As discussed earlier, the resonant column test is based on estimating the material properties from the first-mode resonance characteristics of a specimen with known geometry and boundary conditions. Measurement of the frequency response curve of a specimen is performed and the resonant frequency is used in evaluating the shear modulus of the material. The maximum accelerometer output is used in determining the strain amplitude of

the test. Material damping ratio is calculated from both the frequency response curve and the free-vibration decay curve.

A.4.1.1 Shear Modulus and Shearing Strain

Shear Modulus

Calculation of the shear modulus is based on the one-dimensional wave propagation equation for a specimen fixed at the bottom and free at the top, with a rigid added mass attached at the top of the specimen. The equation is:

$$\frac{\Sigma I}{I_o} = \frac{\omega_n \times l}{V_s} \times \tan\left(\frac{\omega_n \times l}{V_s}\right) \qquad (A.1)$$

where, $\Sigma I = I_s + I_m$ (A.2)

I_s = mass polar moment of inertia of the specimen ($= \frac{1}{2} m r^2$ for a solid right-circular cylinder),

I_m = mass polar moment of inertia of the membrane,

I_o = mass polar moment of inertia of the rigid end mass (top cap and drive plate) at the top of specimen plus any added mass of the O-ring and membrane on the top cap,

l = length of the specimen,

V_s = shear wave velocity of specimen, and

ω_n = undamped natural angular frequency of the system ($= 2\pi f_n$).

The value of I_o, ΣI, and l are determined from the calibration of the drive plate, weight and dimensions of the top cap, weight of the membrane and O-ring and from the dimensions and weight of the specimen. Once the first-mode resonant frequency, f_r, is determined, the shear wave velocity, V_s, is calculated using Equation A.1 by assuming that f_r and f_n are equal. Since resonant frequency is measured rather than the undamped natural frequency, shear wave velocity of the specimen is calculated using f_r. The relationship between f_r and f_n is :

$$f_r = f_n \times \sqrt{1 - 2\ D^2} \qquad \text{(A.3)}$$

If the damping ratio of the specimen, D, is zero, f_r is equal to f_n. Typical damping ratios of soils evaluated in the resonant column tests are less than 15 %, and the difference between f_r and f_n resulting from it is less than 3 %. Thus, f_r is assumed to be the same as f_n throughout this study. Once the shear wave velocity is determined, shear modulus is calculated from the following equation:

$$G = \rho \times V_s^2 \qquad \text{(A.4)}$$

where ρ is the total mass density of the soil.

Shearing Strain

During torsional vibration of the specimen with the added mass at the top, torsional displacement can be assumed to be linearly distributed along the height of the specimen, with a maximum displacement at the top and zero displacement at the bottom (Drnevich et al., 1967). The shearing strain, however, varies radially from zero at the center of a solid specimen to a maximum at the outer boundary. The strain can be expressed as a linear function of the distance from the longitudinal axis as illustrated in Figure A.12 (Chen and Stokoe, 1979).

Chen and Stokoe (1979) studied the radial distribution of shearing strain in the specimen to find a value of the equivalent radius, r_{eq}, of the specimen tested in the RCTS apparatus. They found that the value of r_{eq} varies from 0.82 times the radius of the specimen, r_o, at peak shearing strain amplitudes below 0.001% to 0.79 r_o at a peak shearing strain of 0.1 % for a solid specimen. For a hollow specimen, however, they recommended using the average of the inside and outside radii for r_{eq}. These values of r_{eq} have been adopted in this study. The shearing strain in the resonant column test is expressed by:

$$\gamma_{eq} = C \times \gamma_{max} \times 100\ \% \qquad \text{(A.5)}$$

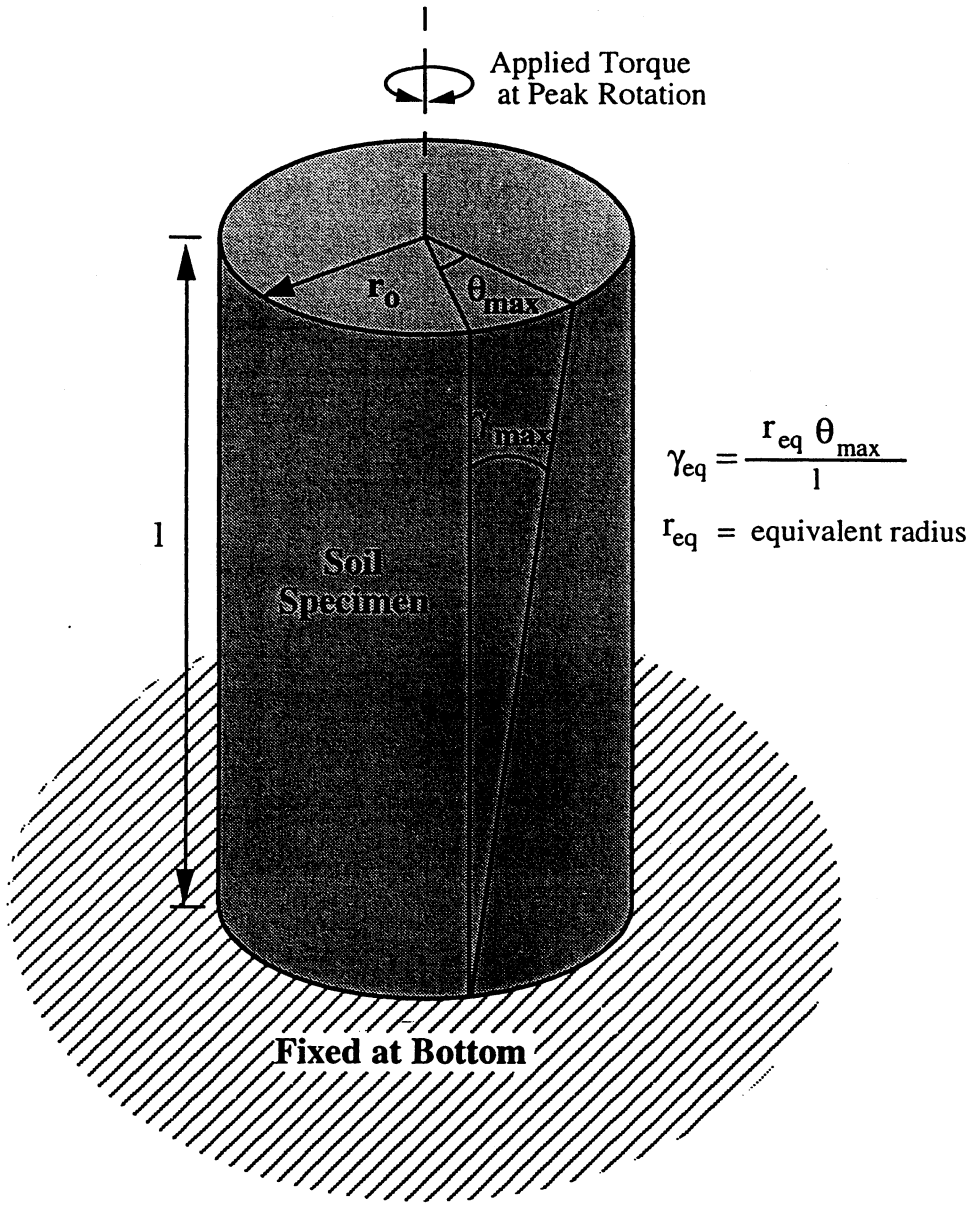

Figure A.12 Illustration of the Shearing Strain in a Soil Specimen Tested in the RCTS Apparatus (from Hwang 1997)

where, γ_{eq} : equivalent shearing strain of specimen (%),

$C = \frac{r_{eq}}{r_o}$ (= 0.79 for a solid specimen) (Chen and Stokoe, 1979) ,

r_{eq} : equivalent radius of specimen,

r_o : radius of a solid specimen, and

$$\gamma_{max} = \frac{r_o \times \theta_{max}}{\ell} \tag{A.6}$$

where, θ_{max} : maximum rotation of the top of the specimen, and

ℓ : height of specimen.

To calculate the shearing strain from the accelerometer output, the distance from the center of specimen to the location of accelerometer, r_a, must be known. (The value of r_a is 2 in. (5.08 cm) in the RCTS equipment at The University of Texas at Austin.) The value of peak acceleration measured by the accelerometer can be expressed as:

$$\ddot{z}_a = \frac{\sqrt{2} \times \frac{(32.2 \frac{ft}{sec^2})}{g} \times \frac{V_a}{1000}}{F_{ac}} \tag{A.7}$$

where, $\ddot{z}_a$: peak acceleration measured by the accelerometer ($\frac{ft}{sec^2}$),

V_a : output voltage(rms) of the accelerometer (mV),

g : acceleration of gravity (= 32.2 $\frac{ft}{sec^2}$),

γ_{max} : shearing strain at the outer edge of specimen (%), and

F_{ac} : calibration factor of the accelerometer ($= 2.5234 \times \frac{volt}{g}$).

The peak value of horizontal motion (essentially equals peak rotational motion at the small strains in the RCTS tests) can be expressed as:

$$\ddot{z}_a = z_a \times \omega^2 \tag{A.8}$$

$$\ddot{z}_a = z_a \times (2 \times \pi \times f_r)^2 \tag{A.9}$$

where, ω : angular frequency of the specimen($= 2 \times \pi \times f_r$),

f_r : resonant frequency of specimen (Hz), and

$$z_a = \frac{\ddot{z}_a}{4 \times \pi^2 \times f_r^2} \tag{A.10}$$

Therefore, the equivalent shearing strain of the specimen in the resonant column test can be obtained using following equation:

$$\gamma = 7.882 \times \frac{2\, r_o \times V_a}{\ell \times F_{ac} \times f_r^2} \times 10^{-3}\ \% \tag{A.11}$$

A.4.1.2 Material Damping Ratio

In the RCTS device, the material damping ratio of a soil sample is evaluated by either the half-power bandwidth method or by the free-vibration decay curve. The equation of a single-degree-of-freedom system is:

$$m\ \ddot{z}(t) + c\ \dot{z}(t) + k\ z(t) = F(t) \qquad (A.12)$$

where, m = mass of the system,

c = the constant of a viscous dashpot,

k = a spring constant proportional to the modulus,

F(t) = force as a function of time, t, applied to the system, and

$\ddot{z}(t)$, $\dot{z}(t)$, z(t) represent the acceleration, velocity, and displacement as a function of time, respectively.

If the excitation force is assumed to be a steady-state harmonic function $F(t) = F \cos \omega t$, then Equation A.12 becomes a second-order linear differential equation. The complete solution of this equation is the algebraic sum of the transient (or complementary) solution, obtained by solving the homogeneous equation, for which the right-hand side of Equation A.12 is set equal to zero, and a steady-state (or particular) solution of the equation including the forcing function on the right-hand side. The transient solution of this equation can be shown to be of the form:

$$z_c(t) = e^{-at} (A_1 \sin \omega_d t + A_2 \cos \omega_d t) \qquad (A.13)$$

where, $z_c(t)$: displacement of the system for transient state

$$a = \frac{c}{2\ m} \qquad (A.14)$$

ω_d = damped natural circular frequency,

$$\omega_d = \omega_n \sqrt{1 - D^2} \qquad \text{(A.15)}$$

ω_n = undamped natural circular frequency ($= \sqrt{\frac{k}{m}}$),

D = damping ratio ($= \frac{c}{c_c}$),

c_c = critical damping coefficient ($= 2\sqrt{k\,m}$), and

A_1, A_2 = arbitrary constants obtained by substituting the initial boundary conditions into the complete solution of the equation.

This transient oscillation at the damped natural circular frequency is a harmonic response of the system that depends on the initial conditions, in which the amplitude decays rapidly with time. Therefore, for most soil dynamic studies, the transient solution is often neglected.

The steady-state solution, $z_p(t)$, is any function, z(t), that satisfies Equation A.13. For harmonic excitation, the solution can be expressed as:

$$z_p(t) = \frac{F \cos(\omega t - \varphi)}{\sqrt{(k - m\omega^2)^2 + \omega^2 c^2}} \qquad \text{(A.16a)}$$

$$z_p(t) = \frac{\frac{F}{k} \cos(\omega t - \varphi)}{\sqrt{\left(1 - \frac{m\omega^2}{k}\right)^2 + \left(\frac{\omega c}{k}\right)^2}} \qquad \text{(A.16b)}$$

$$z_p(t) = \frac{\frac{F}{k} \cos(\omega t - \varphi)}{\sqrt{\left(1 - \left(\frac{\omega}{\omega_n}\right)^2\right)^2 + \left(2D\frac{\omega}{\omega_n}\right)^2}} \qquad \text{(A.16c)}$$

$$\text{where, } \tan\varphi = \frac{\frac{\omega c}{k}}{1 - \frac{m\omega^2}{k}} = \frac{2D\left(\frac{\omega}{\omega_n}\right)}{1 - \left(\frac{\omega}{\omega_n}\right)^2} \quad . \tag{A.17}$$

It should be noted that the resonant circular frequency, ω_r, for which strain amplitude reaches a maximum value is obtained when the denominator in Equation A.16c has a minimum value. Therefore, by differentiating the denominator in Equation A.16c with respect to ω and equating it to zero gives:

$$2\left(1 - \left(\frac{\omega}{\omega_n}\right)^2\right)\left(-\frac{2\omega}{\omega_n^2}\right) + \left(\frac{2D}{\omega_n^2}\right)^2 (2\omega) = 0 \tag{A.18}$$

$$\omega = \omega_r = \omega_n \sqrt{1 - 2D^2} \tag{A.19}$$

Thus the complete solution of Equation A.12 is:

$$z(t) = z_c(t) + z_p(t)$$

$$z(t) = e^{-at}\left(A_1 \sin\omega_d t + A_2 \cos\omega_d t\right) + A_3 \cos(\omega t - \varphi) \tag{A.20}$$

$$\text{where, } A_3 = \frac{\frac{F}{k}}{\sqrt{\left(1 - \left(\frac{\omega}{\omega_n}\right)^2\right)^2 + \left(2D\frac{\omega}{\omega_n}\right)^2}} \quad . \tag{A.21}$$

Free-Vibration Decay Method

The free-vibration decay curve is generated by shutting off the current to the driving coils after soil specimen is excited at first-mode resonance in steady-state vibration. The data are recorded on the digital oscilloscope and are transferred to the computer for calculation of the material damping ratio. The ratio of the natural logarithm of two successive peaks in the free-vibration decay curve is termed the logarithmic decrement, δ, and is expressed as :

$$\delta = \ln \frac{z_n}{z_{n+1}} \qquad \text{(A.22)}$$

where z_n and z_{n+1} = two successive peak amplitudes in the free-vibration decay curve. From Equation A.13, two successive peak amplitudes at time t_0 and $(t_0 + \frac{2\pi}{\omega_d})$ can be obtained, and the logarithmic decrement is expressed as follows:

$$\delta = \frac{\pi\ c}{m\ \omega_d} \qquad \text{(A.23)}$$

Dividing both numerator and denominator of right hand side of Equation A.23 with c_c and rearranging the equation results in:

$$\delta = \frac{2\ \pi\ D}{\sqrt{1\ -\ D^2}} \qquad \text{(A.24)}$$

Material damping ratio is then expressed as follows:

$$D = \sqrt{\frac{\delta^2}{4\,\pi^2 + \delta^2}} \qquad \text{(A.25)}$$

A typical free-vibration decay curve of remolded washed mortar sand and the resulting damping ratio measurement using Equation A.25 are shown in Figures A.3a and A.3b, respectively.

Typical frequency response curves showing the effect of the strain amplitude are presented in Figure A.13. Curves I, II and III correspond to three RC tests at different strain amplitudes. The shear modulus decreases and the material damping ratio increases with increasing strain amplitude. Figure A.14 presents the free-vibration curves at the three strain amplitudes illustrated in Figure A.13. The logarithmic decrement curves for the different strain amplitudes are presented in Figure A.15. This figure also shows that the exponential decay of the oscillation results in a decrease in strain amplitude and also a decrease in damping after a few cycles. In this study, the logarithmic decrement is calculated from the first three cycles of free oscillation. Thus, the material damping ratio calculated from the free-vibration decay curve does not actually correspond to the maximum strain amplitude. As a result, the average strain amplitude of the first three cycles of the free-vibration decay curve is used as the representative strain amplitude.

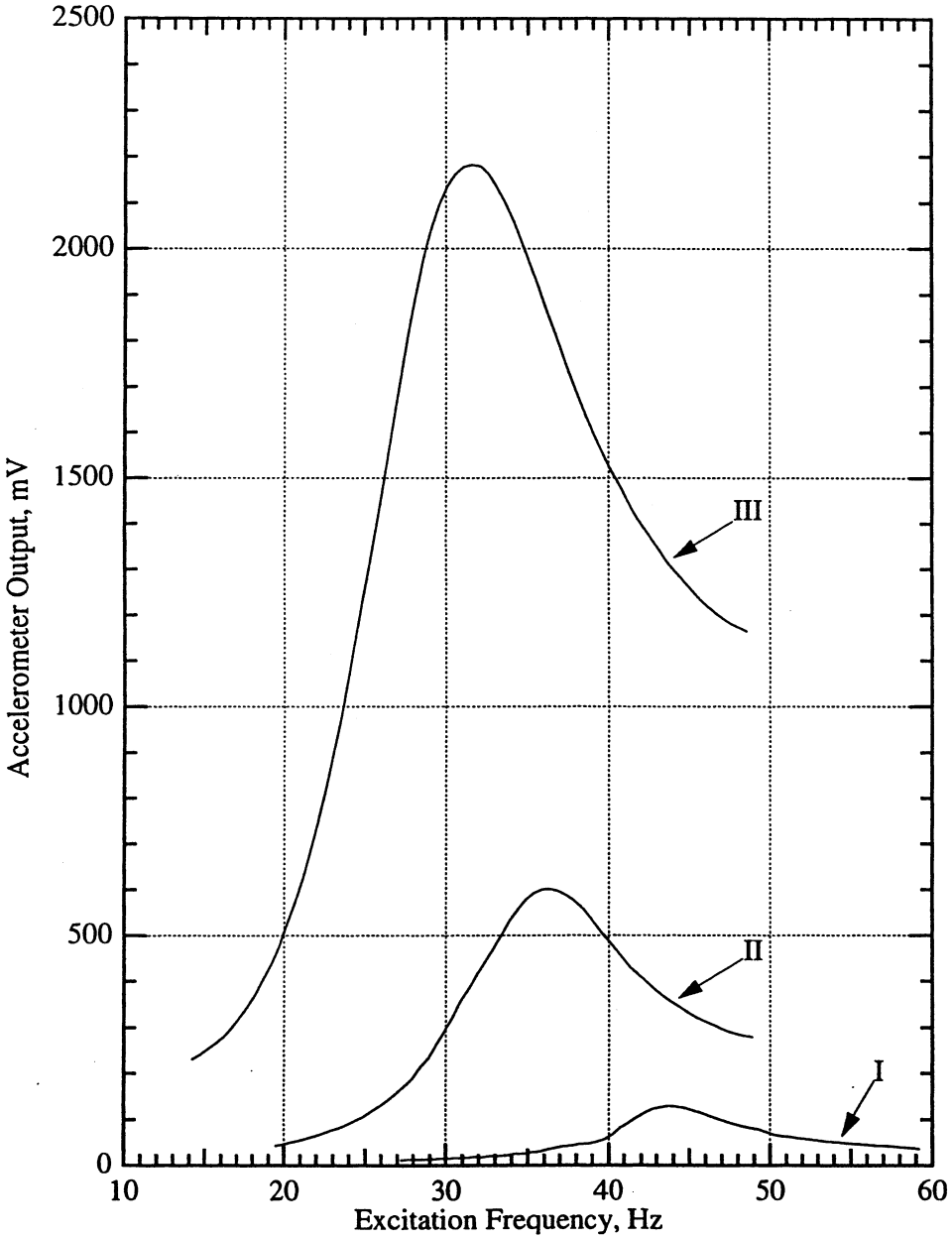

Figure A.13 Typical Frequency Response Curves Showing the Effect of Strain Amplitude on the Measurement of Material Damping Ratio During Resonant Column Testing of a Soil Specimen (from Hwang 1997)

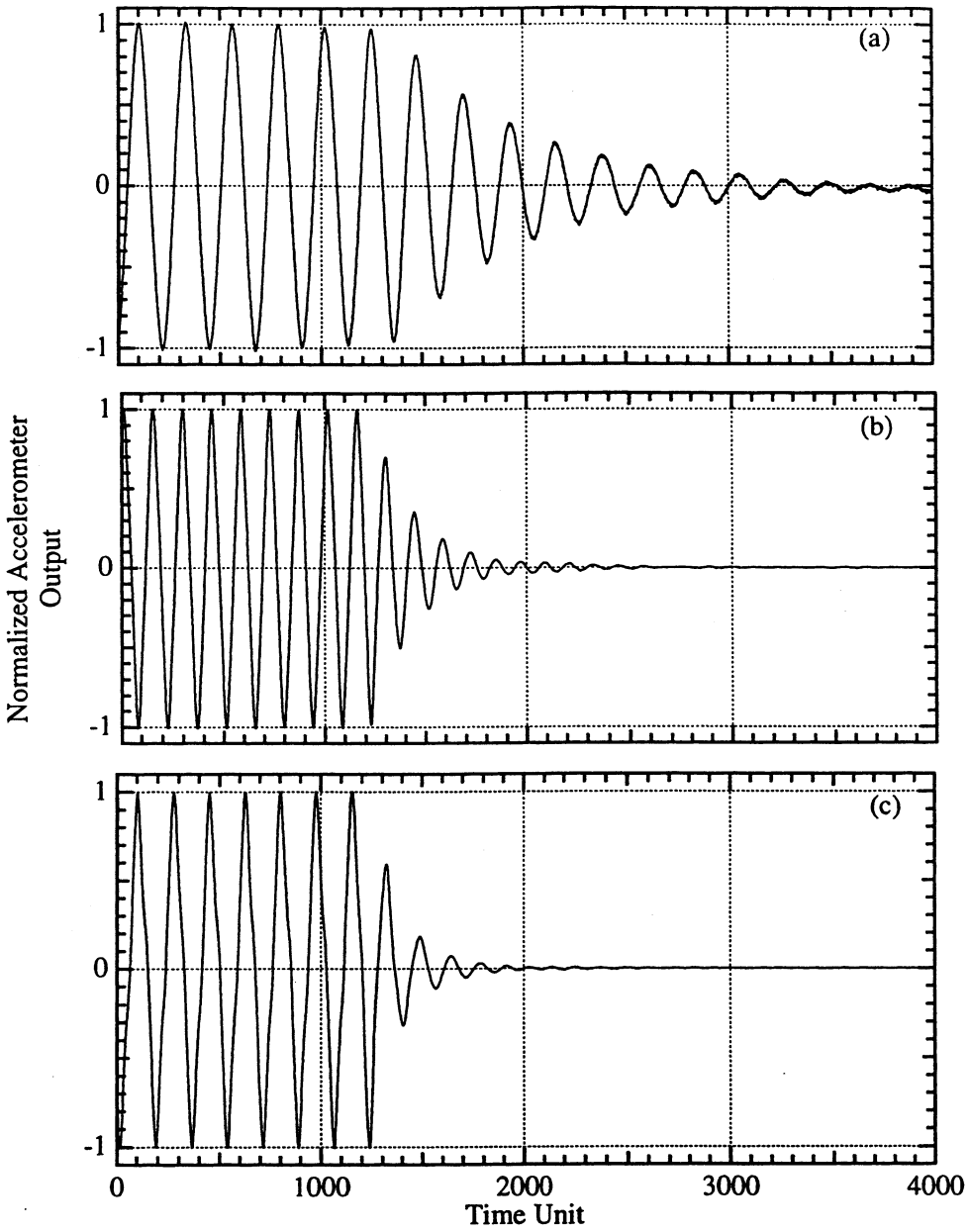

Figure A.14 Typical Free-Vibration Decay Curves Showing the Effect of Strain Amplitude on the Measurement of Material Damping Ratio During Resonant Column Testing of a Soil Specimen (from Hwang 1997)

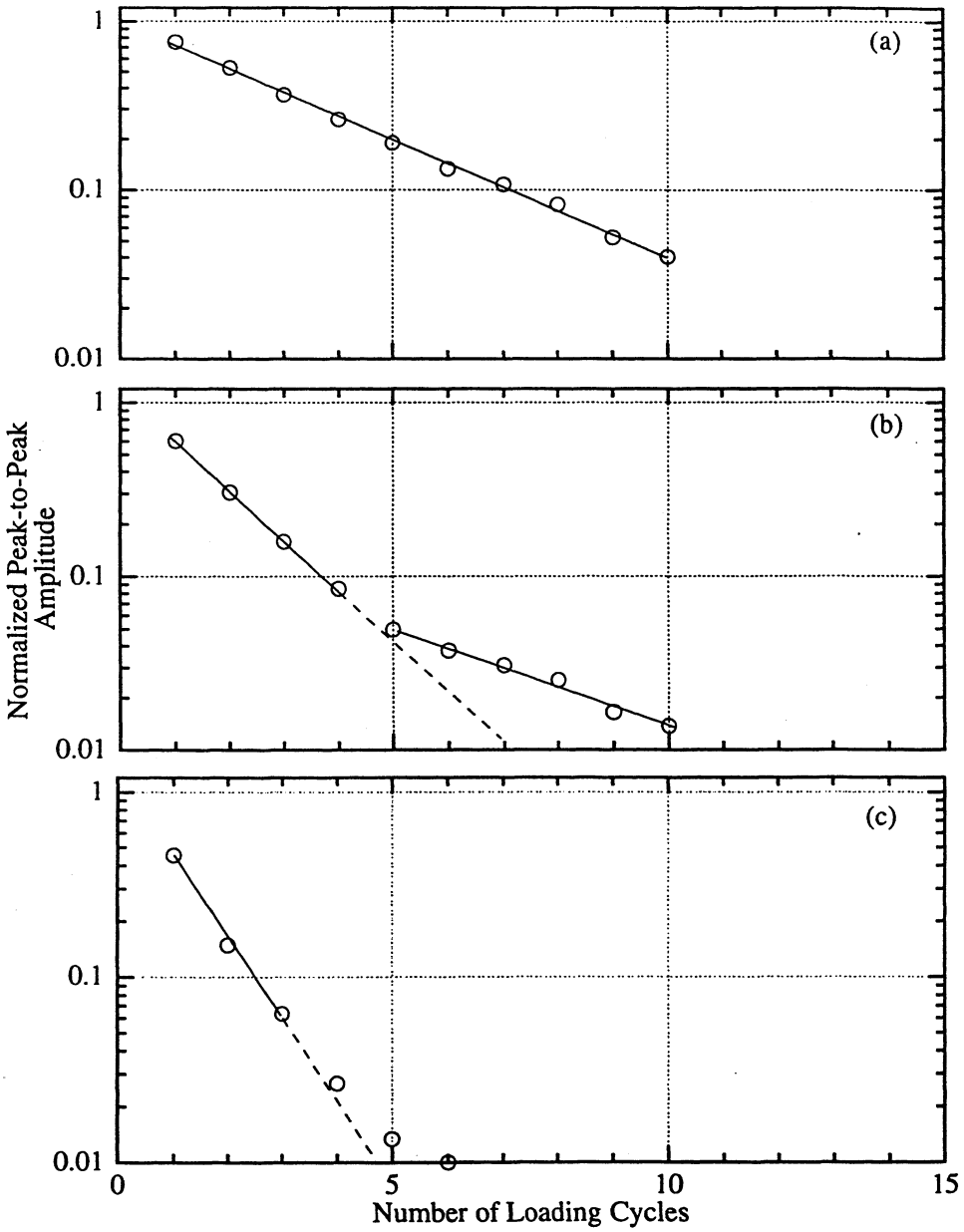

Figure A.15 Typical Plots Showing Effects of Strain Amplitude and Number of Loading Cycles on the Measurement of Material Damping Ratio During Resonant Column Testing of a Soil Specimen (from Hwang 1997)

Half-Power Bandwidth Method

The other method used in measuring the material damping ratio is the half-power bandwidth method based on the vibration of a single-degree-of-freedom system with equivalent viscoelastic damping.

A portion of the frequency response curve, which is around the resonant peak, is used in calculating an estimate of the material damping ratio. The method relates the shape (height to width ratio) of the frequency response curve to damping characteristics.

From the frequency response curve, the maximum amplitude at resonance can be obtained from Equation A.21 by assuming $\omega_r = \omega_n$. If the material damping ratio is small, the equation becomes:

$$A_3 = \frac{F}{k}\,\frac{1}{2D} \tag{A.26}$$

To find the frequencies at which the amplitude is equal to $\frac{1}{\sqrt{2}}$ A_3, A_3 in Equation A.21 is replaced with $\frac{1}{\sqrt{2}}$ A_3 and after calculating the square of both sides, we get:

$$\frac{1}{2}\left(\frac{1}{2D}\right) = \frac{1}{\left(1-\left(\frac{\omega}{\omega_n}\right)^2\right)^2 + \left(2D\frac{\omega}{\omega_n}\right)^2} \tag{A.27a}$$

By rearranging Equation A.27a, the equation becomes:

$$\left(\frac{\omega}{\omega_n}\right)^4 - 2(1 - 2D^2)\left(\frac{\omega}{\omega_n}\right)^2 + (1 - 8D^2) = 0 \qquad \text{(A.27b)}$$

Solving for $\left(\frac{\omega}{\omega_n}\right)^2$ gives:

$$\left(\frac{\omega}{\omega_n}\right)^2 = (1 - 2D^2) \pm 2D\sqrt{1 - D^2} \qquad \text{(A.28)}$$

Since material damping is assumed to be small, neglecting the second-order term of D in Equation A.28 gives:

$$\left(\frac{\omega}{\omega_n}\right)^2 = 1 \pm 2D \qquad \text{(A.29)}$$

Letting ω_1, ω_2 be the two frequencies corresponding to the roots of Equation A.28 gives:

$$4D = \left(\frac{\omega_1^2 - \omega_2^2}{\omega_n^2}\right) \cong 2\left(\frac{\omega_1 - \omega_2}{\omega_n}\right) \qquad \text{(A.30)}$$

Thus the material damping ratio from the half-power bandwidth method is:

$$D \cong \left(\frac{\omega_1 - \omega_2}{2\,\omega_n}\right) \qquad \text{(A.31)}$$

This method is based on the assumption that the material damping ratio is small. The method performs well for material damping ratios smaller than 5%. As the strain amplitude increases as illustrated in Figure A.13, the frequency response curve becomes non-symmetrical. Thus, this method

should not be used in the measurement of material damping ratio at high strain amplitudes.

In this study, the results from the free-vibration decay curves are used at high strain amplitudes. On the other hand, the signal used in free-vibration decay method becomes very weak at low strains. Thus, the half-power bandwidth method is employed in calculation of material damping ratio at low strains (strain amplitudes less than 0.001 %).

A.4.2 Torsional Shear Test

In case of torsional shear tests, the dynamic soil properties (G and D) are determined in a completely different way. Slow cyclic loading of the specimen is excited while the response (displacement at the top of the specimen) of the specimen is measured. The input and output signals are converted into shearing stress and shearing strain, respectively. Then, the hysteresis loop (that forms from plotting of the two measurements) is used in calculating the soil properties. Shear modulus is calculated from the slope of the hysteresis loop and material damping ratio is calculated using the area of the hysteresis loop as illustrated in Figure A.5b.

A.4.2.1 Shear Modulus and Shearing Strain

In the torsional shear test, shear modulus is determined from the stress-strain curve. Shear modulus is evaluated as the secant slope of the

hysteresis loop at which shearing strain reaches its maximum value. It is expressed as:

$$G = \frac{\tau}{\gamma} \tag{A.32}$$

where G is the shear modulus, τ is the peak shearing stress and γ is the peak shearing strain.

Shearing Stress

When a specimen is subjected to a torsional force, T (= F × 2 r_o), as shown in Figure A.16, the shearing stress, τ, increases linearly with radius, r. The shearing force acting over a unit area, dA, is $\tau \times dA$, and the moment of this force about the longitudinal axis of the specimen is $r \times \tau \times dA$. The total torque, T, is the summation of such moments over the entire cross-sectional area. Thus the equation of the total torque applied to the specimen can be written as:

$$T = \int_{r = r_1}^{r = r_2} r \times \tau \times dA \tag{A.33}$$

where, $dA = (2 \times \pi \times r) \times dr$. The shearing stress at the center of dA can be expressed as:

$$\tau = \tau_{max} \times \frac{r}{r_o} \tag{A.34}$$

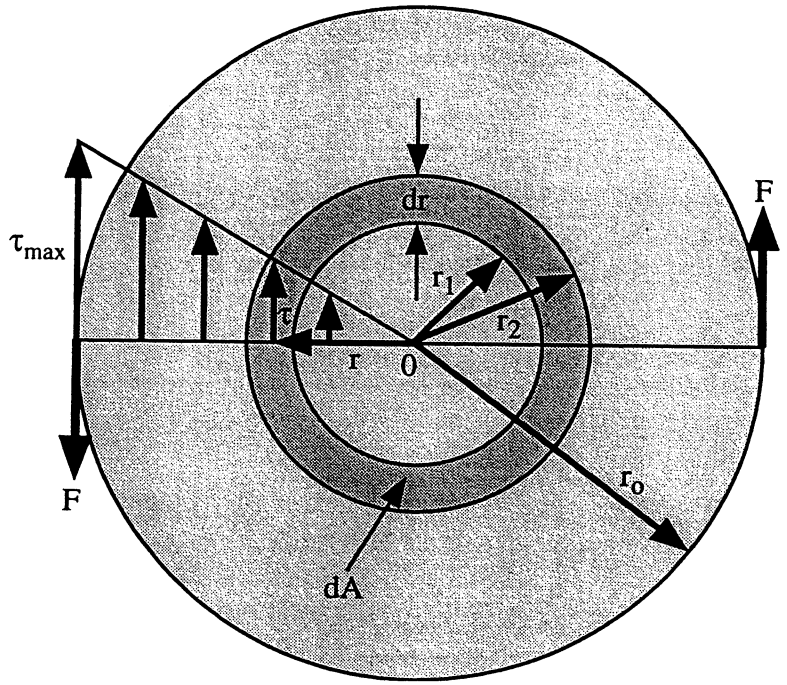

Figure A. 16 Cross-Sectional View of the Specimen in the Torsional Shear Test (from Hwang 1997)

Thus, Equation A.33 can be rewritten as:

$$T = \frac{2 \times \pi \times \tau_{max}}{R} \int_{r = r_1}^{r = r_2} r^3 \, dr$$

$$= \frac{\tau_{max}}{r_o} \times \frac{\pi}{2} \times (r_2^4 - r_1^4) = \frac{\tau_{max}}{r_o} \times J_p \qquad (A.35)$$

where J_p is the area polar moment of inertia. The maximum shearing stress from Equation A.35 can be expressed as:

$$\tau_{max} = r_o \times \frac{T}{J_p} \qquad (A.36)$$

Because shearing stress is assumed to vary linearly across the radius, the equivalent torsional shearing stress can be defined as:

$$\tau_{eq} = r_{eq} \times \frac{T}{J_p} \qquad (A.37)$$

The value of equivalent radius, r_{eq}, is the same value as discussed in the resonant column analysis for calculation of shearing strain (Section A.4.1.1). The value of applied torque, T, is calculated from the input voltage applied to the drive system, V_T (volt), and the torque calibration factor, K_T ($\frac{\text{torque}}{\text{volt}}$).

Therefore, the equivalent shearing stress applied to the specimen is:

$$\tau_{eq} = r_{eq} \times K_T \times \frac{V_T}{J_p} \qquad (A.38)$$

Shearing Strain

The shearing strain is determined from the displacement measured at the top of the specimen. The proximitor output voltage, V_P (volt), is converted to displacement by using the proximitor calibration factor, K_P ($\frac{rad}{volt}$). Thus, the equivalent shearing strain is:

$$\gamma_{eq} = r_{eq} \times K_P \times \frac{V_P}{l} \qquad (A.39)$$

Shear Modulus

After calculating the values of shearing stress and shearing strain following the procedure discussed above, the shear modulus is obtained by using Equation A.32.

A.4.2.2 Damping Ratio From The Hysteresis Loop

The hysteresis loop (that forms from plotting shearing stress versus shear strain) is used in determining the material damping ratio in torsional shear test. Material damping ratio is defined as the ratio of the total amount of energy dissipated and the peak strain energy stored in the specimen in one complete loading cycle. Based on this definition, material damping ratio can be written as:

$$D = \frac{1}{4\pi} \times \frac{W_d}{W_s} \qquad (A.40)$$

where W_d is the area of the hysteresis loop and W_s is the area of triangle as shown in Figure A.17. The derivation of Equation A.40 can be found in Thompson (1965).

A.5 Calibration Of The Combined Resonant Column And Torsional Shear Equipment

The combined RCTS equipment is composed of several pieces that have to be calibrated. Accelerometers, LVDT's and proximitors on each drive plate are some of the components that have to be calibrated. The polar moment of inertia and damping characteristics of each drive plate, and the characteristics of each drive system need to be determined. The calibration factors recommended by the manufacturer of each component of the system (such as accelerometers, LVDT's and proximitors) are verified before integrating these components into the RCTS device. Also, all monitoring devices in the system (such as voltmeter, frequency counter, digital oscilloscope, function generator and digital filter) are verified to be in proper operation conditions by checking them with NIST traceable equipment. Thus, only calibrations related with the mechanical, physical and electro-magnetic properties of the system are explained briefly in this section. Further details can be found in Hwang (1997).

To facilitate the calibration process, a total of eighteen brass specimens have been fabricated in the Civil Engineering machine shop by Mr. James

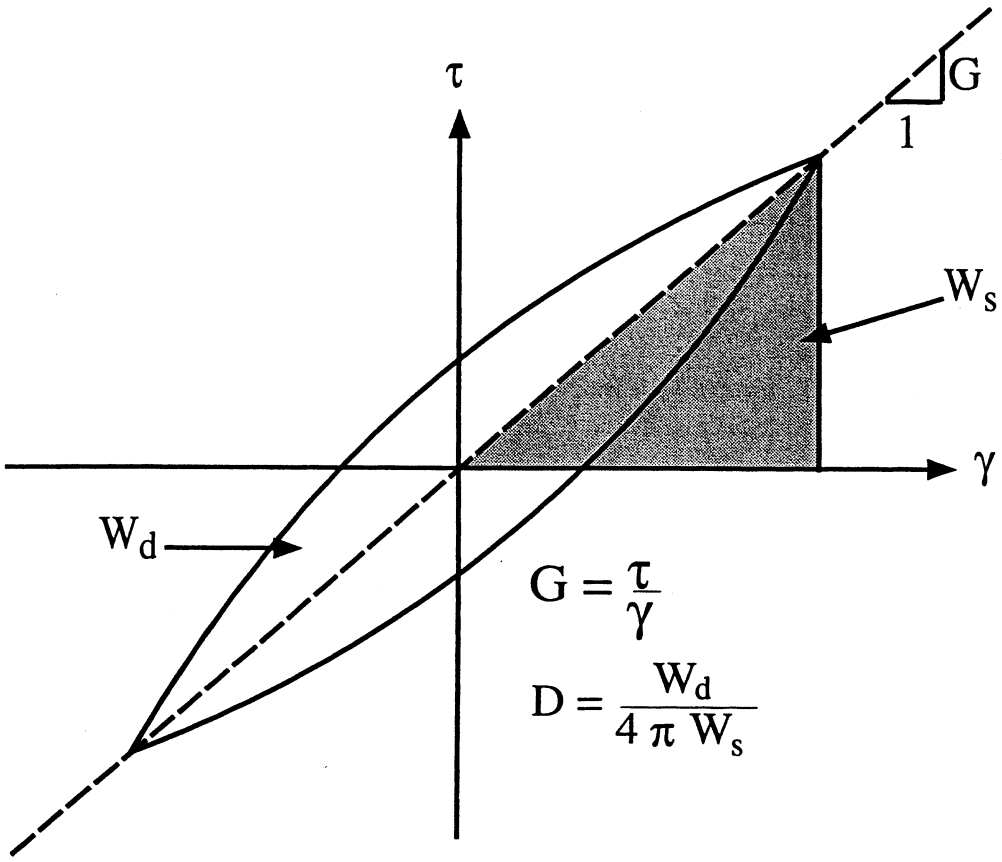

Figure A.17 Illustration of Hysteresis Loop Measured in the Torsional Shear Test Showing the Evaluation of Shear Modulus (G) and Material Damping Ratio (D) (from Hwang 1997)

Stewart at The University of Texas at Austin. The physical properties of these specimens are listed in Table A.1, and a side view of a typical specimen is presented in Figure A.18. These metal specimens are used throughout the calibration process.

A.5.1 Resonant Column Test

A.5.1.1 Calibration of Mass Polar Moment of Inertia of the Drive Plate

As indicated in Equation A.1, the calculation of the shear wave velocity (and therefore the shear modulus) is a function of the mass polar moment of inertia of the top cap and the drive plate. Since it would be very difficult to calculate the actual value of the mass polar moment of inertia, I_o, accurately, an indirect approach is employed in this part of the calibration procedure. The fabricated metal specimens are tested with a drive plate combined with different sets of fabricated metal plates of known mass polar moments of inertia. The resonant frequencies measured for each case (sets of known plates) are recorded.

The resonant frequency of a specimen is:

$$f_r = f_n \times \sqrt{1 - 2\ D^2} \qquad \text{(A.3)}$$

Table A.1 Metal Specimens Used to Calibrate RCTS Equipment (from Hwang 1997)

Specimen Number	Outside Diameter		Inside Diameter		Height		Weight
	inch	mm	inch	mm	inch	mm	gram
1(Brass Tube)	1.000	25.40	0.875	22.23	4.98	126.5	132.35
2(Brass Tube)	0.875	22.23	0.813	20.64	6.96	176.8	79.96
3(Brass Tube)	0.875	22.23	0.813	20.64	8.49	215.6	97.07
4(Brass Tube)	0.750	19.05	0.688	17.46	6.97	177.0	70.72
5(Brass Tube)	0.750	19.05	0.688	17.46	8.49	215.7	85.87
6(Brass Tube)	0.625	15.88	0.563	14.29	6.96	176.8	58.45
7(Brass Tube)	0.625	15.88	0.563	14.29	8.49	215.7	70.94
8(Brass Tube)	0.375	9.53	0.313	7.94	6.94	176.3	33.69
9(Brass Tube)	0.375	9.53	0.313	7.94	8.44	214.5	40.86
10(Brass Rod)	0.313	7.94	0.000	0.00	6.92	175.7	74.46
11(Brass Rod)	0.313	7.94	0.000	0.00	8.44	214.4	90.30
12(Brass Rod)	0.500	12.70	0.000	0.00	7.00	177.8	191.22
13(Brass Rod)	0.750	19.05	0.000	0.00	7.00	177.5	429.52
14(Brass Rod)	0.250	6.35	0.000	0.00	6.96	176.7	47.53
15(Brass Rod)	1.500	38.10	0.000	0.00	7.00	177.8	1731.64
16(Brass Tube)	0.500	12.70	0.438	11.11	6.97	177.1	44.63
17(Brass Tube)	0.500	12.70	0.438	11.11	8.48	215.3	54.29
18(Brass Tube)	1.000	25.40	0.875	22.23	6.97	177.0	178.50

Unit Weight of Brass = 8490 kg/m3 (=0.316 lbs/in3)

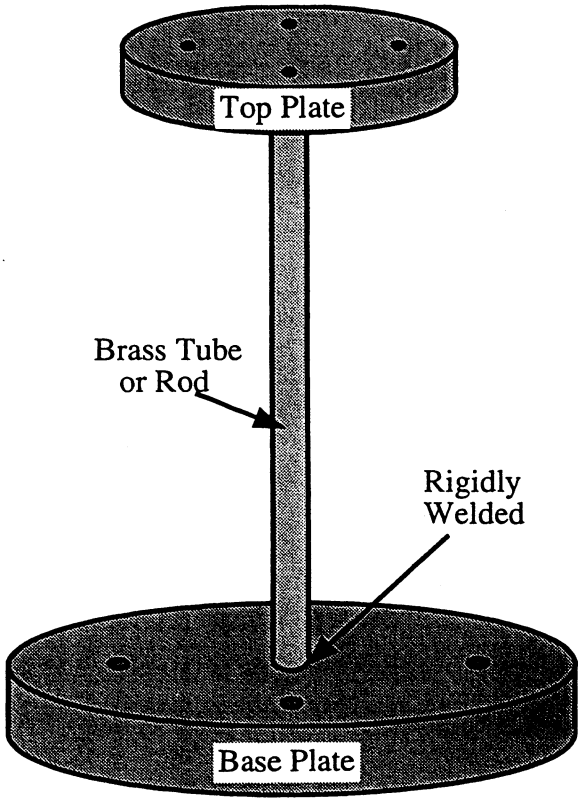

Figure A.18 Side View of a Typical Brass Specimen Used in the Calibration of the Combined RCTS Equipment (from Hwang 1997)

Since $f_n = \frac{1}{2\pi} \times \sqrt{\frac{k}{I_o+I_t}}$, Equation A.3 becomes:

$$f_r = \frac{1}{2\pi} \times \sqrt{\frac{k}{I_o+I_t}} \times \sqrt{1 - 2D^2} \qquad (A.41)$$

where, f_n = natural frequency of the brass specimen,

D = material damping ratio of the brass specimen ($\approx$ 0 %),

k = stiffness of the brass specimen,

I_o= mass polar moment of inertia of the mass (including everything such as drive plate, accelerometer, counter weight for accelerometer, proximitor target, LVDT core, magnets) on top of the brass specimen, and

I_t = mass polar moment of inertia of added top plate(s).

Equations for two different cases can be combined to yield:

$$\left(\frac{f_{ro}}{f_{r1}}\right)^2 = \frac{(I_o + I_t + \Delta I_1)}{(I_o+I_t)} \qquad (A.42)$$

Equation A.42 can be solved to calculate the mass polar moment of inertia of the drive plate as illustrated in Table A.2.

Table A.2 Calculation of the Mass Polar Moment of Inertia for Drive Plate No. 5 (from Hwang 1997)

Using Metal Specimen No. 1

Added Mass Plate No.	I of Added Masses ($lb\text{-}ft\text{-}sec^2$) (Known)	Resonant Frequency f_r (Hz) (Measured)	I of the Drive Plate, I_o, ($lb\text{-}ft\text{-}sec^2$) (Unknown)	Torsional Stiffness of Specimen (ft-lb/rad) (Unknown)
Top Cap	4.623E-05	203.988	-	
1	5.772E-04	181.309	1.9514E-03	3206
1+2	1.109E-03	166.143	2.0483E-03	3365
1+2+3	1.640E-03	154.351	2.0889E-03	3431
		Ave. I_o =	2.0295E-03	3334

Using Metal Specimen No. 2

Top Cap	4.623E-05	106.297	-	
1	5.772E-04	94.965	2.0533E-03	916
1+2	1.109E-03	86.659	2.0602E-03	919
1+2+3	1.640E-03	80.188	2.0589E-03	918
		Ave. I_o =	2.0575E-03	918

Using Metal Specimen No. 16

Top Cap	4.623E-05	45.156	-	
1	5.772E-04	40.302	2.0330E-03	164
1+2	1.109E-03	36.800	2.0557E-03	165
1+2+3	1.640E-03	33.996	2.0393E-03	164
		Ave. I_o =	2.0427E-03	164

Average I_o of Drive Plate No. 5 = $((2.0295+2.0575+2.0427)/3)*10^{-3}$

= $2.0432*10^{-3}$ ($lb_m\text{-}ft^2$)

A.5.1.2 Calibration of Equipment-Generated Damping in The Drive System

In the last few years, an equipment generated damping has been found to exist in the resonant column system. Tests on metal specimens revealed that this damping exists whenever a specimen is driven with the current in the drive coils and it is frequency dependent (as shown in Figure A.19). Since the material damping ratio of brass is negligible (less than 0.01 % in these tests), the damping of the metal specimens measured in the course of calibration is a result of the equipment. The testing is based on a fixed-free boundary condition and the coil-magnet interaction at the drive system violates this assumption and causes second order effects that change the damping measurements. The analysis of the test results of metal specimens suggest that there is a damping coefficient associated with each drive plate, and the equipment generated damping is equal to:

$$D_{eq} = \frac{c}{4 \pi I_{\psi} f_r} \tag{A.43}$$

Figures A.20 and A.21 present equipment generated damping of drive plate No.4 measured by the half-power bandwidth method and by the free-vibration decay curve. Tables A.3 and A.4 present the calculated values of c based on these measurements. The tests of metal specimens also suggest that

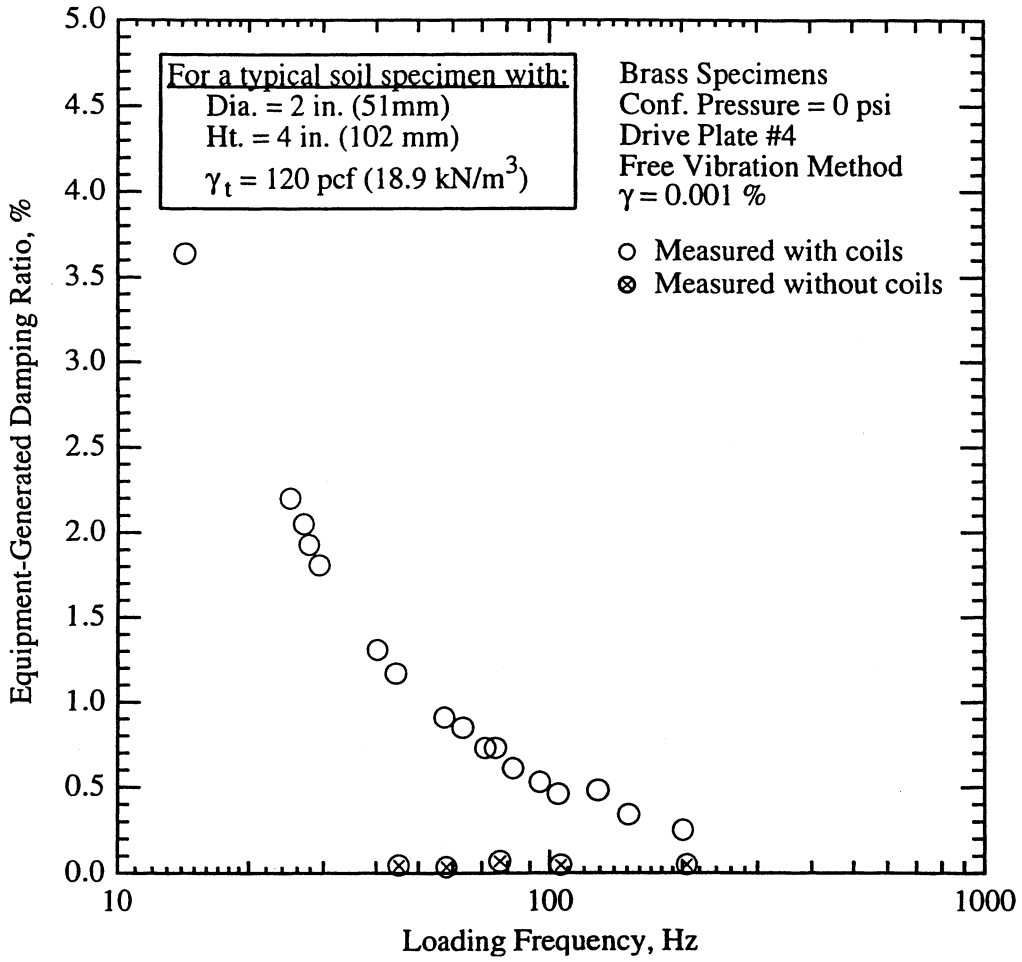

Figure A.19 Comparison of Equipment-Generated Damping Ratios Measured in Free Vibration RC Tests With and Without the Electrical Coils in Place (from Hwang 1997)

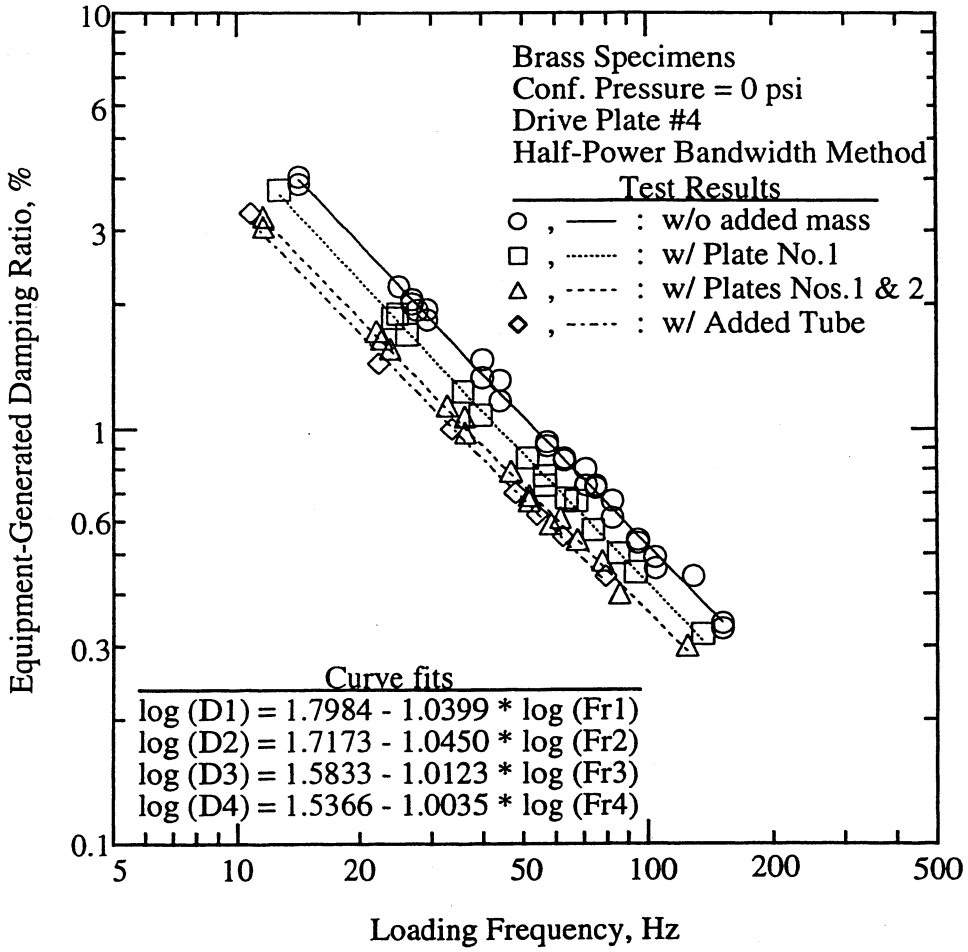

Figure A.20 Variation of the Equipment-Generated Damping Ratio Measured by Half-Power Bandwidth Method with Three Different Masses Added on Top of Drive Plate No. 4 (from Hwang 1997)

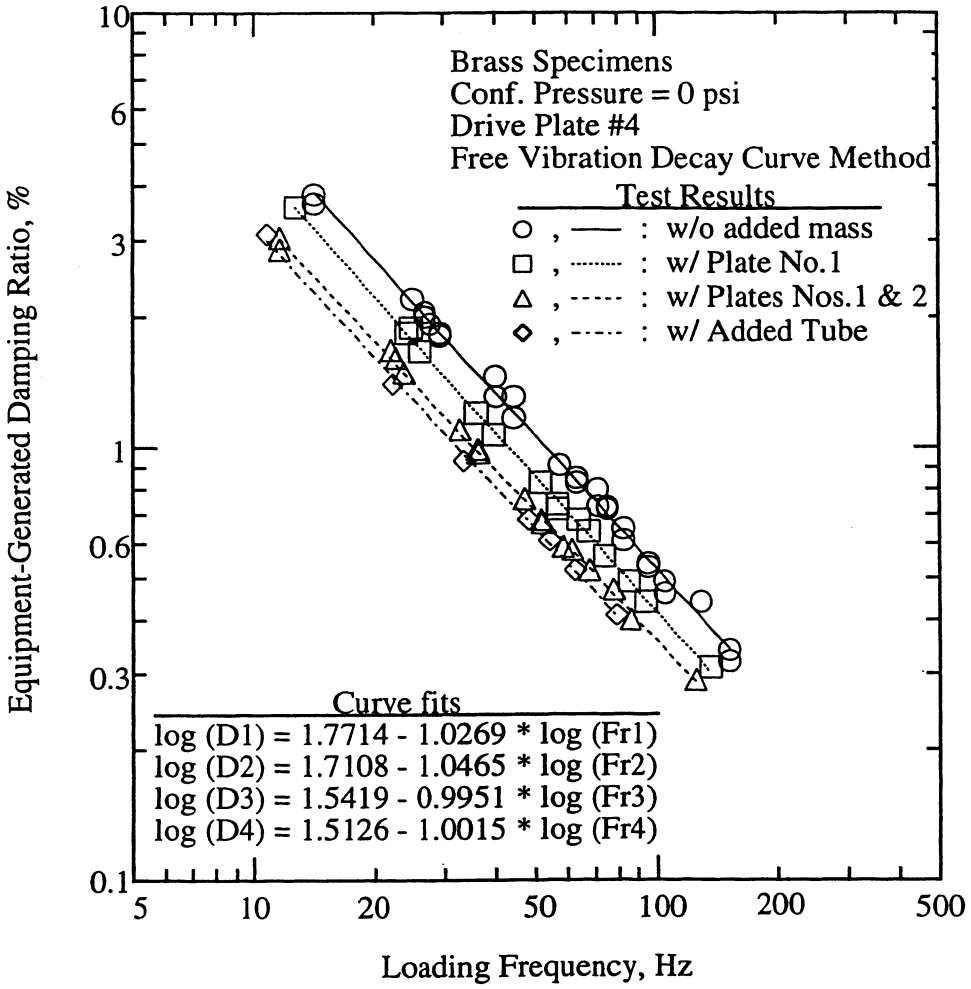

Figure A.21 Variation of the Equipment-Generated Damping Ratio Measured by Free Vibration Decay Curve Method with Three Different Masses Added on Top of Drive Plate No. 4 (from Hwang 1997)

Table A.3 Summary of the Calculation Results Used in the Calibration of the Equipment-Generated Damping Using Half-Power Bandwidth Method From Resonant Column Tests of Metal Specimens (from Hwang 1997)

Metal Specimen Number	Without Added Mass				With Plate No. 1				With Plate No. 1 and 2				With a Tube			
	f_r [1] Hz	c_c [2]	D_{hp} [3] %	c [4]	f_r [1] Hz	c_c [2]	D_{hp} [3] %	c [4]	f_r [1] Hz	c_c [2]	D_{hp} [3] %	c [4]	f_r [1] Hz	c_c [2]	D_{hp} [3] %	c [4]
2	104.5	2.89	0.46	0.013	93.6	3.22	0.45	0.014	85.8	3.52	0.40	0.014	79.3	3.88	0.44	0.017
3	94.9	2.63	0.53	0.014	85.2	2.93	0.50	0.015	77.9	3.20	0.48	0.015				
4	82.4	2.28	0.61	0.014	73.9	2.54	0.57	0.014	67.7	2.78	0.54	0.015	62.5	3.06	0.55	0.017
5	75.1	2.08	0.73	0.015	67.4	2.31	0.67	0.016	61.6	2.53	0.61	0.015				
6	63.2	1.75	0.85	0.015	56.7	1.95	0.73	0.014	51.8	2.12	0.67	0.014	48.0	2.35	0.70	0.016
7	57.3	1.58	0.93	0.015	51.4	1.76	0.85	0.015	47.0	1.93	0.79	0.015				
8	27.7	0.77	1.93	0.015	24.8	0.85	2.08	0.018	22.7	0.93	1.65	0.015				
9	25.0	0.69	2.20	0.015												
10	29.3	0.81	1.83	0.015	26.1	0.90	1.69	0.015	23.8	0.98	1.56	0.015	22.3	1.09	1.44	0.016
11	26.9	0.74	2.05	0.015	24.1	0.83	1.85	0.015	22.0	0.90	1.72	0.016				
12	71.2	1.97	0.73	0.014	63.8	2.19	0.68	0.015	58.4	2.40	0.59	0.014	54.2	2.65	0.62	0.016
13	151.2	4.19	0.34	0.014	135.6	4.66	0.32	0.015	124.4	5.11	0.30	0.015	113.7	5.57	0.49	0.027
14	14.2	0.39	4.03	0.016	12.7	0.44	3.75	0.016	11.6	0.48	3.06	0.015	10.8	0.53	3.30	0.017
16	44.3	1.22	1.17	0.014	39.7	1.36	1.08	0.015	36.4	1.49	0.98	0.015	33.7	1.65	1.00	0.016
17	40.1	1.11	1.33	0.015	36.0	1.24	1.23	0.015	32.9	1.35	1.14	0.015				
18	128.8	3.57	0.48	0.017	115.2	3.97	0.48	0.019	105.7	4.35	0.44	0.019	93.4	4.58	0.58	0.027

Note:

1. f_r = first-mode resonant frequency of the metal specimen
2. c_c = critical damping coefficient of the metal specimen (lb-sec/rad)
3. D_{hp} = equipment-generated damping ratio determined by half-power bandwidth method
4. c = damping coefficient of the metal specimen (lb-sec/rad)

Table A.4 Summary of the Calculation Results Used in the Calibration of the Equipment-Generated Damping Using Free-Vibration Decay Curve Method From Resonant Column Tests of Metal Specimens (from Hwang 1997)

Metal Specimen Number	Without Added Mass				With Plate No. 1				With Plate No. 1 and 2				With a Tube			
	f_r [1] Hz	c_c [2]	D_{fv} [3] %	c [4]	f_r [1] Hz	c_c [2]	D_{fv} [3] %	c [4]	f_r [1] Hz	c_c [2]	D_{fv} [3] %	c [4]	f_r [1] Hz	c_c [2]	D_{fv} [3] %	c [4]
2	104.5	2.89	0.46	0.013	93.6	3.22	0.44	0.014	85.8	3.52	0.40	0.014	79.3	3.88	0.41	0.016
3	94.9	2.63	0.53	0.014	85.2	2.93	0.49	0.014	77.9	3.20	0.47	0.015				
4	82.4	2.28	0.61	0.014	73.9	2.54	0.56	0.014	67.7	2.78	0.52	0.014	62.5	3.06	0.52	0.016
5	75.1	2.08	0.73	0.015	67.4	2.31	0.64	0.015	61.6	2.53	0.58	0.015				
6	63.2	1.75	0.85	0.015	56.7	1.95	0.72	0.014	51.8	2.12	0.67	0.014	48.0	2.35	0.68	0.016
7	57.3	1.58	0.91	0.014	51.4	1.76	0.83	0.015	47.0	1.93	0.76	0.015				
8	27.7	0.77	1.93	0.015	24.8	0.85	1.89	0.016	22.7	0.93	1.61	0.015				
9	25.0	0.69	2.20	0.015												
10	29.3	0.81	1.81	0.015	26.1	0.90	1.67	0.015	23.8	0.98	1.49	0.015	22.3	1.09	1.40	0.015
11	26.9	0.74	2.05	0.015	24.1	0.83	1.84	0.015	22.0	0.90	1.68	0.015				
12	71.2	1.97	0.73	0.014	63.8	2.19	0.68	0.015	58.4	2.40	0.59	0.014	54.2	2.65	0.61	0.016
13	151.2	4.19	0.34	0.014	135.6	4.66	0.31	0.014	124.4	5.11	0.29	0.015	113.7	5.57	0.39	0.022
14	14.2	0.39	3.64	0.014	12.7	0.44	3.57	0.016	11.6	0.48	2.86	0.014	10.8	0.53	3.10	0.016
16	44.3	1.22	1.17	0.014	39.7	1.36	1.07	0.015	36.4	1.49	0.97	0.014	33.7	1.65	0.93	0.015
17	40.1	1.11	1.31	0.015	36.0	1.24	1.20	0.015	32.9	1.35	1.10	0.015				
18	128.8	3.57	0.48	0.017	115.2	3.97	0.48	0.019	105.7	4.35	0.44	0.019	93.4	4.58	0.52	0.024

Note:

1. f_r = first-mode resonant frequency of the metal specimen
2. c_c = critical damping coefficient of the metal specimen (lb-sec/rad)
3. D_{fv} = equipment-generated damping ratio determined by free-vibration decay curve method
4. c = damping coefficient of the metal specimen (lb-sec/rad)

the equipment generated damping is independent of strain amplitude (as presented in Figure A.22).

The equipment generated damping can be treated as a phase shift in the displacement signal (accelerometer output) relative to the driving signal (current in the coils). The phase shift of a sinusoidal wave is additive, in other words, one can subtract or add a phase to a signal without changing its nature. A parametric study of two signals in phase yielded that change of phase is proportional to the change of the area of the hysteresis loop associated with the two signals at small phase angles. Therefore, it is believed to be reasonable to subtract equipment generated damping from the measured values.

A.5.2 Torsional Shear Test

As discussed above, the torsional shear test is based on monitoring the forcing function (current in the drive coil) and the displacement function (proximitor output). The shear modulus and material damping ratio are measured using the resulting hysteresis loop from these two signals.

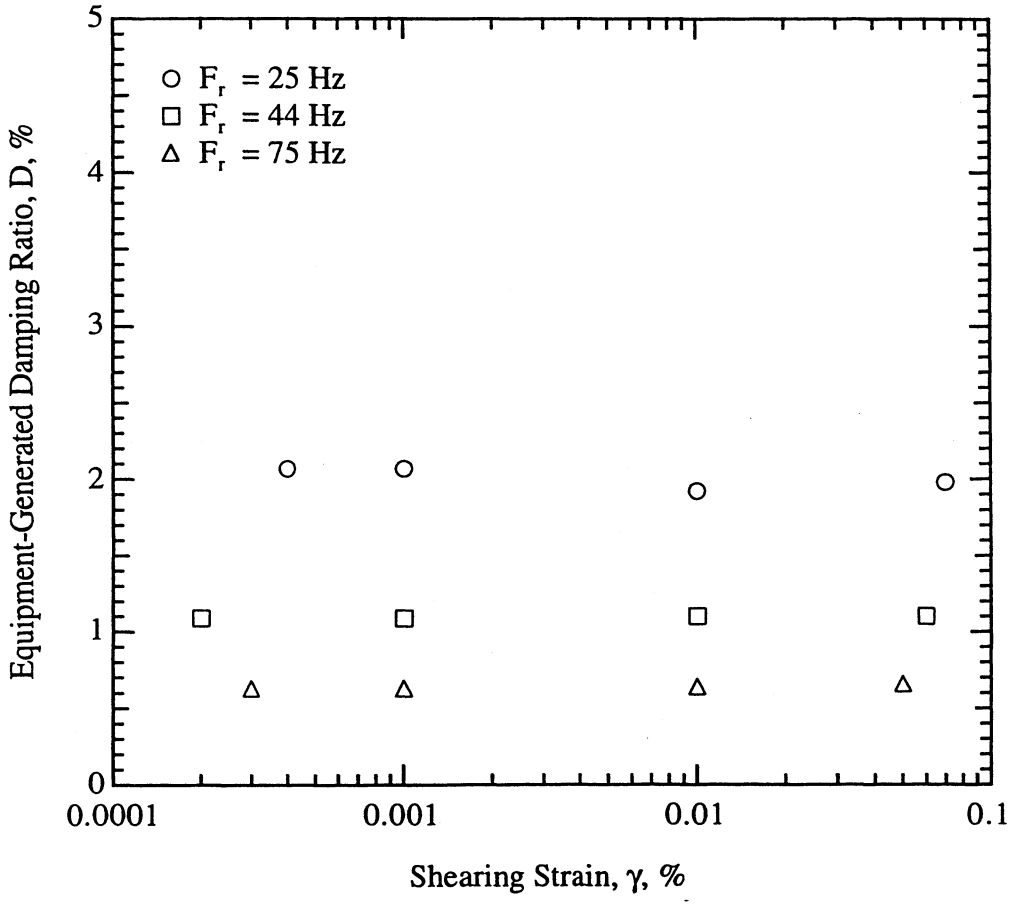

Figure A.22 Effect of Shearing Strain Amplitude on Equipment-Generated Damping Ratio for Drive Plate No. 9 (from Hwang 1997)

A.5.2.1 Calibration of Monitoring System

Calibration of the monitoring system is accomplished by evaluating the complete system together. A metal specimen with known stiffness (the shear modulus determined by the RC test is used to calculate this value) is employed in this procedure.

Calibration Factor of Proximitor System, K_p

As illustrated in Figures A.23 and A.24, the calibration factor of each proximitor is evaluated at different input voltages. Also, the range over which the proximitors are linear is determined. Then, the relationship between the displacement of the target and the distance of the proximitor probe to the center of rotation is established (Figure A.25). The angle of twist from Figure A.25 is then related to the proximitor output at 0.4 in. from the center of the drive plate (which is the location of the proximitor probes during testing). The calibration factor of the proximitor system, K_p, is the slope of the resulting curve fit through the data points in Figure A.26 and is defined as the twist angle per unit proximitor output voltage, $(\frac{rad}{volt})$.

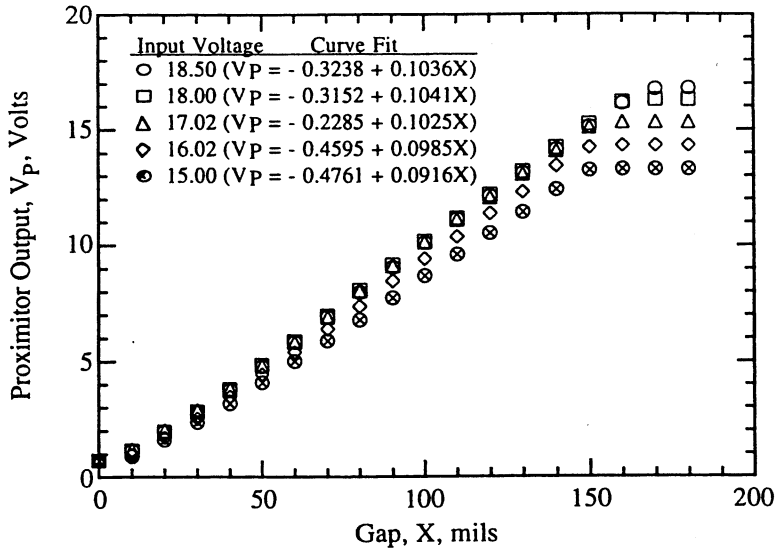

Figure A.23 Relationship Between Gap Size and Proximitor Output Voltage (from Hwang 1997)

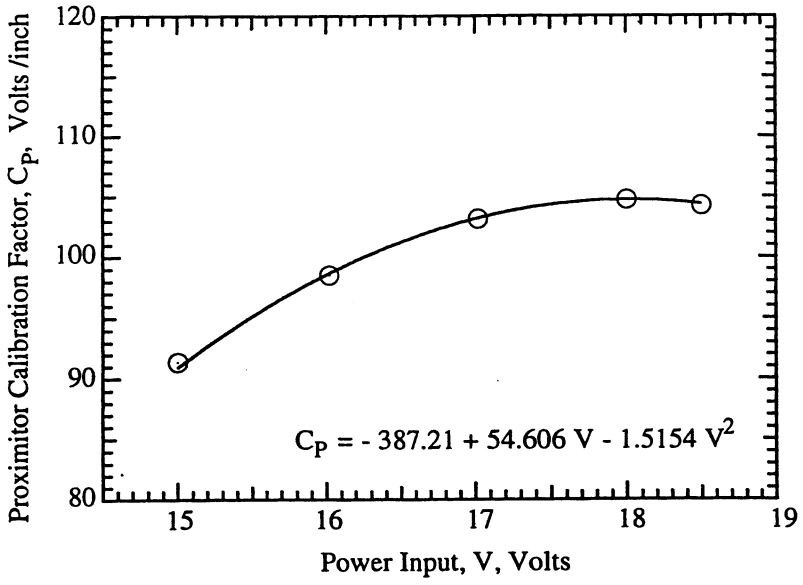

Figure A.24 Relationship Between DC Input Voltage and Proximitor Calibration Factor (from Hwang 1997)

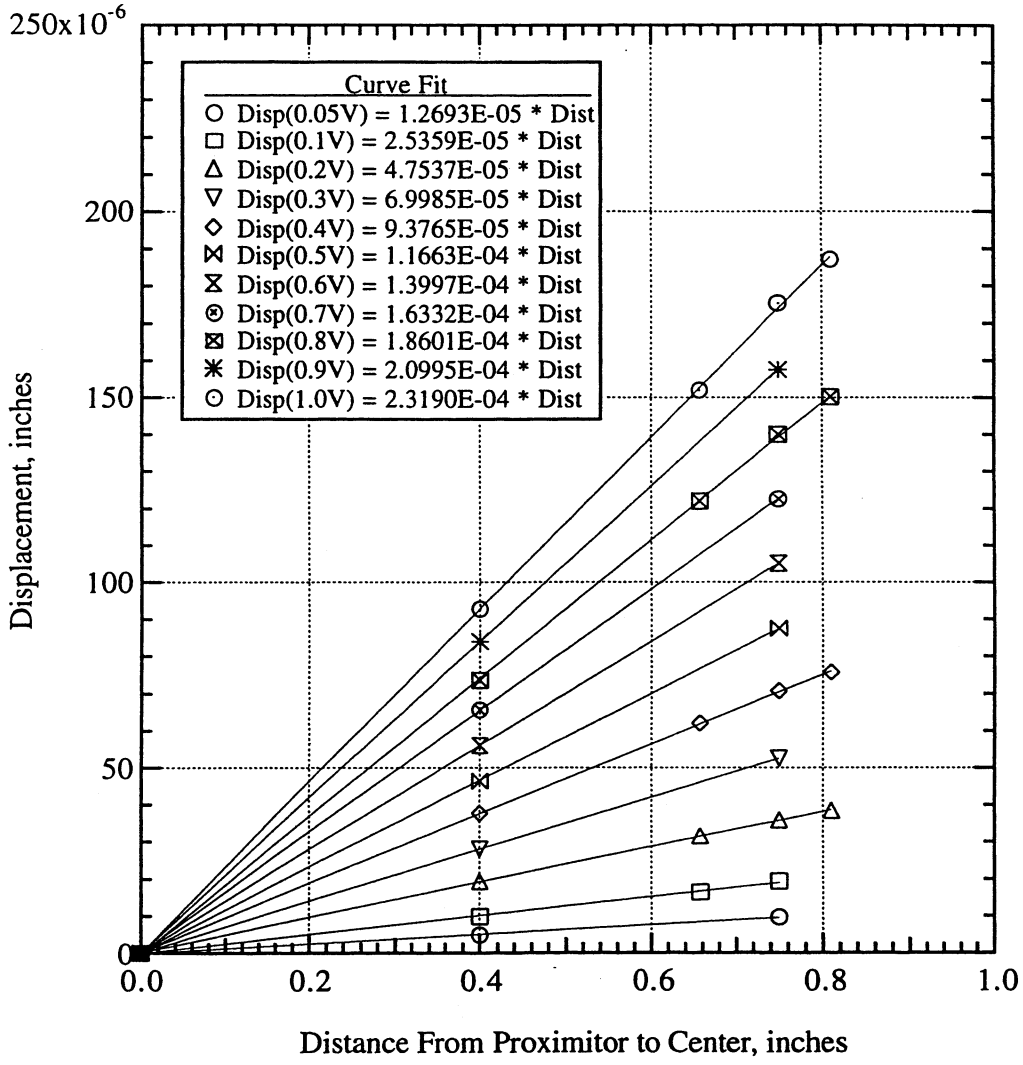

Figure A.25 Determination of Twist Angle at Several Different DC Input Voltages for Calibration of the Proximitor System of Drive Plate No. 4 (from Hwang 1997)

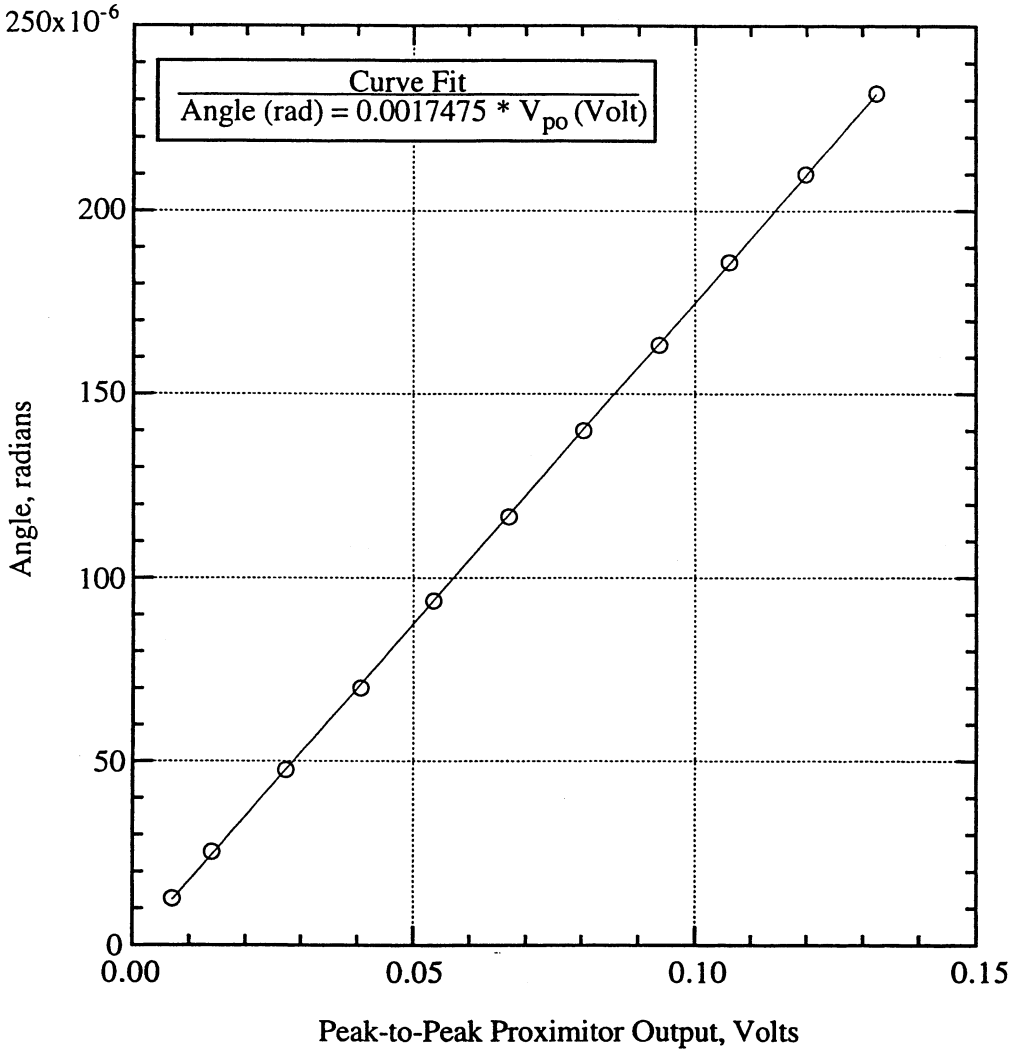

Figure A.26 Determination of the Calibration Factor, K_p, of the Proximitor System (from Hwang 1997)

Torque Calibration Factor, K_T

The torque applied to the brass specimen at a given excitation voltage in the above calibration process can be calculated using Equation A.44:

$$\text{Torque (ft·lb)} = K_\psi \left(\frac{\text{ft·lb}}{\text{rad}}\right) \times \psi \text{ (rad)} \qquad \text{(A.44)}$$

in which the torsional stiffness of the brass specimen, K_ψ, and the calculated twist angle, ψ, at a given excitation voltage are measured.

The calculated torque versus excitation voltage is plotted in Figure A.27 in which the slope of the fitted line through the data points is the torque calibration factor, K_T, defined as the torque per unit excitation voltage, $\left(\frac{\text{ft·lb}}{\text{volt}}\right)$. In other words, the torque calibration factor is calculated by using the shear modulus of the metal specimen obtained from the RC test.

A.5.2.2 Calibration of Equipment-Generated Damping Ratio

As presented in Figure A.28 the equipment damping generated during TS testing is observed to be a linear function of the excitation frequency and it is also observed to be independent of the strain amplitude. The approach explained in the section related with the equipment damping generated from

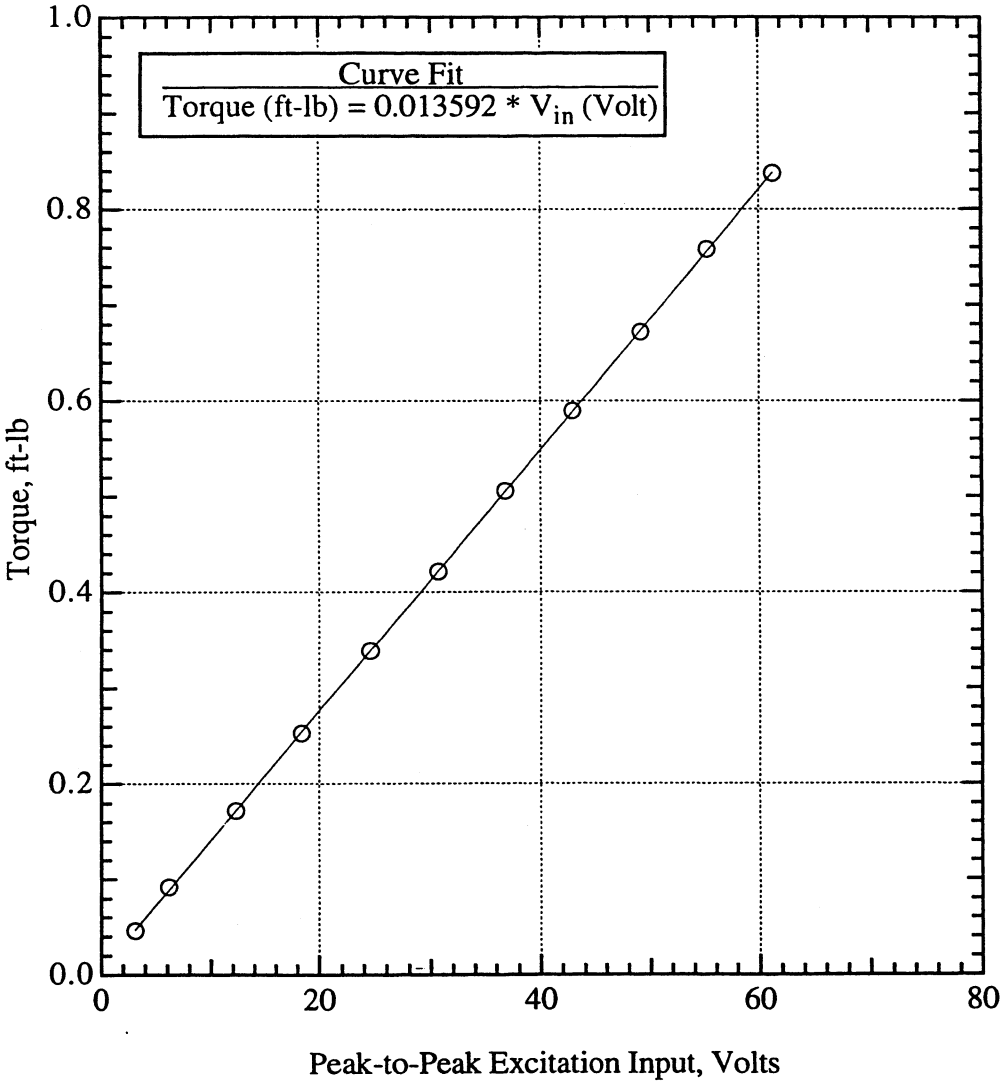

Figure A.27 Determination of Torque Calibration Factor, K_T, of the Proximitor System of Drive Plate No. 4 (from Hwang 1997)

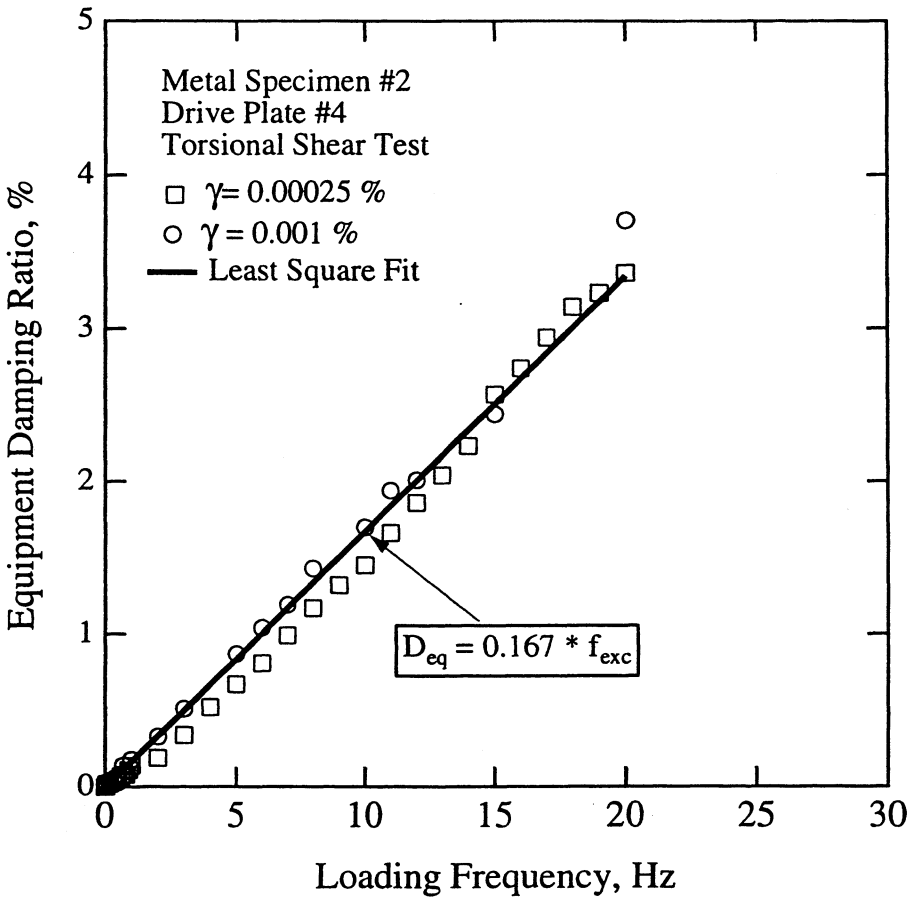

Figure A.28 Variation of the Equipment-Generated Damping Ratio with Excitation Frequency Determined in the Torsional Shear Test Equipment (after Hwang 1997)

RC tests (Section A.5.1.2) is also used in evaluating the correction to the measurements in the TS tests.

In case of the RC tests, the equipment generated damping is observed to be inversely proportional to the testing frequency (resonant frequency of the specimen). In case of the TS tests, equipment generated damping is observed to be proportional to the testing frequency.

The difference between the two cases is evidently the result of the difference of the testing procedures. In case of the resonant column test, the measurements are made at the resonant frequency. The inertia of the drive plate and the back EMF currents in the drive coils cause the equipment damping. In case of the torsional shear test, the voltage level in the drive coils is much higher (since there is not any specimen amplification during a TS test, more torque is necessary to achieve the same strain amplitude of an RC test). The higher voltages associated with the torsional shear test are believed to do work on the magnet (making them weaker in the long run) and generate heat during testing.

A.6 SUMMARY

The RCTS equipment was described in this appendix. The theory of testing was presented along with the measurement techniques involved in this study. The calibration process was also briefly discussed. The recent developments in explaining equipment generated damping were also presented. However, further research would be beneficial to validate more completely the theories associated with this subject.

APPENDIX B

UTA-10-A

BOREHOLE ID : 98 - 20

SAMPLE NO. = 27

DEPTH = 27.5 ft (8.4 m)

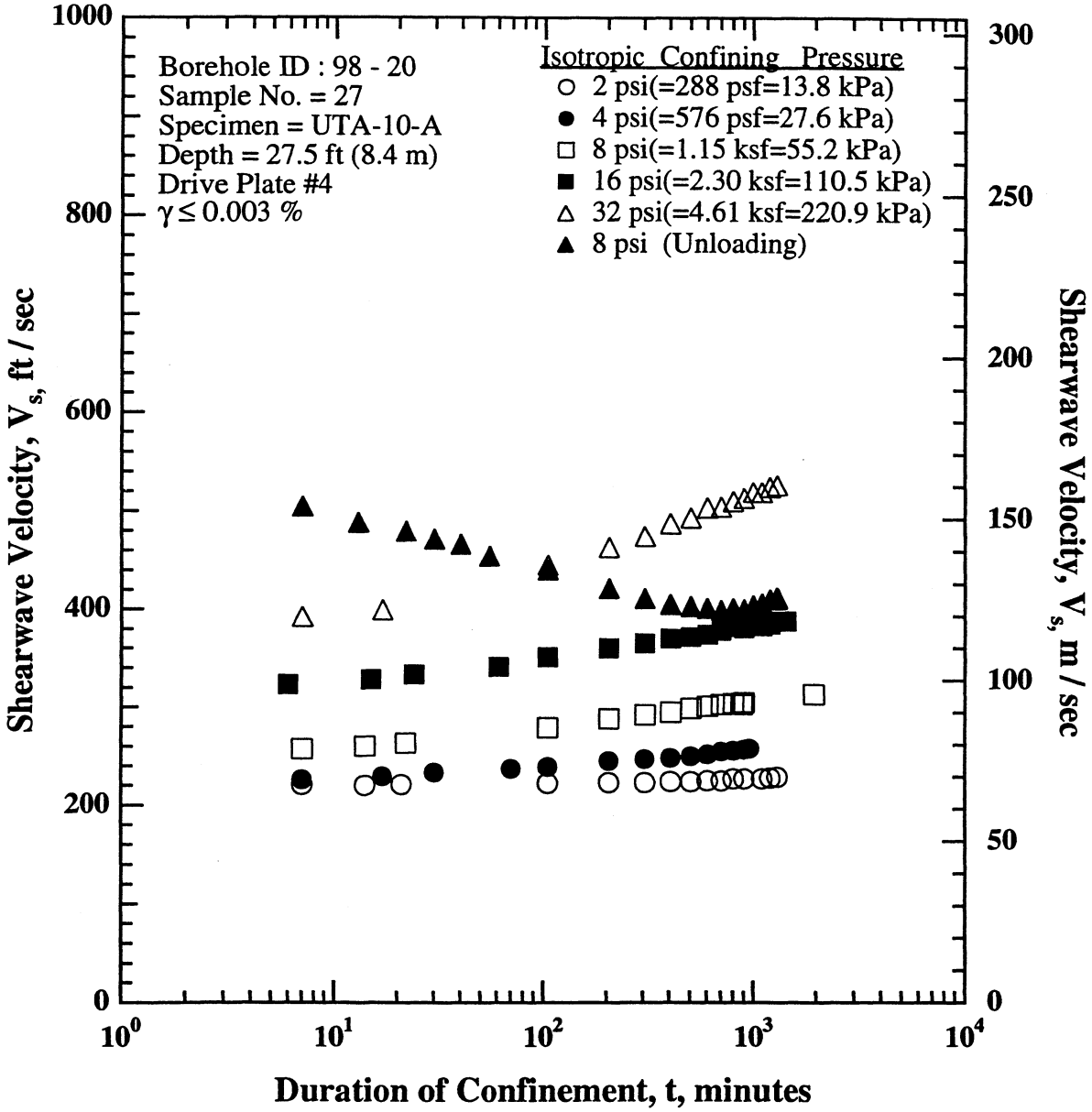

Figure B.1 Variation in Low-Amplitude Shear Wave Velocity with Magnitude and Duration of Isotropic Confining Pressure from Resonant Column Tests of Specimen UTA-10-A from the East Bay Bridge Site.

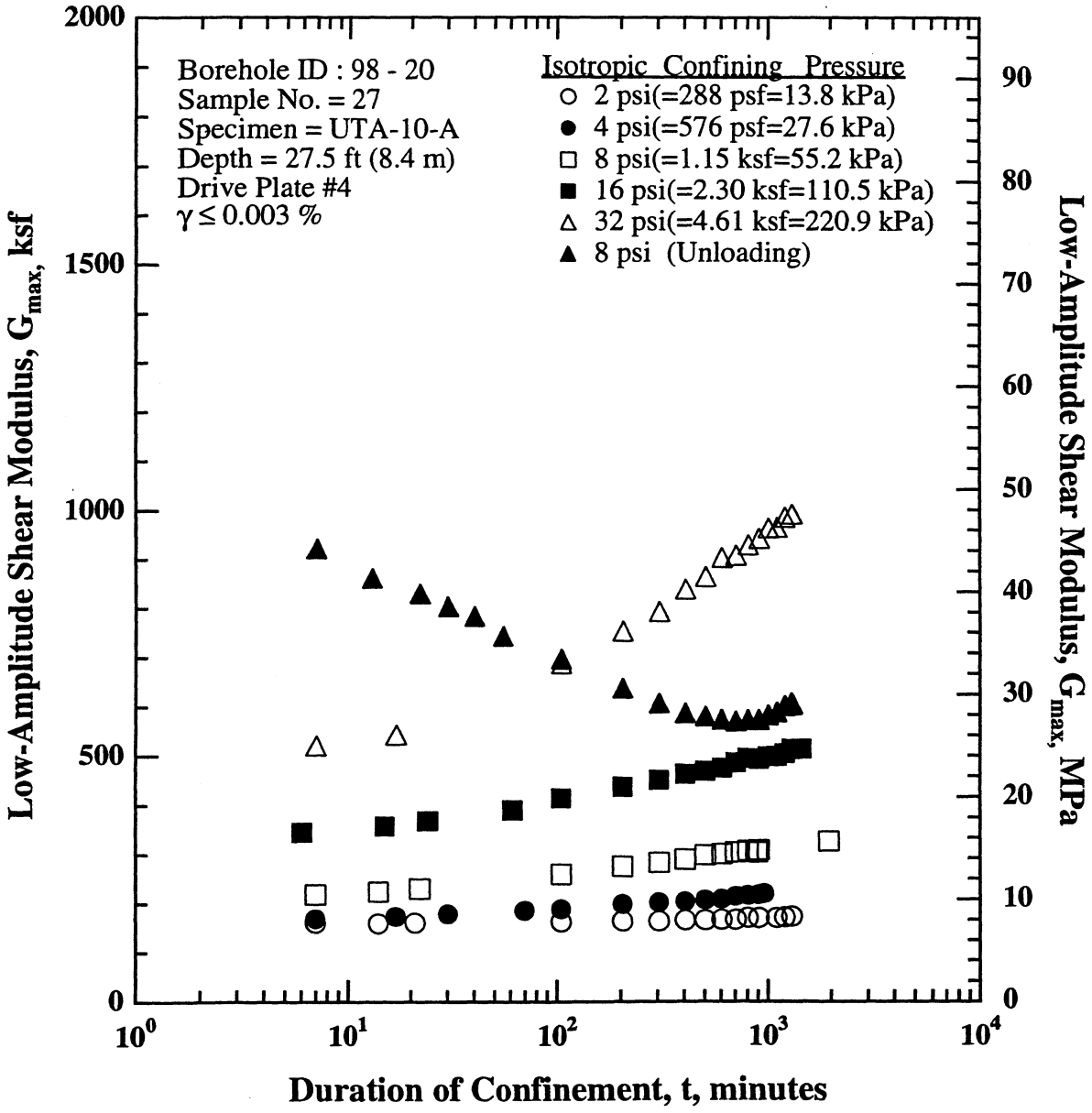

Figure B.2 Variation in Low-Amplitude Shear Modulus with Magnitude and Duration of Isotropic Confining Pressure from Resonant Column Tests of Specimen UTA-10-A from the East Bay Bridge Site.

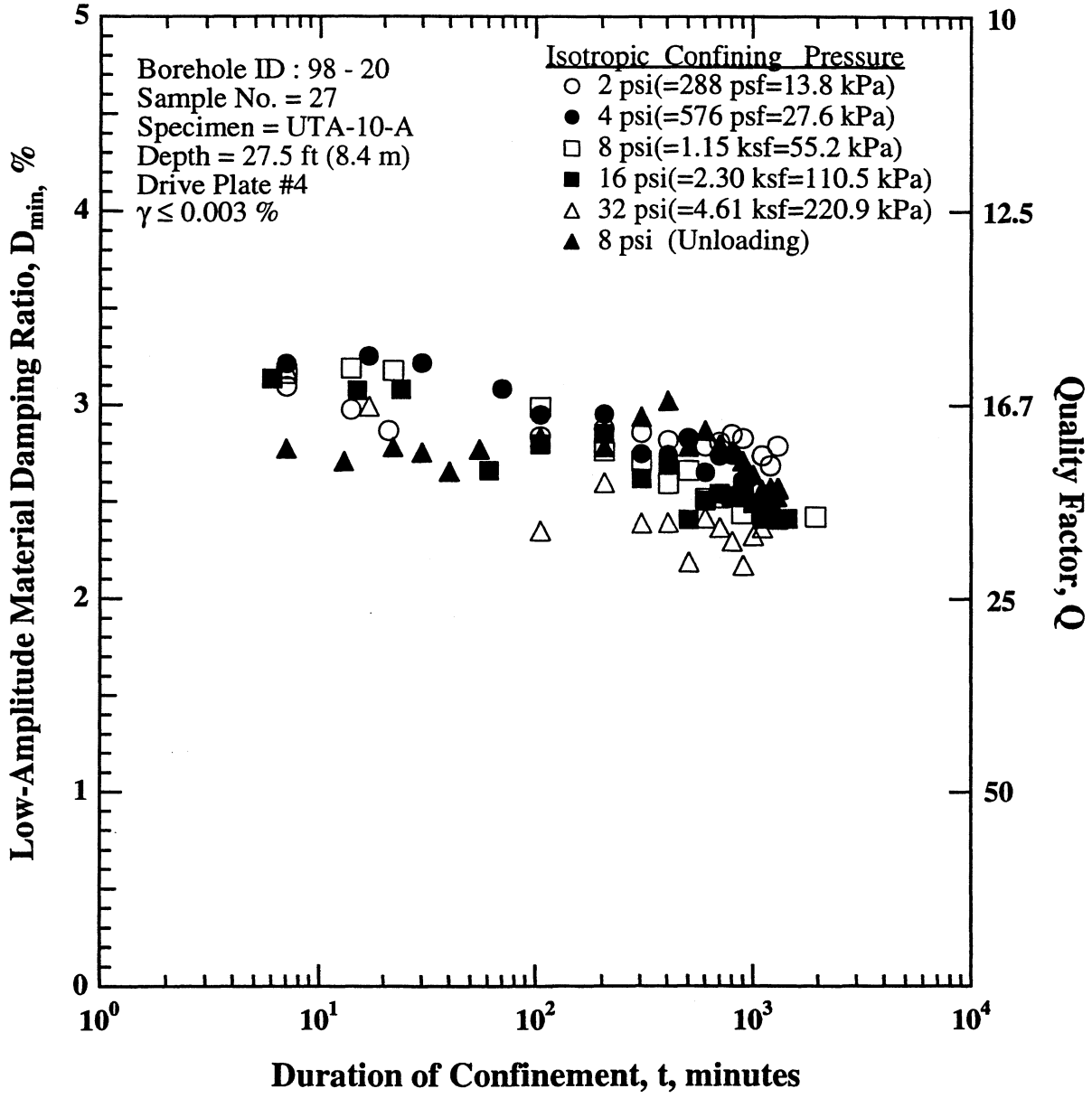

Figure B.3 Variation in Low-Amplitude Material Damping Ratio with Magnitude and Duration of Isotropic Confining Pressure from Resonant Column Tests of Specimen UTA-10-A from the East Bay Bridge Site.

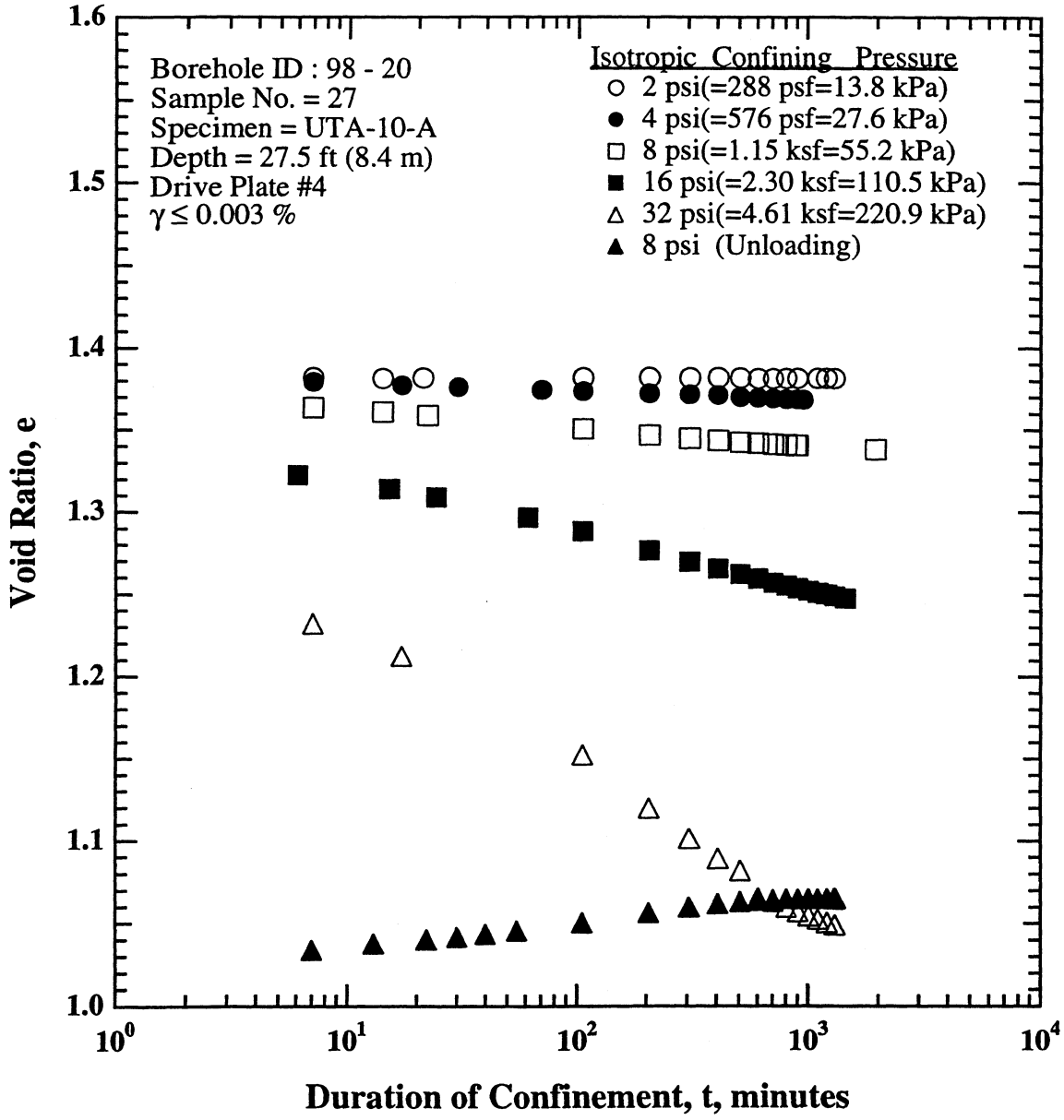

Figure B.4 Variation in Void Ratio with Magnitude and Duration of Isotropic Confining Pressure from Resonant Column Tests of Specimen UTA-10-A from the East Bay Bridge Site.

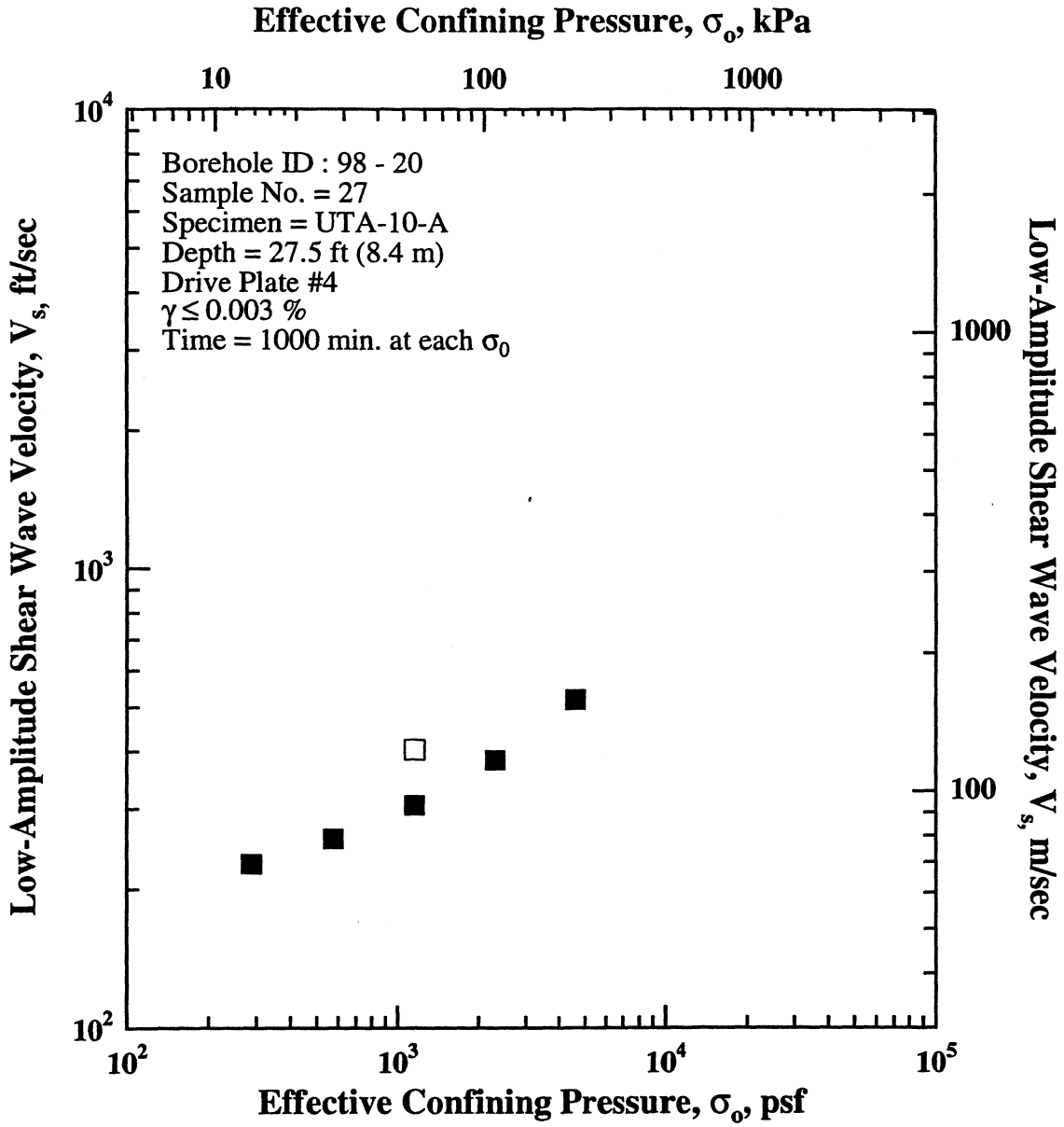

Figure B.5 Variation in Low-Amplitude Shear Wave Velocity with Effective Confining Pressure from Resonant Column Tests of Specimen UTA-10-A from the East Bay Bridge Site.

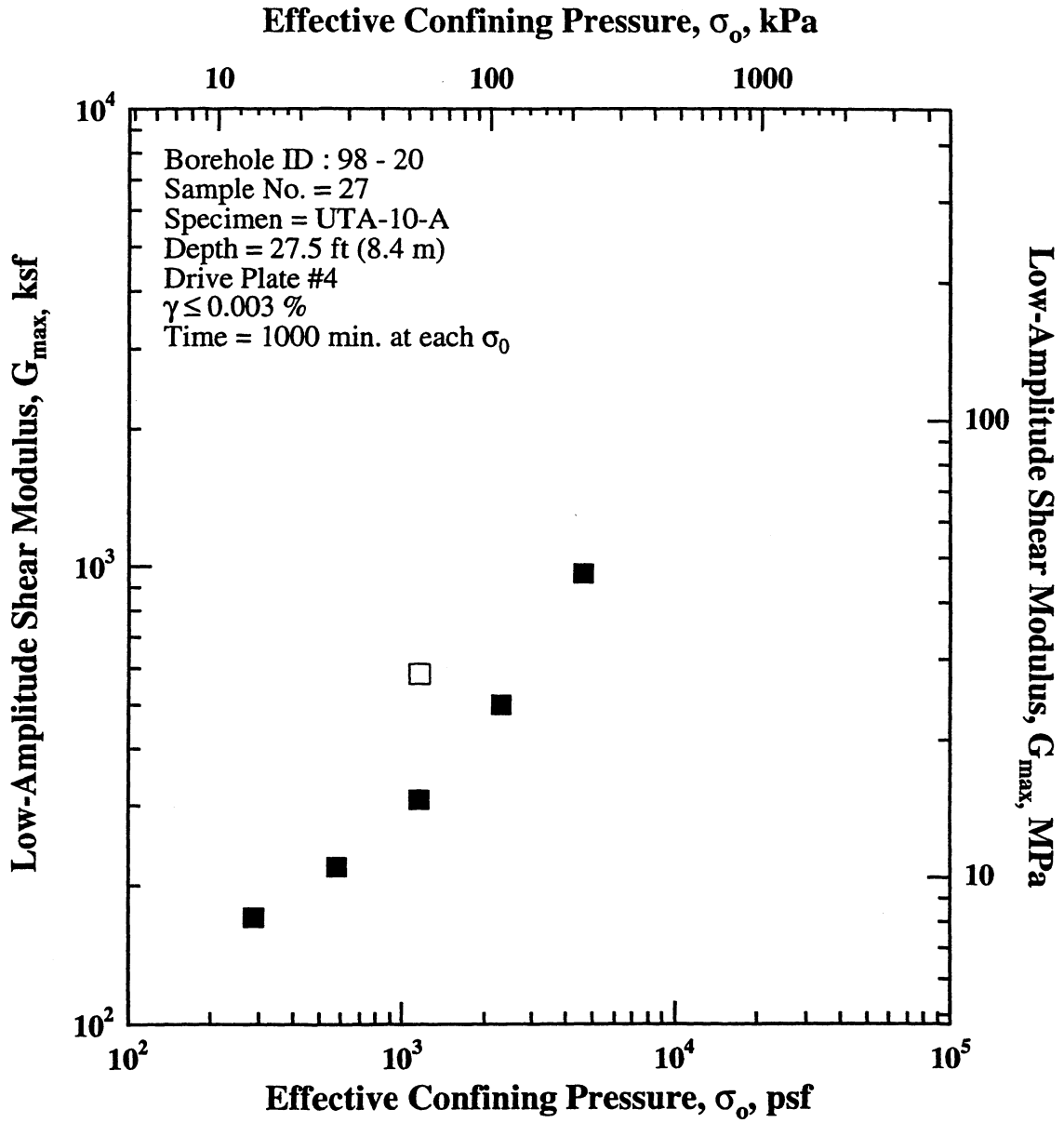

Figure B.6 Variation in Low-Amplitude Shear Modulus with Effective Confining Pressure from Resonant Column Tests of Specimen UTA-10-A from the East Bay Bridge Site.

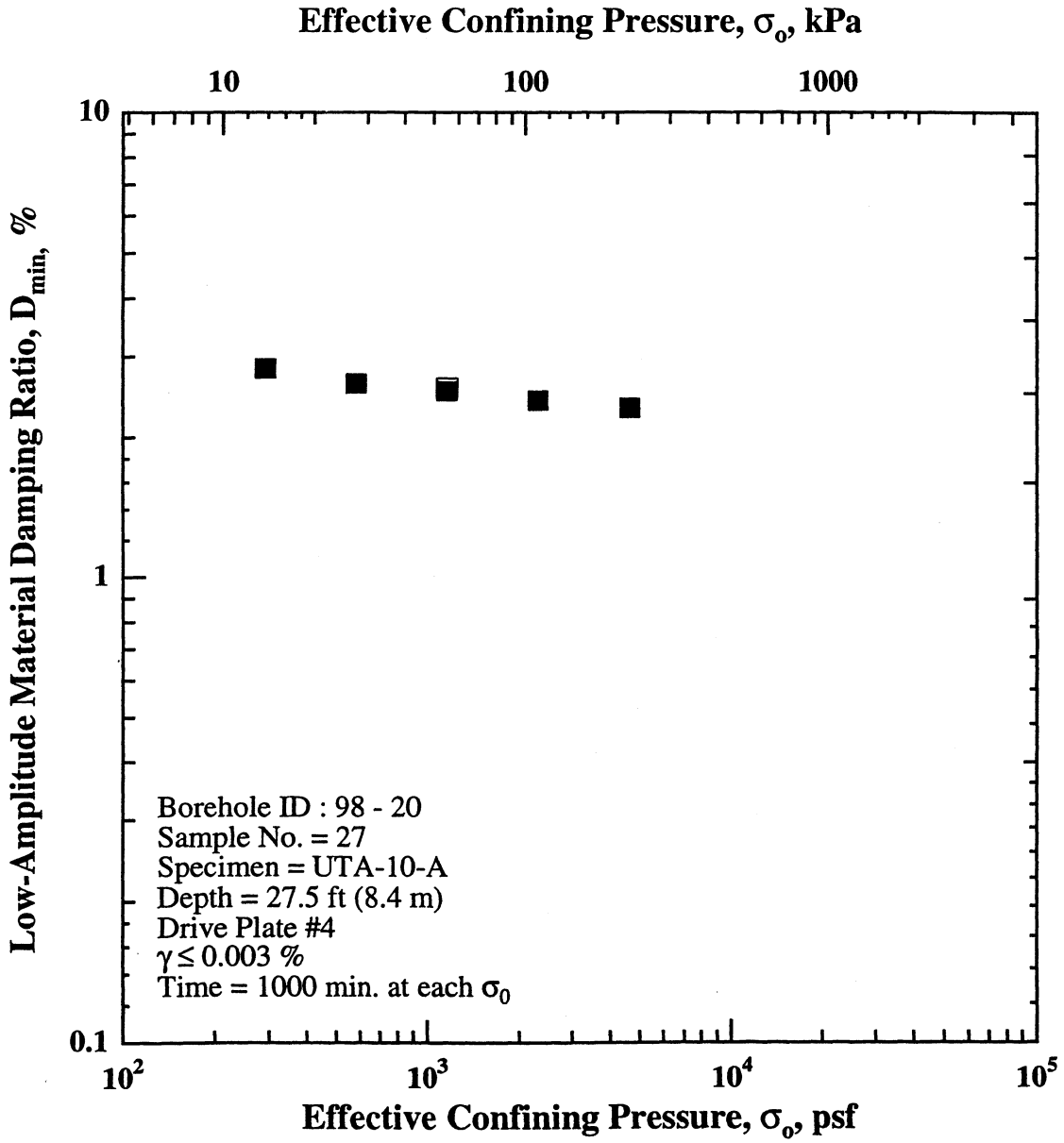

Figure B.7 Variation in Low-Amplitude Material Damping Ratio with Effective Confining Pressure from Resonant Column Tests of Specimen UTA-10-A from the East Bay Bridge Site.

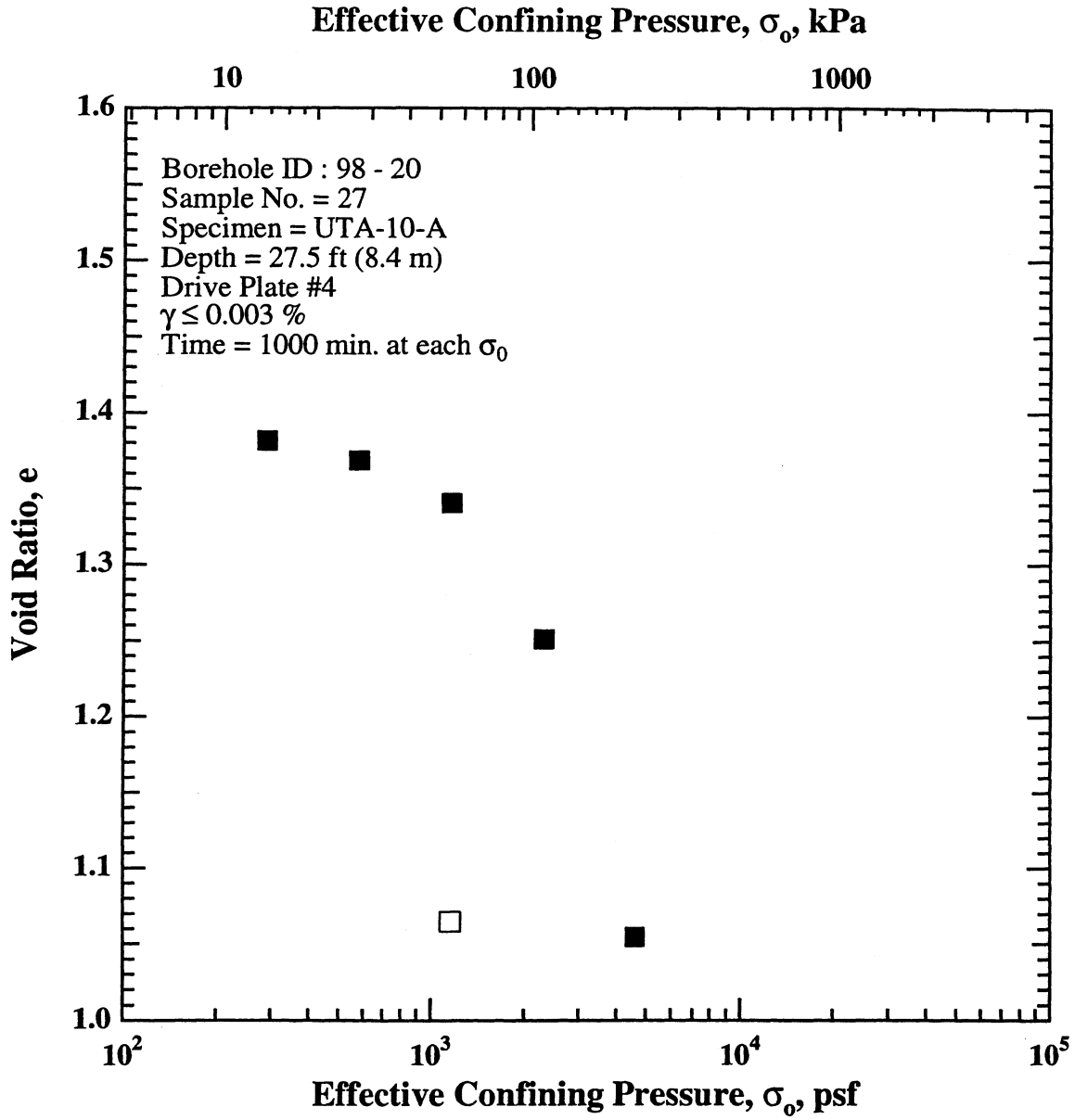

Figure B.8 Variation in Void Ratio with Effective Confining Pressure from Resonant Column Tests of Specimen UTA-10-A from the East Bay Bridge Site.

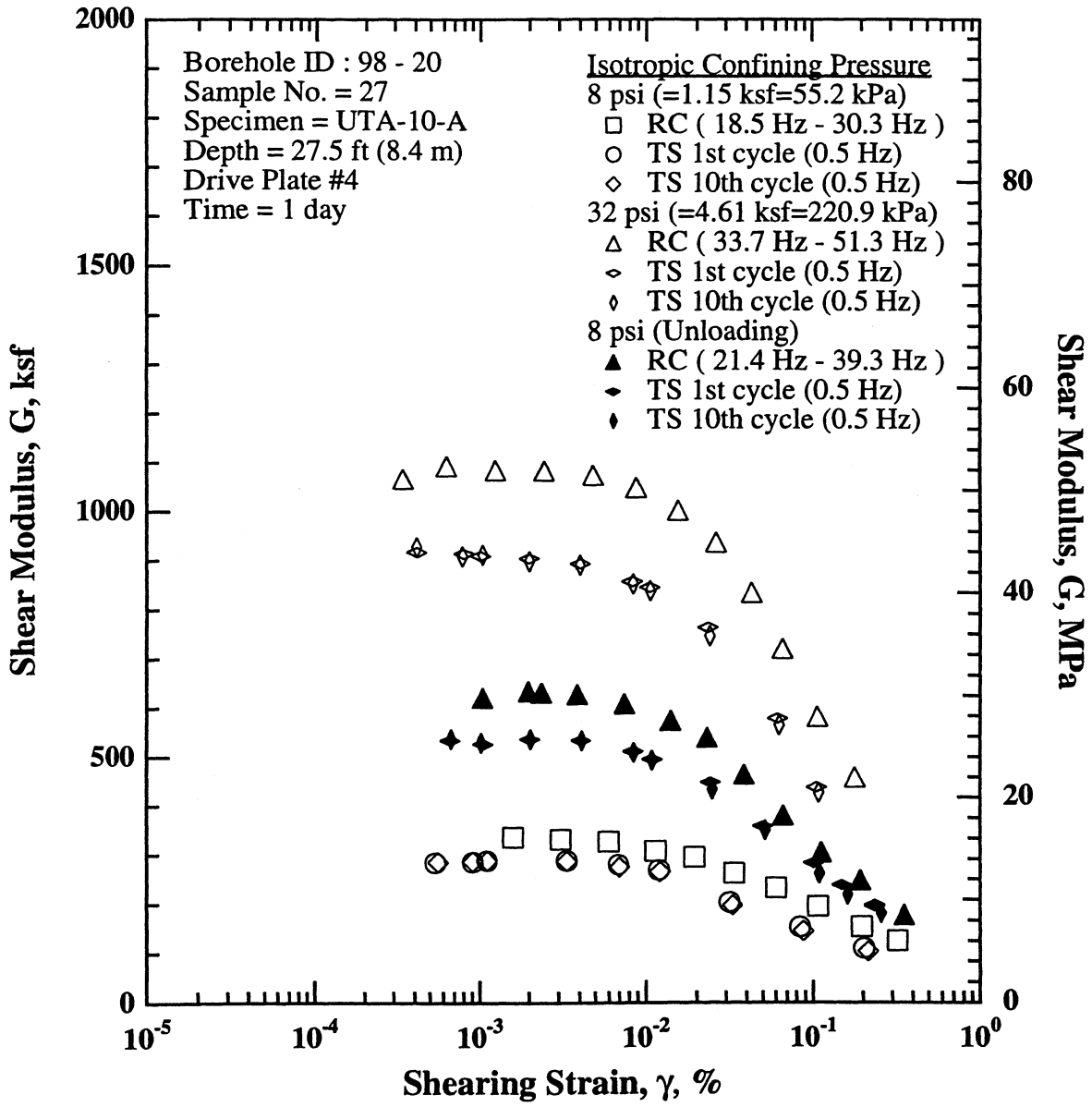

Figure B.9 Comparison of the Variation in Shear Modulus with Shearing Strain, Stress History and Isotropic Effective Confining Pressure from RCTS Tests of Specimen UTA-10-A from the East Bay Bridge Site.

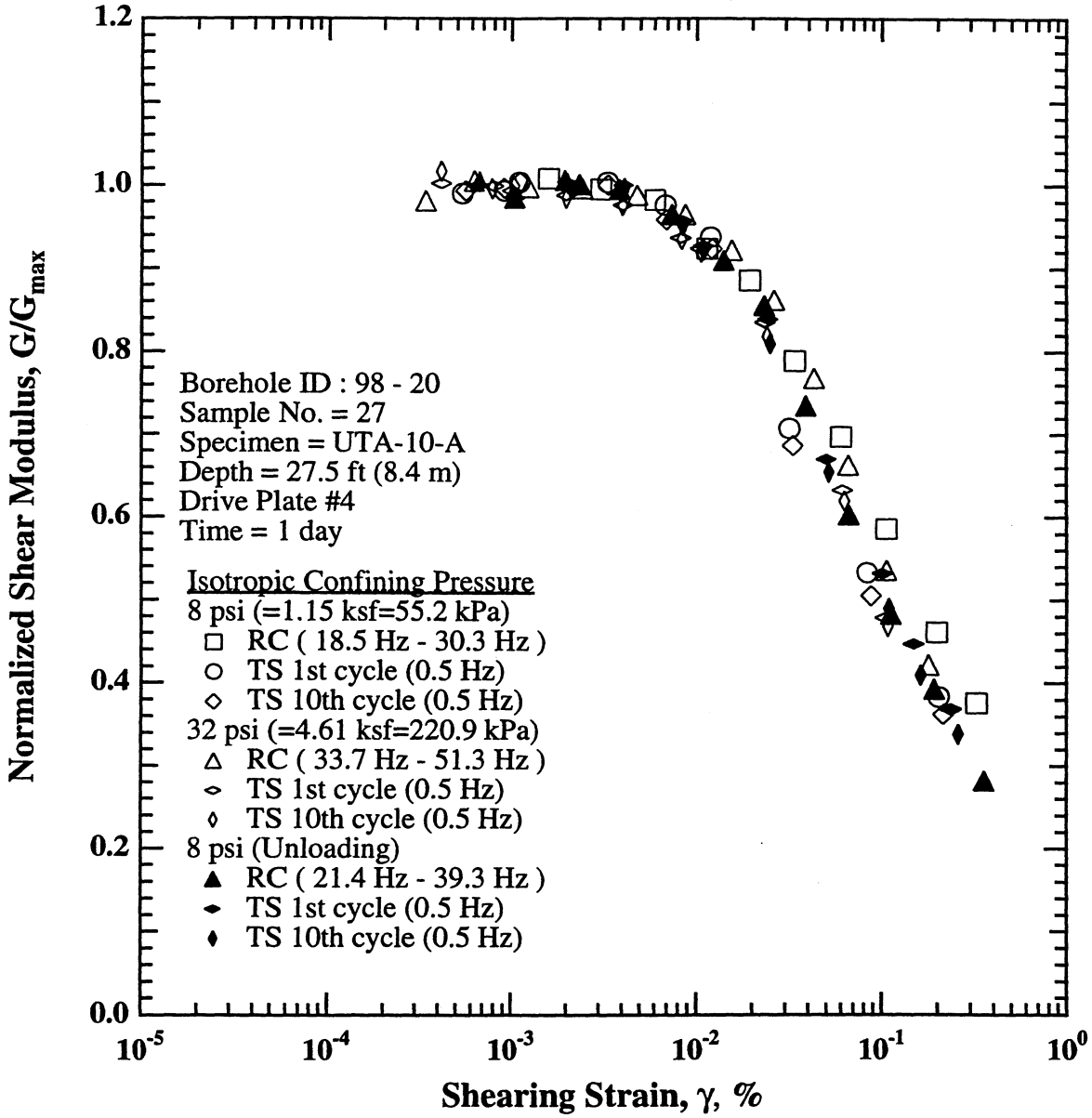

Figure B.10 Comparison of the Variation in Normalized Shear Modulus with Shearing Strain, Stress History and Isotropic Effective Confining Pressure from RCTS Tests of Specimen UTA-10-A from the East Bay Bridge Site.

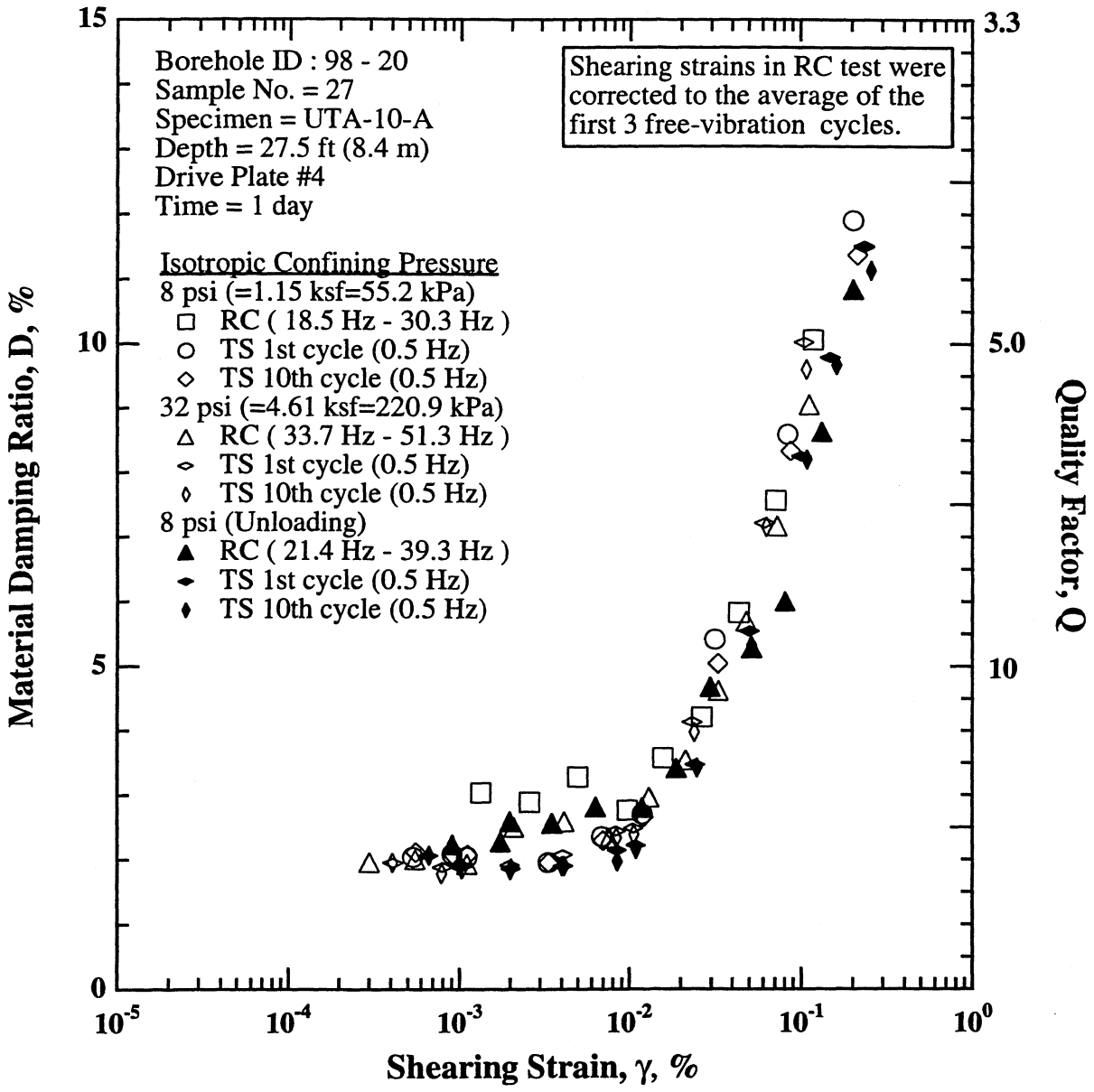

Figure B.11 Comparison of the Variation in Material Damping Ratio with Shearing Strain, Stress History and Isotropic Effective Confining Pressure from RCTS Tests of Specimen UTA-10-A from the East Bay Bridge Site.

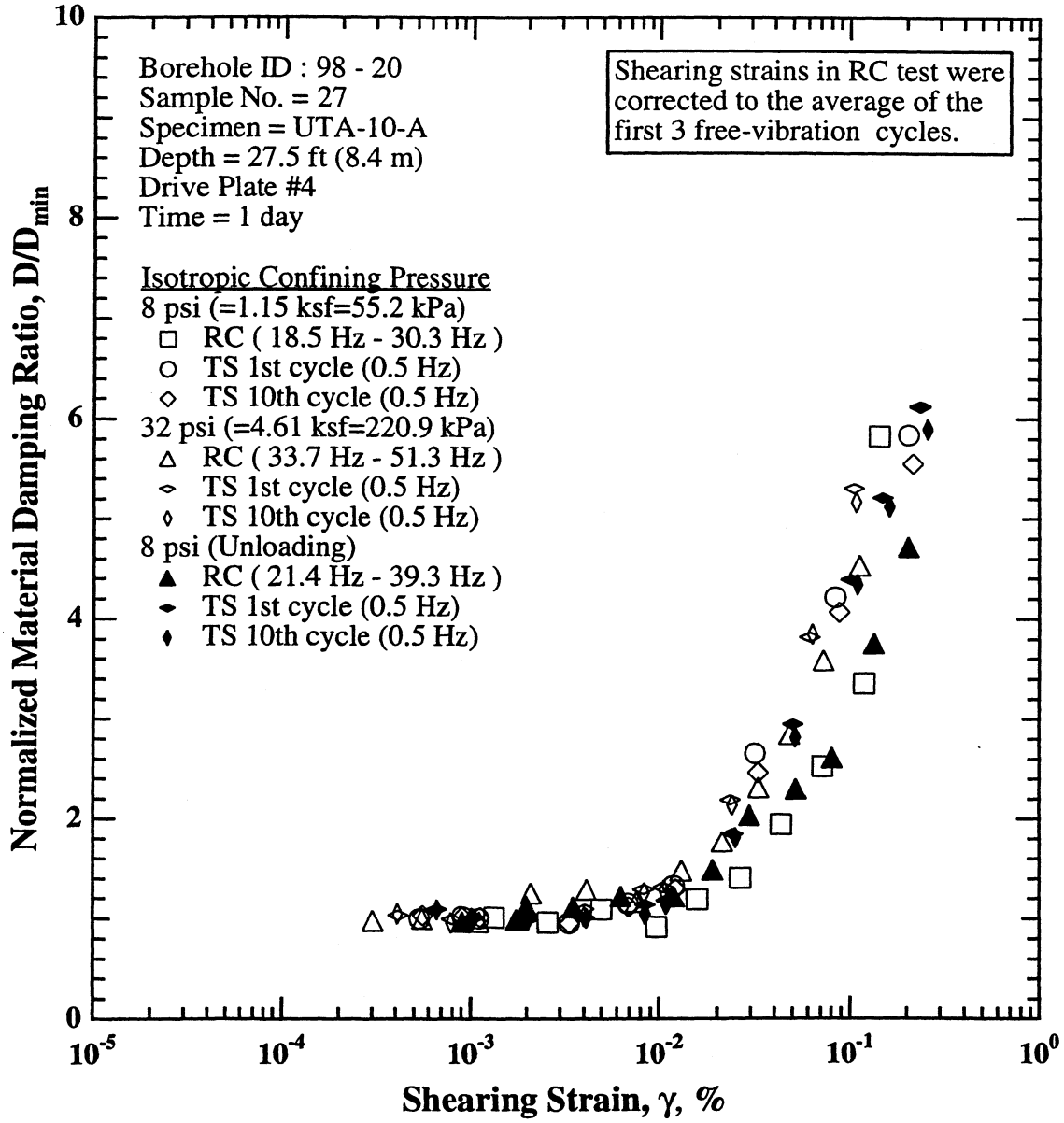

Figure B.12 Comparison of the Variation in Normalized Material Damping Ratio with Shearing Strain, Stress History and Isotropic Effective Confining Pressure from RCTS Tests of Specimen UTA-10-A from the East Bay Bridge Site.

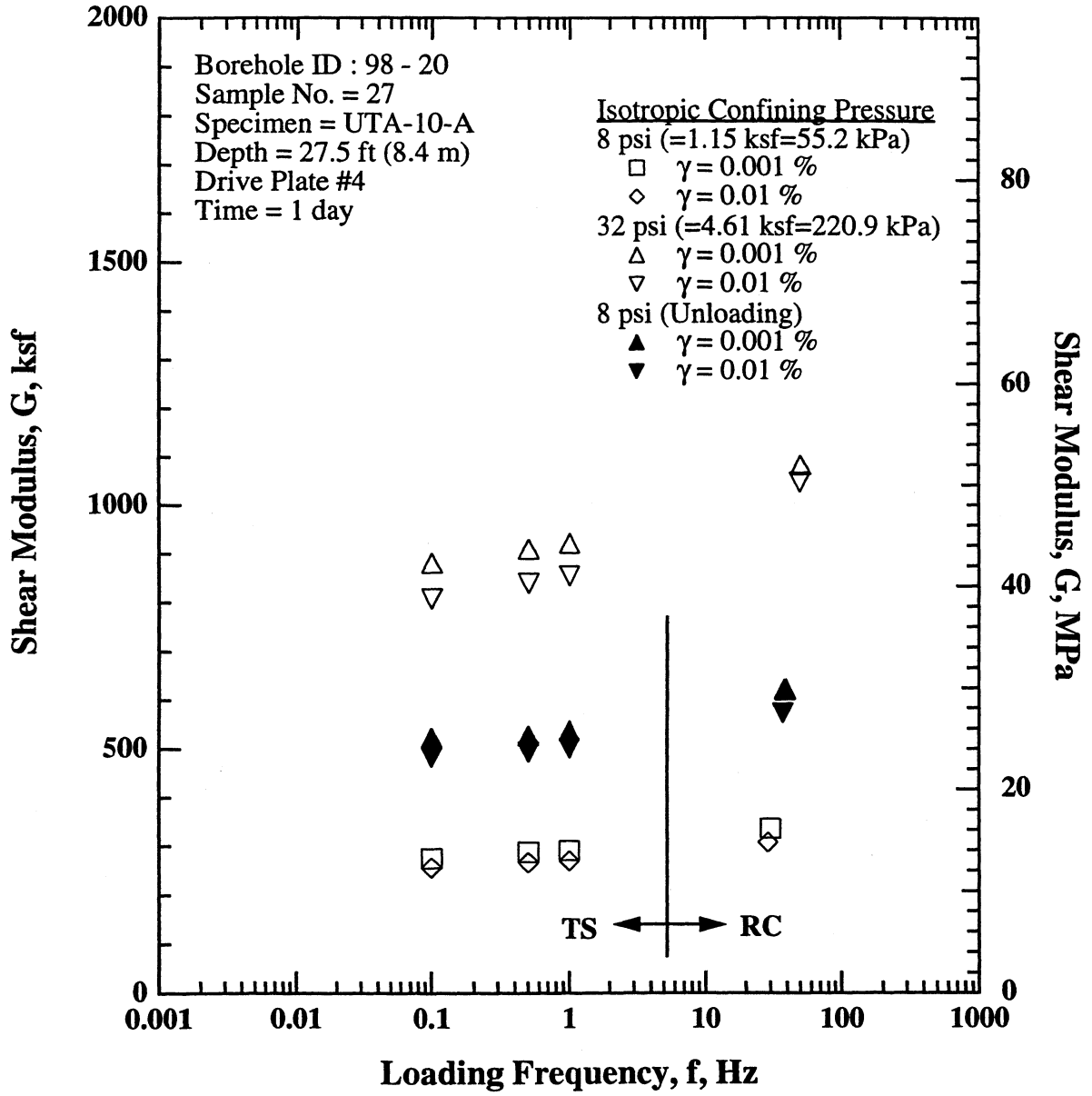

Figure B.13 Comparison of the Variation in Shear Modulus with Loading Frequency, Shearing Strain, Stress History and Isotropic Effective Confining Pressure from RCTS Tests of Specimen UTA-10-A from the East Bay Bridge Site.

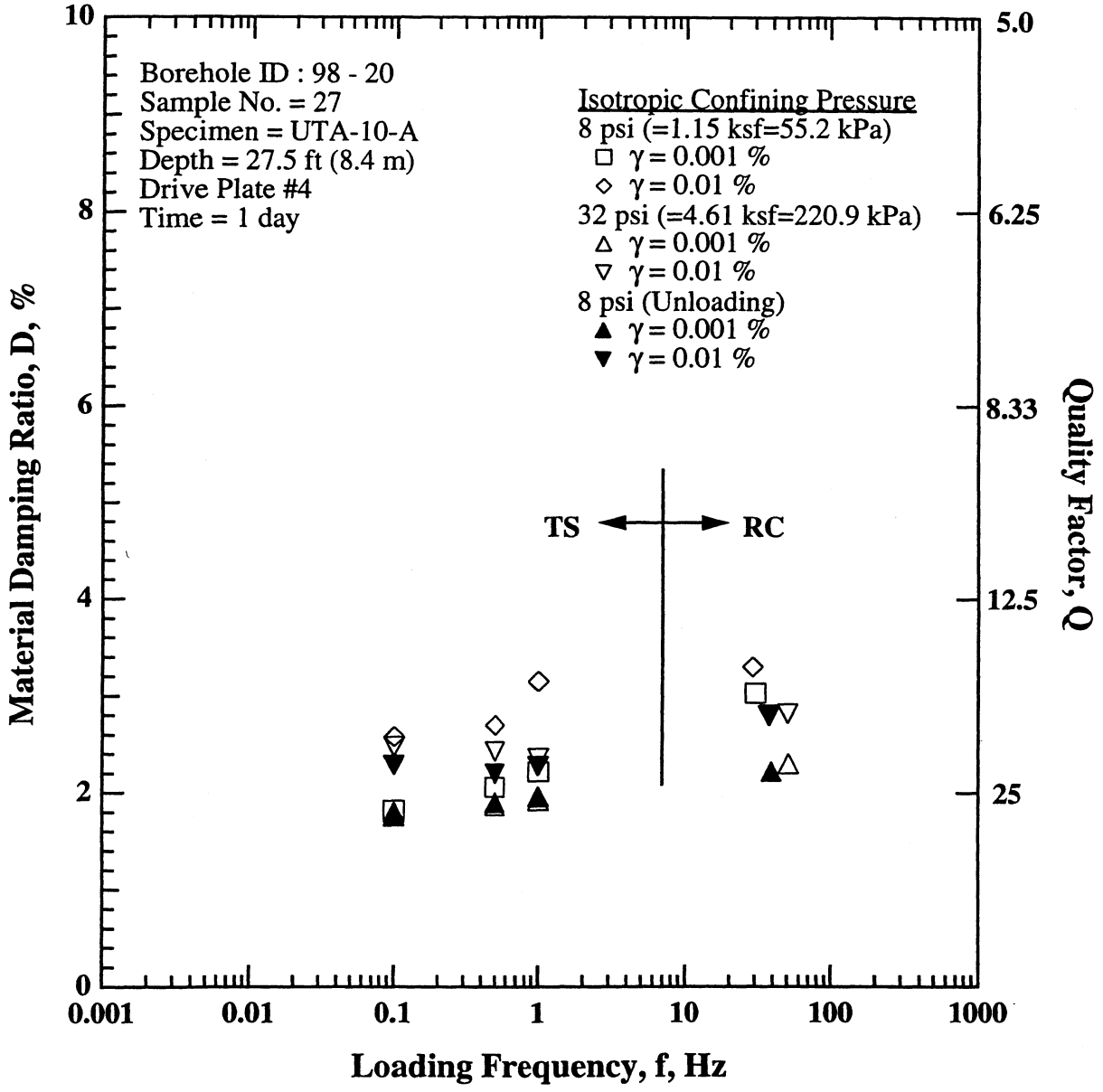

Figure B.14 Comparison of the Variation in Material Damping Ratio with Loading Frequency, Shearing Strain, Stress History and Isotropic Effective Confining Pressure from RCTS Tests of Specimen UTA-10-A from the East Bay Bridge Site.

Table B.1 Variation in Low-Amplitude Shear Modulus, Low-Amplitude Material Damping Ratio and Void Ratio with Effective Isotropic Confining Pressure from RC Tests of Specimen UTA-10-A (Boring 98 - 20) from the East Bay Bridge Site

Effective Isotropic Confining Pressure, σ_o'			Low-Amplitude Shear Modulus, G_{max}		Low-Amplitude Material Damping Ratio,	Void Ratio, e
(psi)	(psf)	(kPa)	(ksf)	(MPa)	Dmin, %	
2	288	13.8	171	8.2	2.83	1.381
4	576	27.6	220	10.6	2.62	1.369
8	1152	55.2	309	14.8	2.53	1.341
16	2304	110.5	499	23.9	2.41	1.251
32	4608	220.9	964	46.2	2.32	1.055
8	1152	55.2	583	28.0	2.56	1.065

Table B.2 Variation in Shear Modulus, Normalized Shear Modulus and Material Damping Ratio with Shearing Strain from RC Tests of Specimen UTA-10-A (Boring 98 - 20) from the East Bay Bridge Site; Effective Confining Pressure, σ_o' = 8 psi (1.15 ksf = 55.2 kPa)

Peak Shearing Strain, %	Shear Modulus, G, ksf	Normalized Shear Modulus, G/G_{max}	Average[+] Shearing Strain, %	Material Damping Ratio[x], D, %
1.59E-03	336	1.01	1.33E-03	3.03
3.06E-03	331	0.99	2.58E-03	2.88
6.01E-03	327	0.98	4.96E-03	3.28
1.14E-02	308	0.92	9.70E-03	2.76
1.94E-02	295	0.89	1.58E-02	3.57
3.36E-02	263	0.79	2.64E-02	4.21
6.00E-02	232	0.70	4.35E-02	5.83
1.07E-01	195	0.59	7.13E-02	7.56
1.97E-01	154	0.46	1.18E-01	10.06
3.23E-01	125	0.38	1.43E-01	17.46

[+] Average Shearing Strain from the First Three Cycles of the Free Vibration Decay Curve

[x] Average Damping Ratio from the First Three Cycles of the Free Vibration Decay Curve

Table B.3 Variation in Shear Modulus, Normalized Shear Modulus and Material Damping Ratio with Shearing Strain from TS Tests of Specimen UTA-10-A (Boring 98 - 20) from the East Bay Bridge Site; Effective Confining Pressure, σ_o' = 8 psi (1.15 ksf = 55.2 kPa)

First Cycle				Tenth Cycle			
Peak Shearing Strain, %	Shear Modulus, G, ksf	Normalized Shear Modulus, G/G_{max}	Material Damping Ratio, D, %	Peak Shearing Strain, %	Shear Modulus, G, ksf	Normalized Shear Modulus, G/G_{max}	Material Damping Ratio, D, %
5.34E-04	284	0.99	2.04	5.56E-04	285	0.99	2.11
9.04E-04	285	0.99	2.08	9.05E-04	286	1.00	2.08
1.10E-03	288	1.00	2.04	1.11E-03	288	1.00	2.07
3.34E-03	288	1.00	1.95	3.35E-03	287	1.00	1.95
6.85E-03	280	0.98	2.35	6.95E-03	275	0.96	2.29
1.19E-02	269	0.94	2.70	1.21E-02	265	0.92	2.65
3.15E-02	203	0.71	5.41	3.28E-02	197	0.69	5.04
8.35E-02	153	0.53	8.59	8.76E-02	145	0.51	8.33
2.03E-01	110	0.38	11.90	2.15E-01	104	0.36	11.37

Table B.4 Variation in Shear Modulus, Normalized Shear Modulus and Material Damping Ratio with Shearing Strain from RC Tests of Specimen UTA-10-A (Boring 98 - 20) from the East Bay Bridge Site; Effective Confining Pressure, σ_o' = 32 psi (4.61 ksf = 220.9 kPa)

Peak Shearing Strain, %	Shear Modulus, G, ksf	Normalized Shear Modulus, G/G_{max}	Average[+] Shearing Strain, %	Material Damping Ratio[x], D, %
3.38E-04	1066	0.98	3.00E-04	1.96
6.21E-04	1092	1.00	5.51E-04	2.00
1.23E-03	1084	1.00	1.10E-03	1.93
2.43E-03	1083	1.00	2.10E-03	2.50
4.81E-03	1074	0.99	4.12E-03	2.58
8.72E-03	1048	0.96	7.58E-03	2.33
1.55E-02	1002	0.92	1.30E-02	2.95
2.61E-02	937	0.86	2.12E-02	3.54
4.28E-02	834	0.77	3.29E-02	4.62
6.59E-02	721	0.66	4.80E-02	5.69
1.06E-01	582	0.54	7.22E-02	7.17
1.79E-01	458	0.42	1.12E-01	9.05

[+] Average Shearing Strain from the First Three Cycles of the Free Vibration Decay Curve

[x] Average Damping Ratio from the First Three Cycles of the Free Vibration Decay Curve

Table B.5 Variation in Shear Modulus, Normalized Shear Modulus and Material Damping Ratio with Shearing Strain from TS Tests of Specimen UTA-10-A (Boring 98 - 20) from the East Bay Bridge Site; Effective Confining Pressure, σ_o' = 32 psi (4.61 ksf = 220.9 kPa)

First Cycle				Tenth Cycle			
Peak Shearing Strain, %	Shear Modulus, G, ksf	Normalized Shear Modulus, G/G_{max}	Material Damping Ratio, D, %	Peak Shearing Strain, %	Shear Modulus, G, ksf	Normalized Shear Modulus, G/G_{max}	Material Damping Ratio, D, %
4.10E-04	917	1.00	1.95	4.08E-04	927	1.02	1.95
7.92E-04	914	1.00	1.88	7.80E-04	908	1.00	1.78
9.97E-04	909	0.99	1.89	1.03E-03	911	1.00	1.85
1.98E-03	904	0.99	1.91	1.99E-03	898	0.98	1.84
4.03E-03	893	0.98	2.07	4.00E-03	890	0.98	1.90
8.28E-03	857	0.94	2.44	8.34E-03	852	0.93	2.33
1.05E-02	845	0.92	2.48	1.06E-02	838	0.92	2.38
2.33E-02	764	0.83	4.13	2.39E-02	746	0.82	3.97
6.13E-02	579	0.63	7.21	6.28E-02	565	0.62	7.15
1.05E-01	438	0.48	10.02	1.08E-01	427	0.47	9.60

Table B.6 Variation in Shear Modulus, Normalized Shear Modulus and Material Damping Ratio with Shearing Strain from RC Tests of Specimen UTA-10-A (Boring 98 - 20) from the East Bay Bridge Site; Effective Confining Pressure, σ_o' = 8 psi (1.15 ksf = 55.2 kPa), Unloading

Peak Shearing Strain, %	Shear Modulus, G, ksf	Normalized Shear Modulus, G/G_{max}	Average[+] Shearing Strain, %	Material Damping Ratio[x], D, %
2.35E-03	631	1.00	1.98E-03	2.59
1.03E-03	622	0.99	9.05E-04	2.23
1.96E-03	635	1.01	1.74E-03	2.27
3.86E-03	628	1.00	3.51E-03	2.56
7.42E-03	609	0.96	6.29E-03	2.81
1.40E-02	574	0.91	1.19E-02	2.80
2.31E-02	540	0.86	1.89E-02	3.41
3.86E-02	464	0.73	2.96E-02	4.68
6.62E-02	380	0.60	5.18E-02	5.28
1.12E-01	305	0.48	8.03E-02	6.00
1.92E-01	248	0.39	1.33E-01	8.63
3.56E-01	178	0.28	2.03E-01	10.84

[+] Average Shearing Strain from the First Three Cycles of the Free Vibration Decay Curve

[x] Average Damping Ratio from the First Three Cycles of the Free Vibration Decay Curve

Table B.7 Variation in Shear Modulus, Normalized Shear Modulus and Material Damping Ratio with Shearing Strain from TS Tests of Specimen UTA-10-A (Boring 98 - 20) from the East Bay Bridge Site; Effective Confining Pressure, σ_o' = 8 psi (1.15 ksf = 55.2 kPa), Unloading

First Cycle				Tenth Cycle			
Peak Shearing Strain, %	Shear Modulus, G, ksf	Normalized Shear Modulus, G/G_{max}	Material Damping Ratio, D, %	Peak Shearing Strain, %	Shear Modulus, G, ksf	Normalized Shear Modulus, G/G_{max}	Material Damping Ratio, D, %
6.57E-04	534	1.00	2.06	6.64E-04	537	1.00	2.06
1.04E-03	526	0.99	1.90	1.01E-03	529	0.99	1.90
2.01E-03	536	1.00	1.86	2.02E-03	536	1.00	1.86
4.06E-03	534	1.00	1.90	4.11E-03	533	1.00	1.90
8.42E-03	511	0.96	2.14	8.44E-03	509	0.95	1.97
1.09E-02	495	0.93	2.22	1.09E-02	493	0.92	2.16
2.41E-02	448	0.84	3.47	2.48E-02	433	0.81	3.42
5.00E-02	358	0.67	5.54	5.15E-02	350	0.65	5.32
1.01E-01	284	0.53	8.25	1.09E-01	262	0.49	8.20
1.49E-01	239	0.45	9.79	1.62E-01	219	0.41	9.67
2.35E-01	197	0.37	11.50	2.57E-01	181	0.34	11.13

APPENDIX C

UTA-10-B

BOREHOLE ID : 98 - 19

SAMPLE NO. = 34

DEPTH = 36.5 ft (11.1 m)

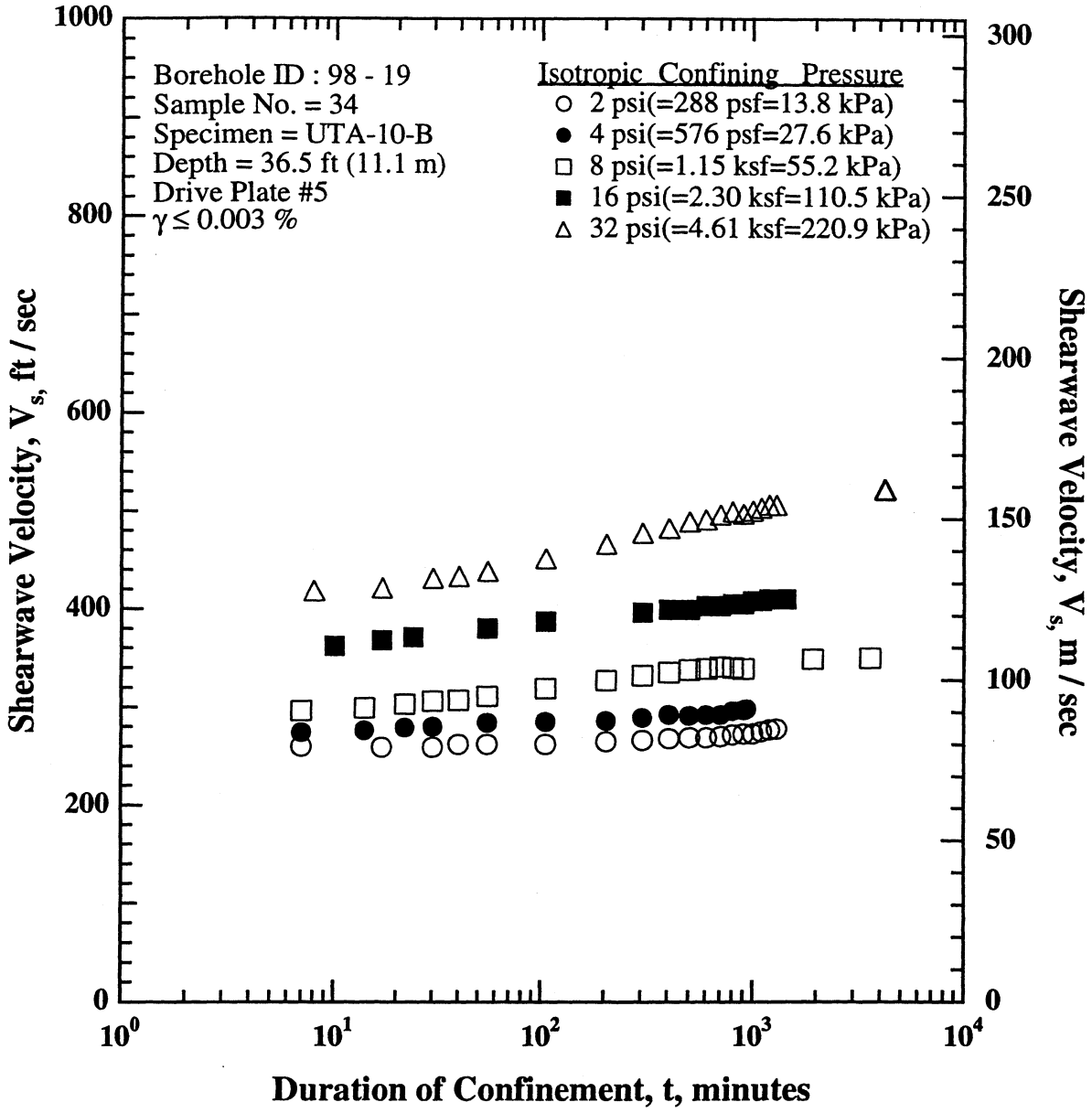

Figure C.1 Variation in Low-Amplitude Shear Wave Velocity with Magnitude and Duration of Isotropic Confining Pressure from Resonant Column Tests of Specimen UTA-10-B from the East Bay Bridge Site.

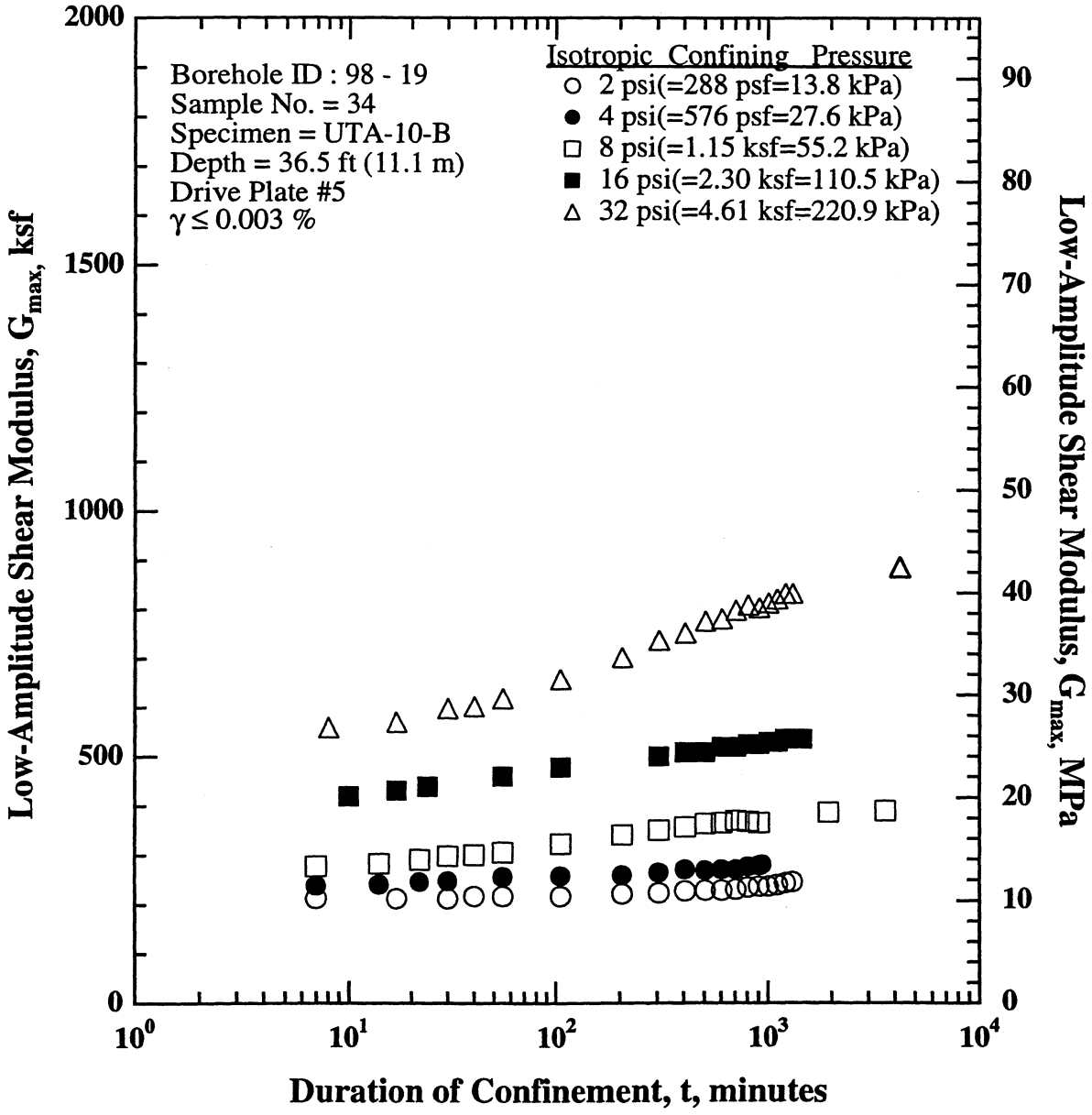

Figure C.2 Variation in Low-Amplitude Shear Modulus with Magnitude and Duration of Isotropic Confining Pressure from Resonant Column Tests of Specimen UTA-10-B from the East Bay Bridge Site.

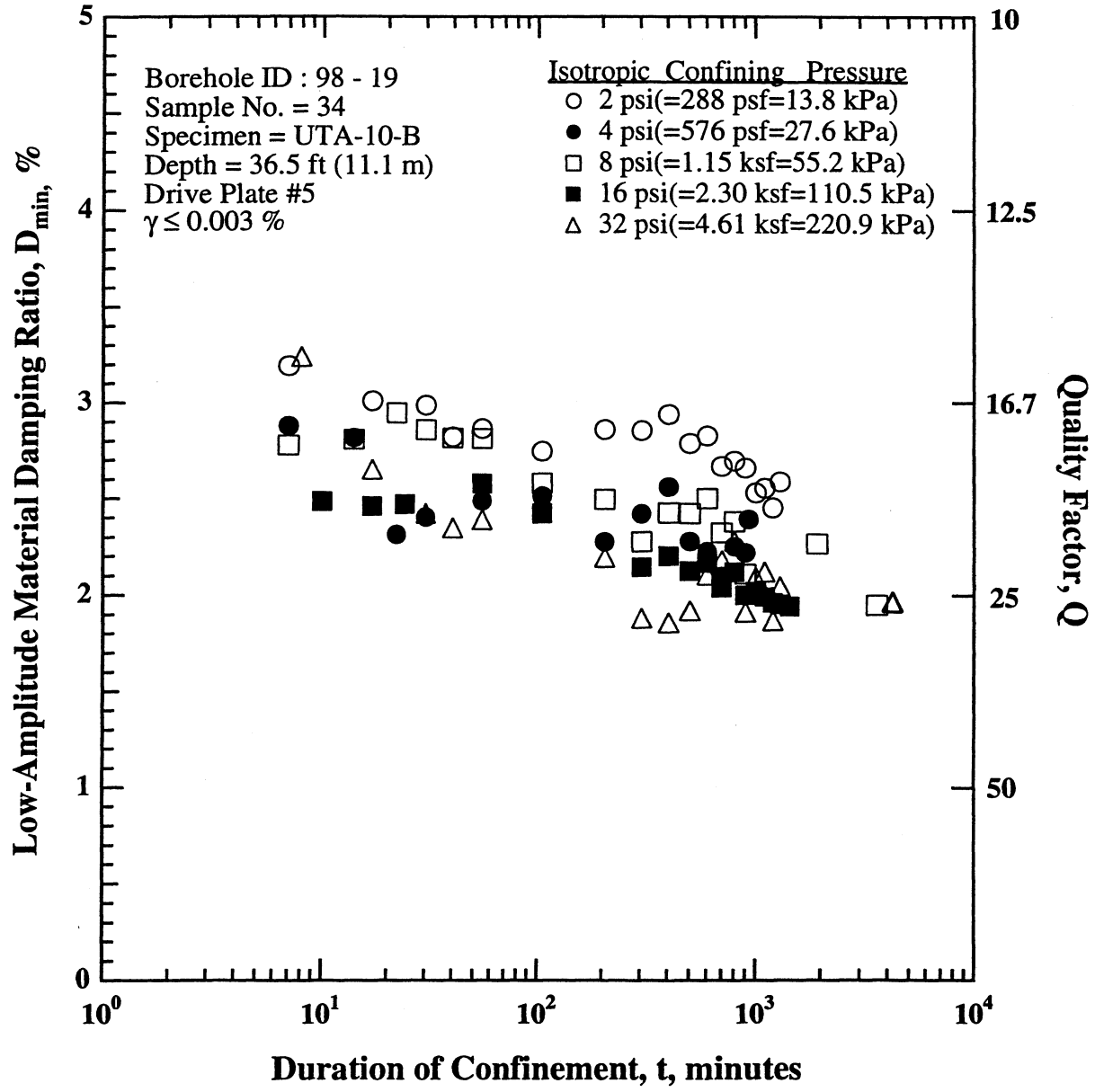

Figure C.3 Variation in Low-Amplitude Material Damping Ratio with Magnitude and Duration of Isotropic Confining Pressure from Resonant Column Tests of Specimen UTA-10-B from the East Bay Bridge Site.

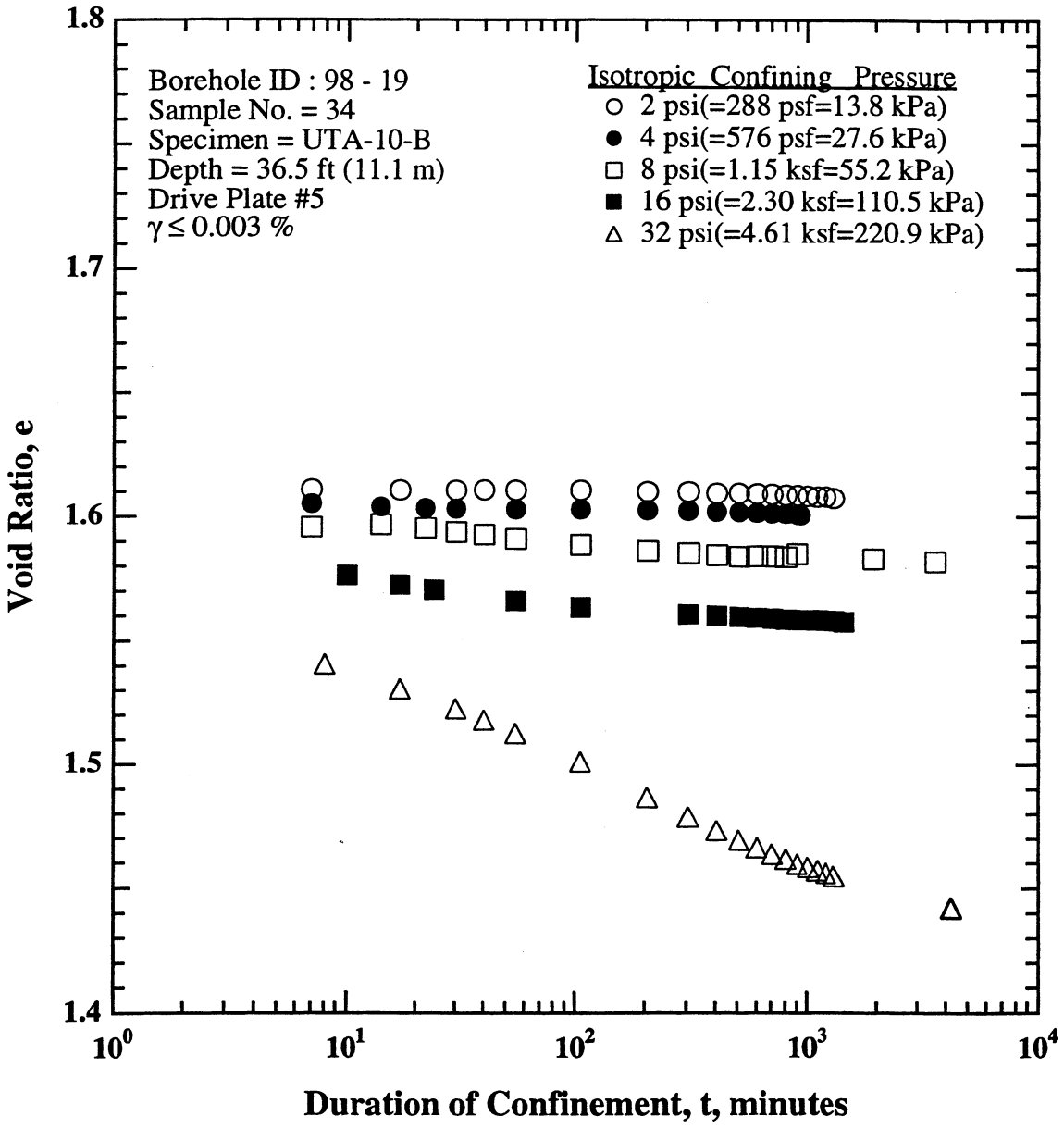

Figure C.4 Variation in Void Ratio with Magnitude and Duration of Isotropic Confining Pressure from Resonant Column Tests of Specimen UTA-10-B from the East Bay Bridge Site.

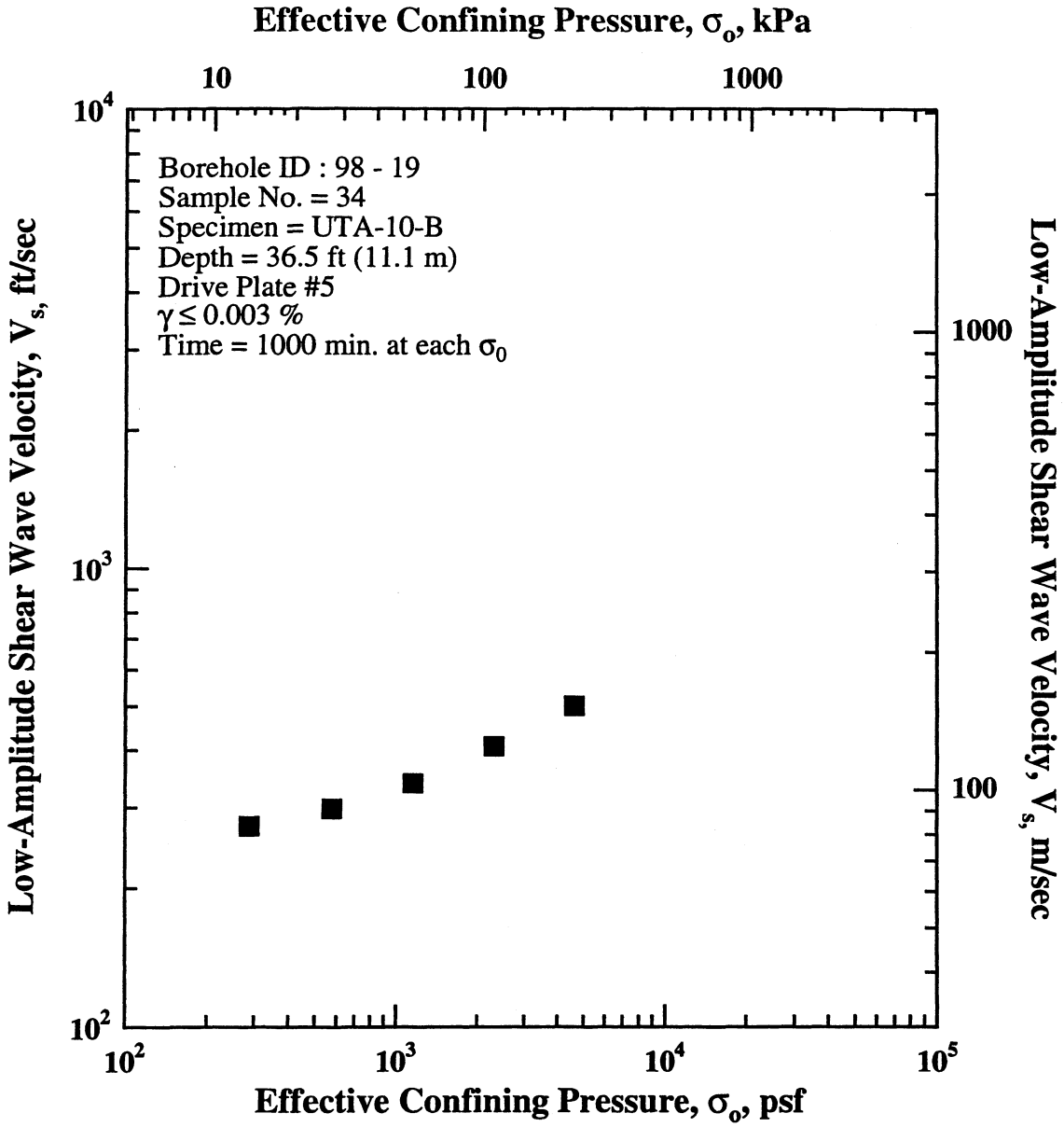

Figure C.5 Variation in Low-Amplitude Shear Wave Velocity with Effective Confining Pressure from Resonant Column Tests of Specimen UTA-10-B from the East Bay Bridge Site.

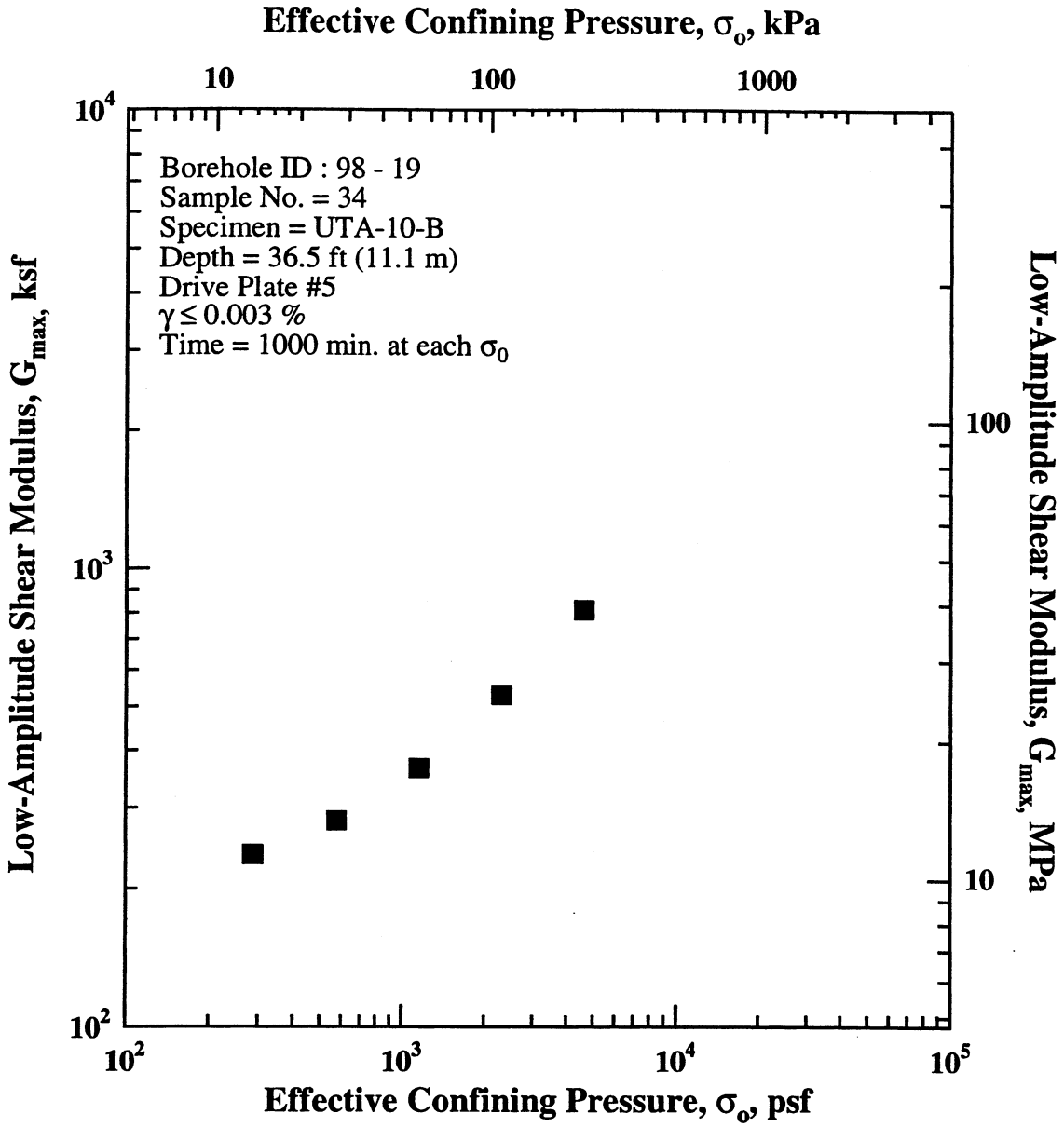

Figure C.6 Variation in Low-Amplitude Shear Modulus with Effective Confining Pressure from Resonant Column Tests of Specimen UTA-10-B from the East Bay Bridge Site.

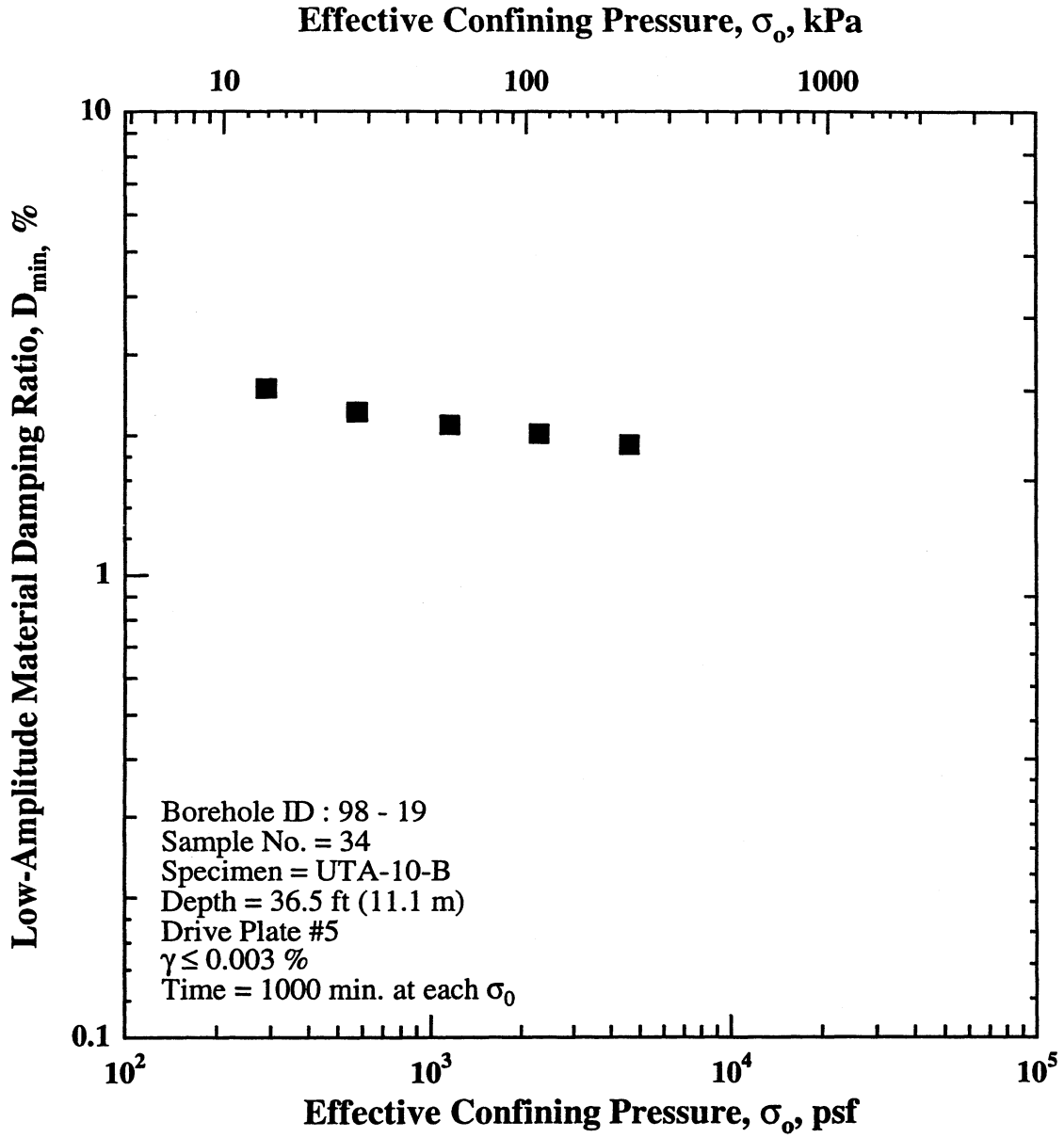

Figure C.7 Variation in Low-Amplitude Material Damping Ratio with Effective Confining Pressure from Resonant Column Tests of Specimen UTA-10-B from the East Bay Bridge Site.

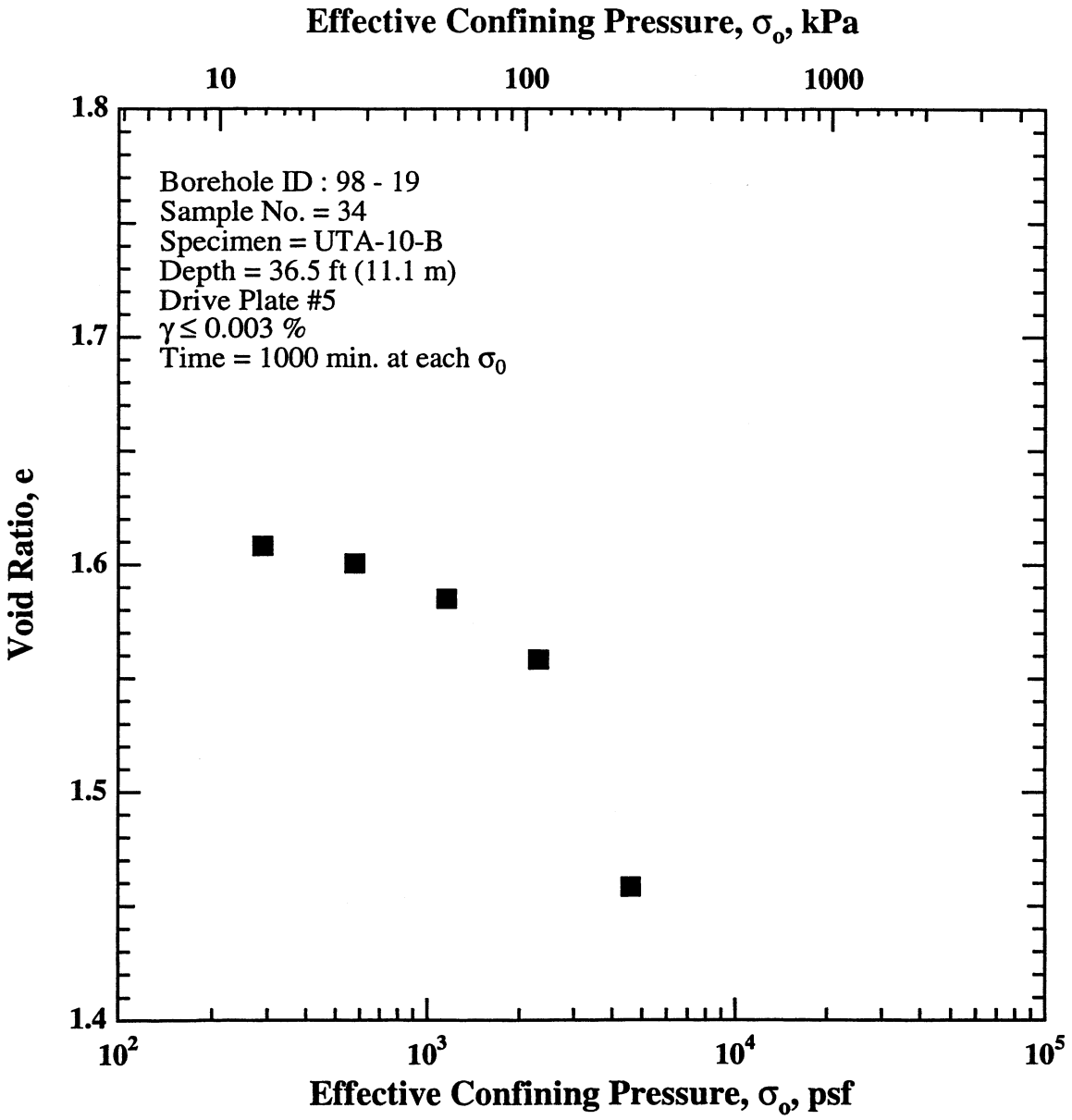

Figure C.8 Variation in Void Ratio with Effective Confining Pressure from Resonant Column Tests of Specimen UTA-10-B from the East Bay Bridge Site.

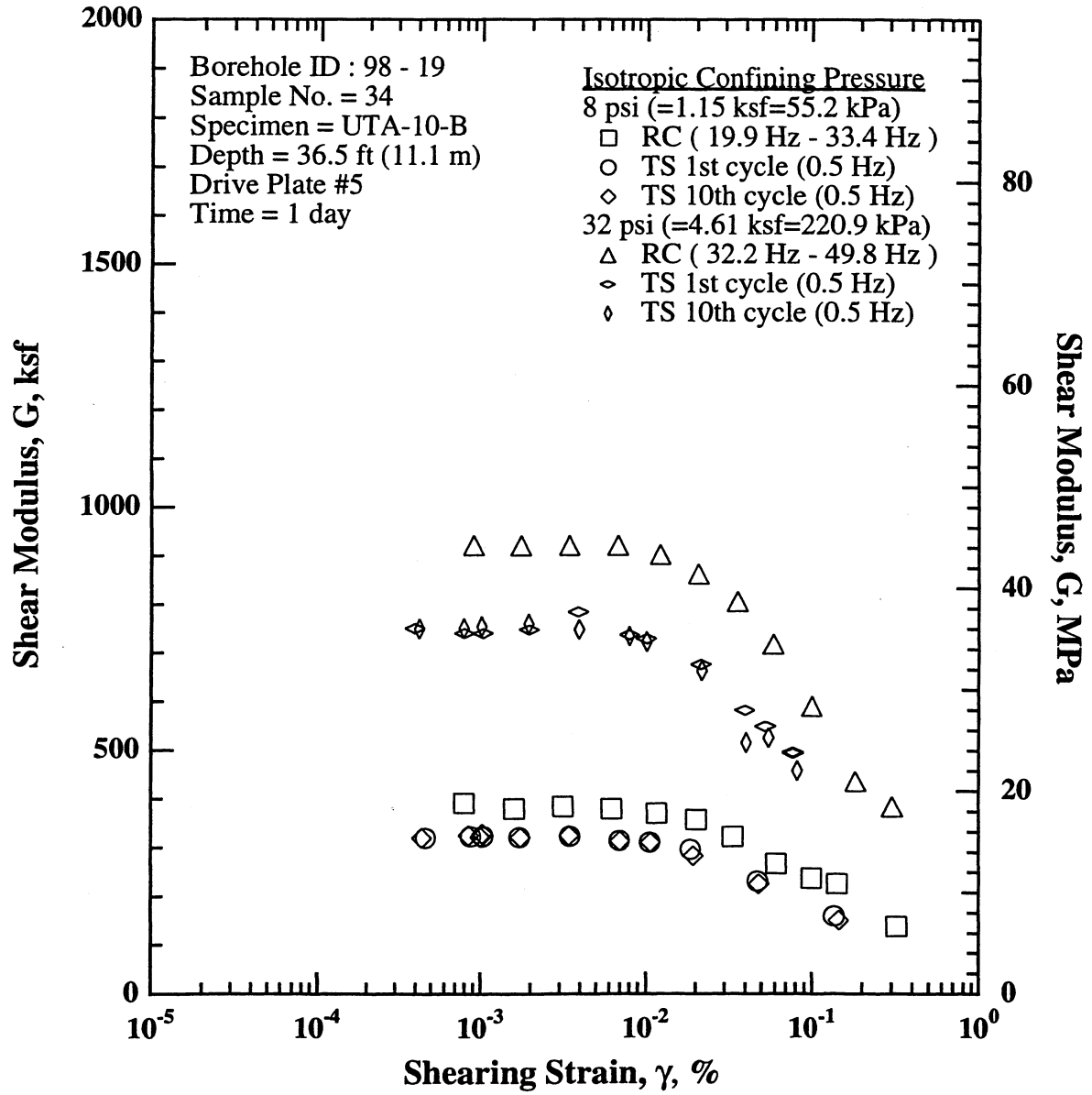

Figure C.9 Variation in Shear Modulus with Shearing Strain and Isotropic Effective Confining Pressure from Resonant Column Tests of Specimen UTA-10-B from the East Bay Bridge Site.

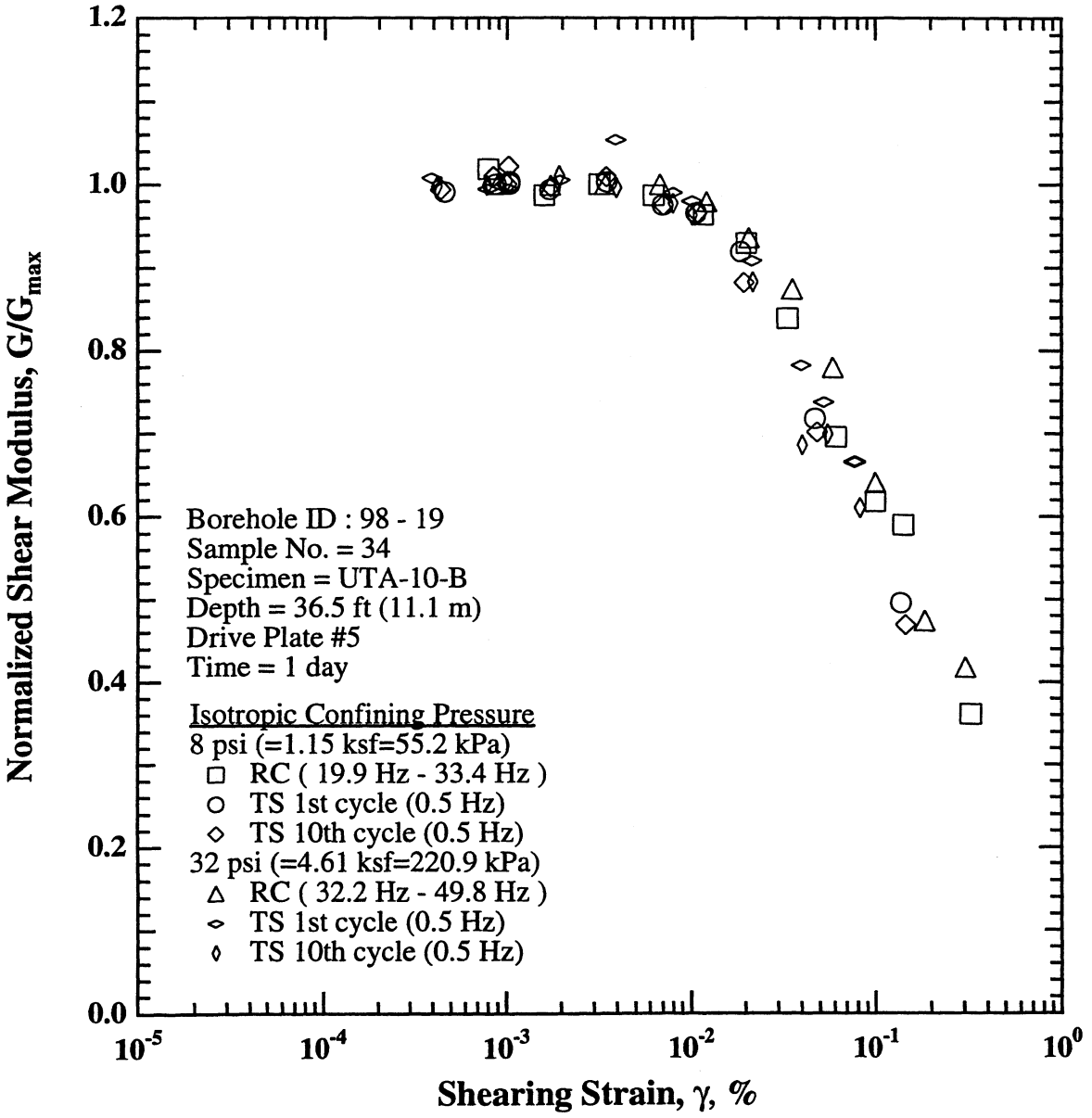

Figure C.10 Variation in Normalized Shear Modulus with Shearing Strain and Isotropic Effective Confining Pressure from Resonant Column Tests of Specimen UTA-10-B from the East Bay Bridge Site.

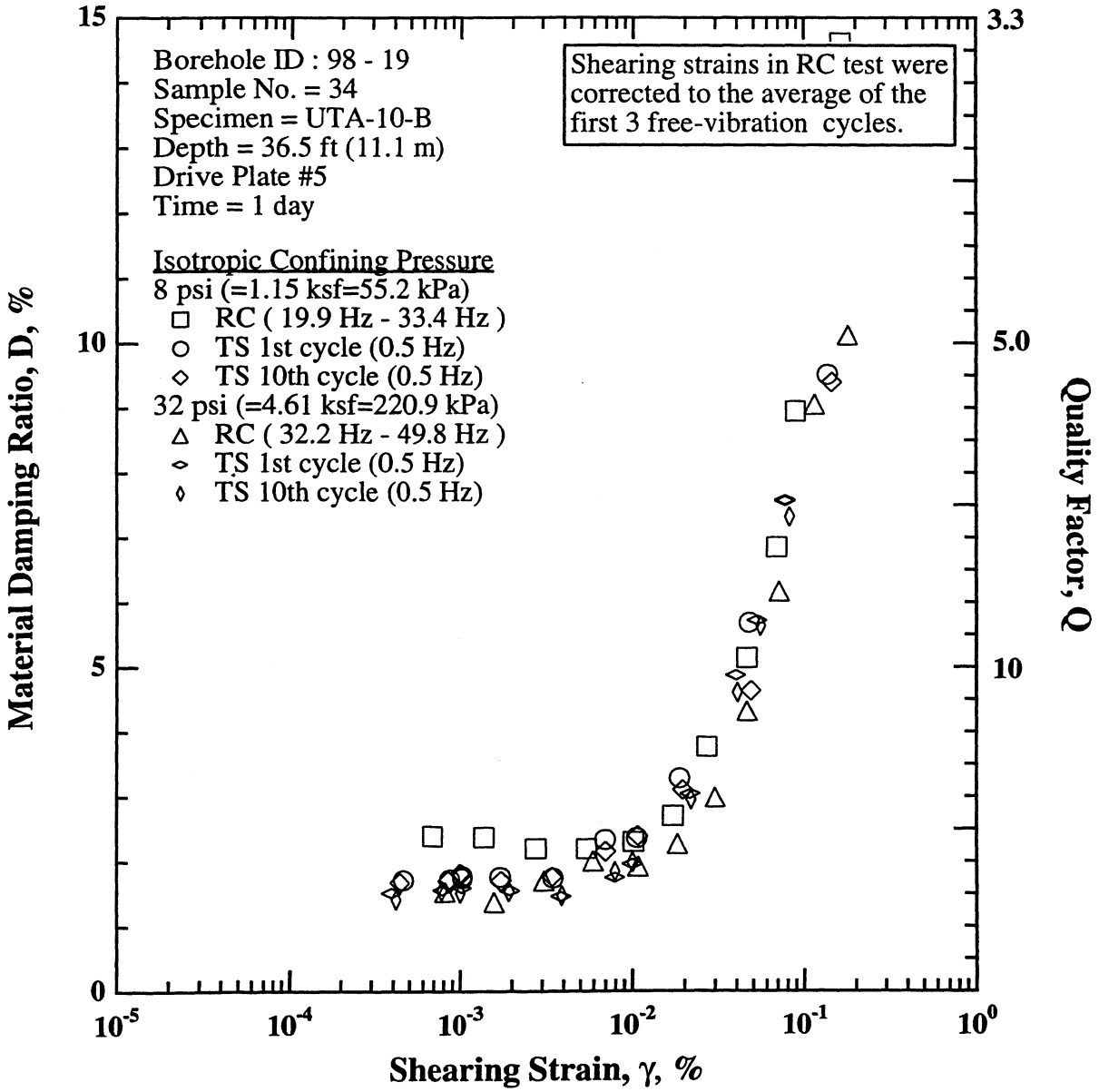

Figure C.11 Variation in Material Damping Ratio with Shearing Strain and Isotropic Effective Confining Pressure from Resonant Column Tests of Specimen UTA-10-B from the East Bay Bridge Site.

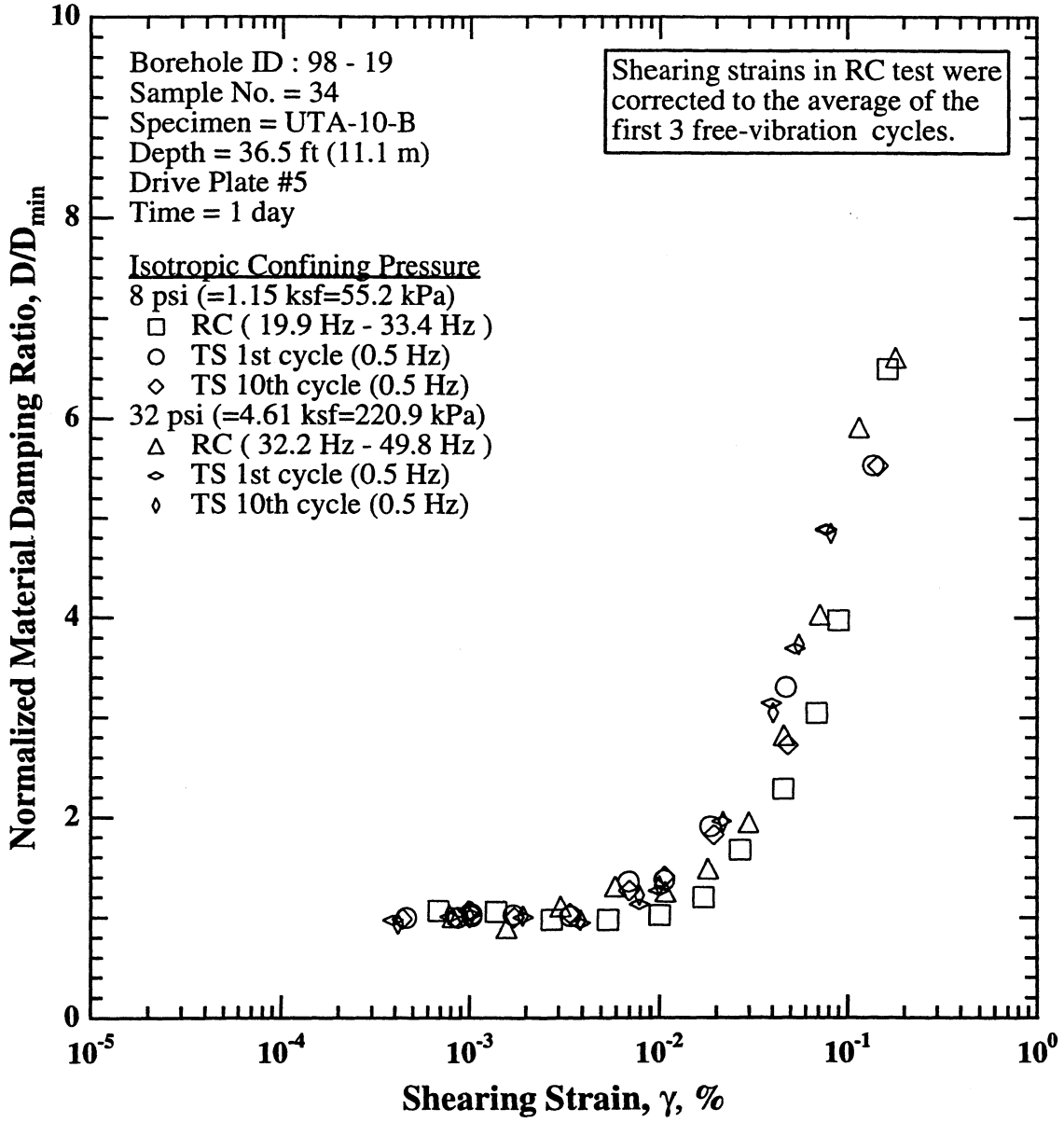

Figure C.12 Variation in Normalized Material Damping Ratio with Shearing Strain and Isotropic Effective Confining Pressure from Resonant Column Tests of Specimen UTA-10-B from the East Bay Bridge Site.

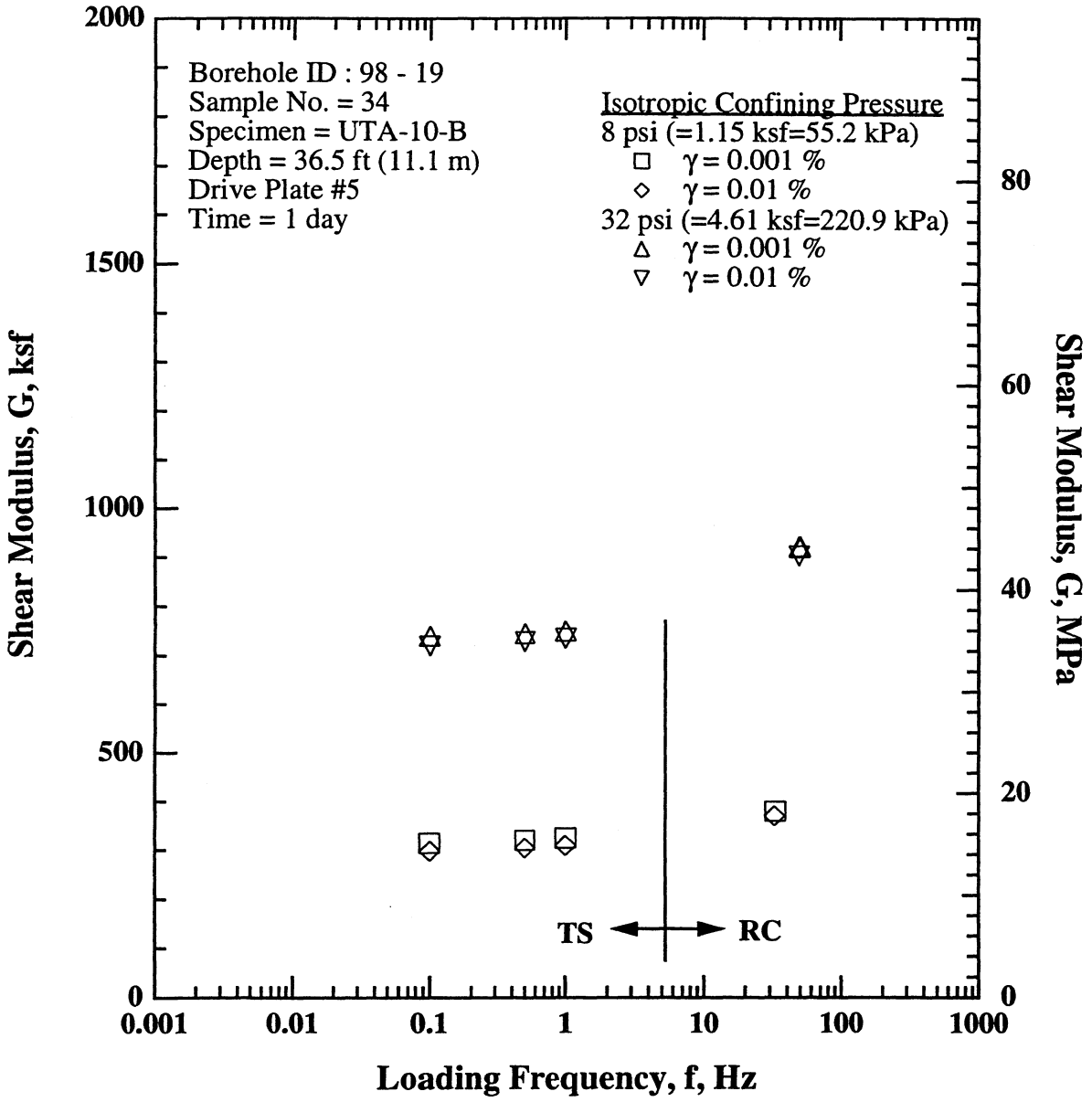

Figure C.13 Comparison of the Variation in Shear Modulus with Loading Frequency, Shearing Strain and Isotropic Effective Confining Pressure from RCTS Tests of Specimen UTA-10-B from the East Bay Bridge Site.

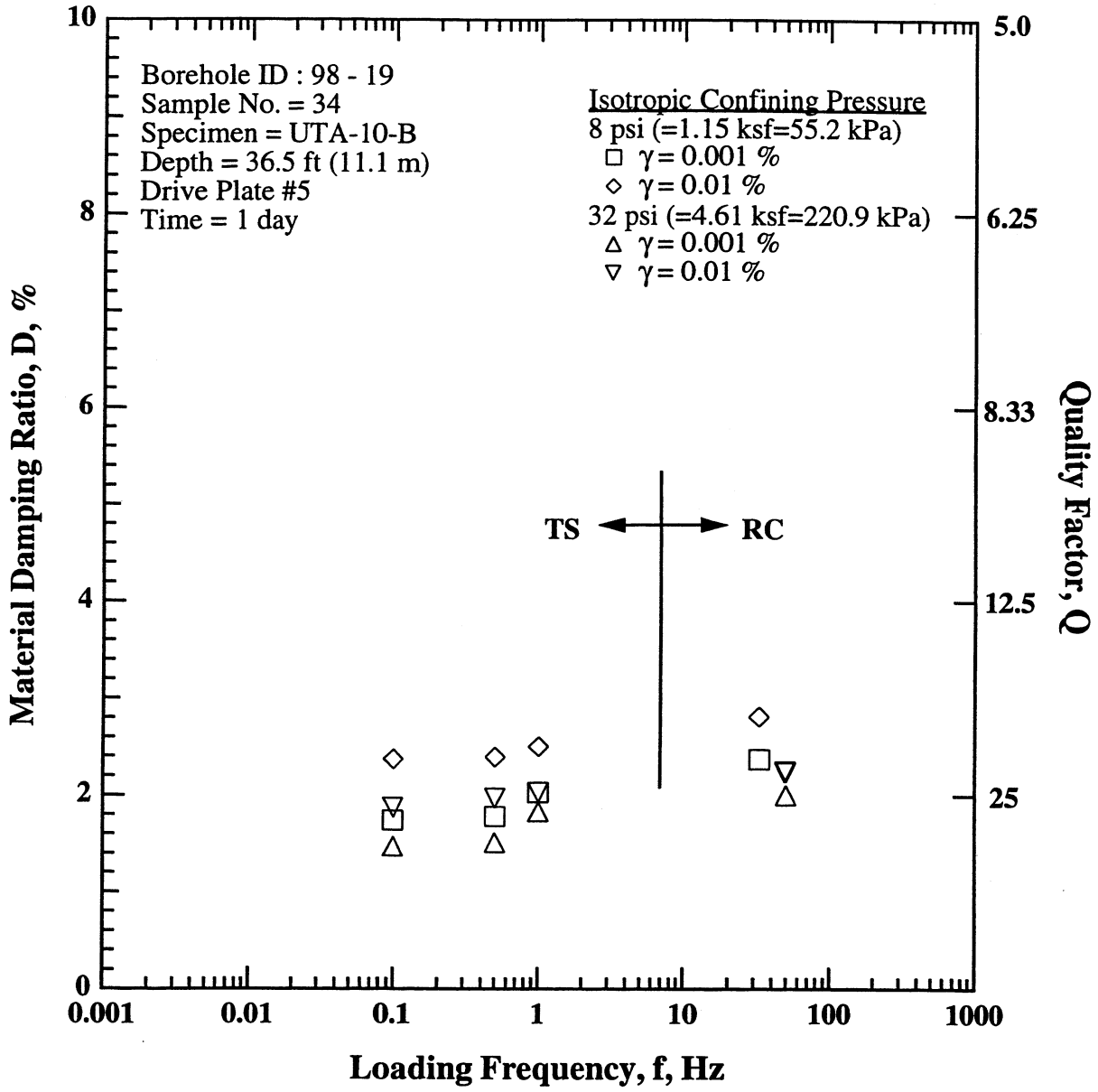

Figure C.14 Comparison of the Variation in Material Damping Ratio with Loading Frequency, Shearing Strain and Isotropic Effective Confining Pressure from RCTS Tests of Specimen UTA-10-B from the East Bay Bridge Site.

Table C.1 Variation in Low-Amplitude Shear Modulus, Low-Amplitude Material Damping Ratio and Void Ratio with Effective Isotropic Confining Pressure from RC Tests of Specimen UTA-10-B (Boring 98 - 19) from the East Bay Bridge Site

Effective Isotropic Confining Pressure, σ_o'			Low-Amplitude Shear Modulus, G_{max}		Low-Amplitude Material Damping Ratio,	Void Ratio, e
(psi)	(psf)	(kPa)	(ksf)	(MPa)	Dmin, %	
2	288	13.8	237	11.4	2.53	1.608
4	576	27.6	281	13.5	2.25	1.601
8	1152	55.2	366	17.5	2.11	1.585
16	2304	110.5	530	25.4	2.02	1.558
32	4608	220.9	813	39.0	1.91	1.458

Table C.2 Variation in Shear Modulus, Normalized Shear Modulus and Material Damping Ratio with Shearing Strain from RC Tests of Specimen UTA-10-B (Boring 98 - 19) from the East Bay Bridge Site; Effective Confining Pressure, σ_o' = 8 psi (1.15 ksf = 55.2 kPa)

Peak Shearing Strain, %	Shear Modulus, G, ksf	Normalized Shear Modulus, G/G_{max}	Average[+] Shearing Strain, %	Material Damping Ratio[x], D, %
7.89E-04	392	1.02	6.84E-04	2.39
1.59E-03	380	0.99	1.38E-03	2.38
3.15E-03	385	1.00	2.76E-03	2.20
6.19E-03	380	0.99	5.43E-03	2.19
1.16E-02	371	0.96	1.01E-02	2.30
2.00E-02	358	0.93	1.70E-02	2.70
3.35E-02	323	0.84	2.69E-02	3.76
6.12E-02	268	0.70	4.58E-02	5.14
9.96E-02	238	0.62	6.87E-02	6.85
1.42E-01	227	0.59	8.94E-02	8.94
3.23E-01	139	0.36	1.64E-01	14.61

[+] Average Shearing Strain from the First Three Cycles of the Free Vibration Decay Curve

[x] Average Damping Ratio from the First Three Cycles of the Free Vibration Decay Curve

Table C.3 Variation in Shear Modulus, Normalized Shear Modulus and Material Damping Ratio with Shearing Strain from TS Tests of Specimen UTA-10-B (Boring 98 - 19) from the East Bay Bridge Site; Effective Confining Pressure, σ_o' = 8 psi (1.15 ksf = 55.2 kPa)

First Cycle				Tenth Cycle			
Peak Shearing Strain, %	Shear Modulus, G, ksf	Normalized Shear Modulus, G/G_{max}	Material Damping Ratio, D, %	Peak Shearing Strain, %	Shear Modulus, G, ksf	Normalized Shear Modulus, G/G_{max}	Material Damping Ratio, D, %
4.60E-04	320	0.99	1.71	4.37E-04	320	0.99	1.67
8.68E-04	323	1.00	1.72	8.44E-04	325	1.01	1.70
1.03E-03	323	1.00	1.77	9.95E-04	322	1.00	1.81
1.03E-03	324	1.00	1.74	1.02E-03	329	1.02	1.80
1.71E-03	321	0.99	1.76	1.73E-03	321	1.00	1.70
3.46E-03	324	1.00	1.74	3.43E-03	325	1.01	1.76
6.94E-03	315	0.98	2.33	6.97E-03	314	0.98	2.15
1.06E-02	312	0.97	2.36	1.07E-02	311	0.97	2.39
1.86E-02	297	0.92	3.28	1.94E-02	284	0.88	3.10
4.72E-02	232	0.72	5.68	4.84E-02	226	0.70	4.63
1.37E-01	160	0.50	9.51	1.45E-01	151	0.47	9.39

Table C.4 Variation in Shear Modulus, Normalized Shear Modulus and Material Damping Ratio with Shearing Strain from RC Tests of Specimen UTA-10-B (Boring 98 - 19) from the East Bay Bridge Site; Effective Confining Pressure, σ_o' = 32 psi (4.61 ksf = 220.9 kPa)

Peak Shearing Strain, %	Shear Modulus, G, ksf	Normalized Shear Modulus, G/G_{max}	Average[+] Shearing Strain, %	Material Damping Ratio[x], D, %
8.92E-04	922	1.00	8.13E-04	1.53
1.72E-03	921	1.00	1.58E-03	1.37
3.40E-03	922	1.00	3.07E-03	1.70
6.68E-03	922	1.00	5.92E-03	2.00
1.21E-02	903	0.98	1.08E-02	1.92
2.07E-02	863	0.94	1.81E-02	2.27
3.56E-02	806	0.87	2.99E-02	2.98
5.88E-02	719	0.78	4.59E-02	4.31
9.99E-02	591	0.64	7.11E-02	6.16
1.84E-01	437	0.47	1.15E-01	9.04
3.04E-01	385	0.42	1.80E-01	10.11

[+] Average Shearing Strain from the First Three Cycles of the Free Vibration Decay Curve

[x] Average Damping Ratio from the First Three Cycles of the Free Vibration Decay Curve

Table C.5 Variation in Shear Modulus, Normalized Shear Modulus and Material Damping Ratio with Shearing Strain from TS Tests of Specimen UTA-10-B (Boring 98 - 19) from the East Bay Bridge Site; Effective Confining Pressure, σ_o' = 32 psi (4.61 ksf = 220.9 kPa)

First Cycle				Tenth Cycle			
Peak Shearing Strain, %	Shear Modulus, G, ksf	Normalized Shear Modulus, G/G_{max}	Material Damping Ratio, D, %	Peak Shearing Strain, %	Shear Modulus, G, ksf	Normalized Shear Modulus, G/G_{max}	Material Damping Ratio, D, %
3.90E-04	751	1.01	1.51	4.14E-04	750	1.00	1.41
7.85E-04	741	0.99	1.56	7.79E-04	751	1.00	1.55
1.02E-03	741	0.99	1.59	1.00E-03	755	1.00	1.51
1.94E-03	749	1.01	1.55	1.92E-03	760	1.01	1.53
3.86E-03	785	1.05	1.46	3.91E-03	749	1.00	1.47
7.90E-03	738	0.99	1.75	7.90E-03	735	0.98	1.84
1.00E-02	730	0.98	1.96	1.00E-02	724	0.96	1.98
2.14E-02	677	0.91	3.04	2.17E-02	664	0.88	2.95
3.96E-02	583	0.78	4.87	4.03E-02	516	0.69	4.60
5.27E-02	550	0.74	5.72	5.51E-02	526	0.70	5.63
7.72E-02	496	0.67	7.57	8.18E-02	459	0.61	7.32

APPENDIX D

UTA-10-C

BOREHOLE ID : 98 - 8

SAMPLE NO. = 71

DEPTH = 79.0 ft (24.1 m)

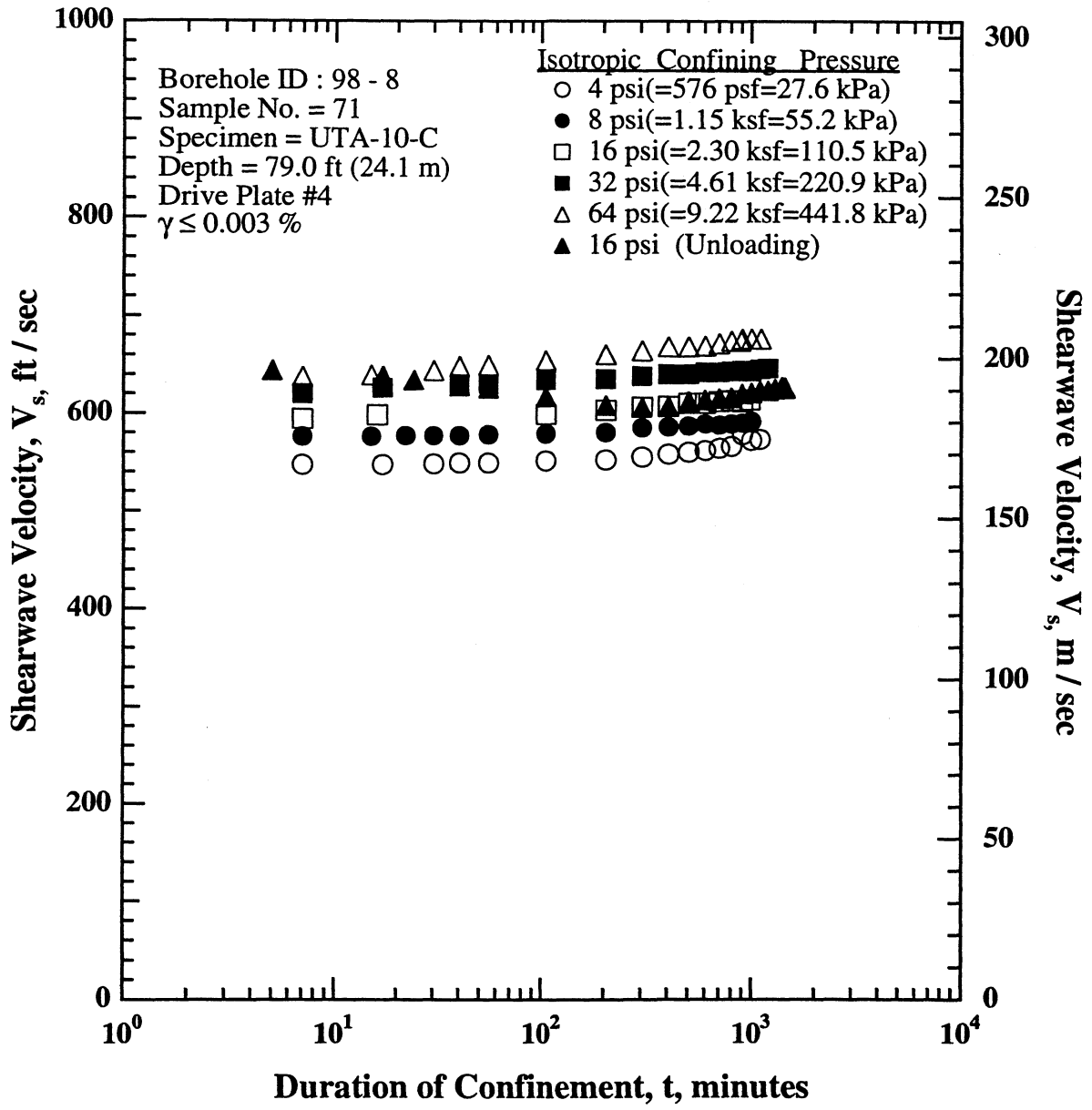

Figure D.1 Variation in Low-Amplitude Shear Wave Velocity with Magnitude and Duration of Isotropic Confining Pressure from Resonant Column Tests of Specimen UTA-10-C from the East Bay Bridge Site.

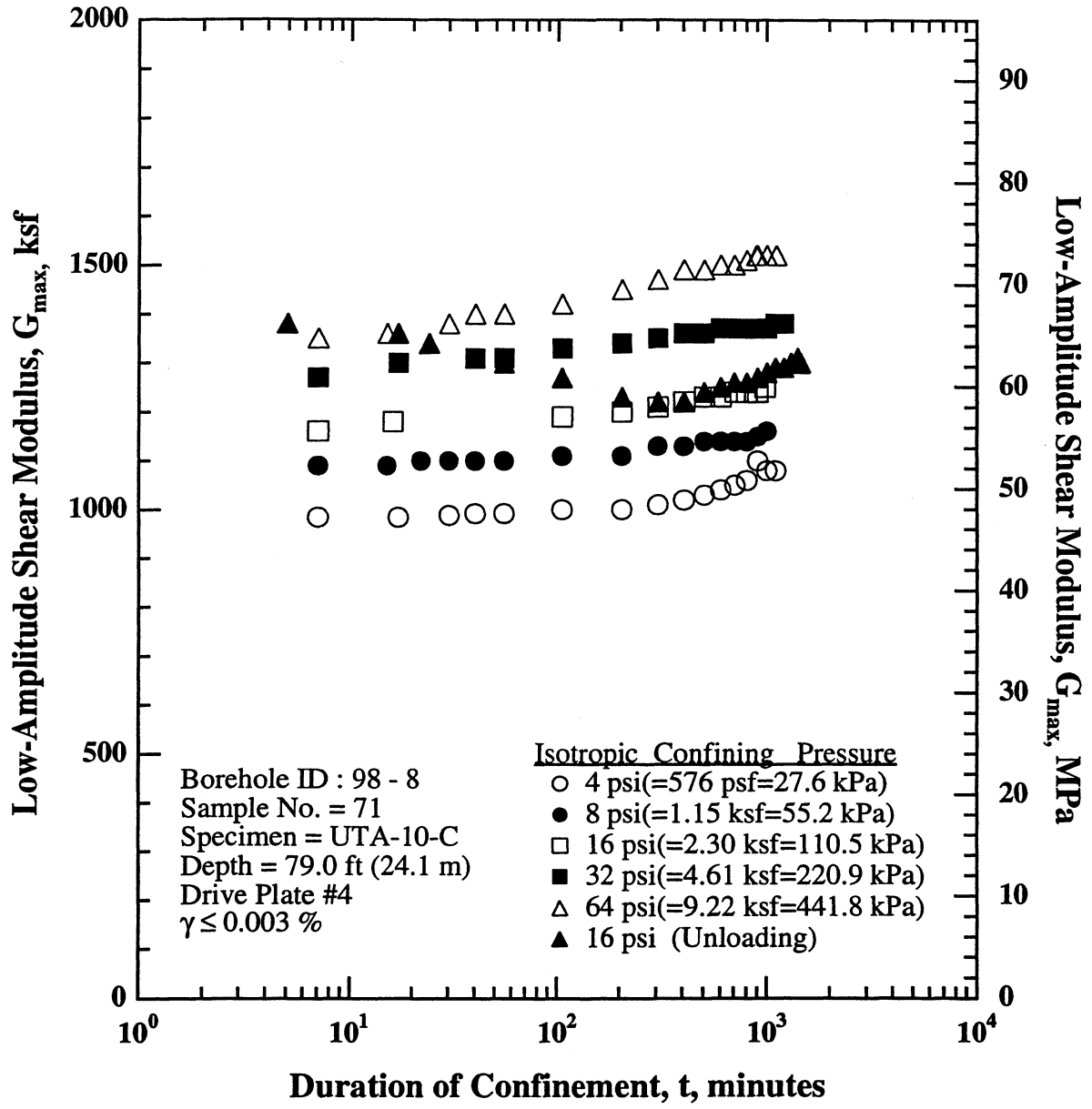

Figure D.2 Variation in Low-Amplitude Shear Modulus with Magnitude and Duration of Isotropic Confining Pressure from Resonant Column Tests of Specimen UTA-10-C from the East Bay Bridge Site.

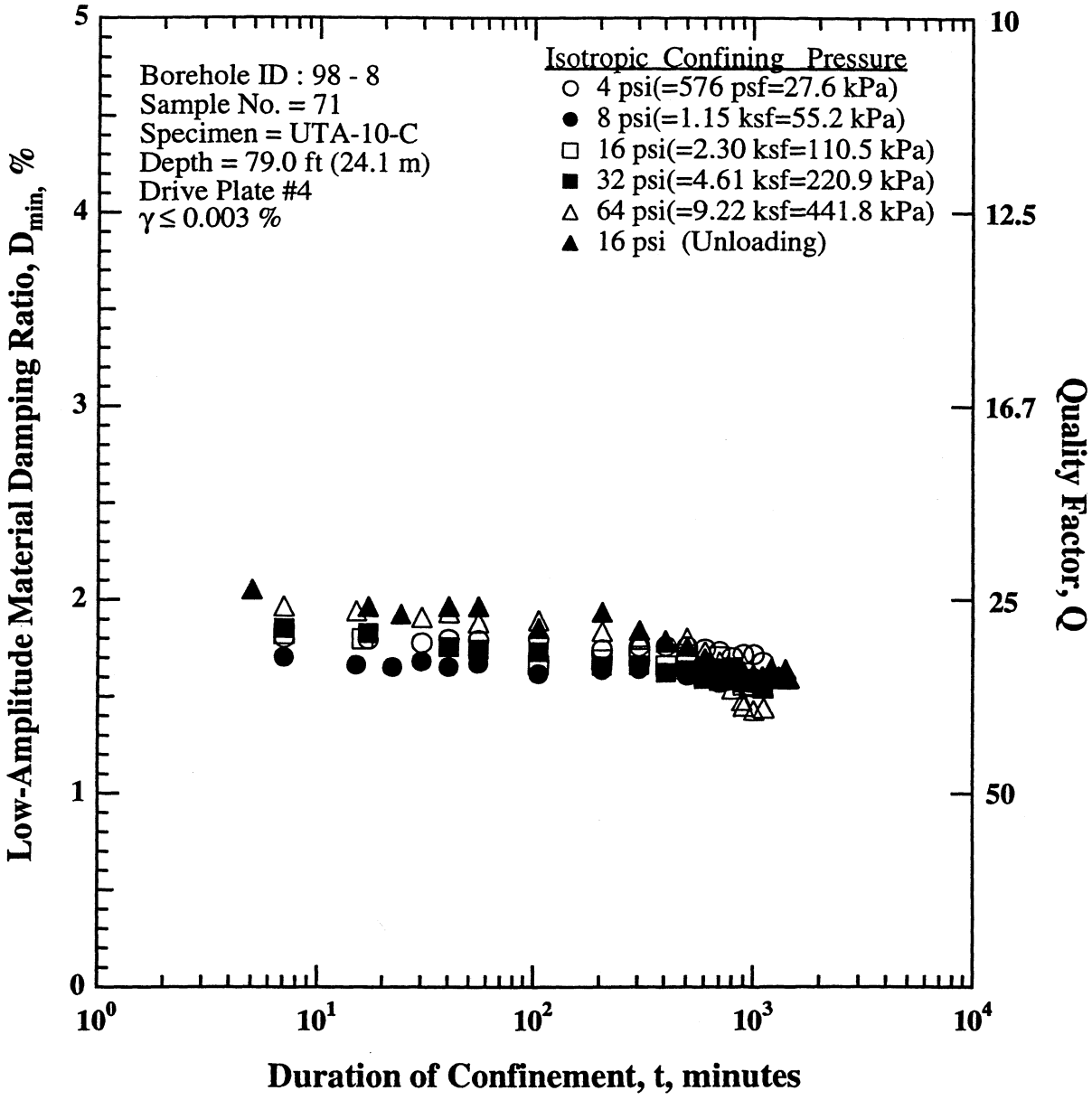

Figure D.3 Variation in Low-Amplitude Material Damping Ratio with Magnitude and Duration of Isotropic Confining Pressure from Resonant Column Tests of Specimen UTA-10-C from the East Bay Bridge Site.

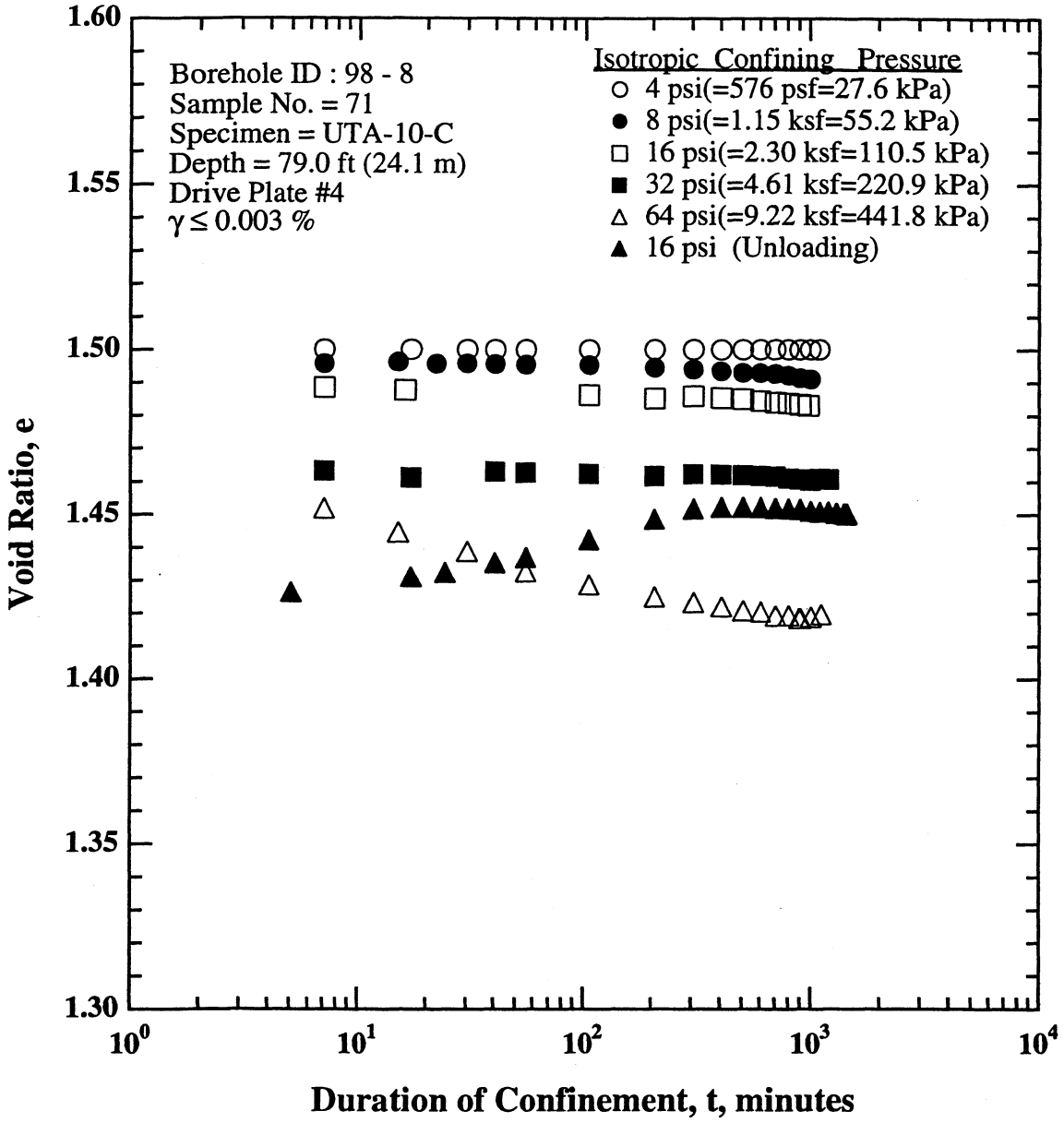

Figure D.4 Variation in Void Ratio with Magnitude and Duration of Isotropic Confining Pressure from Resonant Column Tests of Specimen UTA-10-C from the East Bay Bridge Site.

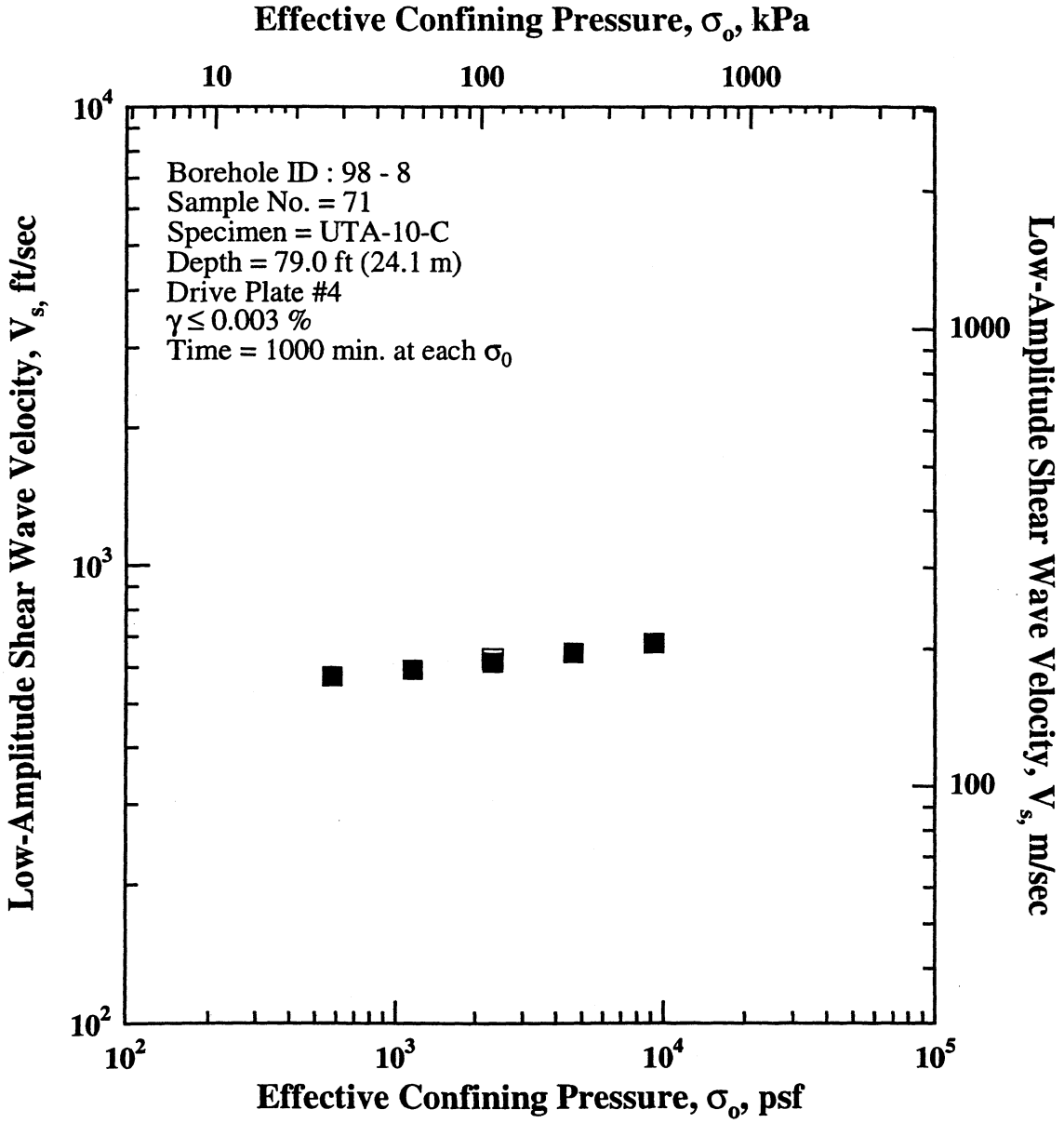

Figure D.5 Variation in Low-Amplitude Shear Wave Velocity with Effective Confining Pressure from Resonant Column Tests of Specimen UTA-10-C from the East Bay Bridge Site.

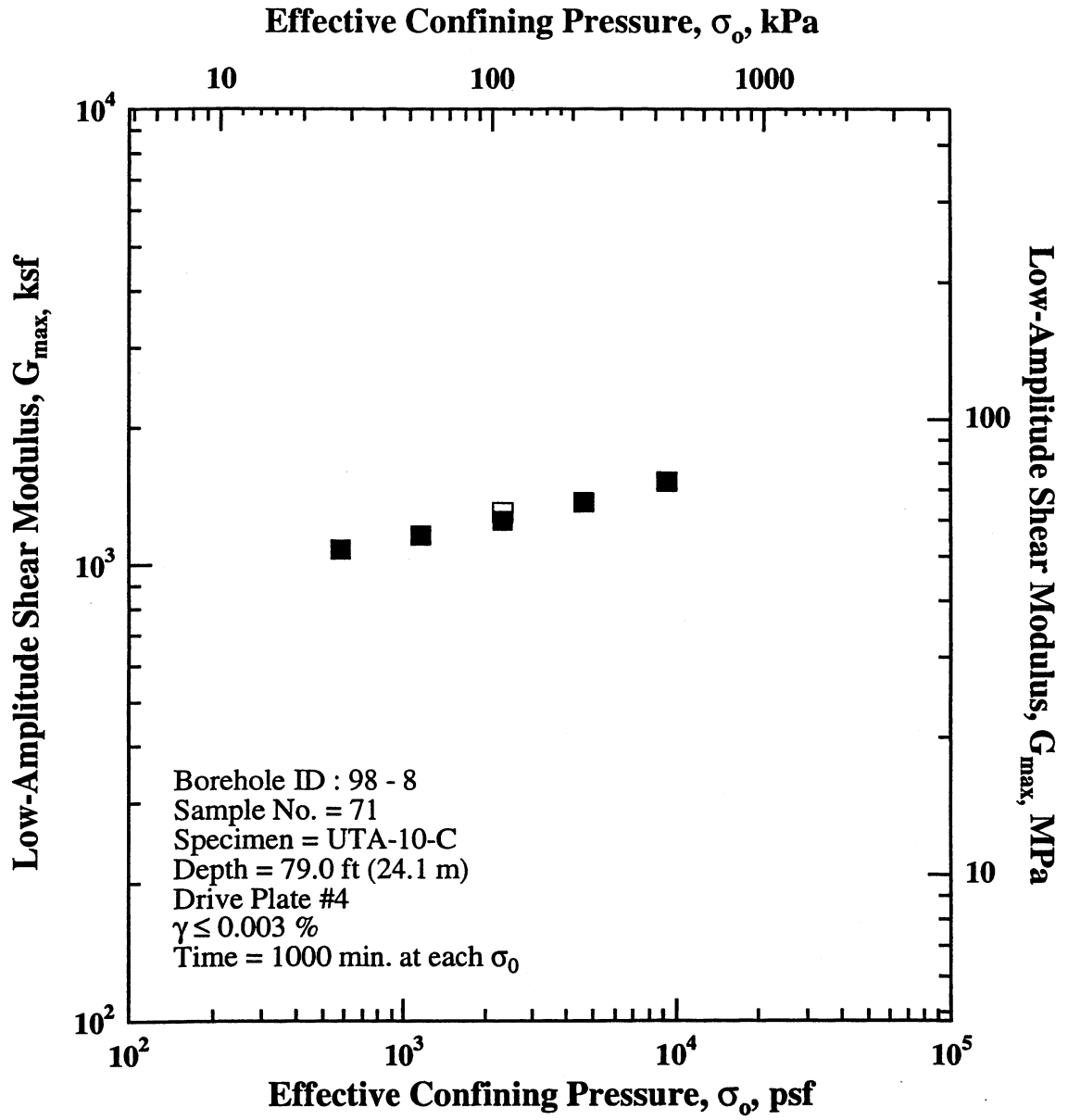

Figure D.6 Variation in Low-Amplitude Shear Modulus with Effective Confining Pressure from Resonant Column Tests of Specimen UTA-10-C from the East Bay Bridge Site.

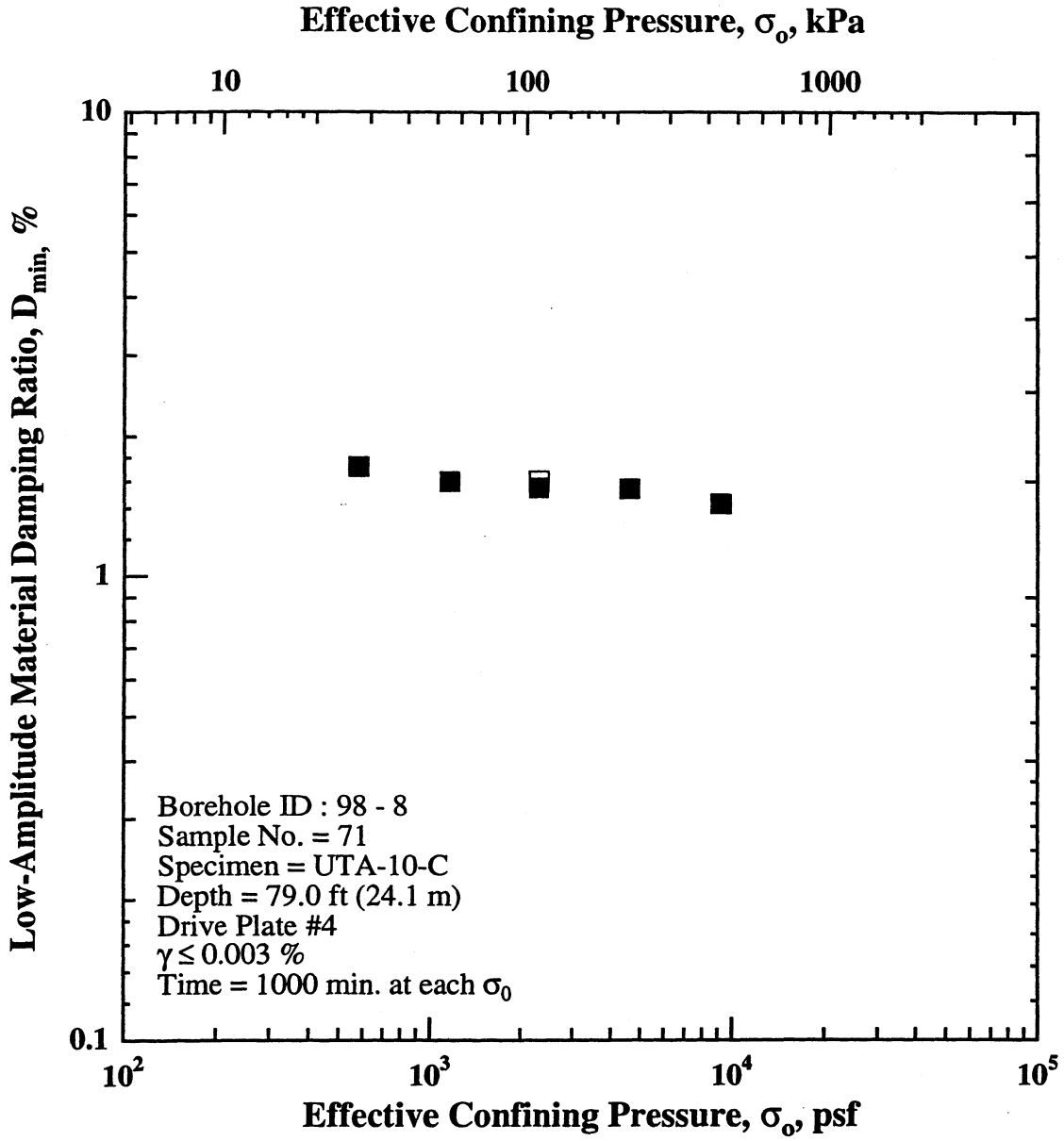

Figure D.7 Variation in Low-Amplitude Material Damping Ratio with Effective Confining Pressure from Resonant Column Tests of Specimen UTA-10-C from the East Bay Bridge Site.

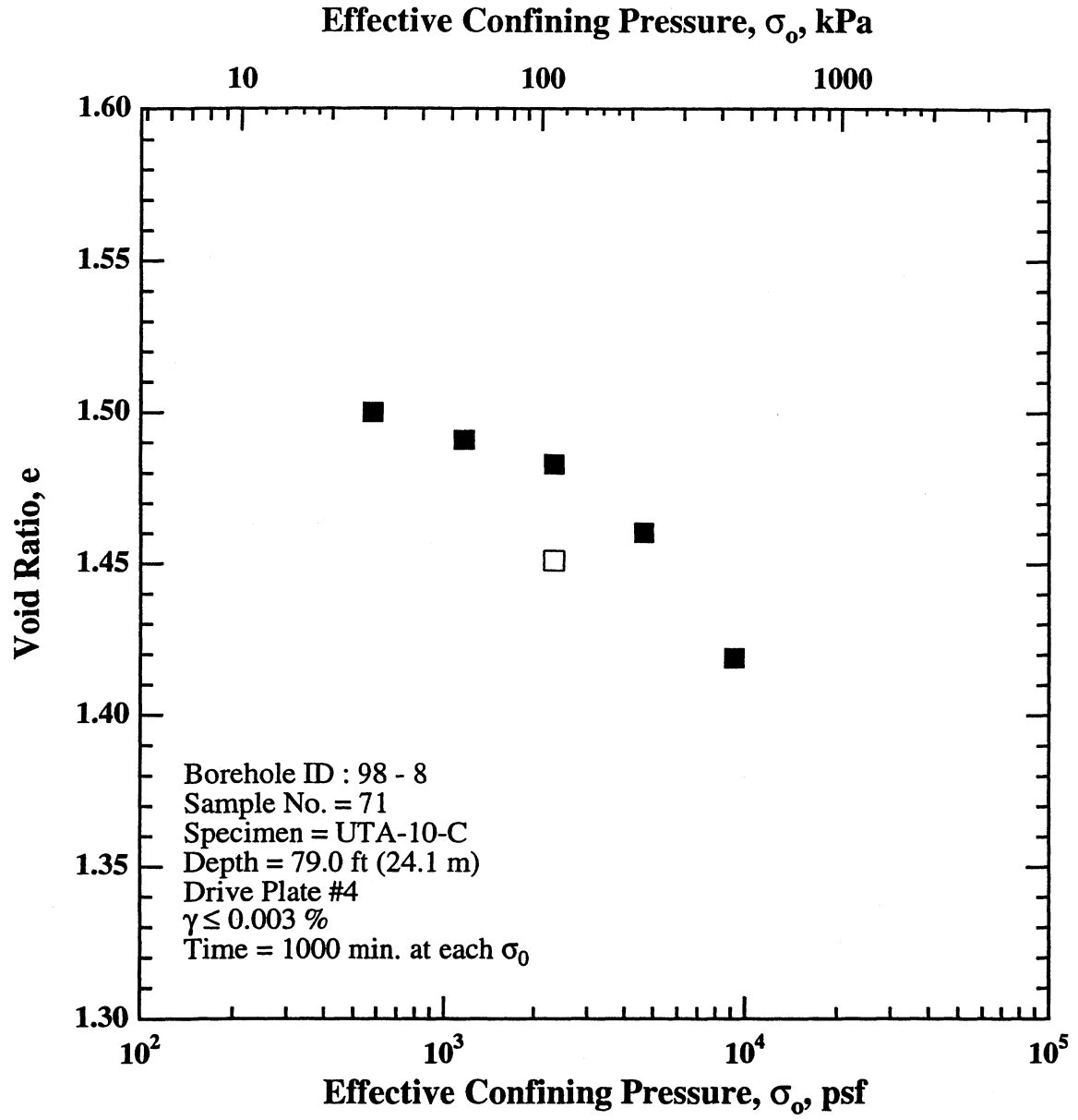

Figure D.8 Variation in Void Ratio with Effective Confining Pressure from Resonant Column Tests of Specimen UTA-10-C from the East Bay Bridge Site.

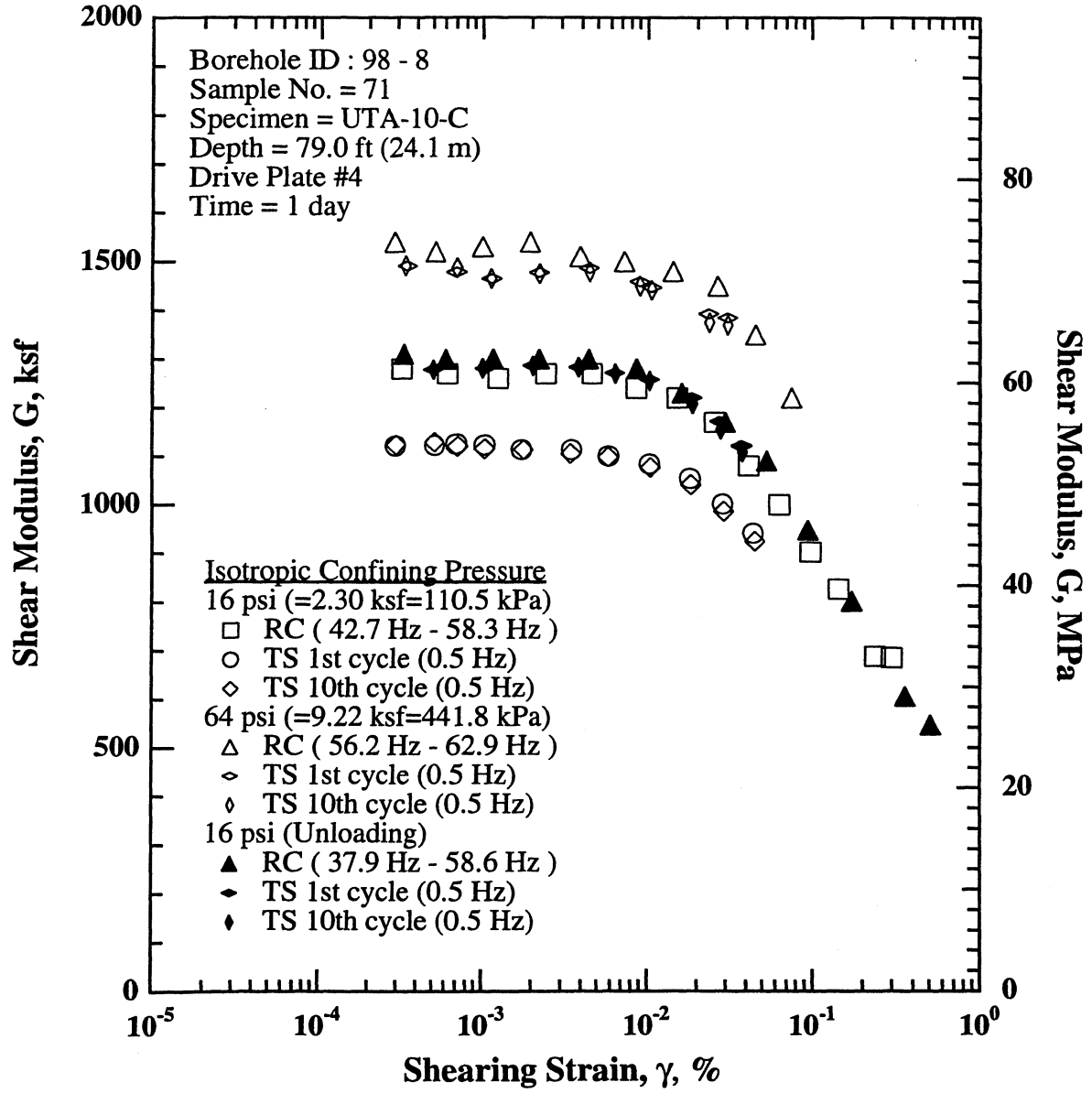

Figure D.9 Comparison of the Variation in Shear Modulus with Shearing Strain, Stress History and Isotropic Effective Confining Pressure from RCTS Tests of Specimen UTA-10-C from the East Bay Bridge Site.

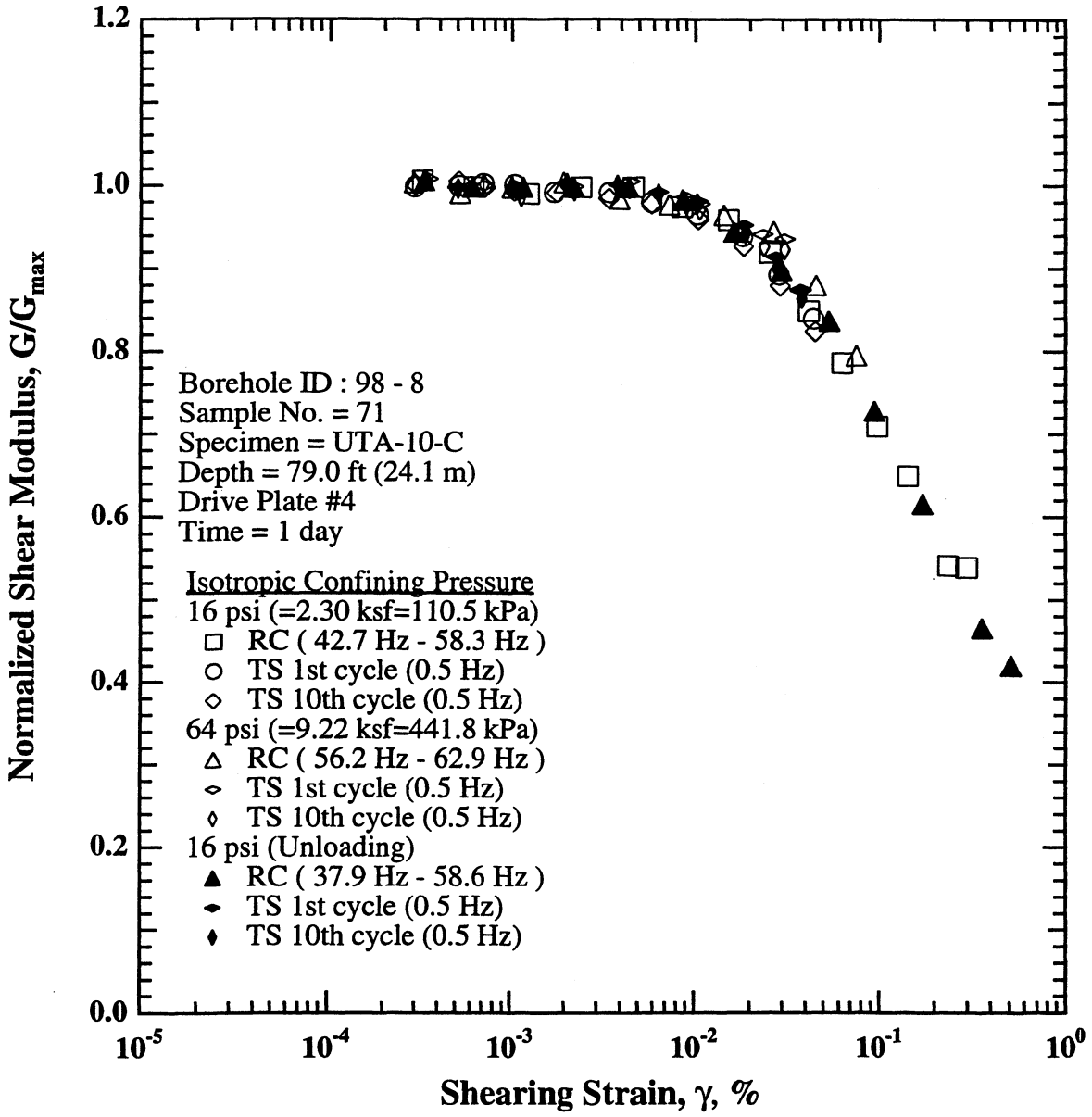

Figure D.10 Comparison of the Variation in Normalized Shear Modulus with Shearing Strain, Stress History and Isotropic Effective Confining Pressure from RCTS Tests of Specimen UTA-10-C from the East Bay Bridge Site.

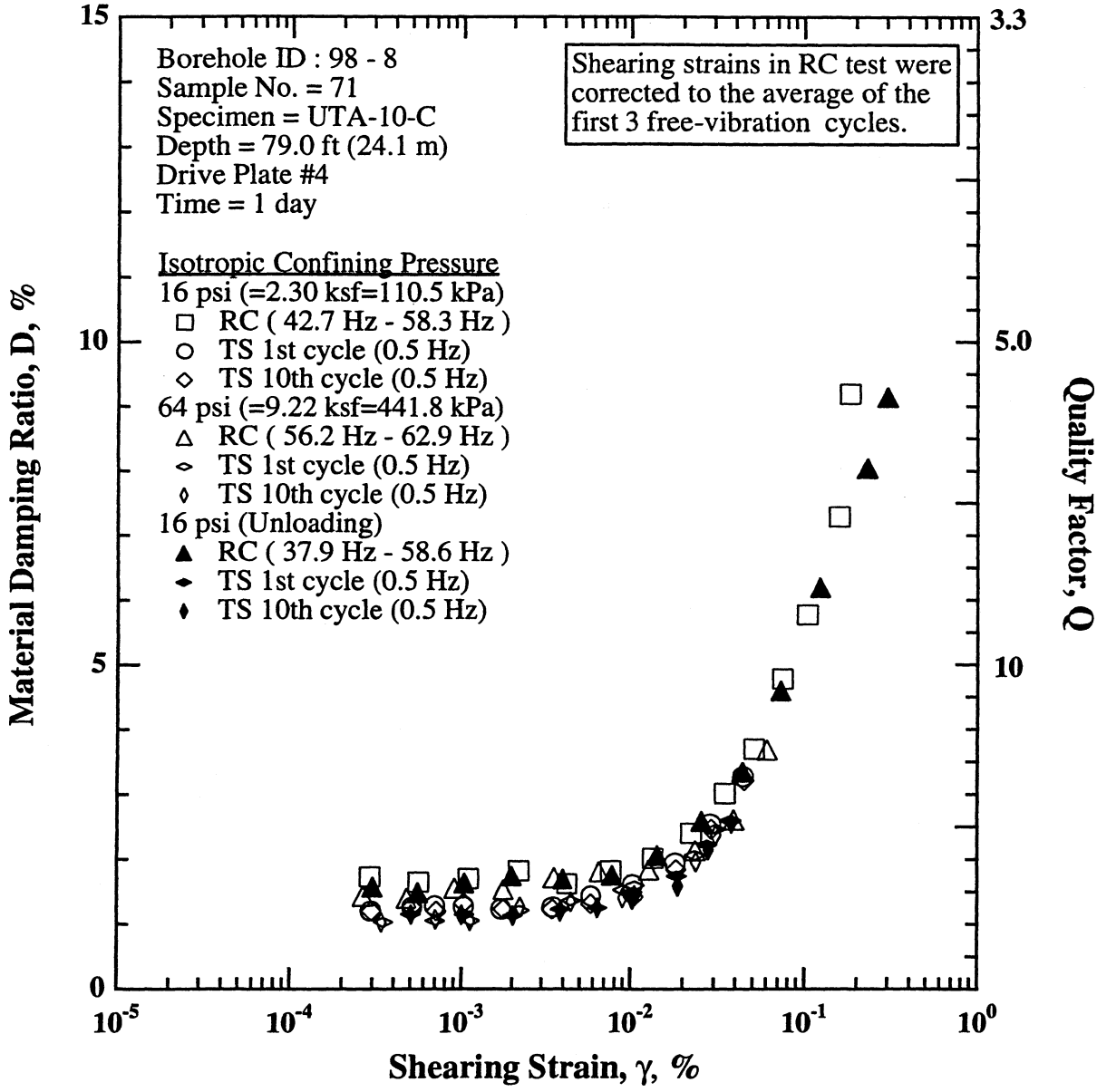

Figure D.11 Comparison of the Variation in Material Damping Ratio with Shearing Strain, Stress History and Isotropic Effective Confining Pressure from RCTS Tests of Specimen UTA-10-C from the East Bay Bridge Site.

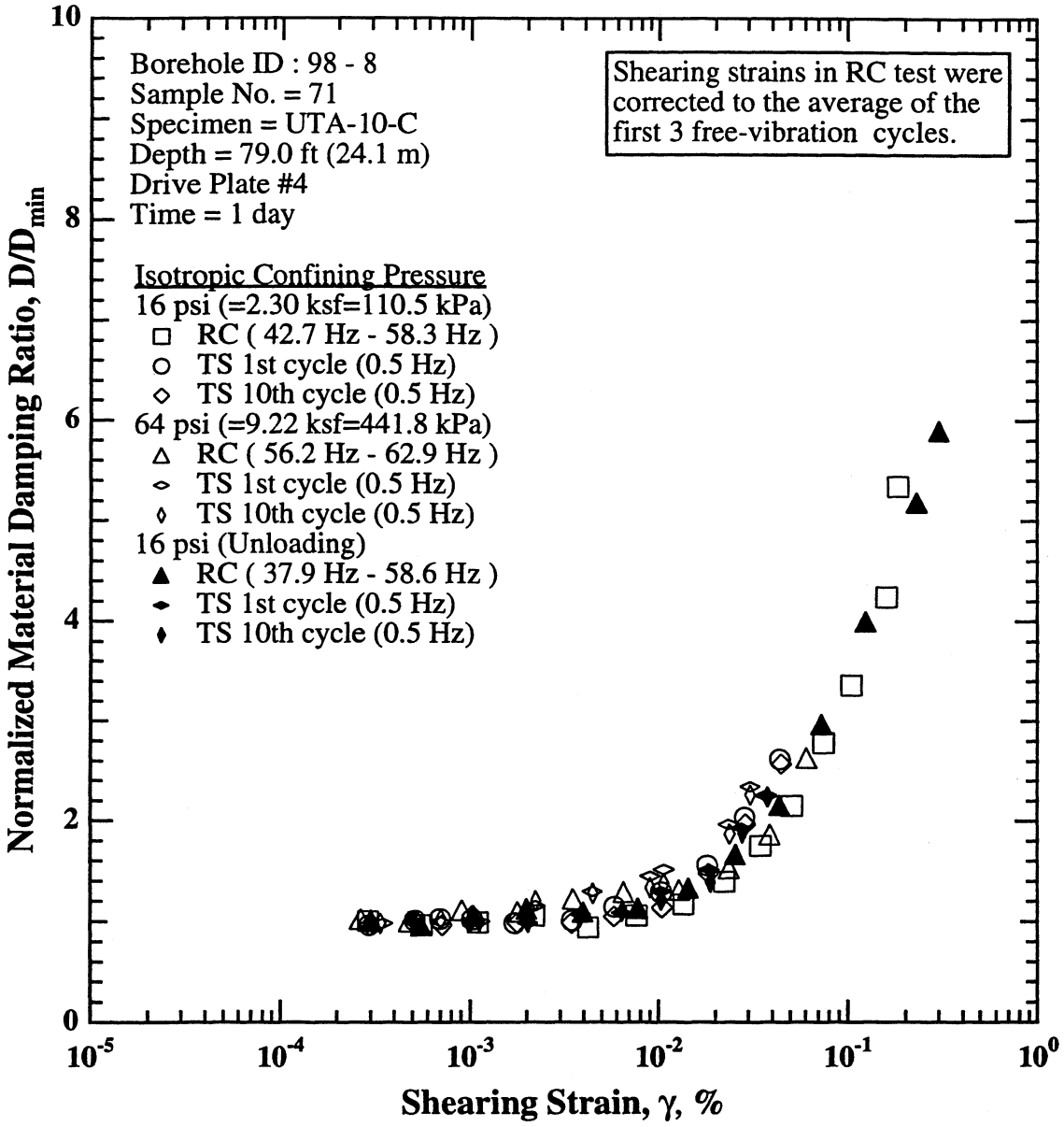

Figure D.12 Comparison of the Variation in Normalized Material Damping Ratio with Shearing Strain, Stress History and Isotropic Effective Confining Pressure from RCTS Tests of Specimen UTA-10-C from the East Bay Bridge Site.

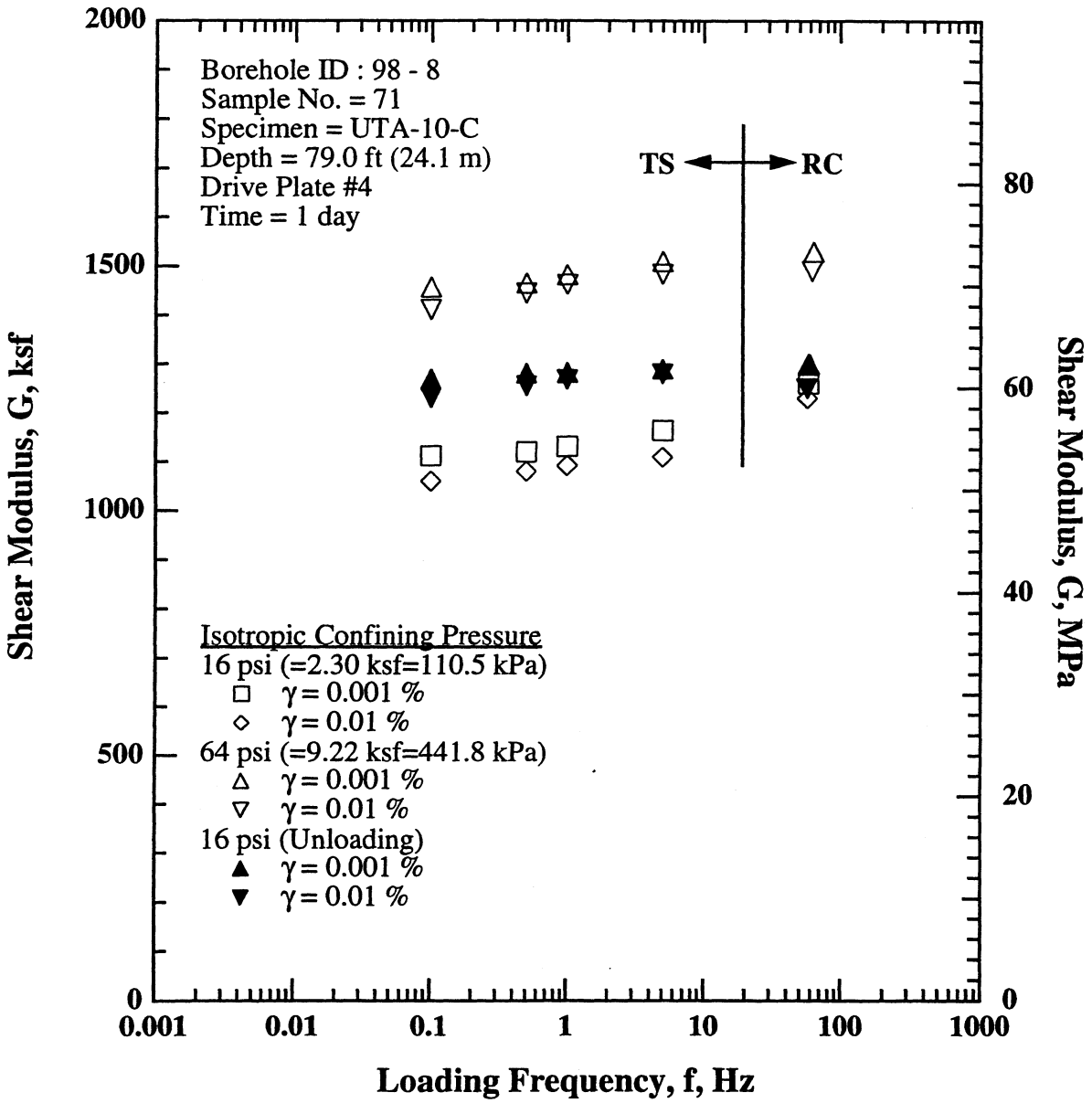

Figure D.13 Comparison of the Variation in Shear Modulus with Loading Frequency, Shearing Strain, Stress History and Isotropic Effective Confining Pressure from RCTS Tests of Specimen UTA-10-C from the East Bay Bridge Site.

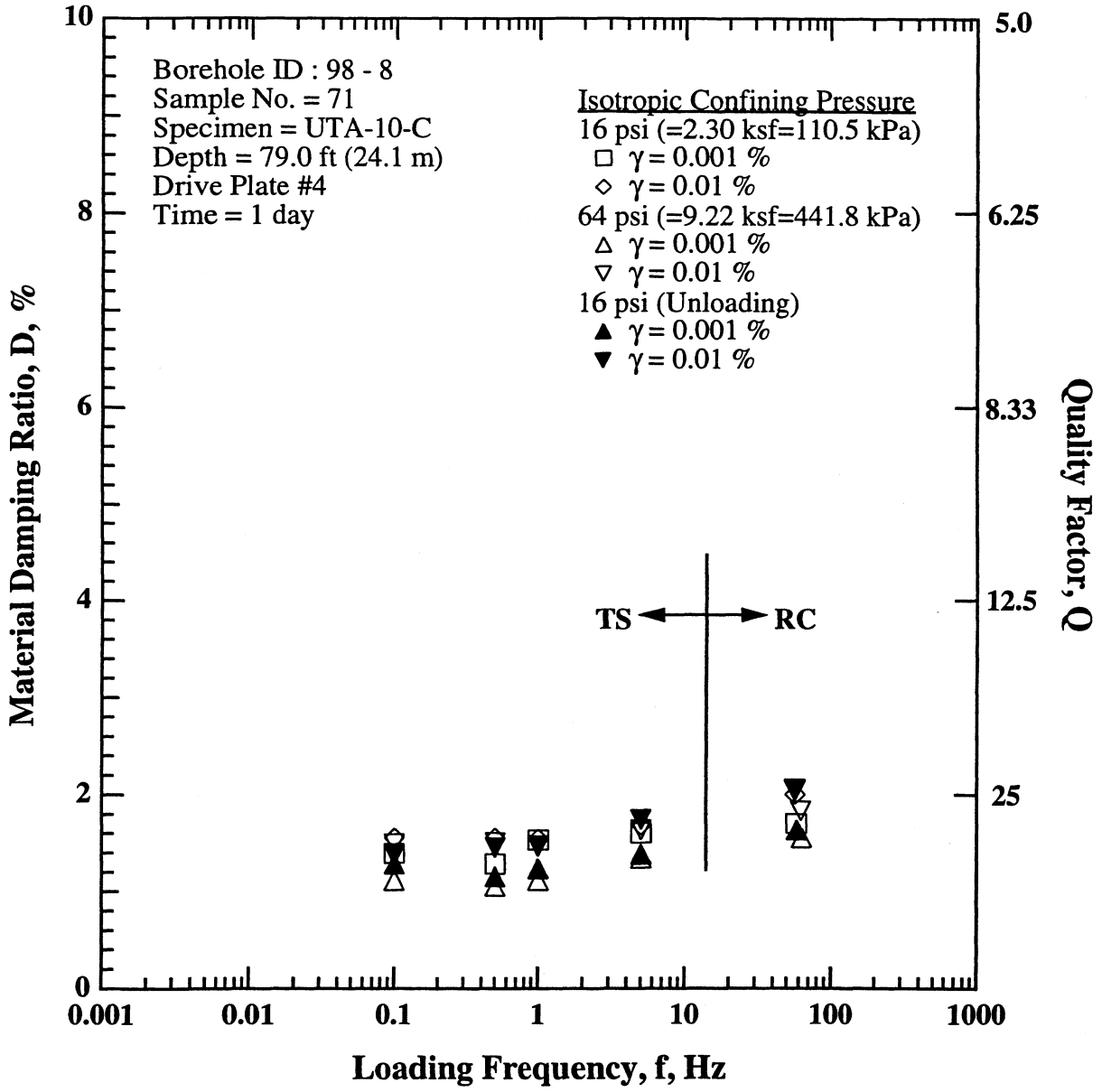

Figure D.14 Comparison of the Variation in Material Damping Ratio with Loading Frequency, Shearing Strain, Stress History and Isotropic Effective Confining Pressure from RCTS Tests of Specimen UTA-10-C from the East Bay Bridge Site.

Table D.1 Variation in Low-Amplitude Shear Modulus, Low-Amplitude Material Damping Ratio and Void Ratio with Effective Isotropic Confining Pressure from RC Tests of Specimen UTA-10-C (Boring 98 - 8) from the East Bay Bridge Site

Effective Isotropic Confining Pressure, σ_o'			Low-Amplitude Shear Modulus, G_{max}		Low-Amplitude Material Damping Ratio,	Void Ratio, e
(psi)	(psf)	(kPa)	(ksf)	(MPa)	Dmin, %	
4	576	27.6	1080	51.8	1.72	1.500
8	1152	55.2	1160	55.6	1.60	1.491
16	2304	110.5	1250	59.9	1.55	1.483
32	4608	220.9	1370	65.7	1.54	1.460
64	9216	441.8	1520	72.9	1.43	1.419
16	2304	110.5	1300	62.3	1.60	1.451

Table D.2 Variation in Shear Modulus, Normalized Shear Modulus and Material Damping Ratio with Shearing Strain from RC Tests of Specimen UTA-10-C (Boring 98 - 8) from the East Bay Bridge Site; Effective Confining Pressure, σ_o' = 16 psi (2.30 ksf = 110.5 kPa)

Peak Shearing Strain, %	Shear Modulus, G, ksf	Normalized Shear Modulus, G/G_{max}	Average[+] Shearing Strain, %	Material Damping Ratio[x], D, %
3.22E-04	1280	1.01	2.90E-04	1.72
6.17E-04	1270	1.00	5.58E-04	1.65
1.24E-03	1260	0.99	1.10E-03	1.70
2.43E-03	1270	1.00	2.18E-03	1.82
4.64E-03	1270	1.00	4.21E-03	1.62
8.53E-03	1240	0.97	7.64E-03	1.82
1.52E-02	1220	0.96	1.35E-02	2.01
2.56E-02	1170	0.92	2.22E-02	2.39
4.14E-02	1080	0.85	3.47E-02	3.01
6.31E-02	1000	0.79	5.09E-02	3.69
9.77E-02	903	0.71	7.45E-02	4.78
1.44E-01	827	0.65	1.04E-01	5.77
2.37E-01	689	0.54	1.59E-01	7.29
2.98E-01	686	0.54	1.83E-01	9.19

[+] Average Shearing Strain from the First Three Cycles of the Free Vibration Decay Curve

[x] Average Damping Ratio from the First Three Cycles of the Free Vibration Decay Curve

Table D.3 Variation in Shear Modulus, Normalized Shear Modulus and Material Damping Ratio with Shearing Strain from TS Tests of Specimen UTA-10-C (Boring 98 - 8) from the East Bay Bridge Site; Effective Confining Pressure, σ_o' = 16 psi (2.30 ksf = 110.5 kPa)

First Cycle				Tenth Cycle			
Peak Shearing Strain, %	Shear Modulus, G, ksf	Normalized Shear Modulus, G/G_{max}	Material Damping Ratio, D, %	Peak Shearing Strain, %	Shear Modulus, G, ksf	Normalized Shear Modulus, G/G_{max}	Material Damping Ratio, D, %
2.94E-04	1121	1.00	1.20	2.96E-04	1123	1.00	1.20
5.14E-04	1122	1.00	1.26	5.11E-04	1128	1.00	1.26
6.97E-04	1125	1.00	1.28	7.12E-04	1120	1.00	1.20
1.03E-03	1123	1.00	1.27	1.03E-03	1115	0.99	1.32
1.72E-03	1113	0.99	1.23	1.77E-03	1113	0.99	1.23
3.46E-03	1113	0.99	1.26	3.44E-03	1105	0.98	1.23
5.82E-03	1100	0.98	1.43	5.80E-03	1098	0.98	1.31
1.03E-02	1084	0.97	1.61	1.04E-02	1077	0.96	1.42
1.81E-02	1054	0.94	1.94	1.83E-02	1041	0.93	1.84
2.86E-02	1002	0.89	2.54	2.90E-02	987	0.88	2.46
4.40E-02	942	0.84	3.27	4.48E-02	925	0.82	3.21

Table D.4 Variation in Shear Modulus, Normalized Shear Modulus and Material Damping Ratio with Shearing Strain from RC Tests of Specimen UTA-10-C (Boring 98 - 8) from the East Bay Bridge Site; Effective Confining Pressure, σ_o' = 64 psi (9.22 ksf = 441.8 kPa)

Peak Shearing Strain, %	Shear Modulus, G, ksf	Normalized Shear Modulus, G/G_{max}	Average[+] Shearing Strain, %	Material Damping Ratio[x], D, %
5.19E-04	1520	0.99	4.77E-04	1.40
2.89E-04	1540	1.00	2.65E-04	1.43
9.95E-04	1530	1.00	9.05E-04	1.55
1.94E-03	1540	1.00	1.77E-03	1.53
3.91E-03	1510	0.98	3.50E-03	1.71
7.25E-03	1500	0.98	6.50E-03	1.81
1.43E-02	1480	0.96	1.28E-02	1.83
2.67E-02	1450	0.94	2.35E-02	2.13
4.54E-02	1350	0.88	3.89E-02	2.61
7.51E-02	1220	0.79	6.06E-02	3.68

[+] Average Shearing Strain from the First Three Cycles of the Free Vibration Decay Curve

[x] Average Damping Ratio from the First Three Cycles of the Free Vibration Decay Curve

Table D.5 Variation in Shear Modulus, Normalized Shear Modulus and Material Damping Ratio with Shearing Strain from TS Tests of Specimen UTA-10-C (Boring 98 - 8) from the East Bay Bridge Site; Effective Confining Pressure, σ_o' = 64 psi (9.22 ksf = 441.8 kPa)

First Cycle				Tenth Cycle			
Peak Shearing Strain, %	Shear Modulus, G, ksf	Normalized Shear Modulus, G/G_{max}	Material Damping Ratio, D, %	Peak Shearing Strain, %	Shear Modulus, G, ksf	Normalized Shear Modulus, G/G_{max}	Material Damping Ratio, D, %
3.47E-04	1491	1.01	1.03	3.38E-04	1491	1.00	1.03
7.00E-04	1479	1.00	1.05	7.02E-04	1487	1.00	1.07
1.13E-03	1465	0.99	1.05	1.12E-03	1465	0.99	1.05
2.21E-03	1478	1.00	1.21	2.22E-03	1475	0.99	1.26
4.44E-03	1487	1.00	1.36	4.45E-03	1479	1.00	1.34
8.98E-03	1459	0.99	1.52	8.99E-03	1450	0.98	1.40
1.06E-02	1447	0.98	1.59	1.06E-02	1441	0.97	1.44
2.34E-02	1393	0.94	2.06	2.37E-02	1375	0.93	1.96
3.07E-02	1385	0.94	2.46	3.07E-02	1370	0.92	2.37

Table D.6 Variation in Shear Modulus, Normalized Shear Modulus and Material Damping Ratio with Shearing Strain from RC Tests of Specimen UTA-10-C (Boring 98 - 8) from the East Bay Bridge Site; Effective Confining Pressure, σ_o' = 16 psi (2.30 ksf = 110.5 kPa), Unloading

Peak Shearing Strain, %	Shear Modulus, G, ksf	Normalized Shear Modulus, G/G_{max}	Average[+] Shearing Strain, %	Material Damping Ratio[x], D, %
3.30E-04	1310	1.01	3.00E-04	1.57
6.04E-04	1300	1.00	5.52E-04	1.48
1.15E-03	1300	1.00	1.04E-03	1.63
2.21E-03	1300	1.00	1.98E-03	1.74
4.39E-03	1300	1.00	3.96E-03	1.69
8.61E-03	1280	0.98	7.75E-03	1.75
1.62E-02	1230	0.94	1.43E-02	2.06
2.97E-02	1170	0.90	2.55E-02	2.58
5.32E-02	1090	0.84	4.38E-02	3.34
9.43E-02	948	0.73	7.25E-02	4.60
1.73E-01	802	0.62	1.23E-01	6.19
3.58E-01	606	0.47	2.29E-01	8.03
5.07E-01	547	0.42	3.00E-01	9.14

[+] Average Shearing Strain from the First Three Cycles of the Free Vibration Decay Curve

[x] Average Damping Ratio from the First Three Cycles of the Free Vibration Decay Curve

Table D.7 Variation in Shear Modulus, Normalized Shear Modulus and Material Damping Ratio with Shearing Strain from TS Tests of Specimen UTA-10-C (Boring 98 - 8) from the East Bay Bridge Site; Effective Confining Pressure, σ_o' = 16 psi (2.30 ksf = 110.5 kPa), Unloading

First Cycle				Tenth Cycle			
Peak Shearing Strain, %	Shear Modulus, G, ksf	Normalized Shear Modulus, G/G_{max}	Material Damping Ratio, D, %	Peak Shearing Strain, %	Shear Modulus, G, ksf	Normalized Shear Modulus, G/G_{max}	Material Damping Ratio, D, %
5.04E-04	1279	1.00	1.15	5.04E-04	1278	1.00	1.15
1.04E-03	1281	1.00	1.15	1.00E-03	1281	1.00	1.14
2.01E-03	1286	1.00	1.13	2.02E-03	1286	1.00	1.13
3.84E-03	1283	1.00	1.23	3.82E-03	1283	1.00	1.19
6.36E-03	1272	0.99	1.25	6.37E-03	1270	0.99	1.25
1.03E-02	1258	0.98	1.49	1.03E-02	1255	0.98	1.38
1.85E-02	1221	0.95	1.74	1.87E-02	1208	0.94	1.58
2.74E-02	1172	0.91	2.22	2.78E-02	1155	0.90	2.14
3.74E-02	1121	0.87	2.59	3.78E-02	1108	0.86	2.55

APPENDIX E

UTA-10-D

BOREHOLE ID : 98 - 20

SAMPLE NO. = 91

DEPTH = 231 ft (70.4 m)

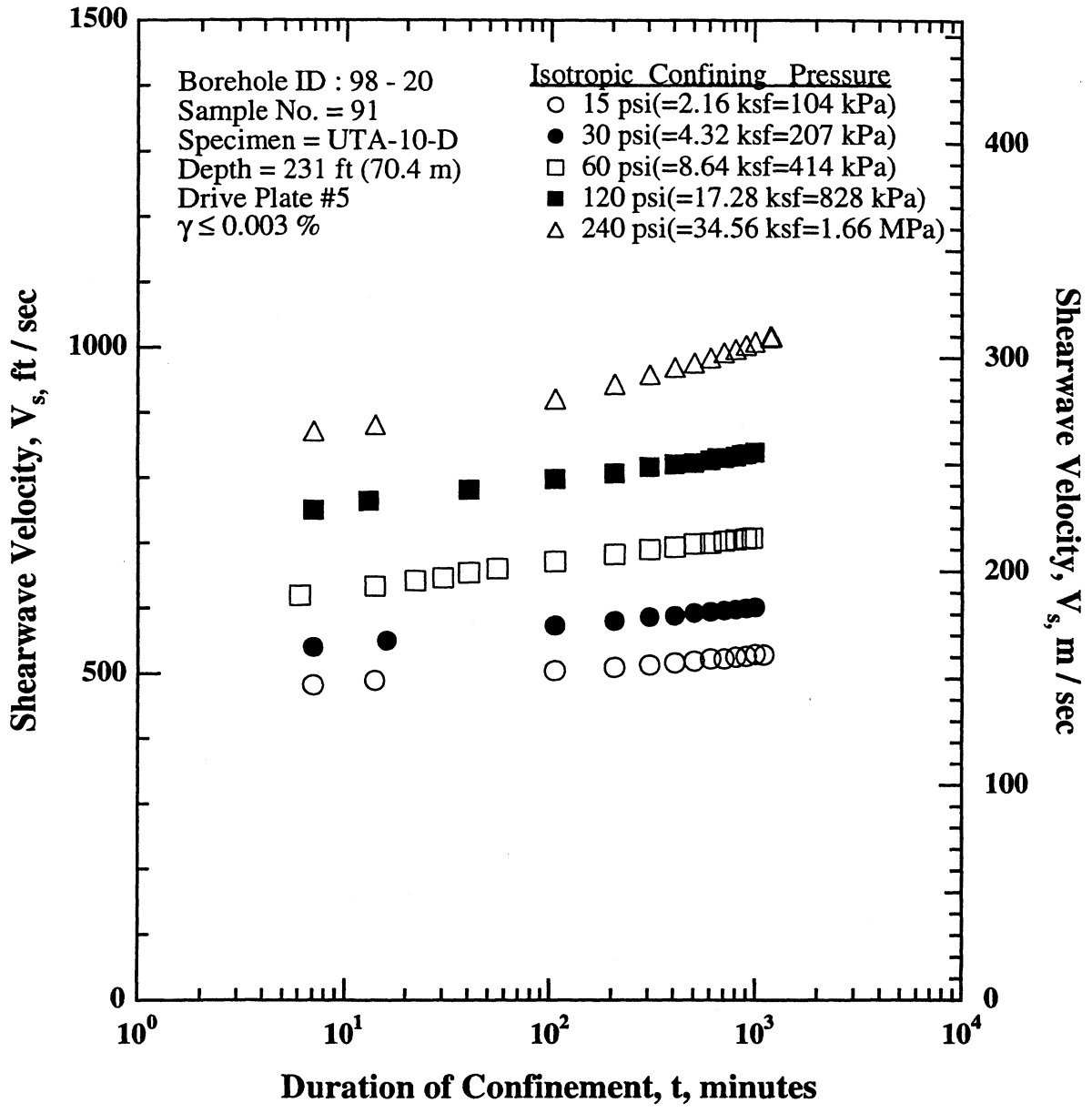

Figure E.1 Variation in Low-Amplitude Shear Wave Velocity with Magnitude and Duration of Isotropic Confining Pressure from Resonant Column Tests of Specimen UTA-10-D from the East Bay Bridge Site.

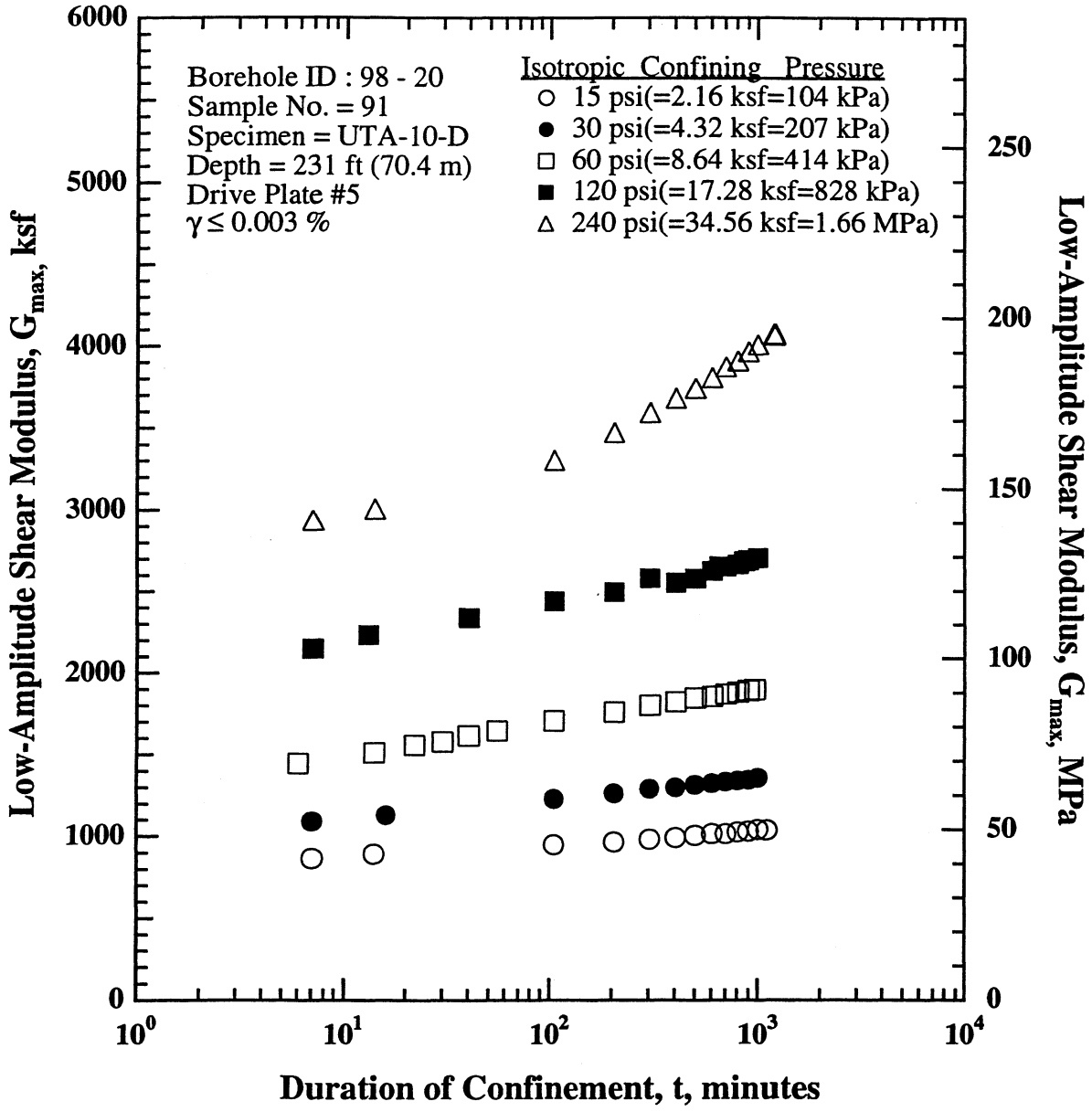

Figure E.2 Variation in Low-Amplitude Shear Modulus with Magnitude and Duration of Isotropic Confining Pressure from Resonant Column Tests of Specimen UTA-10-D from the East Bay Bridge Site.

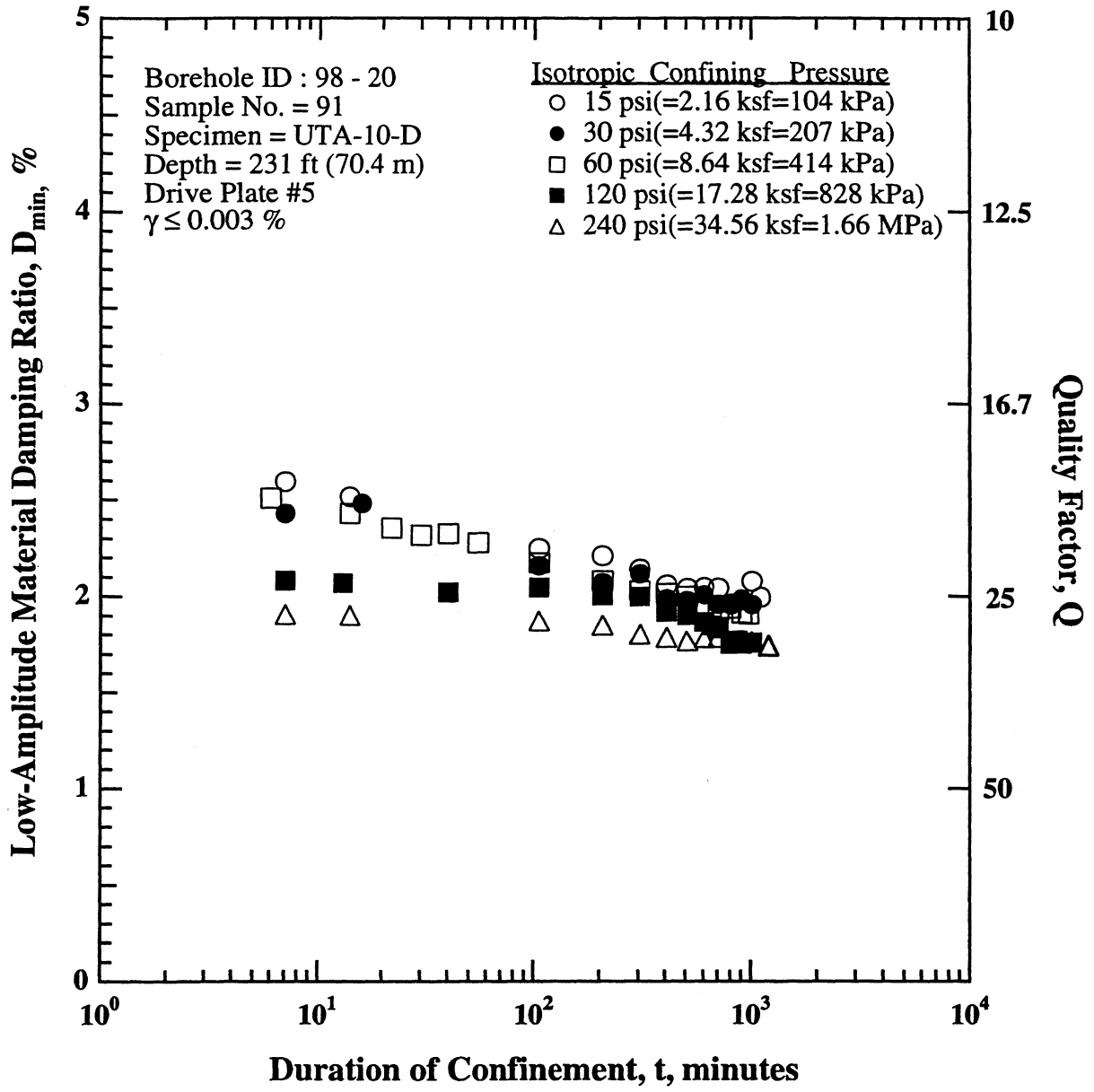

Figure E.3 Variation in Low-Amplitude Material Damping Ratio with Magnitude and Duration of Isotropic Confining Pressure from Resonant Column Tests of Specimen UTA-10-D from the East Bay Bridge Site.

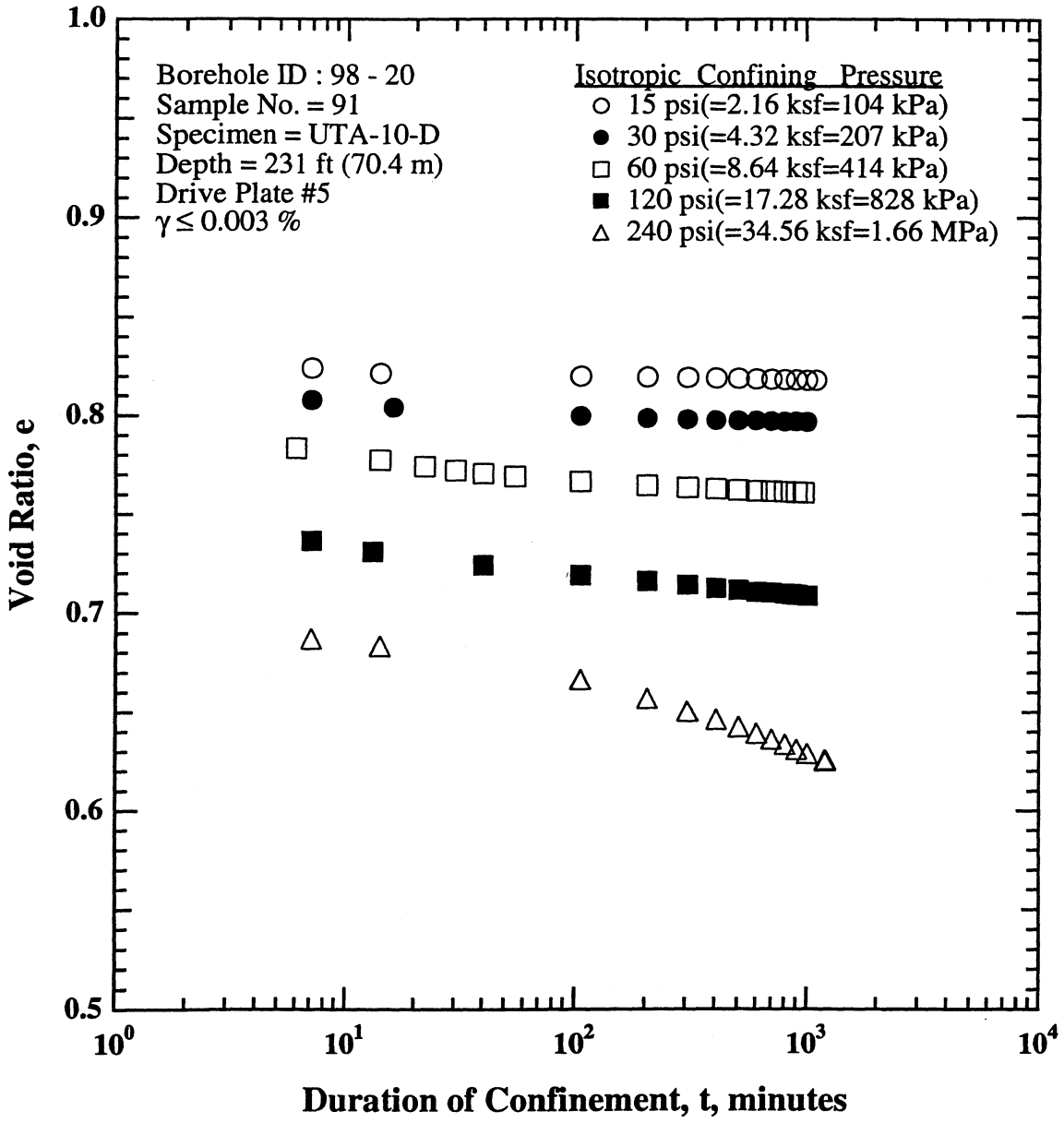

Figure E.4 Variation in Void Ratio with Magnitude and Duration of Isotropic Confining Pressure from Resonant Column Tests of Specimen UTA-10-D from the East Bay Bridge Site.

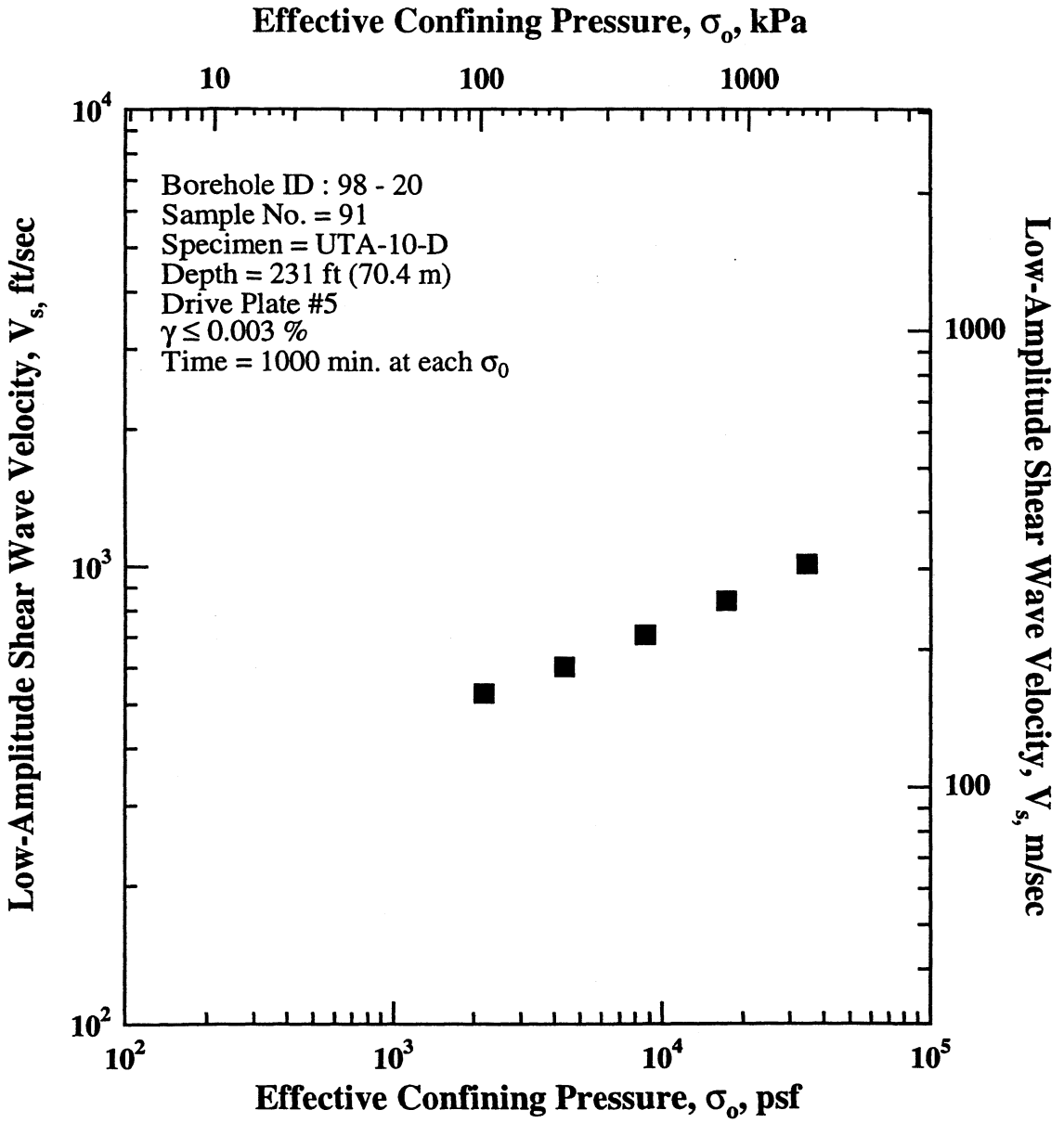

Figure E.5 Variation in Low-Amplitude Shear Wave Velocity with Effective Confining Pressure from Resonant Column Tests of Specimen UTA-10-D from the East Bay Bridge Site.

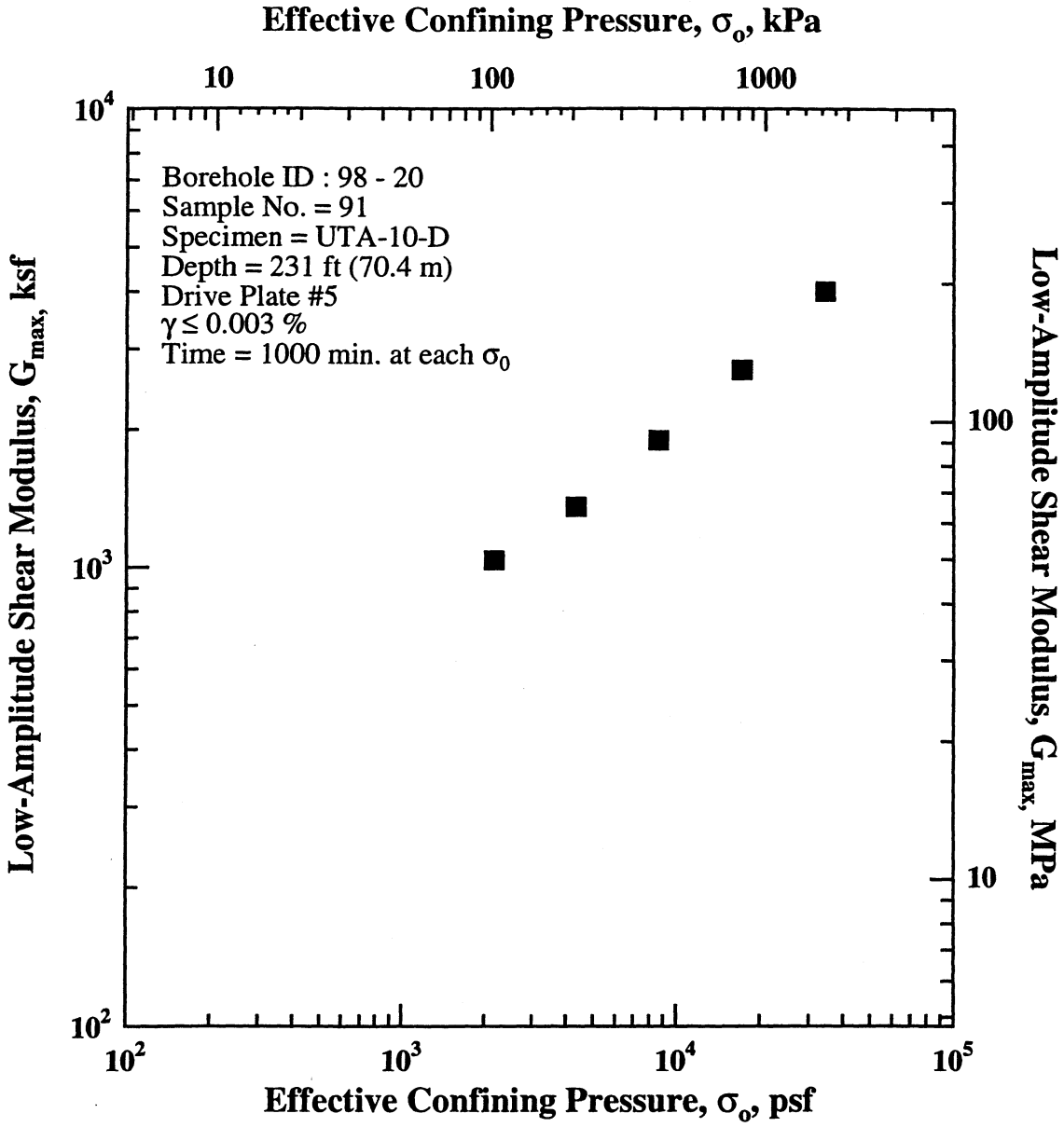

Figure E.6 Variation in Low-Amplitude Shear Modulus with Effective Confining Pressure from Resonant Column Tests of Specimen UTA-10-D from the East Bay Bridge Site.

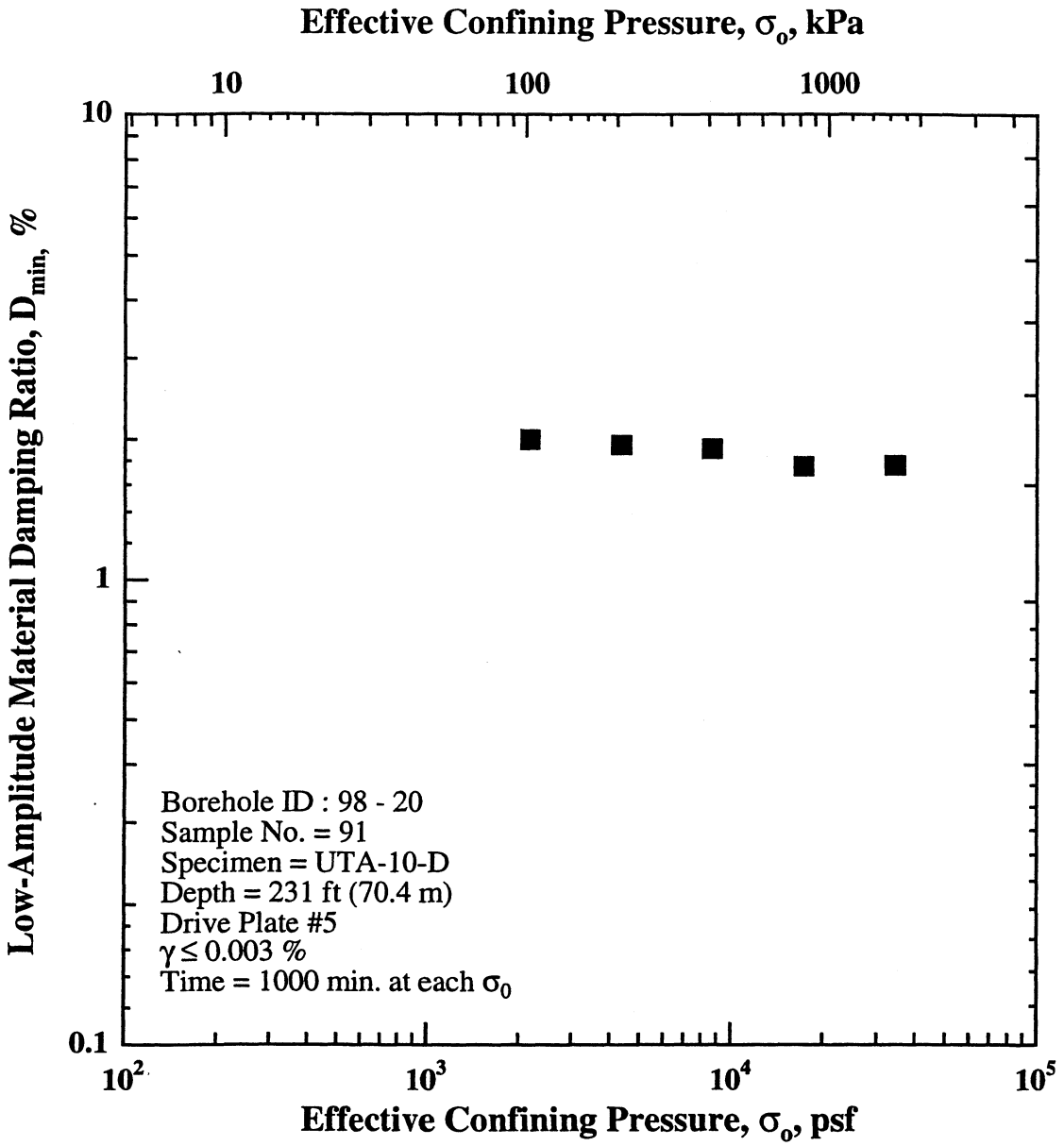

Figure E.7 Variation in Low-Amplitude Material Damping Ratio with Effective Confining Pressure from Resonant Column Tests of Specimen UTA-10-D from the East Bay Bridge Site.

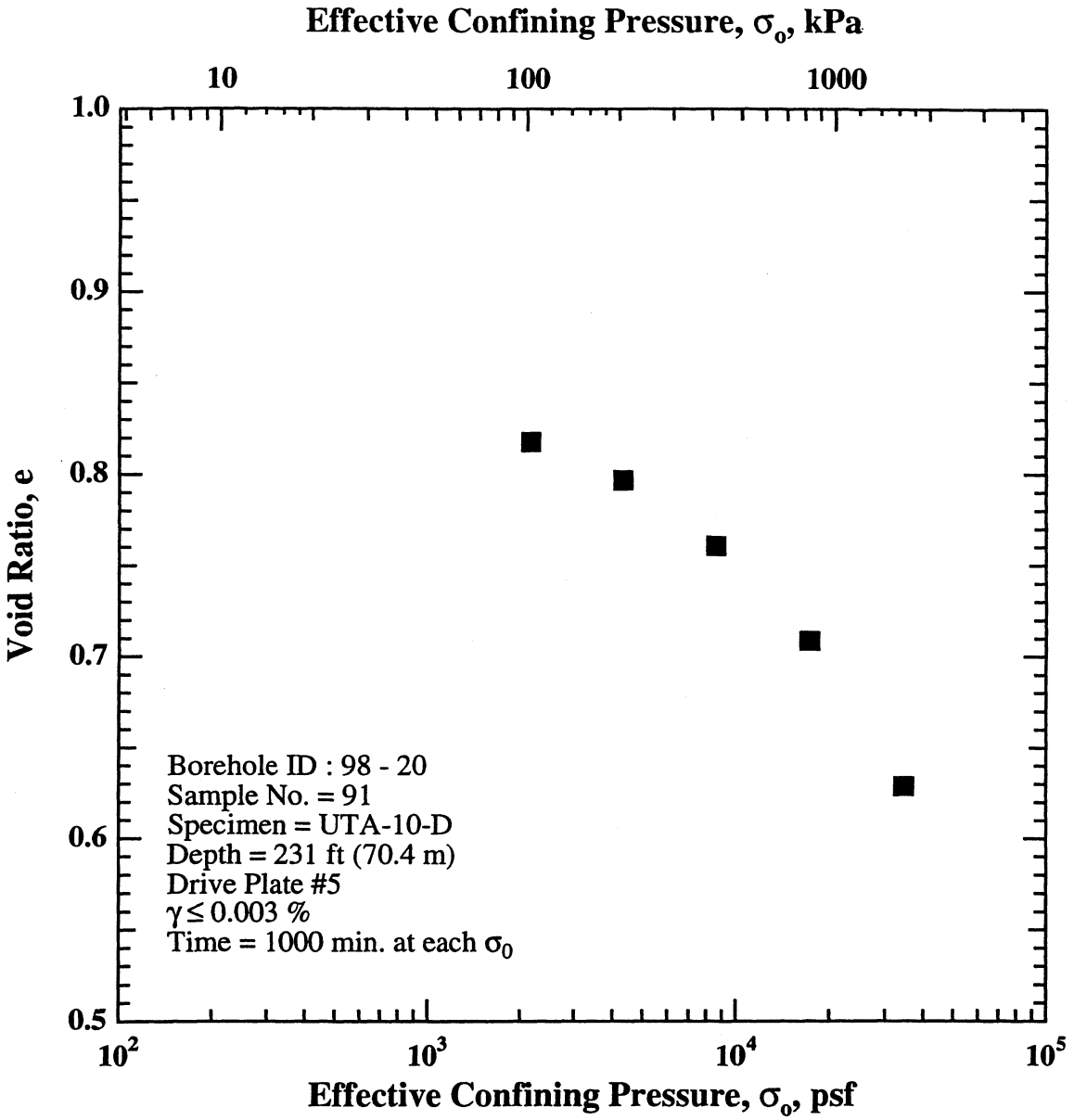

Figure E.8 Variation in Void Ratio with Effective Confining Pressure from Resonant Column Tests of Specimen UTA-10-D from the East Bay Bridge Site.

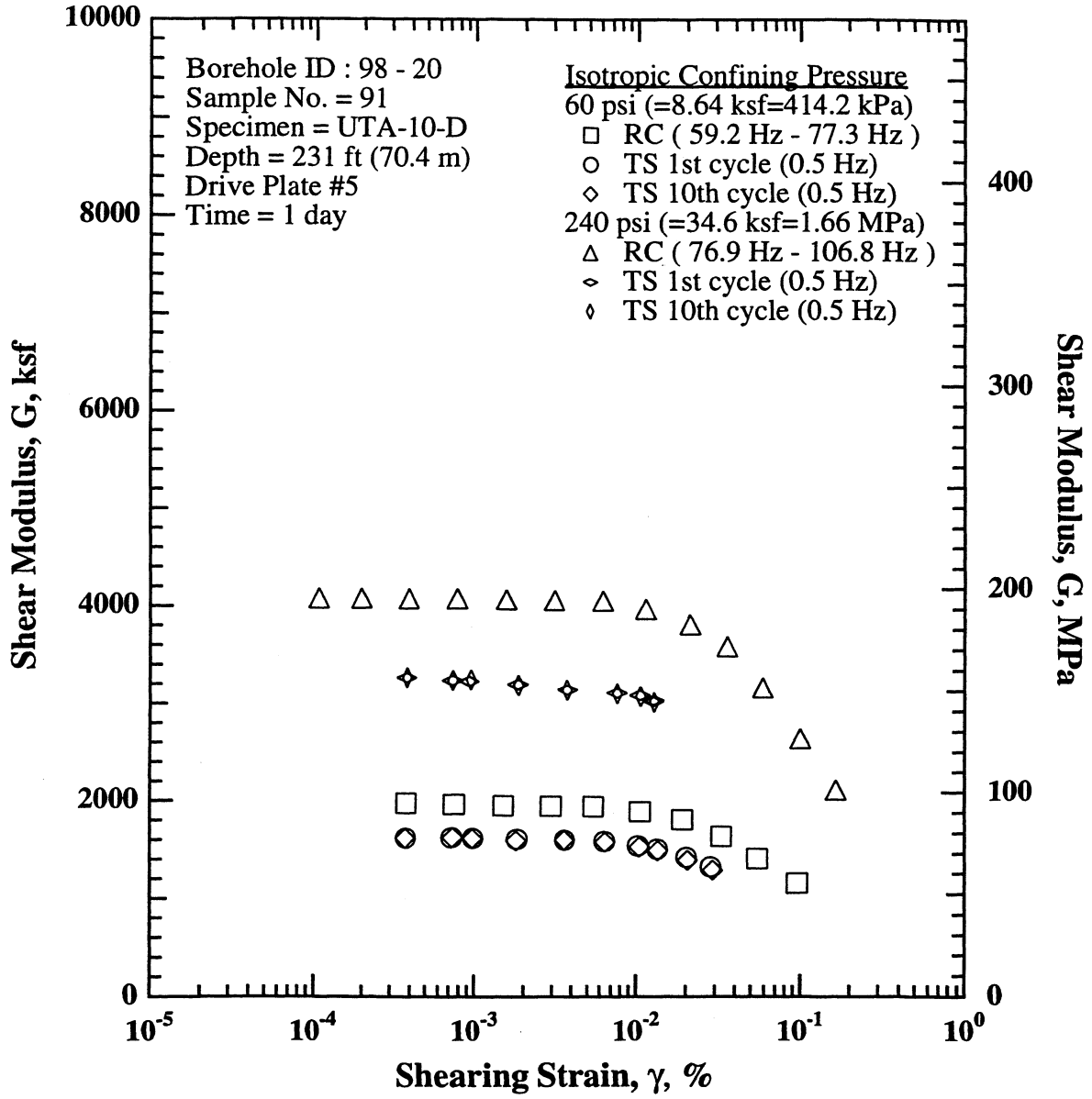

Figure E.9 Variation in Shear Modulus with Shearing Strain and Isotropic Effective Confining Pressure from Resonant Column Tests of Specimen UTA-10-D from the East Bay Bridge Site.

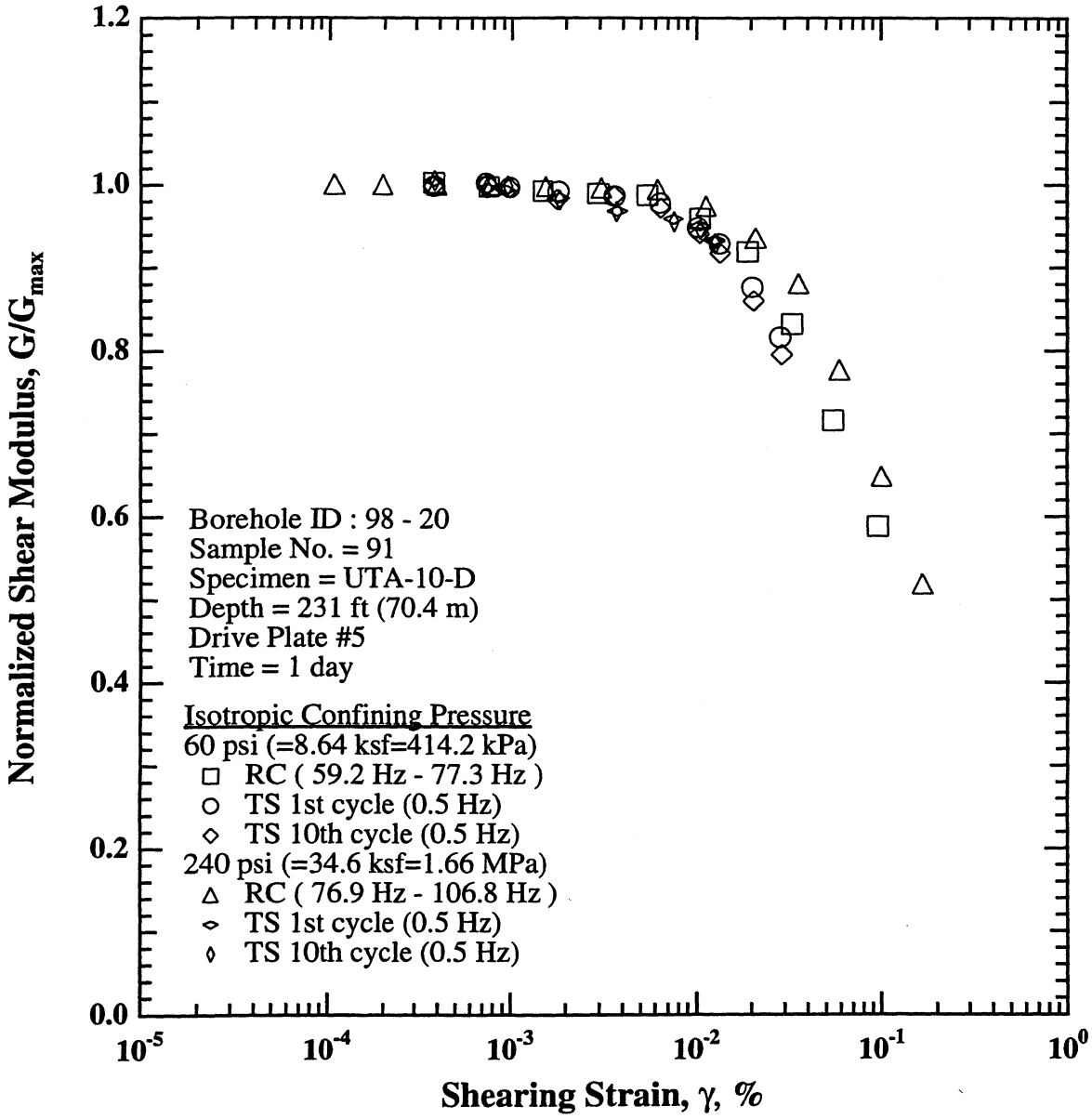

Figure E.10 Variation in Normalized Shear Modulus with Shearing Strain and Isotropic Effective Confining Pressure from Resonant Column Tests of Specimen UTA-10-D from the East Bay Bridge Site.

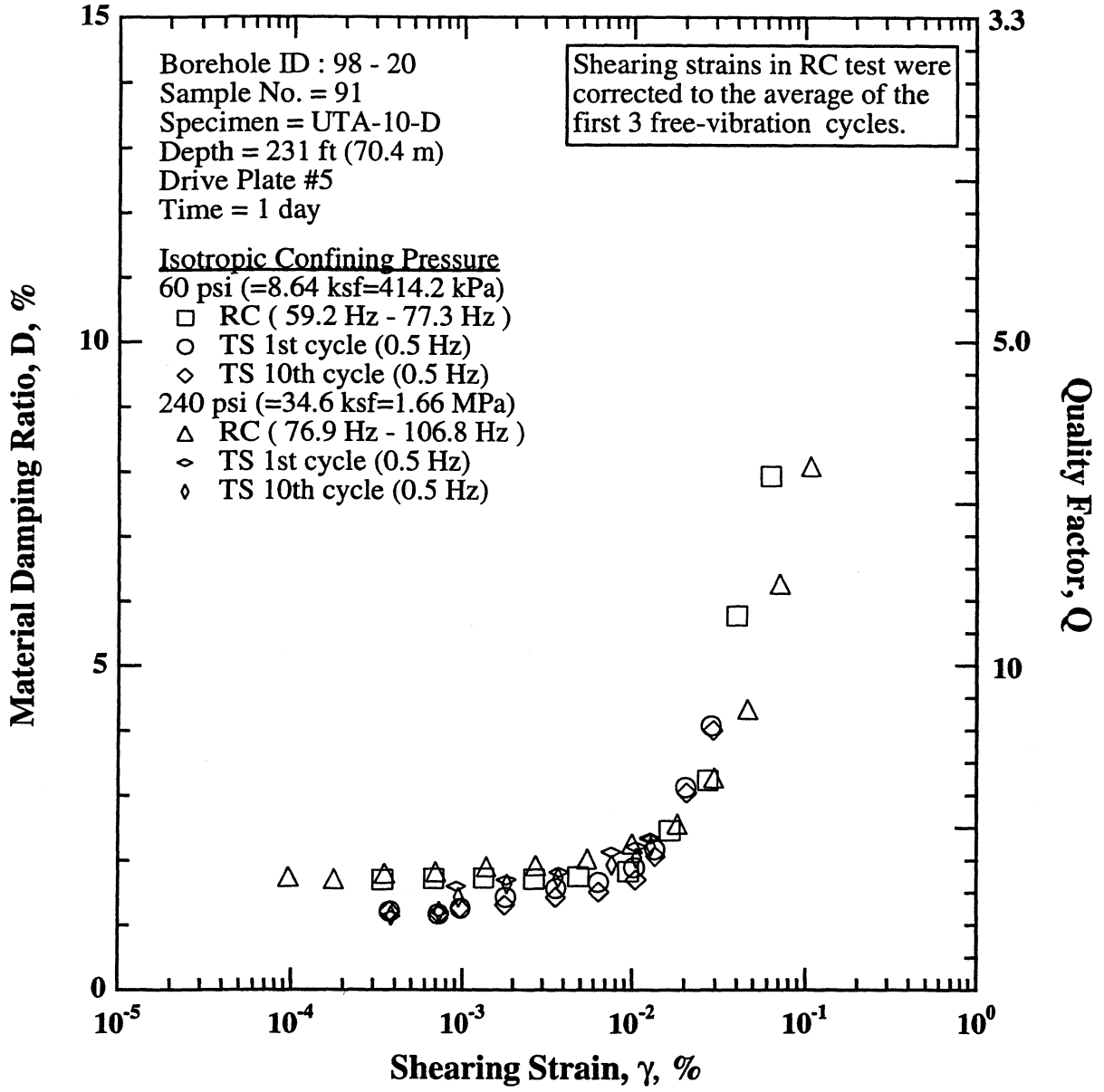

Figure E.11 Variation in Material Damping Ratio with Shearing Strain and Isotropic Effective Confining Pressure from Resonant Column Tests of Specimen UTA-10-D from the East Bay Bridge Site.

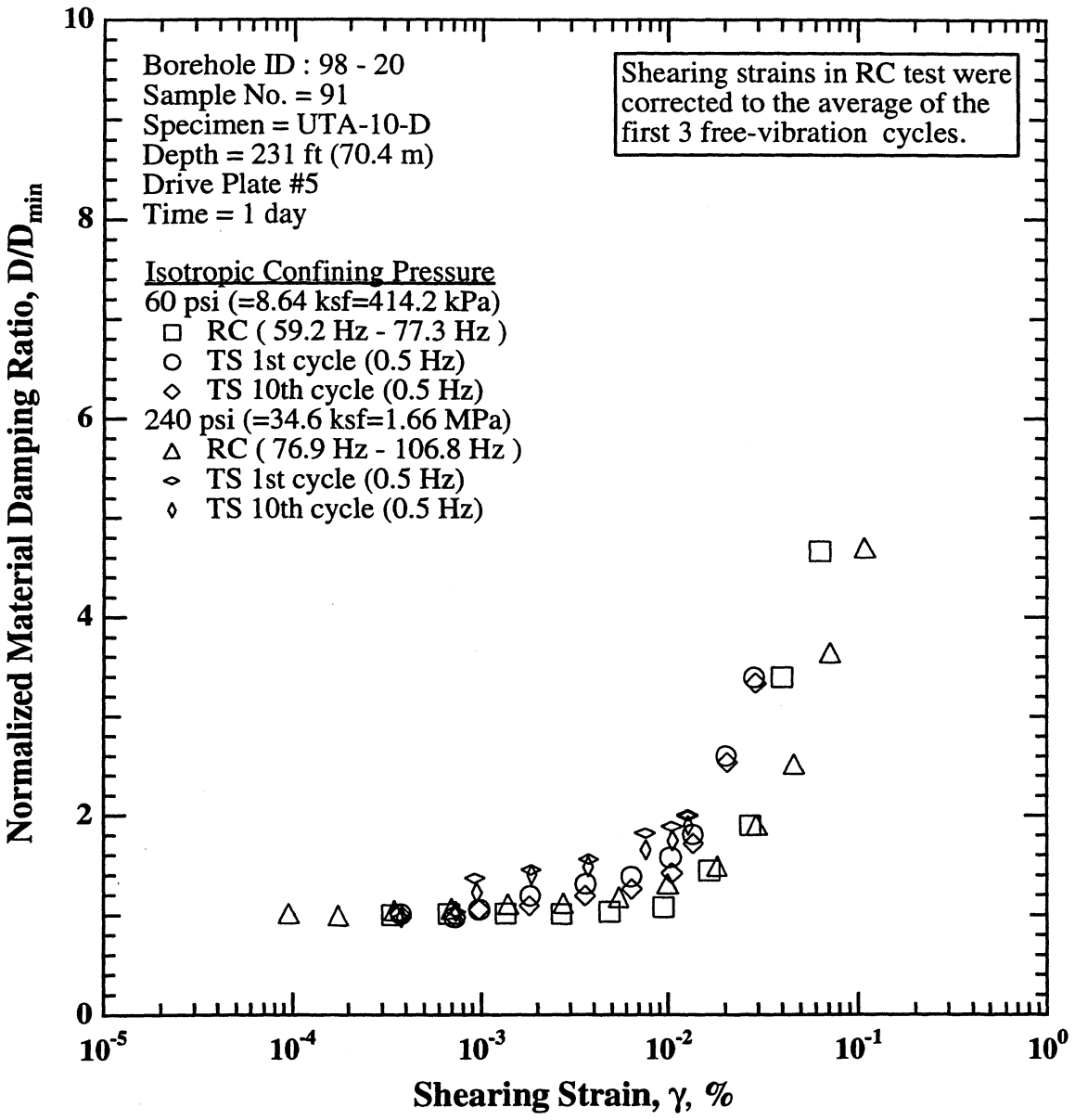

Figure E.12 Variation in Normalized Material Damping Ratio with Shearing Strain and Isotropic Effective Confining Pressure from Resonant Column Tests of Specimen UTA-10-D from the East Bay Bridge Site.

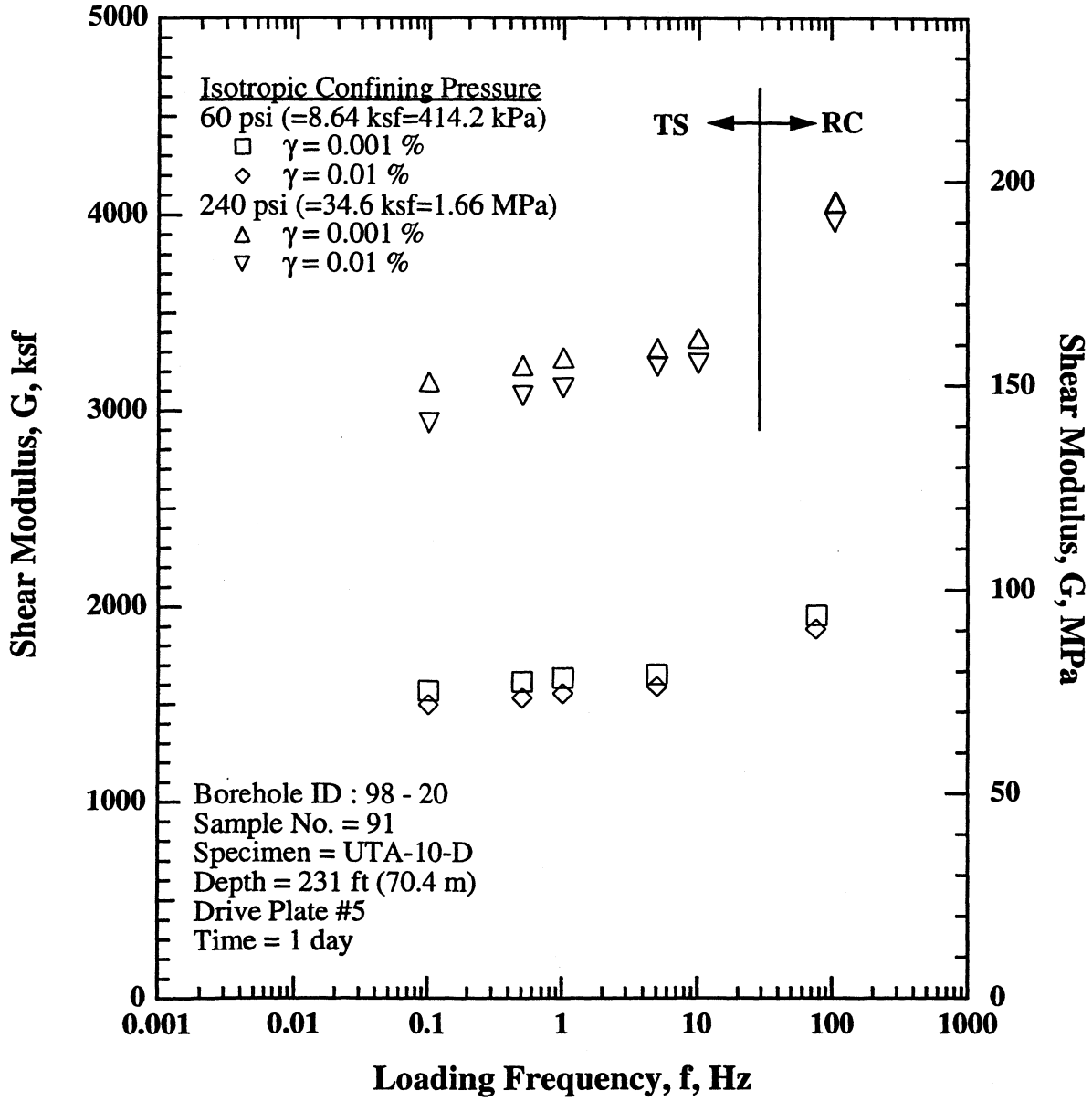

Figure E.13 Comparison of the Variation in Shear Modulus with Loading Frequency, Shearing Strain and Isotropic Effective Confining Pressure from RCTS Tests of Specimen UTA-10-D from the East Bay Bridge Site.

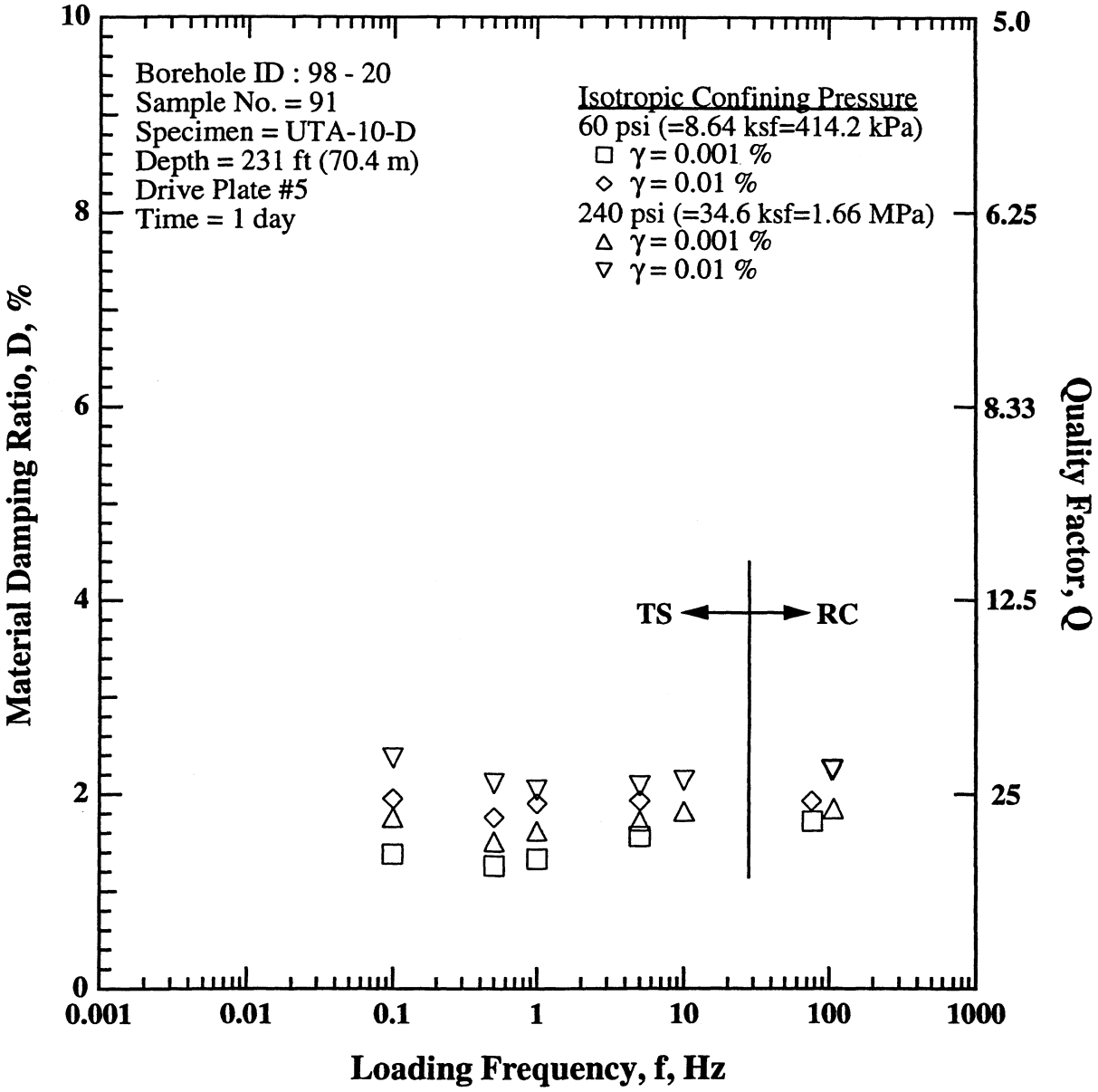

Figure E.14 Comparison of the Variation in Material Damping Ratio with Loading Frequency, Shearing Strain and Isotropic Effective Confining Pressure from RCTS Tests of Specimen UTA-10-D from the East Bay Bridge Site.

Table E.1 Variation in Low-Amplitude Shear Modulus, Low-Amplitude Material Damping Ratio and Void Ratio with Effective Isotropic Confining Pressure from RC Tests of Specimen UTA-10-D (Boring 98 - 20) from the East Bay Bridge Site

Effective Isotropic Confining Pressure, σ_o'			Low-Amplitude Shear Modulus, G_{max}		Low-Amplitude Material Damping Ratio,	Void Ratio, e
(psi)	(psf)	(kPa)	(ksf)	(MPa)	Dmin, %	
15	2160	103.5	1039	49.8	2.00	0.818
30	4320	207.1	1357	65.0	1.95	0.797
60	8640	414.2	1895	90.8	1.91	0.761
120	17280	828.4	2703	129.6	1.75	0.709
240	34560	1656.8	4008	192.2	1.76	0.629

Table E.2 Variation in Shear Modulus, Normalized Shear Modulus and Material Damping Ratio with Shearing Strain from RC Tests of Specimen UTA-10-D (Boring 98 - 20) from the East Bay Bridge Site; Effective Confining Pressure, σ_o' = 60 psi (8.64 ksf = 414.2 kPa)

Peak Shearing Strain, %	Shear Modulus, G, ksf	Normalized Shear Modulus, G/G_{max}	Average[+] Shearing Strain, %	Material Damping Ratio[x], D, %
3.75E-04	1971	1.00	3.39E-04	1.70
7.47E-04	1961	1.00	6.73E-04	1.72
1.49E-03	1951	0.99	1.34E-03	1.73
2.96E-03	1945	0.99	2.67E-03	1.71
5.41E-03	1941	0.99	4.86E-03	1.75
1.05E-02	1886	0.96	9.43E-03	1.83
1.90E-02	1807	0.92	1.64E-02	2.46
3.28E-02	1635	0.83	2.71E-02	3.23
5.46E-02	1407	0.72	3.97E-02	5.77
9.56E-02	1156	0.59	6.29E-02	7.92

[+] Average Shearing Strain from the First Three Cycles of the Free Vibration Decay Curve

[x] Average Damping Ratio from the First Three Cycles of the Free Vibration Decay Curve

Table E.3 Variation in Shear Modulus, Normalized Shear Modulus and Material Damping Ratio with Shearing Strain from TS Tests of Specimen UTA-10-D (Boring 98 - 20) from the East Bay Bridge Site; Effective Confining Pressure, σ_o' = 60 psi (8.64 ksf = 414.2 kPa)

First Cycle				Tenth Cycle			
Peak Shearing Strain, %	Shear Modulus, G, ksf	Normalized Shear Modulus, G/G_{max}	Material Damping Ratio, D, %	Peak Shearing Strain, %	Shear Modulus, G, ksf	Normalized Shear Modulus, G/G_{max}	Material Damping Ratio, D, %
3.74E-04	1617	1.00	1.21	3.70E-04	1617	1.00	1.21
7.20E-04	1623	1.00	1.17	7.30E-04	1622	1.00	1.17
9.74E-04	1615	1.00	1.26	9.70E-04	1614	1.00	1.26
1.81E-03	1607	0.99	1.43	1.79E-03	1591	0.98	1.31
3.60E-03	1598	0.99	1.57	3.58E-03	1598	0.99	1.43
6.36E-03	1584	0.98	1.66	6.40E-03	1574	0.97	1.51
1.02E-02	1536	0.95	1.89	1.04E-02	1524	0.94	1.70
1.34E-02	1504	0.93	2.17	1.35E-02	1486	0.92	2.06
2.01E-02	1419	0.88	3.12	2.05E-02	1392	0.86	3.04
2.83E-02	1322	0.82	4.07	2.90E-02	1288	0.80	4.00

Table E.4 Variation in Shear Modulus, Normalized Shear Modulus and Material Damping Ratio with Shearing Strain from RC Tests of Specimen UTA-10-D (Boring 98 - 20) from the East Bay Bridge Site; Effective Confining Pressure, σ_o' = 240 psi (34.56 ksf = 1.66 MPa)

Peak Shearing Strain, %	Shear Modulus, G, ksf	Normalized Shear Modulus, G/G_{max}	Average[+] Shearing Strain, %	Material Damping Ratio[x], D, %
1.95E-04	4071	1.00	1.75E-04	1.71
1.06E-04	4072	1.00	9.53E-05	1.74
3.87E-04	4068	1.00	3.47E-04	1.80
7.75E-04	4069	1.00	6.94E-04	1.82
1.55E-03	4062	1.00	1.38E-03	1.90
3.07E-03	4054	1.00	2.73E-03	1.92
6.15E-03	4046	0.99	5.45E-03	2.02
1.13E-02	3964	0.97	9.91E-03	2.26
2.10E-02	3807	0.94	1.80E-02	2.56
3.55E-02	3582	0.88	2.93E-02	3.27
5.89E-02	3160	0.78	4.60E-02	4.33
9.99E-02	2639	0.65	7.08E-02	6.26
1.66E-01	2110	0.52	1.08E-01	8.08

[+] Average Shearing Strain from the First Three Cycles of the Free Vibration Decay Curve

[x] Average Damping Ratio from the First Three Cycles of the Free Vibration Decay Curve

Table E.5 Variation in Shear Modulus, Normalized Shear Modulus and Material Damping Ratio with Shearing Strain from TS Tests of Specimen UTA-10-D (Boring 98 - 20) from the East Bay Bridge Site; Effective Confining Pressure, σ_o' = 240 psi (34.56 ksf = 1.66 MPa)

First Cycle				Tenth Cycle			
Peak Shearing Strain, %	Shear Modulus, G, ksf	Normalized Shear Modulus, G/G_{max}	Material Damping Ratio, D, %	Peak Shearing Strain, %	Shear Modulus, G, ksf	Normalized Shear Modulus, G/G_{max}	Material Damping Ratio, D, %
3.76E-04	3261	1.00	1.14	3.78E-04	3261	1.00	1.14
7.26E-04	3233	1.00	1.21	7.30E-04	3233	1.00	1.21
9.19E-04	3225	0.99	1.60	9.45E-04	3240	1.00	1.43
1.83E-03	3193	0.98	1.70	1.84E-03	3185	0.98	1.64
3.73E-03	3141	0.97	1.82	3.70E-03	3139	0.97	1.73
7.53E-03	3110	0.96	2.13	7.55E-03	3099	0.96	1.93
1.04E-02	3083	0.95	2.21	1.05E-02	3068	0.95	2.04
1.26E-02	3025	0.93	2.34	1.27E-02	3012	0.93	2.22